

Optimization of the assessment of cerebral autoregulation in neurocritical care

Xiuyun Liu

Newnham College



University of Cambridge



This dissertation is submitted for the degree of Doctor of Philosophy

05/2017

DECLARATION

This dissertation is the result of my own work and includes nothing which is the outcome of work done in collaboration except as declared in the preface and specified in the text.

This dissertation is not substantially the same as any that I have submitted, or, is being concurrently submitted for a degree or diploma or other qualification at the University of Cambridge or any other University or similar institution except as declared in the preface and specified in the text. I further state that no substantial part of my dissertation has already been submitted, or, is being concurrently submitted for any such degree, diploma or other qualification at the University of Cambridge or any other University of similar institution except as declared in the Preface and specified in the text.

This dissertation does not exceed the word limit of 60 000 words.

Xiuyun Liu

31/05/2017

Table of Contents

| | |
|---|-----------|
| SUMMARY | 5 |
| ACKNOWLEDGEMENTS..... | 8 |
| LIST OF PUBLICATIONS..... | 9 |
| DISTINCTIONS | 13 |
| LIST OF FIGURES | 14 |
| LIST OF TABLES | 18 |
| LIST OF ABBREVIATIONS AND ACRONYMS | 19 |
| LIST OF EQUATIONS AND CONDITIONS | 24 |
| CHAPTER 1 AIMS AND HYPOTHESES..... | 27 |
| 1.1 The validation of relationships between currently widely used CA parameters..... | 28 |
| 1.2 Introduction of a new time–frequency-based analysis method for CA assessment..... | 29 |
| 1.3 Calculation of optimal CPP for clinical TBI patients..... | 30 |
| 1.4 Outline of the thesis | 30 |
| CHAPTER 2 BASIC OF CEREBRAL PHYSIOLOGY – REVIEW..... | 32 |
| 2.1 Monro–Kellie hypothesis and pressure–volume curve | 32 |
| 2.2 Global model of CBF and circulation of CSF..... | 33 |
| 2.3 Cerebral autoregulation | 34 |
| 2.4 Traumatic brain injury..... | 38 |
| 2.5 Disturbance of cerebral autoregulation after TBI..... | 39 |
| 2.6 Clinical Problems in treating TBI..... | 40 |
| CHAPTER 3 STATE OF THE ART FOR CURRENT METHODOLOGY OF AUTOREGULATION MONITORING | 42 |
| 3.1 Current widely used methods for cerebral autoregulation assessment | 43 |
| 3.2 Wavelet analysis for CA autoregulation | 51 |
| 3.3 Clinical application of CA assessment | 52 |
| CHAPTER 4 METHODOLOGICAL CONSIDERATIONS REGARDING PROJECTS INCLUDED IN THE THESIS..... | 58 |
| 4.1 General overview of the original projects included in this thesis | 58 |

| | |
|--|------------|
| 4.2 Data collection | 59 |
| 4.3 The database | 65 |
| 4.4 Statistical analysis..... | 67 |
| CHAPTER 5 RELATIONSHIP BETWEEN DIFFERENT CA PARAMETERS IN TBI..... | 69 |
| 5.1 Cross-validation and cross-calibration of CA indices – a modelling study | 69 |
| 5.2 Comparison of frequency- and time-domain methods of CA assessment in TBI..... | 80 |
| 5.3 Conclusion..... | 88 |
| CHAPTER 6 INTRODUCTION OF A NEW, TIME-FREQUENCY ANALYSIS METHOD FOR CA ASSESSMENT | 89 |
| 6.1 Introduction | 89 |
| 6.2 Validation of Cerebral Autoregulation Assessment Using Wavelet Method | 90 |
| 6.3 Cerebovascular pressure reactivity using wavelet analysis in TBI..... | 104 |
| 6.4 Conclusion..... | 112 |
| CHAPTER 7 AN INNOVATIVE METHOD TO MONITOR CPPopt IN TBI..... | 114 |
| 7.1 Introduction | 114 |
| 7.2 Monitoring of CPPopt in TBI using a multi-window weighting algorithm based on PRx | 114 |
| 7.3 Monitoring of CPPopt in TBI using a multi-window weighting algorithm based on wPRx..... | 123 |
| 7.4 Discussion | 129 |
| 7.5 Conclusion..... | 130 |
| CHAPTER 8 CEREBRAL AUTOREGULATION DURING INTRACRANIAL HYPERTENSION..... | 131 |
| 8.1 Cerebral autoregulation assessment in plateau waves | 133 |
| 8.2 Wavelet method for CA assessment in TBI patients with refractory ICP | 139 |
| 8.3 Conclusion..... | 143 |
| CHAPTER 9 CONCLUSIONS AND FUTURE DIRECTIONS..... | 144 |
| REFERENCES | 147 |

SUMMARY

Introduction

Cerebral autoregulation (CA) refers to the physiological mechanisms in the brain to maintain constant blood flow despite changes in cerebral perfusion pressure (CPP). It plays an important protective role against the danger of ischaemia at low perfusion pressure, and the risk of brain oedema at higher CPP. Over the years, various methods for CA assessment have been proposed, including both static and dynamic CA. Whereas ‘static’ CA is assessed by analysing the cerebral blood flow (CBF) response to slow manipulations of arterial blood pressure (ABP) or cerebral perfusion pressure (CPP), the dynamic CA is assessed from analysing the CBF velocity (CBFV) response to transient changes in ABP, either externally induced or occurring spontaneously. One dynamic method known as the leg-cuff test uses a sudden drop in ABP produced by a rapid deflation of thigh cuffs to grade the ensuing CBFV response with a parametric, second order-model, Tiecks’ model. The resulting CA index, the autoregulation index (ARI), grades CA into ten levels (from 0 - 9), while ARI = 0 represents absent autoregulation and ARI = 9 indicates hyperactive autoregulation. However, direct calculation of ARI in such a manner requires substantial decreases/increases in ABP, which, for traumatic brain injury (TBI) patients, should be avoided in some cases.

One attractive method that takes advantage of spontaneous fluctuations in ABP and CBFV is transfer function (TF) analysis, an approach that sheds light on the dynamic properties of CA from the perspective of linear response theory. This type of analysis assumes that functional CA can be described as a high pass filter that readily transmits rapid (high frequency) changes in ABP to CBFV, but attenuates the transmission of slower (low frequency, usually lower than 0.05 Hz) ABP perturbations to CBFV. Parameters derived from TF include phase shift, gain and coherence. In 1998, Panerai and colleagues combined the Tiecks’ model with TF analysis in low frequency range to yield the impulse response (IR)-based ARI, defined as the best match between the IR estimated from patients’ real data with IR of Tiecks’ model.

Another commonly used measure, the mean flow index (Mx), estimates CA through the correlation coefficient between slow fluctuations (20 sec to 3 minutes) of mean CBFV and CPP. It is a purely time domain measurement, based on the concept that if CA is intact, there will be no correlation between changes in CPP and changes in CBFV ($Mx = \text{zero or negative}$), whereas when CA is exhausted changes in CPP will be directly correlated with changes in CBFV ($Mx \approx +1$). In traumatic brain injury, where frequent, repeated assessment of CA is highly desirable, a technique based on analysis of the relationship between two routinely monitored modalities, ABP and intracranial pressure (ICP) has gained wide popularity. Given that changes in ICP may be interpreted as surrogates for changes in cerebral blood volume, pressure reactivity index (PRx), calculated as a moving correlation coefficient between mean ABP and ICP, is well suited for real-time, continuous monitoring of CA and is by now routinely used in many head trauma centres.

These methods mentioned above, all describe CA, but perhaps reflect its slightly different aspects. Until now, how these parameters are related with each other is still not clear. Especially that in reality, their properties will be affected by issues related to their estimation from the measurement data, as well as by the degree of misfit of the models used to describe the underlying physiology. A comprehensive investigation of the relationship between all these parameters using measurements taken from a particular patient population is therefore needed. In addition, the methods mentioned above mostly assume the system being analysed is linear and the signals are stationary, the assumption has been shown not to reflect the reality very well. A more robust method, in particular suitable for non-stationary signal analysis, needs therefore to be explored.

The clinical benefit of PRx monitoring lies in the fact that plotting PRx against CPP will often generate a ‘U’-shape curve, the minimum of which represents the CPP corresponding to the smallest value of PRx, where the CA response is most active, and the point is termed optimal CPP (CPPopt). Observational studies have confirmed that patients whose median CPP is closer to their determined CPPopt seem to have better clinical outcomes. The problem with the current algorithm of CPPopt is the fact that CPPopt can only be generated during approximately 55% of the monitoring time. An improved method which can create more stable and continuous CPPopt is needed, to make CPPopt-guided management more likely to be accepted into clinical practice.

Objectives, Methods and Results

This thesis addresses three primary questions:

1. What are the relationships between currently widely used CA parameters, i.e. Mx, ARI, TF parameters, from theoretical and practical point of view?
2. Is there an effective method that can be introduced to assess CA, which is suitable for analyses of non-stationary signals?
3. How can bedside monitoring of cerebral autoregulation be improved in traumatic brain injury patients ?

These general aims have been translated into a series of experiments, retrospective analyses and background studies which are presented in different chapters of this thesis. As part of this project, all the methods used in this thesis have been implemented in ICM+ (<http://www.neurosurg.cam.ac.uk/icmplplus>) using custom built plugins (written in C and compiled into dll libraries) where necessary. Most of the chapters of this work have been also written up as manuscripts for peer-review journals and are either published already or are in currently under review (see list of publications).

First, a validation study of the relationship between different established CA parameters, such as Mx, TF, ARI, was applied to a group of simulated data and a database of TBI patients. The result showed that the impulse-response-

based ARI correlates significantly with the time-correlation-based index Mx and TF phase. Both Mx and ARI were significantly related to patients' outcome, although Mx correlates more strongly than ARI.

Second, a new time – frequency analytical method, the wavelet transform, is introduced to assess CA, which is suitable for non-stationary signals. The new method, termed wavelet transform pressure reactivity index (wPRx), was validated through two groups of experimental piglets' data. Subsequently, the wPRx was applied to a big cohort of TBI patients. The results showed a significantly positive relationship between wPRx and the time-correlation-based index, PRx, with wPRx demonstrating more stable behaviour than PRx.

Third, an improved approach for optimal CPP estimation for TBI patients is described. This mathematical approach was based on a multi-window algorithm and applying a weighting system which incorporates more characteristics of the PRx-CPP plot. The result showed significant improvement of CPPopt yield using the multi-window approach, with more stable results. This methodological improvement is essential for its clinical application in future CPPopt trials.

Finally, the thesis tests whether the CA parameters used in this project also work in other clinical situations. The result showed that the CA parameters (i.e. ARI, Mx, PRx, wPRx) demonstrated deteriorated CA during high ICP, such as ICP plateau and refractory ICP.

Conclusion

This PhD project carefully scrutinised currently used CA assessment methodologies in TBI patients, demonstrating significant relationships between ARI, Mx and TF phase. The new introduced wavelet-transform-based method, wPRx was validated and showed more stable result for CA assessment than the well-established parameter, PRx. A multi-window approach with weighting system for optimal CPP estimation was described. The result showed a significant improvement in the continuity and stability of CPPopt estimation, which made it possible to be applied in the future clinical management of TBI patients.

ACKNOWLEDGEMENTS

First and foremost, I would like to thank my supervisors Dr. Peter Smielewski and Prof. Marek Czosnyka, who have been unfailingly generous with their time, encouragement and support and who have been able to impart to me the intellectual excitement of research. In the four years' study, from collecting data to analysing data, from selecting the best papers to read to making a good plan for each project, they showed great patience to me and help me to grow up in academic field.

I would like to thank Dr. Zofia Czosnyka for helping me to understand the infusion study and the cerebral spinal fluid mechanism. She was always so kind to help me with any trouble in life. I am grateful to Prof. Peter Hutchinson, who supported me a lot in both research projects and academic meetings. Mr Joseph Donnelly and Dr. George Varsos helped me get familiar with my research very fast and they supported me a lot on my publications. Dr. Marcel Aries and Dr Ari Ercole gave me suggestions in combing research with clinical practice. Mr Danilo Cardim and Mr Manuel Cabeleira helped me with collecting data from bedside. Dr. Ken Brady, Dr. Marek Sykora and Dr. Natalie Finnigan were so generous to share part of their data with me for my new method calibration. Dr. Celeste Dias and Ms Corien Weersink were very supportive and encouraging in my first year. I'd like to thank the members of the brain physics lab and department of clinical neurosciences, Prof. Christina Haubrich, Ms Chiara Robba, Ms Cristine Sortica, Ms Jeanette Tas, Ms Despina Aphroditis Lalou, Ms Leanne Calviello, Mr Piotrek Czosnek and our visiting scholars, they have been a constant source of practical support and advice over the past four years, particularly their friendship help me overcome difficulties.

My research has been entirely funded by Gates Cambridge Scholarship, a scholarship established by the Bill and Melinda Gates Foundation in 2000 to enable outstanding graduate students from outside the United Kingdom to study at the University of Cambridge. The awardees are given funding for postgraduate study at the University for the duration of the degree. I am grateful to everyone who has contributed to the Gates Foundation and allowed me to undertake this PhD research at University of Cambridge.

Last but not the least, I would like to thank my family and friends for their love and encouragement during these years. It was a great experience to study at University of Cambridge, and it was such a great honour to work in the Brain Physics Lab, Department of Clinical Neurosciences. I will keep paying attention to the achievement of the lab in the future. I will carry on with my hard working spirit, my enthusiasm, passion and tenacious efforts to realise my dream.

LIST OF PUBLICATIONS

This is a current list (21.12.2016) of manuscripts, abstracts and presentation which have resulted from the work performed as part of this thesis.

Manuscripts published or accepted for publication

1. Liu X, Czosnyka M, Donnelly J, Budohoski KP, Varsos GV, Nasr N, Brady KM, Reinhard M, Hutchinson PJ, Smielewski P. Comparison of frequency and time domain methods of assessment of cerebral autoregulation in traumatic. **J. Cereb. Blood Flow Metab.** 2014, **11:1-9**.
2. Liu X, Czosnyka M, Pickard JD, Varsos GV, Nasr N, Smielewski P. Derangement of cerebral blood flow autoregulation during intracranial pressure plateau waves as detected by time and frequency-based methods. **Acta Neurochir Suppl.** 2016; **122:233-8**.
3. Li Xiong*; Xiuyun Liu*; Ty Shang; Peter Smielewski; Joseph Donnelly; Zhen-ni Guo; Yi Yang; Thomas Leung; Marek Czosnyka; Rong Zhang; Jia Liu; Ka Sing Wong. Clinical applications of measuring impaired cerebral autoregulation in stroke. **Journal of Neurology, Neurosurgery & Psychiatry** (2017)

Manuscripts under review or in submission

1. Xiuyun Liu, Marek Czosnyka, Joseph Donnelly, Danilo Cardim, Georgios V. Varsos, Manuel Cabeleira, Peter J. Hutchinson, Peter Smielewski. Scrutiny of transcranial Doppler based cerebral autoregulation measures – a modelling perspective (**In submission**).
2. Xiuyun Liu, MSc, Marek Czosnyka, PhD, Joseph Donnelly, MB ChB, Danilo Cardim, MSc, Manuel Cabeleira, MSc, Peter J. Hutchinson, PhD, Peter Smielewski*, PhD, Ken Brady*, Validation of wavelet method for assessing cerebral autoregulation. - submitted to **JCBFM (under review)**.
3. Xiuyun Liu, MSc, Marek Czosnyka, Joseph Donnelly, Marcel J. H. Aries, Ken Brady, Danilo Cardim, Chiara Robba, Manuel Cabeleira, Dong-Joo Kim, Christina Haubrich, Peter Smielewski. Cerebrovascular Pressure Reactivity Monitoring Using Wavelet Analysis in Traumatic Brain Injury Patients - submitted to **PLOS Medicine (under review)**.
4. Xiuyun Liu, Natasha M. Maurits, Marcel J.H. Aries, Marek Czosnyka, Joseph Donnelly, Danilo Cardim, Dong-Joo Kim, Celeste Dias, Manuel Cabeleira, Peter Smielewski. Monitoring of optimal cerebral perfusion pressure in traumatic brain injured patients using a multi-window weighting algorithm. submitted to **Critical Care Medicine (under review)**.

Conference presentations

1. April, 2013: the 18th conference of the European Society of Neurosonology and Cerebral Hemodynamics, Porto, Portugal

2. November 2013: 15th International Conference on Intracranial Pressure & Brain Monitoring (ICP), Singapore

1) Oral presentation: Dearrangement of cerebral blood flow autoregulation during intracranial pressure plateau waves as detected by time and frequency based methods

2) Poster 1: Comparison of frequency and time domain methods of assessment of cerebral autoregulation in traumatic injury patients

3) Poster 2: Cross-validation and cross-calibration of mean flow index Mx with the phase, gain and ARI measures of cerebral autoregulation

3. July 2015: CARNet conference: Southampton

Oral Presentation: Comparison between wavelet phaseshift and pressure reactivity index in determination of optimal cerebral perfusion pressure

4. March 2016: Annual meeting of the British Neurosurgical Research Group (BNRG), Cambridge

1) Oral presentation: Wavelet analysis in Traumatic Brain Injury Patients

2) Poster: Cerebral Autoregulation Using Wavelet Method: wPRx

5. July 2016: 16th International Symposium on Intracranial Pressure and Neuromonitoring in conjunction with the 6th Annual Meeting of the Cerebral Autoregulation Research Network and the 3rd ICM+ User Meeting

Poster presentation: Cerebral Autoregulation Using Wavelet Method: wPRx

Co-authored publications

The following list includes a current (24.10.2016) overview of publications and abstracts to which I was a co-author during the period of my PhD research.

1. Varsos GV, Budohoski KP, Czosnyka M, Koliass AG, Nasr N, Donnelly J, Liu X, Kim DJ, Hutchinson PJ, Kirkpatrick PJ, Varsos VG, Smielewski P. Cerebral Vasospasm affects Arterial Critical Closing Pressure. **J Cereb Blood Flow Metab.** 2015; 35(2):285-91.
2. Donnelly J, Czosnyka M, Harland S, Varsos GV, Cardim D, Robba C, Liu X, Ainslie PN, Smielewski P. Cerebral haemodynamics during experimental intracranial hypertension. **J Cereb Blood Flow Metab.** 2016;18.
3. Young AM, Donnelly J, Czosnyka M, Jalloh I, Liu X, Aries MJ, Fernandes HM, Garnett MR, Smielewski P, Hutchinson PJ, Agrawal S. Continuous Multimodality Monitoring in Children after Traumatic Brain Injury- Preliminary Experience. **PLoS One.** 2016 Mar 15;11(3).
4. Zhang Y, Liu X, Steiner L, Smielewski P, Feen E, Pickard JD, Czosnyka M. Correlation between cerebral autoregulation and carbon dioxide reactivity in patients with traumatic brain injury. **Acta Neurochir Suppl.** 2016;122:205-9.
5. Varsos GV, Czosnyka M, Smielewski P, Garnett MR, Liu X, Adams H, Pickard JD, Czosnyka Z. Cerebral critical closing pressure during infusion tests. **Acta Neurochir Suppl.** 2016;122:215-20.
6. Cardim D, Robba C, Bohdanowicz M, Donnelly J, Cabella B, Liu X, Cabeleira M, Smielewski P, Schmidt B, Czosnyka M. Non-invasive Monitoring of Intracranial Pressure Using Transcranial Doppler Ultrasonography: Is It Possible? **Neurocrit Care.** 2016 Mar 3.
7. Sykora M, Czosnyka M, Liu X, Donnelly J, Nasr N, Diedler J, Okoroafor F, Hutchinson P, Menon D, Smielewski P. Autonomic Impairment in Severe Traumatic Brain Injury. **Crit Care Med.** 2016 Jun;44(6):1173-81.
8. Cardim D, Czosnyka M, Donnelly J, Robba C, Cabella BC, Liu X, Cabeleira MT, Smielewsky P, Haubrich C, Garnett MR, Pickard JD, Czosnyka Z. Assessment of non-invasive ICP during CSF infusion test: an approach with Transcranial Doppler. **Acta Neurochir (Wien).** 2016 Feb;158(2):279-87.
9. Weersink CS, Aries MJ, Dias C, Liu MX, Koliass AG, Donnelly J, Czosnyka M, van Dijk JM, Regtien J, Menon DK, Hutchinson PJ, Smielewski P. Clinical and Physiological Events That Contribute to the Success Rate of Finding “Optimal” Cerebral Perfusion Pressure in Severe Brain Trauma Patients. **Crit Care Med.** 2015 Sep;43(9):1952-63.
10. Varsos GV, Czosnyka M, Smielewski P, Garnett MR, Liu X, Kim DJ, Donnelly J, Adams H, Pickard JD, Czosnyka Z. Cerebral critical closing pressure in hydrocephalus patients undertaking infusion tests. **Neurol Res.** 2015 Aug;37(8):674-82.

11. Sekhon MS, Griesdale DE, Czosnyka M, Donnelly J, Liu X, Aries MJ, Robba C, Lavinio A, Menon DK, Smielewski P, Gupta AK. The Effect of Red Blood Cell Transfusion on Cerebral Autoregulation in Patients with Severe Traumatic Brain Injury. **Neurocrit Care.** 2015 Oct;**23(2):210-6.**
12. J Simpson, N Sudhan, H Hare, J Donnelly, X Liu, F Aigbirhio, T Fryer, G Stocks-Gee, P Smielewski, D Bulte, and J Coles. Comparison of ¹⁵oxygen positron emission tomography and near-infrared spectroscopy for measurement of cerebral physiology. **Crit Care.** 2015; **19(Suppl 1): P445.**
13. Meel-van den Abeelen AS, Simpson DM, Wang LJ, Slump CH, Zhang R, Tarumi T, Rickards CA, Payne S, Mitsis GD, Kostoglou K, Marmarelis V, Shin D, Tzeng YC, Ainslie PN, Gommer E, Müller M, Dorado AC, Smielewski P, Yelicich B16, Puppo C, Liu X, Czosnyka M, Wang CY, Novak V, Panerai RB, Claassen JA. Between-centre variability in transfer function analysis, a widely used method for linear quantification of the dynamic pressure-flow relation: the CARNet study. **Med Eng Phys.** 2014 May;**36(5):620-7.**
14. Nasr N, Czosnyka M, Pavy-Le Traon A, Custaud MA, Liu X, Varsos GV, Larrue V. Baroreflex and Cerebral Autoregulation Are Inversely Correlated. **Circ J.** 2014;**78(10):2460-7.**
15. Donnelly J, Czosnyka M, Sudhan N, Varsos GV, Nasr N, Jalloh I, Liu X, Dias C, Sekhon MS, Carpenter KL, Menon DK, Hutchinson PJ, Smielewski P. Increased Blood Glucose is Related to Disturbed Cerebrovascular Pressure Reactivity After Traumatic Brain Injury. **Neurocrit Care.** 2015 Feb;**22(1):20-5.**
16. Varsos GV, Budohoski KP, Koliass AG, Liu X, Smielewski P, Varsos VG, Hutchinson PJ, Pickard JD, Czosnyka M. Relationship of Vascular Wall Tension and Autoregulation Following Traumatic Brain Injury. **Neurocrit Care.** 2014 Oct;**21(2):266-74.**
17. Cabella Brenno, Donnelly Joseph, Cardim Danilo, Liu Xiuyun, Cabeleira Manuel, Smielewski Peter, Haubrich Christina, Hutchinson Peter, Kim Dong Joo, Czosnyka Marek. An association between ICP-derived data and outcome in TBI patients: The role of sample size. **Journal of Neurocritical Care,** 2016.

DISTINCTIONS

The following list includes a current (24.10.2014) overview of scholarships and grants, which have been awarded for the results of my work, performed as part of this thesis.

Scholarship

Gates Cambridge Scholarship (2012-2016)

Gates Academic development funding (2014)

Chinese Government Award for outstanding students abroad (2016)

Grants

Travel Grants, International Universities Innovation Alliance (2016)

Travel Grants, Western Returned Scholars Association Chinese Overseas-Educated Scholars Association (2015)

LIST OF FIGURES

| Number | Description. | Page |
|-------------------|--|-------------|
| Figure 1.1 | The framework of this research | 27 |
| Figure.2.1 | Anatomy of the intracranial compartment and intracranial pressure-volume curve | 32 |
| Figure 2.2 | Hydrodynamic equivalent of the model, comprising pathways of CBF and the CSF circulation | 34 |
| Figure 2.3 | The Lassen autoregulatory curve by plotting CBF vs perfusion pressure relationship | 35 |
| Figure 2.4 | Effect of changes in ABP, and cerebral vascular resistance on cerebral blood flow | 36 |
| Figure 2.5 | The effect of PaCO ₂ , PaO ₂ , ABP on CBF in a healthy population | 37 |
| Figure 2.6 | Leading causes of traumatic brain injury | 39 |
| Figure 2.7 | Cerebrovascular autoregulation in health, chronic hypertension and during autoregulation loss. | 40 |
| Figure 2.8 | The inter-relationship between primary and secondary injury in TBI is shown | 41 |
| Figure 3.1 | Example of evaluation of static rate of autoregulation. | 43 |
| Figure.3.2 | Response of cerebral autoregulation model to a step change in blood pressure | 44 |
| Figure 3.3 | Example of deflation of leg cuffs to test cerebral autoregulation | 45 |
| Figure 3.4 | The upper panel shows the step response and impulse response of original Tiecks' model. The lower panel shows the transfer function characteristics of Tiecks' model . | 47 |
| Figure 3.5 | Analysis of the phase shift between slow fluctuation of mean ABP and blood flow velocity. | 49 |
| Figure 3.6 | Graphs comparing the observed difference in analysed indices between favourable/unfavourable outcome and survival/death using CPP and ABP | 50 |
| Figure 4.1 | The framework of this research | 59 |

| | | |
|--------------------|---|-----------|
| Figure 4.2 | Intracranial pressure (ICP) can be highly dynamic in the neuro criticalcare unit. | 60 |
| Figure 4.3 | The waveforms of intracranial pressure (ICP) signal: pulse waves, respiratory waves and slow waves. | 60 |
| Figure 4.4 | Intracranial pressure monitoring. | 61 |
| Figure 4.5 | An example of spectral Doppler frequency display of the middle cerebral artery | 63 |
| Figure 4.6 | Four acoustic windows commonly used in transcranial Doppler examination | 63 |
| Figure 4.7 | Data monitoring in neuro critical care unit in Addenbrooke's hospital, Cambridge | 64 |
| Figure 5.1 | The real blood pressure and 10 artificial flow velocities generated for one patient. | 72 |
| Figure 5.2 | The relationship between mean Mxa and ARI. | 72 |
| Figure.5.3 | The relationship between ARI and the estimated transfer function parameters. | 73 |
| Figure 5.4 | Relationship between Mxa with transfer function parameters. | 74 |
| Figure 5.5 | The relationships between Mxa, TF parameters and ARI with different intensities of added noise. | 75 |
| Figure 5.6 | Comparison of Mxa-ARI relationship between real data and modelled data. | 77 |
| Figure 5.7 | The relationship between ARI and Mx. | 83 |
| Figure 5.8 | The relationship between ARIC and Gain_c at VLF and LF as well as the relationship between ARIC and Phase_c at VLF and LF. | 84 |
| Figure 5.9 | The relationship between ARIa and Gain_a at VLF and LF as well as the relationship between ARIa and Phase_a at VLF and LF. | 85 |
| Figure 5.10 | Mean values and SD in patients with favorable and unfavorable outcomes. | 85 |
| Figure 6.1 | Flow Chart of chapter 6. . | 89 |
| Figure 6.2 | Demonstration of lower limit of autoregulation using laser Doppler cerebral blood flow (CBF) and cerebral perfusion pressure (CPP). | 95 |

| | | |
|--------------------|--|------------|
| Figure 6.3 | Demonstration of WTP and WTC between ABP and ICP of one piglet in the PEEP Group. | 96 |
| Figure 6.4 | The distribution of wavelet transform coherence of 10000 simulations using Monte Carlo simulations. | 97 |
| Figure 6.5 | Relationships between PRx and wPRx in the PEEP wave-manipulated group and in the spontaneous ABP waves. | 98 |
| Figure 6.6 | Comparison of PRx and wPRx against a standard LLA in PEEP group. | 99 |
| Figure 6.7 | Influences of ICP on lower limit of autoregulation. | 100 |
| Figure 6.8 | Performance of PRx and wPRx in distinguishing good cerebral autoregulation and bad autoregulation. | 101 |
| Figure 6.9 | Example of data analysis using ICM+, showing time trends of ABP, CPP, PRx, wPRx. | 106 |
| Figure 6.10 | Relationship between PRx and wPRx. | 107 |
| Figure 6.11 | The mean values of PRx, and wPRx in different patients' outcome groups. | 108 |
| Figure 6.12 | PRx- vs CPP plot and wPRx-CPP plot for the whole cohort. | 109 |
| Figure 6.13 | Relationship between favourable outcome, unfavourable outcome , mortality rate, severe disability rate and the difference between median cerebral perfusion pressure (CPP) and optimal CPP according to PRx (CPPopt_PRx) and wPRx (CPPopt_wPRx). | 110 |
| Figure 6.14 | The relationship between cerebral autoregulation parameters and age. | 111 |
| Figure 7.1 | The three weighting rules for CPPopt calculation using multi-window approach. | 116 |
| Figure 7.2 | The two Additional fit criteria of the multi-window approach | 117 |
| Figure 7.3 | Examples of CPPopt trends. | 121 |
| Figure 7.4 | Relationship and Bland–Altman plot of CPPopt_S and CPPopt_MA. | 122 |
| Figure 7.5 | Graphs of the relationship between patient outcome and the difference between averaged median cerebral perfusion pressure (CPP) and CPPopt using the moving window of four | 123 |

hours and using weighted multi-window calculation.

| | | |
|-------------------|---|------------|
| Figure 7.6 | Demonstration of CPPopt calculation according to wPRx. | 126 |
| Figure 7.7 | Yield result of CPPopt_wPRx using 4 hour window and multi-window. | 126 |
| Figure 7.8 | Relationship between CPPopt_wPRx using the four-hour window and using multi-window system. | 127 |
| Figure 7.9 | Graphs of the relationship between patient outcome and the difference between CPP and CPPopt_wPRx using the moving window of four hours and using a multi-window calculation. | 128 |
| Figure 8.1 | The complex vasodilatory cascade. | 131 |
| Figure 8.2 | An example of a plateau wave. | 135 |
| Figure 8.3 | Autoregulation indices (ARIa and ARIC) and mean flow indices (Mxa and Mxc) during baseline and plateau. | 136 |
| Figure 8.4 | Mean value of phase and gain and coherence of transfer function at baseline and plateau. | 137 |
| Figure 8.5 | An example of a traumatic brain injury patient with refractory intracranial pressure. | 141 |
| Figure 8.6 | Relationship between wPRx and PRx. | 142 |
| Figure 8.7 | Average value of different CA parameters in two ICP states: baseline and plateau. | 142 |

LIST OF TABLES

| Number | Description | Page |
|------------------|---|-------------|
| Table 3.1 | Parameters related to the autoregulation index | 45 |
| Table 3.2 | Methods for cerebral autoregulation assessment and monitoring | 52 |
| Table 5.1 | The Pearson correlation coefficient (r) between ARI and other cerebral autoregulation parameters. | 76 |
| Table 5.2 | Abbreviations used in this section | 81 |
| Table 5.3 | Patients' Characteristics | 82 |
| Table 5.4 | Mean Value of CA parameters | 82 |
| Table 6.1 | The ability of PRx and wPRx in distinguishing good CA and impaired CA for PEEP Group and non-PEEP Group. | 99 |
| Table 7.1 | Abbreviations of labels for CPPopt calculation | 118 |
| Table 7.2 | Patient demographics, clinical variables, and outcome | |
| Table 7.3 | The yield result and SDD between two consecutive values of CPPopt across the whole recording duration of CPPopt using single-window calculation and using the multi-window algorithm. | 121 |
| Table 7.4 | Abbreviations of codes using wPRx for CPPopt calculation through multi-window or single-window approach. | 124 |
| Table 7.5 | The yield result and SDD between two consecutive values of CPPopt across the whole recording duration of CPPopt using the single-window calculation and the multi-window algorithms. | 126 |
| Table 8.1 | Abbreviations used in this section | 134 |
| Table 8.2 | Mean values of ABP, ICP, CPP and FV at baseline and plateau | 135 |
| Table 8.3 | Mean values of CA parameters during baseline | 136 |

LIST OF ABBREVIATIONS AND ACRONYMS

| | Abbreviation | Full Name |
|----------|---------------------|---|
| A | ABP | Arterial Blood Pressure |
| | ABPhf | Power Spectrum of ABP in high frequency |
| | ABPlf | Power Spectrum of ABP in low frequency |
| | AMP | ICP Pulse Amplitude |
| | ARI | Autoregulation Index |
| | AVDO2 | AVDO2(arteriovenous O2 difference) |
| B | BOLD | Blood Oxygen Level Dependent |
| | BRS | Baroreflex Sensitivity |
| C | Ca | Arterial Compliance |
| | CA | Cerebral Autoregulation |
| | Caa3 | Cytochrome Oxidase AA3 (Caa3) |
| | CARNet | Cerebral Autoregulation Research Network |
| | CBF | Cerebral Blood Flow |
| | CCVF | Cross Covariance Function |
| | CDC | Centres for Disease Control and Prevention |
| | CI | Confidence Interval |
| | CMRO2 | cerebral metabolic rate of oxygen consumption (CMR(O2)) |
| | CO2 | Carbon Dioxide |
| | Coh_a_LF | Coherence between abp and fv at low frequency |

| | | |
|----------|-------------------|--|
| | Coh_a_VLF | Coherence between abp and fv at very low frequency |
| | Coh_c_LF | Coherence between cpp and fv at low frequency |
| | Coh_c_VLF | Coherence between cpp and fv at very low frequency |
| | CPPopt | Optimal Cerebral Blood Pressure |
| | CrCP | Critical Closing Pressure |
| | CSF | Cerebrospinal Fluid |
| | CT | Computed tomography (CT) |
| | Cv | Venous Compliance |
| | CVP | Central Venous Pressure |
| | CVR | Cerebrovascular Resistance |
| F | FFT | Fast Fourier Transform |
| | FV | Cerebral Blood Flow Velocity |
| | FVd | Diastolic Cerebral Blood Flow Velocity |
| | FVm | Mean Cerebral Blood Flow Velocity |
| | FVs | Systolic Cerebral Blood Flow Velocity |
| G | Gain_a_LF | Gain between ABP and FV at Low Frequency |
| | Gain_a_VLF | Gain between ABP and FV at Very Low Frequency |
| | Gain_c_LF | Gain between CPP and FV at Low Frequency |
| | Gain_c_VLF | Gain between CPP and FV at Very Low Frequency |
| | GCS | Glasgow Coma Scale |
| | GM | Gray Matter |

| | | |
|----------|-------------|-------------------------------------|
| | GOS | Glasgow Outcome Scale |
| H | Hb | Deoxygenated Haemoglobin (Hb) |
| | HbO2 | Oxyhaemoglobin (HbO2) |
| | HbT | Hemoglobin |
| | HR | Heart Rate |
| | HRV | Heart Rate Variability |
| I | ICA | Internal Carotid Artery |
| | ICP | Intracranial Pressure |
| | ICU | Intensive Care Unit |
| | IEL | Internal Elastic Lamina |
| | IJV | Internal Jugular Veins |
| | IR | Impulse Response |
| L | LDF | Laser Doppler Flowmetry |
| | LF | Low Frequency |
| | LLA | LLA (lower limit of autoregulation) |
| M | MAD | Median Absolute Deviation |
| | MCA | Middle Cerebral Arteries |
| | MD | Microdialysis |
| | MRI | Magnetic Resonance Imaging |
| | Mx | Mean Flow Index |
| N | NCCU | Neuro Critical Care Unit |

| | | |
|----------|--------------------|---|
| | nICP | non-invasive intracranial pressure |
| | NIRS | Near-Infrared Spectroscopy |
| P | P1 | The Percussion Wave of Intracranial Pressure |
| | P2 | The Tidal Wave of Intracranial Pressure |
| | P3 | The Dicrotic Wave of Intracranial Pressure |
| | PaCO2 | Carbon Dioxide in Arterial Blood |
| | PaO2 | Partial Pressure of Oxygen |
| | PAx | Pressure Amplitude Index |
| | PbTO2 | Brain Tissue Oxygenation PO2 |
| | PEEP | Positive End Expiratory Pressure |
| | PET | Positron Emission Tomography |
| | Phase_a_LF | Phase between ABP and FV at Low Frequency |
| | Phase_c_LF | Phase between CPP and FV at Low Frequency |
| | Phase_c_VLF | Phase between CPP and FV at Very Low Frequency |
| | PI | Pulsatility Index |
| | PRx | Pressure Reactivity Index |
| | ROC | A Receiver-Operator Characteristic Test |
| | RPV | Range of Possible Value |
| R | rSO2 | Regional Cerebral Tissue Hemoglobin Oxygen Saturation |
| S | SAS | Subarachnoid Space |
| | SD | Standard Deviation |

| | | |
|----------|-------------|-----------------------------------|
| | SO2 | Tissue Oxygen Saturation |
| | sROR | Static rate of autoregulation |
| T | TBI | Traumatic Brain Injury |
| | TCD | Transcranial Doppler |
| | TD | Thermal Diffusion |
| | TDF | Thermal Diffusion Flowmetry |
| | TFA | Transfer Function Analysis |
| | THx | Hemoglobin Reactivity Index |
| U | ULA | ULA Upper Limit of Autoregulation |
| V | VIA | Vertebral Artery |
| | VLF | Very Low Frequency |
| | VSM | Vascular Smoothing Muscle |
| | VSMC | Vascular Smooth Muscle Cell |
| W | WT | Wall Tension |
| | WT | Wavelet Transform Method |
| | WTC | Wavelet Transform Coherence |
| X | XWT | Cross Wavelet Transform |

LIST OF EQUATIONS AND CONDITIONS

| Number | Formula | Page |
|----------------------|---|------|
| Equation 3.1 | Impulse response of Tieck's model | 46 |
| | $p(n) = \begin{cases} 0, & n \neq 1; \\ 1, & n = 1; \end{cases}$ | |
| Equation 3.2 | $x_1(n) = x_1(n-1) + \frac{P(n) - x_2(n-1)}{f \cdot T}$ | 46 |
| Equation 3.3 | $x_2(n) = x_2(n-1) + \frac{x_1(n) - 2D \cdot x_2(n-1)}{f \cdot T}$ | 46 |
| Equation 3.4 | $V(n) = 1 + P(n) - K \cdot x_2(n)$ | 46 |
| Equation 3.5 | $f^2 T^2 x'' + 2 \cdot D \cdot f \cdot T x'(n-1) = P - x(n-1)$ | 46 |
| Equation 3.6 | $V(n) = 1 + P(n) - K \cdot x(n)$ | 46 |
| Equation 3.7 | $f^2 T^2 V_n'' + 2DfTK \cdot V_{n-1}' + K \cdot V_{n-1}$ $= f^2 T^2 P_n'' + 2DfTK \cdot P_{n-1}' + K \cdot P_{n-1} - K^2 P_n + K$ | 46 |
| Equation 3.8 | Auto-spectrum of arterial blood pressure | 48 |
| | $Spp(f) = E[P(f) * P(f)]$ | |
| Equation 3.9 | Auto-spectrum of cerebral blood flow velocity | 48 |
| | $Svv(f) = E[V(f) * V(f)]$ | |
| Equation 3.10 | the cross spectrum (Spv(f)) of ABP and FV | 48 |
| | $Spv(f) = E[P(f) * V(f)]$ | |
| Equation 3.11 | The estimation of TF coherence | 48 |
| | $\gamma = \frac{\ Spv(f)\ ^2}{Spp(f)Svv(f)}$ | |
| Equation 3.12 | The estimation of transfer function: | 49 |

$$H_f = \frac{Y_f}{X_f}$$

Equation 3.13 Transfer function can be described as the sum of the real part and imaginary part of H_f : **49**

$$H_f = H_R + H_I \cdot j$$

Equation 3.14 Transfer function gain: **49**

$$|H(f)| = [H_I^2 + H_R^2]^{1/2}$$

Equation 3.15 Transfer function phase: **49**

$$\varphi(f) = \tan^{-1} \left[\frac{H_I(f)}{H_R(f)} \right]$$

Equation 3.16 The impulse response of the system can be obtained by the inverse FFT of transfer function **49**

$$i_f(t) = IFFT[H(f)]$$

Equation 4.1 The relationship between flow velocity and Doppler shift frequency **63**

$$Vr (cm/s) = \frac{Doppler\ shift \times Vp (cm/s)}{2 \times Fi \times \cos(\theta)}$$

Equation 6.1 The definition of wavelet transform **91**

$$W(s, \tau) = \int g(t) \varphi_s(t - \tau) dt$$

Equation 6.2 The definition of Morlet wavelet **91**

$$\varphi_0(t) = \pi^{-\frac{1}{4}} (e^{i2\pi f_0 t} - e^{-(2\pi f_0)^2/2}) e^{-t^2/2}$$

In practice it becomes negligible and can be ignored

Equation 6.3 Estimation of Morlet wavelet while $f_0 \gg 0$ **91**

$$\varphi_0(t) = \pi^{-\frac{1}{4}} e^{i2\pi f_0 t} e^{-t^2/2} \quad (\text{Equation 4.3})$$

Equation 6.4 Estimation of scale s in wavelet transform calculation: **91**

$$f = f_0/s = w_0/2\pi s$$

Equation 6.5 Wavelet transform using morlet wave as mother wave **92**

$$\varphi(t/s) = \pi^{-\frac{1}{4}} e^{iw_0 t/s} e^{-(t/s)^2/2}$$

Equation 6.6 The discrete form of the wavelet transform: **92**

$$W_n(s) = \sum_{n'=0}^{N-1} x_{n'} \varphi^* \left[\frac{(n'-n)\delta t}{s} \right]$$

Equation 6.7 The normalized wavelet function **92**

$$\varphi \left[\frac{(n'-n)\delta t}{s} \right] = \left(\frac{\delta t}{s} \right)^{\frac{1}{2}} \varphi_0 \left[\frac{(n'-n)\delta t}{s} \right]$$

Equation 6.8 The cross-wavelet transform of two time series $W^{XY} = W^X W^{Y*}$ **92**

Equation 6.9 Wavelet transform coherence **92**

$$C_n^2(s) = \frac{|\langle W_n^{xy}(s) \cdot s^{-1} \rangle|^2}{\langle W_n^{xx}(s) \cdot s^{-1} \rangle \langle W_n^{yy}(s) \cdot s^{-1} \rangle}$$

Equation 6.10 The smoothing operator is achieved by a convolution in time and scale: **93**

$$S(W) = S_{scale}(S_{time}(W_n(s)))$$

Equation 6.11 The smoothing operator is applied to wavelet transform: **93**

$$\langle W \rangle = \left[(c_1 W_n(s) * e^{-n^2/2s^2})_n * c_2 \Pi(\delta_j 0 s) \right]_s$$

Equation 7.1 The multi-window weighting process: **116**

$$Weight = \frac{1}{e^{window\ length}} \times \frac{1}{e^{full\ fit\ error}} \times W_{non-parabolic\ window}$$

CHAPTER 1 AIMS AND HYPOTHESES

Survival after traumatic brain injury (TBI) depends on the control of intracranial hypertension and the provision of haemodynamic support to achieve an ‘adequate’ cerebral blood flow with cerebral perfusion pressure (CPP) being one of the main driving forces. Therefore to set an adequate CPP target for the individual TBI patient at the bedside is of great importance, which still remains challenging. Maintaining a CPP above 70 mmHg was proposed as a method for preventing secondary injuries [1], [2]. However, a large randomized controlled trial could not demonstrate a benefit of a fixed CPP-targeted therapy [3], [4]. The recent Brain Trauma Foundation guidelines advocated exploring the feasibility and impact on the outcome of strategies based on individualized autoregulation-guided CPP management [2]. Over the years, a dynamic patient-targeted CPP protocol, based on the cerebral autoregulation (CA) ability of cerebral vasculature has been proposed. Many methodologies for CA assessment have been proposed, including static and dynamic methodologies. However, until now, there is still not a golden standard method for CA assessment in TBI patients. Better understanding and further standards in methodology are still needed.

This thesis looked into details of currently available CA assessment methods and introduced a new time–frequency analytical method, suitable for non-stationary signals. This thesis addresses three primary questions:

1. What are the relationships between currently widely used CA parameters, from theoretical and practical point of view?
2. Is there an effective method that can be introduced to assess CA, which is suitable for analyses of non-stationary signals?
3. How can bedside monitoring of cerebral autoregulation be improved in traumatic brain injury patients ?

The study used the structure described in Figure 1.1.

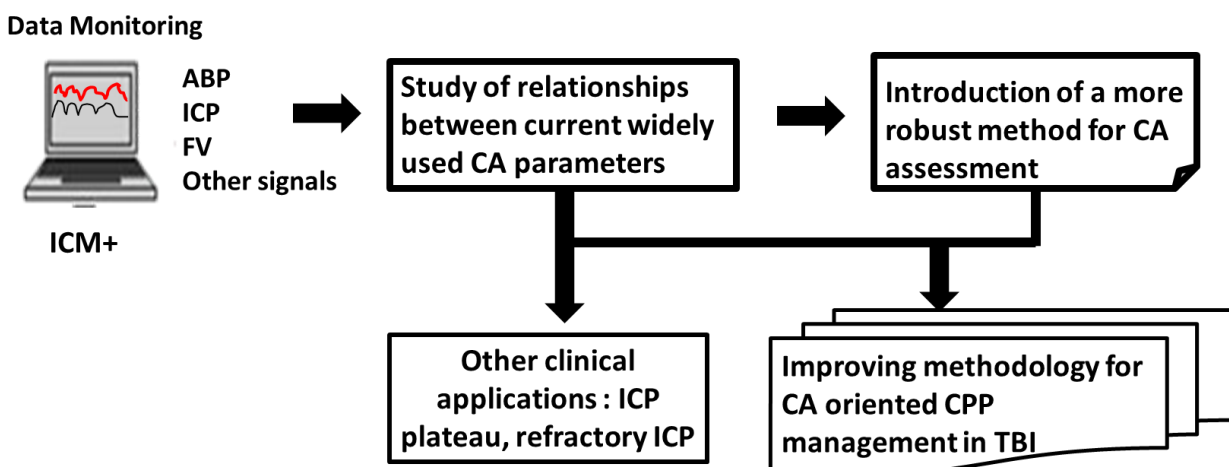


Figure 1.1 Diagram of the framework of this research. CA: cerebral autoregulation; ABP: arterial blood pressure; ICP: intracranial pressure; FV: flow velocity; CPP: cerebral perfusion pressure.

1.1 The validation of relationships between currently widely used CA parameters

CA is an important homeostatic mechanism that protects the brain against injury due to potential insufficient or excessive cerebral blood flow (CBF) caused by an increase or decrease in CPP or arterial blood pressure (ABP). In the last decades, various methods for CA assessment have been proposed, including static and dynamic methods. Initially, clinical studies mainly evaluated CA by analysing the CBF response to slow manipulations of ABP or CPP [5]–[8]. However, this process is not routinely applicable as it requires potentially harmful ABP manipulations [5]. Later on, transcranial Doppler (TCD) ultrasonography was introduced, which allowed dynamic CA assessment by analysing CBFV response to rapid changes in ABP, either externally induced or occurring spontaneously [9]–[11]. The most popular way of grading FV response to rapid changes in ABP, is the autoregulation index (ARI), which grades CA into 10 levels (from 0–9); ARI = 0 represents absence of autoregulation while ARI = 9 indicates hyperactive autoregulation [12], [13]. However, direct calculation of ARI in such a manner requires substantial decreases/increases in ABP, which, for traumatic brain injury (TBI) patients, should be avoided in some cases.

One attractive method that takes advantage of spontaneous fluctuations in ABP and CBFV is transfer function (TF) analysis, an approach that sheds light on the dynamic properties of CA from the perspective of linear response theory [14]–[16]. This type of analysis assumes that functional CA can be described as a high pass filter that readily transmits rapid (high frequency) changes in ABP to CBFV, but attenuates the transmission of slower (low frequency, usually lower than 0.05 Hz) ABP perturbations to CBFV [17]. Parameters derived from TF include phase shift, gain and coherence. In 1998, Panerai and colleagues combined the Tiecks' model with TF analysis in low frequency range to yield the impulse response (IR)-based ARI, defined as the best match between the IR estimated from patients' real data with IR of Tiecks' model [18].

Another commonly used measure, the mean flow index (Mx), estimates CA through the correlation coefficient between slow fluctuations (20 sec to 3 minutes) of mean CBFV and CPP [19]. It is a purely time domain measurement, based on the concept that if CA is intact, there will be no correlation between changes in CPP and changes in CBFV ($Mx = \text{zero or negative}$), whereas when CA is exhausted changes in CPP will be directly correlated with changes in CBFV ($Mx \approx +1$) [20]. In traumatic brain injury, where frequent, repeated assessment of CA is highly desirable, a technique based on analysis of the relationship between two routinely monitored modalities, ABP and intracranial pressure (ICP) has gained wide popularity. Given that changes in ICP may be interpreted as surrogates for changes in cerebral blood volume, pressure reactivity index (PRx), calculated as a moving correlation coefficient between mean ABP and ICP, is well suited for real-time, continuous monitoring of CA and is by now routinely used in many head trauma centres [21].

Despite advances in the application of CA assessment, there remain many uncertainties about the theoretical and pragmatic relationships between the indices. Although a few comparisons have been published [22]–[29] they have been based on real measurements, which inevitably introduces confounding factors to the relationships such as poor fit of the assumed models or the presence of unknown extraneous 'noise' [30], i.e. components in ABP and CBFV

that are not related to each other. The potential for differential sensitivity of the CA indices to these confounding factors makes meaningful comparisons between the different methods difficult. To cross validate the relationships between the CA indices in a more controlled environment, this study generated artificial FV signals according to Tiecks' ARI model of CA [12] using real ABP signals from TBI patients as input.

Hypothesis I: Theoretically, the relationships between the most commonly used indices of CA: ARI, Mx and TF phase and gain, are related to each other. The exogenous noise of signals will influence the accuracy of CA assessment.

After the comparison of CA parameters through modelling data in theoretical level, a further investigation is needed to test how these commonly used parameters correlate with each other in real clinical scenario of TBI patients. The effect of different inputs (ABP or CPP) for CA assessment should also be studied.

Hypothesis II: In TBI patients, different available CA parameters still correlate significantly with each other, while different input (ABP or CPP) demonstrates influences in CA assessment. CA parameters are generally related to patients' outcome.

1.2 Introduction of a new time–frequency-based analysis method for CA assessment

The methods for CA assessment described above are either simple correlation indices (such as PRx) or are assumed to be suitable for linear signal analysis, such as spectral decomposition and TF [31], [32]. With the clarification of the non-stationary nature of CA [28], many attempts are motivated to perform more sophisticated analyses to quantify the coupling mechanism of ABP and ICP. The wavelet-transform (WT) method has been widely applied in analysing noisy, transient and non-stationary signals. One advantage of wavelet analysis is the ability to perform local analysis and reveal signal features with desired temporal–frequency resolution. Noting that CA is altered through low-frequency (LF) arteriole vessel diameter changes [33], wavelet analysis can provide desired resolution for each signal feature simultaneously, higher scale (frequency) resolution for lower frequency and higher temporal resolution for higher frequency [34], [35].

In this study, WT algorithm was introduced to assess CA and was implemented into software ICM+[®](<http://www.neurosurg.cam.ac.uk/icmplus>). To validate the algorithm, a validation study was conducted on two cohorts of experimental hypotensive piglets' data with continuous ABP and ICP monitoring.

Hypothesis III: Wavelet phase shift can be used to assess CA and to distinguish good CA and bad CA. Low wavelet phase shift close to zero should be related with bad CA.

Hypothesis IV: Wavelet coherence might be used as a guarantee of reliable phase relationship between ABP and ICP. Different thresholds should be chosen for different central frequencies of mother wave used for wavelet analysis.

After the wavelet method was validated through the experimental data, it was applied to a cohort of 515 TBI patients admitted to Addenbrooke's Hospital between 2003 and 2015. The wavelet method phase shift between ABP and ICP was calculated in low frequency and was compared with the well-known CA parameter, PRx.

Hypothesis V: Wavelet phase shift is related to PRx and to patients' outcome. Better CA demonstrated by higher phase shift, correlates with a better outcome.

1.3 Calculation of optimal CPP for clinical TBI patients

The final goal of this thesis was trying to find a better way to apply the CA parameters in clinical practise for TBI patients in the future. CA indices, such as PRx, performs in such a way that plotting PRx against CPP will often generate a 'U'-shaped curve, the minimum of which represents the CPP corresponding to the smallest value of PRx, where the CA response is most active [36], [37], the point termed CPPopt. Steiner et al. introduced this concept in 2002 looking at CPPopt calculated from the whole monitoring period [36]. In 2012, Aries et al. proposed and tested an automated CPPopt algorithm based on a moving four-hour calculation window in a different (retrospective) cohort of TBI patients by showing improved outcome in patients with CPP close to averaged automated CPPopt [38]. However, many challenges remain to improve the performance of CPPopt, such as low yield and discontinuity. The object of the present study was to investigate how the yield and continuity of CPPopt can be enhanced through a multi-window algorithm and a weighting system, that can maximally exploit and optimize the potential information about cerebral vascular pressure reactivity.

Hypothesis VI: The multi-window approach can improve the estimation of optimal CPP and increase its potential to make the technique of pressure autoregulation controlled management widely applicable in most ICUs.

1.4 Outline of the thesis

These general aims have been translated in a series of experiments, retrospective analyses and background studies which are presented in different chapters of this thesis.

Chapter 2 provides a further description of the physiology of brain circulation relevant for the thesis starts with a short review of the basic mechanism responsible for ICP circulation with CBF to follow.

Chapter 3 provides background information about methodologies currently used for CA assessment. This review also addresses the problems of current methods.

Chapter 4 describes methodological considerations regarding projects included in this thesis. It explained the materials, the methodologies and statistical analysis used in this PhD projects.

Chapter 5 cross-validates the relationships between the current CA indices through artificial data generated according to Tiecks' ARI model, and also through real data from 288 TBI patients. The parameters being compared includes ARI, Mx, TF phase and gain.

Chapter 6 introduces a new method for CA assessment, which is suitable for non-stationary data analysis, the wavelet method. This chapter compared the new method with traditional PRx using data from 515 TBI patients to validate the new approach.

Chapter 7 describes the development of a multi-window weighting approach for optimal CPP estimation for TBI patients. The association between outcome and the deviation of actual CPP from the calculated optimal CPP was studied. The yield and stability of the new multi-window approach was compared with traditional CPPopt estimation method.

Chapter 8 describes whether the CA parameters studies in this project, could be replicated in other clinical situations, such as ICP plateau or refractory ICP.

Chapter 9 provides a summary and future directions of the methodologies used in this thesis.

CHAPTER 2 BASIC OF CEREBRAL PHYSIOLOGY – REVIEW

This thesis concentrates on the methodology for monitoring the autoregulation of CBF.

Historically, autoregulation can be described as a static relationship between CBF and cerebral arterial blood pressure (ABP), the so-called Lassen curve [39]. The concept of CPP as a difference between ABP and ICP (or central venous pressure, CVP, if $CVP > ICP$), was introduced only in 1970s [40]. The Lassen curve illustrates the relationship between CBF and CPP [41], [42]. Therefore, this chapter describing the physiology of brain circulation relevant for the thesis starts with a short review of the basic mechanism responsible for ICP circulation with CBF to follow.

2.1 Monro–Kellie hypothesis and pressure–volume curve

The concept of ICP being a function of the volume and compliance of each component of the intracranial compartment was proposed by Monro (1783) and his student Kellie (1824) during the late 18th century [43], [44]. The interrelationship came to be known as the Monro–Kellie hypothesis, which states that the cranial compartment is encased in a non-expandable case of bone, and, thus, the volume inside the cranium is fixed [45]. The hypothesis further states that, as a rigid box, the human cranium encloses a fixed volume that is shared by the brain tissue, blood and cerebrospinal fluid (CSF) (Figure 2.1 A), such that an increase in the volume of one of the constituents must be compensated for by reduction in the others [46]. For example, the arterial blood entering the brain requires a continuous outflow of venous blood to make room for it [47], [48]. The intracranial flow of blood and CSF is thus pulsatile, as is the ICP [49].

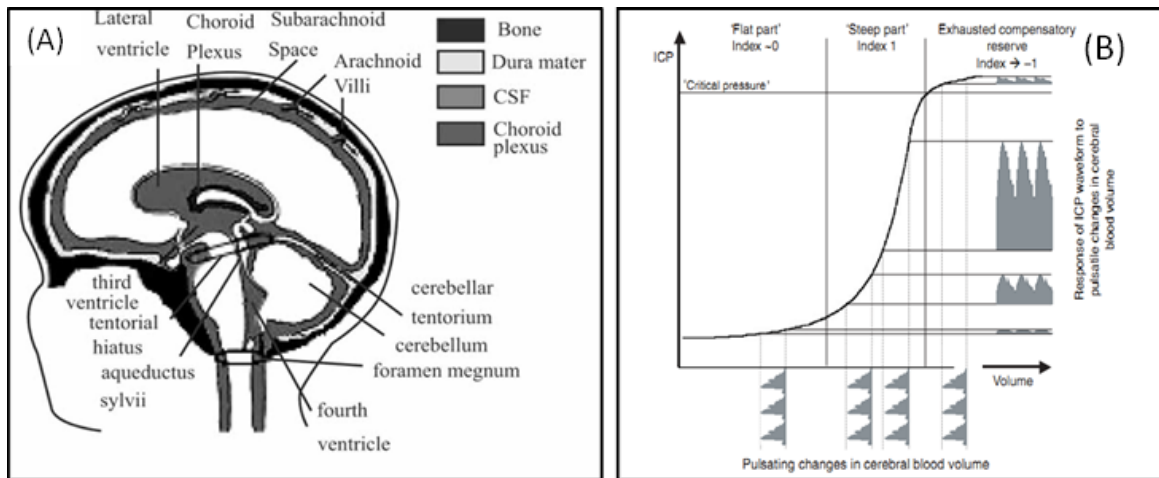


Figure 2.1 (A) Anatomy of the intracranial compartment; (B) Intracranial pressure-volume curve [50] and the relationship between pulse amplitude of ICP and cerebral volume. Index: index of cerebrospinal compensatory reserve calculated as the moving correlation coefficient between the amplitude of the fundamental harmonic of the ICP pulse wave and mean ICP. ICP: intracranial pressure.

Kocher in 1901 described four stages of cerebral compression related to the expansion of intracranial brain tumours [51]. In 1951, Ryder et al. described the pressure–volume relationship as a hyperbolic function, which implies an increase in elastance as ICP increases [52]. The pressure–volume curve has three parts [50]: first, flat at lower intracerebral volumes, where good compensation is observed, therefore ICP remains low and constant even though there are changes in cerebral volume; the second shows that with poor compensatory reserve, ICP rises exponentially with volume, that is, ICP increases considerably even with small increases in intracranial volume; finally, when the critical level of ICP is achieved and the cerebral arterial bed cannot dilate any more, the curve becomes flat again (Fig. 2.1B). The pulse waveform may conceptually be presented as a transformation of regular changes in pulsatile blood volume through the curve. Pulse amplitude is low for good compensatory reserve and does not depend on ICP, then starts to rise with mean ICP and above the ‘critical ICP’ secondarily decreases.

2.2 Global model of CBF and circulation of CSF

As a fragile organ, the brain is only able to withstand very short periods of lack of blood supply (ischaemia), and it has very high energy (ATP) requirement, which needs constant energetic substrate replenishment. The neurons produce energy almost entirely by oxidative metabolism of substrates, including glucose and ketone bodies, with very limited capacity for anaerobic metabolism. Without oxygen, energy-dependent processes cease leading to irreversible cellular injury if blood flow is not re-established rapidly (three to eight minutes under most circumstances) [53]. Therefore, adequate CBF must be maintained to ensure a constant delivery of oxygen and substrates and to remove the waste products of metabolism [54].

In 1997, Czosnyka et al. introduced a mathematical model to interpret cerebrovascular circulation and autoregulation in the brain [55]. As described in Figure 2.2, the CBF pathway starts with the arterial blood inflow to the brain through the resistance of large intracranial arteries (R_a). Arterial blood is contained in a high-pressure arterial compliance C_a . Forward flow through the cerebrovascular resistance vessels is influenced by C_a . Capillary and venous blood are contained in a compliance of C_v . Finally, venous blood flows out to the sagittal sinus through the bridging veins R_b . The CSF pathway encompasses CSF formation (I_f), storage in the distensible fluid structures formed by the ventricles and basal cisterns (C_i) and reabsorption through the arachnoid granulations (R_{csf}) to the sagittal sinus.

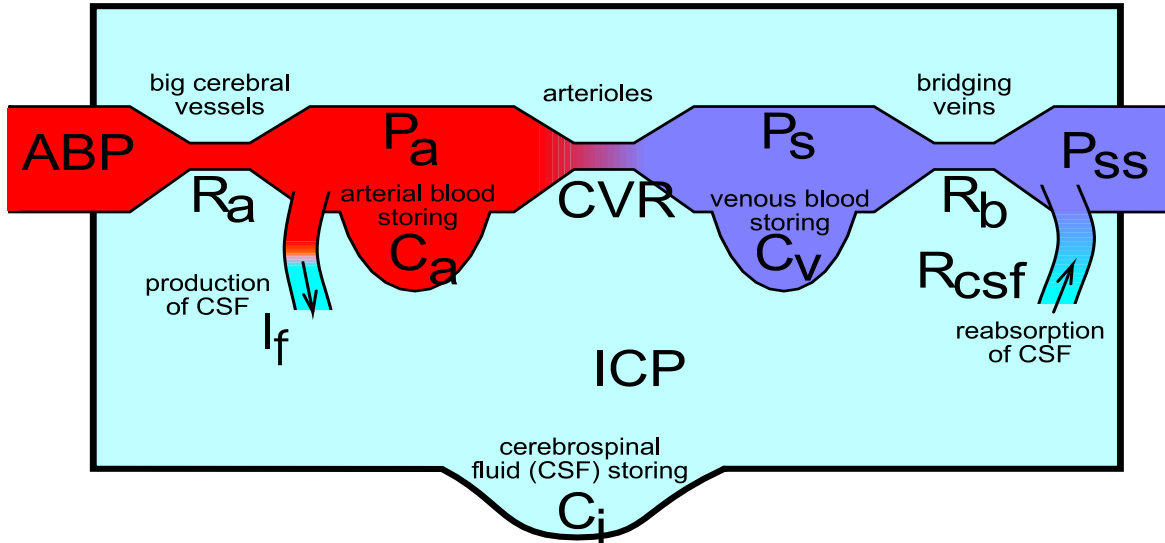


Figure 2.2 Hydrodynamic equivalent of the model, comprising pathways of CBF and the CSF circulation. A rigid skull is represented by the outer box, with a compensatory reserve C_i associated with the compliant dural sac within the lumbar channel [55].

2.3 Cerebral autoregulation

It is estimated that the brain uses around 20% of total oxygen for normal function, making regulation of blood flow and oxygen delivery critical for survival [56], [57]. CA refers to the ability of the brain to keep stable CBF in spite of changes in CPP or if ICP is normal, ABP [10], [58]. It is present in many parts of the vascular bed, but is particularly well developed in the brain (to keep CBF at a constant level, matched to metabolism), probably due to the need for a constant blood supply and water homeostasis [59]. CA is a universal physiological mechanism, the relationship between CBF and CPP that is depicted by the Lassen curve (Figure 2.3), with ABP or CPP along the x-axis and CBF along the y-axis [39], [60].

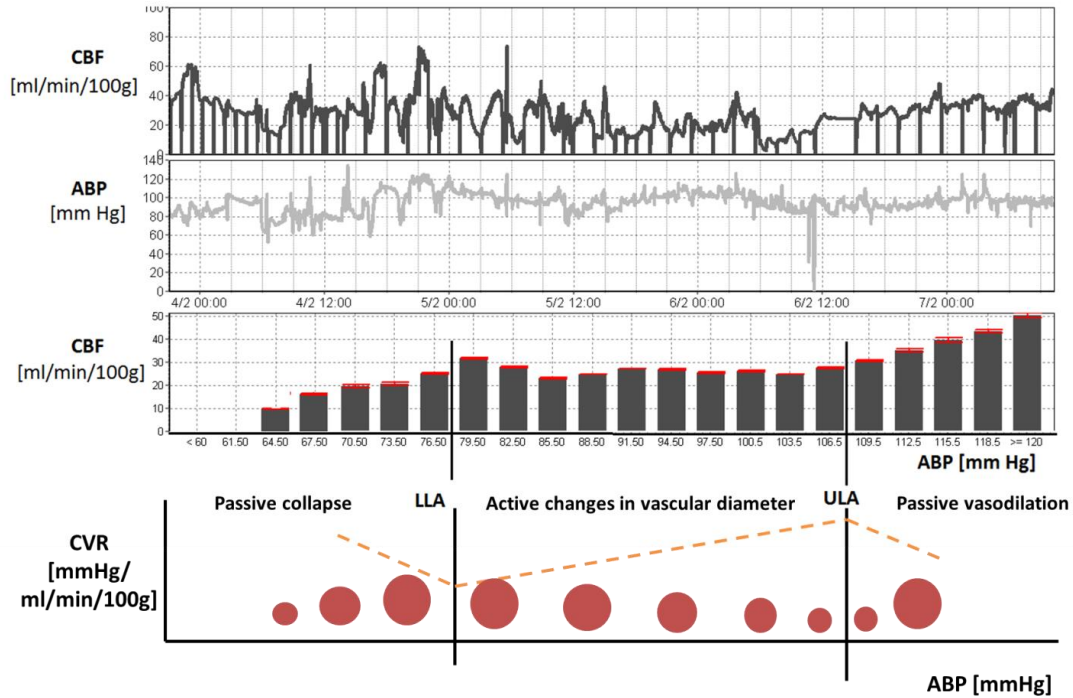


Figure 2.3 The Lassen autoregulatory curve by plotting CBF vs perfusion pressure (in this case approximated by ABP) relationship. It has been obtained from 3.5 days recording of thermodilution CBF and radial artery blood pressure in a patient after a low-grade haemorrhagic stroke. Natural variations of ABP from 60 to 120 mmHg provoked changes in CBF that enabled plotting the curve and visualizing the upper (ULA) and lower (LLA) limits of autoregulation. Stability of blood flow is maintained through active changes in vascular diameter within a certain range of ABP. The changes in diameter lead to changes in cerebral vascular resistance (CVR) and modulate blood flow. Below the LLA, further vasodilation of vessels is impossible and in some cases passive collapse is noted, resulting in a decrease in CBF. Above the ULA, the increased transmural pressure exceeds the ability of vessels to constrict and leads to passive vasodilation, which leads to an increase in blood flow plus cross-capillary water leak and results in cerebral oedema [57].

Classically, four components of CBF regulation have been described: myogenic, metabolic, chemical and neurogenic.

2.3.1 Myogenic CBF regulation (pressure autoregulation)

In normotensive adults, CBF is maintained at around 50 ml per 100 g of brain tissue per minute, provided that the mean ABP calculated as diastolic pressure plus one-third of the pulse pressure) is 60 to 150 mmHg[61]. Strictly speaking, it is the CPP (ABP – ICP) that governs autoregulation. The main myogenic mechanism of CA is vasodilation and constriction guided by CPP-induced changes in CVR (CBF = CPP/CVR)[62]. With functioning autoregulation, CVR changes in proportion to the changes in CPP to keep CBF constant.

Figure 2.3 shows that between CPP of around 70 to 130 mmHg, CBF remains constant. Above and below this limit, autoregulation is lost and CBF becomes dependent on mean arterial pressure in a linear fashion [63], [64]. At the

LLA, cerebral vasodilation is maximal, and below this level the vessels collapse and CBF falls passively with falls in ABP [58], [65]. At the upper limit (ULA), vasoconstriction is maximal and beyond this, the elevated intraluminal pressure may force the vessels to dilate, leading to an increase in CBF and damage to the blood–brain barrier [66], [67](Figure 2.4). It has been demonstrated that myogenic autoregulation is commonly depleted in many acute neurological patients, including brain tumour, subarachnoid haemorrhage, stroke or head injury [68].

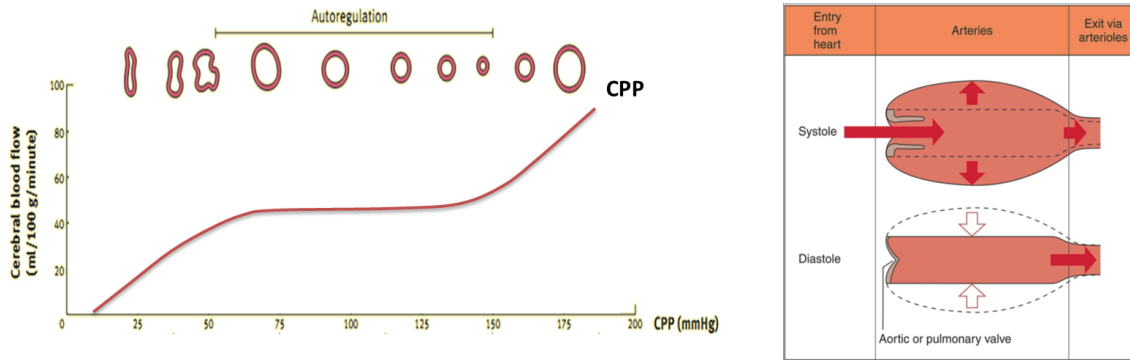


Figure 2.4 Effect of changes in ABP, and cerebral vascular resistance on cerebral blood flow [69]. CPP, cerebral perfusion pressure.

2.3.2 Metabolic regulation of CBF

Changes in CBF and metabolism tend to follow each other, local and global increases in metabolic demand are met rapidly with increase in CBF [70]. These changes are thought to be controlled by several vasoactive metabolic mediators, including hydrogen and potassium ions, adenosine, glycolytic intermediates, phospholipid metabolites and nitric oxide.

Potassium and potassium ions are produced by synaptic transmission, and it has been shown that elevation of these ions stimulates vasodilation [71], [72], thus providing a possible mechanism for neurovascular coupling. The action of H^+ on cerebral arteries mediates the CO_2 reactivity. Nitric oxide (NO) has been implicated as the vasodilatory response to hypercapnia and acidosis is attenuated by NO inhibitors [73]. Metabolites are an attractive option as messengers for flow-metabolism coupling, for obvious reasons [74]. Extracellular levels of adenosine rise sharply with neuronal activity and topical application of adenosine to cerebral microcirculation causes vasodilation [75].

2.3.3 Chemical mechanism of regulation of CBF

At normotension, the relationship between partial pressure of carbon dioxide in arterial blood ($PaCO_2$) and CBF is almost linear [69]. At a $PaCO_2$ of 10.6 kPa (80 mmHg), no further increase in flow is possible as the arterioles are maximally dilated. Conversely, at 2.7 kPa (20 mmHg), flow cannot fall further as the arterioles are maximally vasoconstricted (Figure 2.12). These effects are regulated by a complex and interrelated system of mediators.

The arteriolar tone has an important influence on how PaCO_2 affects CBF, which can help manage patients with increased ICP. Hyperventilation reduces the PaCO_2 and causes vasoconstriction of the cerebral vessels (reduces their radius) and, therefore, reduces cerebral blood volume resulting in decreasing ICP while the intracranial compliance is reduced. However, if the PaCO_2 is reduced too much, the resulting vasoconstriction can reduce CBF to the point of causing or worsening cerebral ischaemia. In contrast, in the situation of exhausted brain compliance, hypercapnia can result in vasodilation which will increase the ICP. Therefore, hyperventilation or hypercapnia to moderate levels is generally considered a short term temporizing measure to control ICP, and overly aggressive operation should be avoided. Results showed impaired cerebral CO_2 vasoreactivity is associated with a poor outcome in patients with TBI [76].

Oxygen has little effect on the radius of blood vessels at partial pressures used clinically. However, while the partial pressure of oxygen (PaO_2) is below 50 mmHg, CBF will increase rapidly [69], [77]. Thus, hypoxia and hypercapnia may significantly increase ICP through increasing CBF. Hypocapnia, on the other hand, significantly decreases CBF and hence ICP.

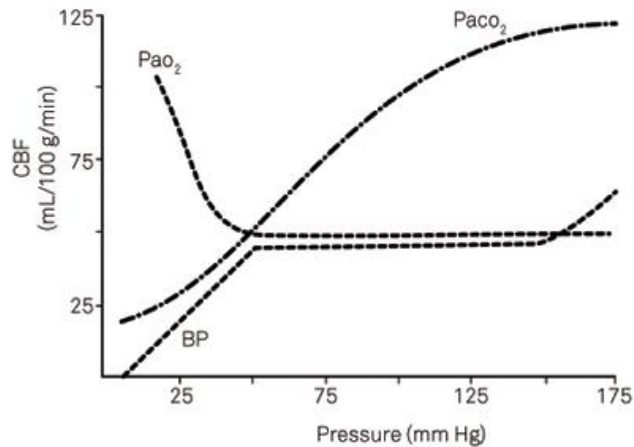


Figure 2.5 The effect of PaCO_2 , PaO_2 , ABP on CBF in a healthy population. Acute hypoxia triggers dilation of cerebral microcirculation and increase in CBF. Hypercapnia causes dilation of cerebral arterioles and CBF elevation, whereas hypocapnia causes vasoconstriction and decrease in CBF [78].

2.3.3 Neurogenic mechanism of CBF regulation

The neurogenic mechanism of CA is still not known clearly, with current theory supporting that the sympathetic and parasympathetic nervous systems can modulate the autoregulatory curve, but do not themselves control autoregulation [79]. It is said the main action of the sympathetic nerves is vasoconstriction, which protects the brain by shifting the autoregulation curve to the right in hypertension [80]. The parasympathetic nerves contribute to vasodilation and may play a part in hypotension and reperfusion injury [57]. Moreover, a recent study suggested that intrinsic innervation may have a role in modulating CA [81].

2.4 Traumatic brain injury

Traumatic brain injury, often referred to as TBI, is a worldwide public health problem typically caused by contact and inertial forces acting on the brain[82]. Every year, over 2,500,000 patients sustain a TBI in the EU, and 75,000 of these die, with a further 100,000 being left handicapped. In the UK, head injury occurs in more than 500,000 persons per year of which about 10% are diagnosed as severe, 15% moderate and the remainder as minor head injuries [83]. In the United States, TBI contributes to about 30% of all injury deaths [84], and in 2013, 50,000 people died due to TBI in USA. According to a survey conducted in 28 European Union countries and all 48 states in Europe, 1,375,974 hospital discharges and 33 415 deaths were related to TBI were identified in 2012 [85] .

The annual costs of TBI are huge and exceed 70 billion dollars per year in the US. It is the leading cause of mortality and morbidity in young people, and in the past decade, the number of TBI seems to be increased in people aged 65 years and older- especially in high income countries [85], [86]. On a global scale, the number of life years lost due to TBI is four times that of diabetes-related loss. According to the report from the United States Centers for Disease Control and Prevention (CDC), there are approximately 1.5 million people in the U.S. who suffer from a TBI each year [84]. Recent statistics show a steep increase in the incidence of TBI, with an increase of 21% over the last five years – threefold greater than the rate of increase in population [87].

The leading causes of TBI vary by age: falls are the leading cause of TBI among persons aged 65 years and older; road traffic accident is the leading cause of TBI among younger patients [88]. The top four causes according to the CDC are: traffic accident (14.3%), strucks (15.5%), assaults (10.7%) and falls (40.5%) (Figure 2.6). Scientists reported that the most common mechanism of injury appears to be shifting in Europe from road traffic incidents to falls [89]. Firearm injuries are often fatal: 9 out of 10 people die from their injuries. Along with a TBI, persons are also susceptible to spinal cord injuries, which are another type of traumatic injury that can result from vehicle crashes, firearms and falls. Prevention of TBI is the best approach because there is no cure.

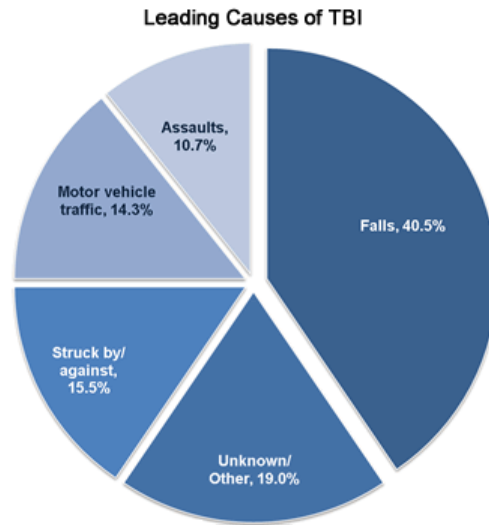


Figure 2.6 Leading causes of traumatic brain injury. The leading causes of TBI vary by age: falls are the leading cause of TBI among persons aged 65 years and older; transportation is the leading cause of TBI among persons under the age of 65 years[88].

The severity of a TBI may range from ‘mild’ (i.e. a loss of consciousness from 20 minutes to 6 hours and a Glasgow Coma Scale of 9 to 12) to ‘severe’ (i.e. a loss of consciousness of greater than 6 hours and a Glasgow Coma Scale of 3 to 8) [90]. The annual incidence of mild TBI is about 131 cases per 100,000 people, the incidence of moderate TBI is about 15 cases per 100,000 people, and the incidence of severe TBI is approximately 14 cases per 100,000 people [91].

Individuals with severe injuries can be left in long-term unresponsive states. For many people with severe TBI, long-term rehabilitation is often necessary to maximize function and independence. Even with mild TBI, the consequences to a person’s life can be dramatic, and they may suffer several months of disabling symptoms. Jacobs reported long-term problems after TBI, including patients’ financial status, behavioural functioning, and psychosocial morbidity which can result in a heavy burden to the patients’ family [92]–[94]. Ghajar pointed out that patients with severe TBI have a big risk of hypotension, hypoxaemia and brain swelling, which can exacerbate brain damage and increase the risk of death if not treated properly [90]. Change in brain function can have a dramatic impact on family, job, social and community interaction.

2.5 Disturbance of cerebral autoregulation after TBI

CA can be impaired in any degree of TBI, even mild, and with normal ICP and mean ABP (ABPm) [95][96]. Once the autoregulatory mechanisms have been completely abolished, CBF passively follows changes in ABP and CPP; sudden increases in mean ABP (ABPm) can be more easily transmitted into the microcirculation and can contribute to either areas of infarction or secondary haemorrhages and edema [97]–[100] [101]. Under these conditions, the brain becomes vulnerable to ischaemic or hyperaemic injuries if perfusion pressure does not remain coupled with

metabolic demands (Fig 2.7). Monitoring of CA in head-injured patients is considered useful for understanding the pathophysiology and effects of therapy, regarding its role as a causative agent and a factor in guiding therapy as well as the determinants of outcome in TBI, although such monitoring has not yet become part of routine patient management in many centres [102][103].

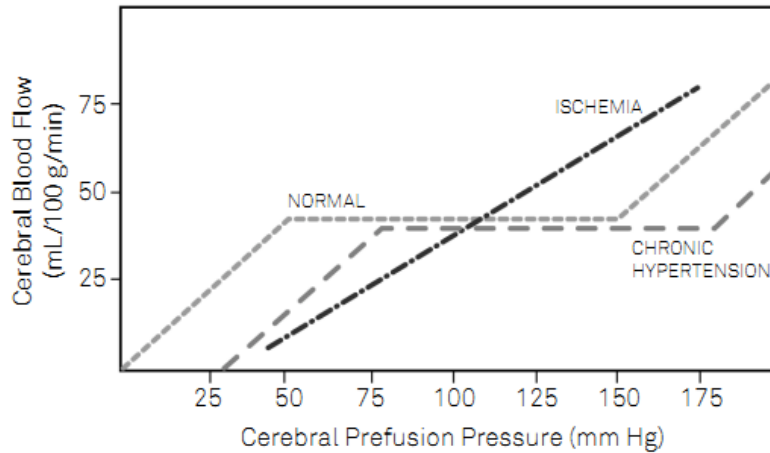


Fig 2.7 Cerebrovascular autoregulation in health, chronic hypertension and during autoregulation loss. In chronic hypertension, values for lower and upper limits of pressure autoregulation are higher than those under normal conditions, resulting in a degree of resetting as high as 40 mmHg. Therefore, acceptable ABP levels for healthy subjects may be associated with lower CBF. Ischemia can impair cerebral autoregulation allowing CBF to vary directly with blood pressure leading to brain lesion[78].

2.6 Clinical Problems in treating TBI

TBI can be divided into primary and secondary injury and the relationship between the two is depicted in figure 2.8 [104]. Normal ICP of healthy people is usually around 5-15 mmHg, while in TBI, an ICP of > 20 mmHg is widely accepted as intracranial hypertension (ICH) [105], [106]. The management of ICP for TBI is based on avoidance of secondary injury, maintenance of cerebral perfusion pressure, and optimization of cerebral oxygenation[107]. The national guidelines recommended treatment of CPP>70 mmHg at the beginning, but reduced this number to 60 mmHg later. However, this guideline ignored individual patient variability and injury- specific factors. Moreover, there is ongoing debate over the importance of ICP monitoring, especially after a recent randomized controlled trial that did not show an outcome benefit in patients undergoing ICP monitoring with a treatment threshold of 20 mmHg when compared to patients that were not monitored .

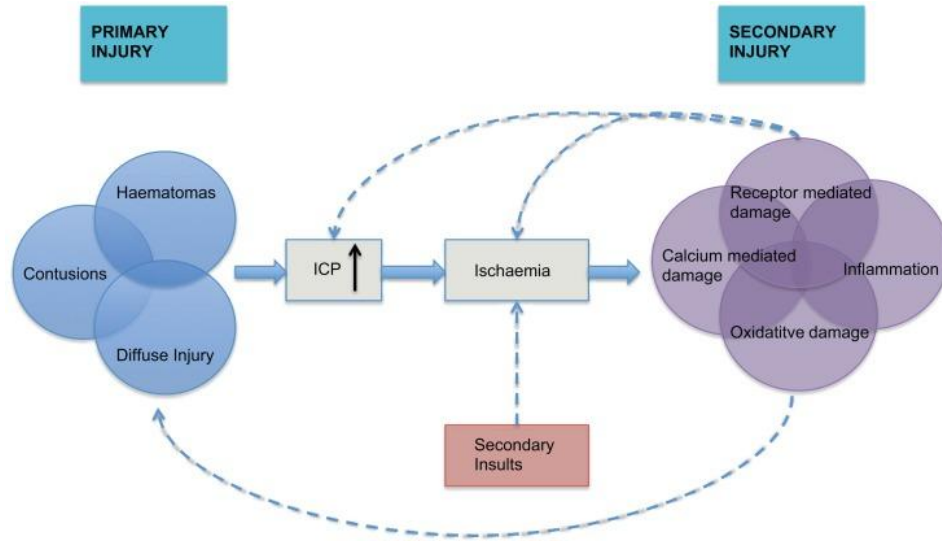


Fig. 2.8 The inter-relationship between primary and secondary injury in TBI is shown[104]. Secondary physiological insults can potentiate ischemia and lead to exacerbation of secondary injury.

However, one of the principle clinical reasons to monitor ICP is to allow calculation of CPP, the main driven force of CBF to meet the need of the brain, regulated by CA. One of the most systematically investigated approach to CA assessment, using ICP as an input, is the pressure reactivity index (PRx) described by Czysnyka et al [21]. It is calculated as the correlation coefficient between slow waves of ABP and ICP, while small PRx is associated with good CA, and big PRx (>0.3) reflects impaired CA [108]. High PRx was also found to be related with worse patient outcome, plateau waves and refractory ICP clinically [31], [109]. In TBI, PRx has also demonstrated a reliable index to calculate 'optimal CPP' for individual patient, with patients whose CPP were close to CPPopt showed best optimal outcome. However, its clinical application has been limited due to its discontinuity and instability.

CHAPTER 3 STATE OF THE ART FOR CURRENT METHODOLOGY OF AUTOREGULATION MONITORING

As described in Chapter 2, CA mechanisms protect against cerebral ischaemia due to hypotension and against excessive flow (hyperaemia) during hypertension, when capillary damage, oedema, diffuse haemorrhage and intracranial hypertension might otherwise result. CA has been monitored in the setting of neuro critical care unit (NCCU) to aid prognostication in many centres and retrospective studies showed failure of autoregulation is associated with a worse outcome in various acute neurological diseases [31], [110]–[112].

CA is a universal physiological mechanism, that has been studied in a similar way across a large number of acute and chronic neurological diseases [30], [113], [114]: changing or observing spontaneous variations in CPP or ABP when ICP is not measured, a situation typical for ischaemic stroke outside NCCUs and recording synchronized changes in CBF or other modalities, believed to be coupled to changes in CBF or cerebral blood volume (such as FV, brain oxygenation).

Clinical methods for assessment of autoregulation can be divided into measurement and monitoring methods. Measurement methods take place when a known stimulus is applied and the CBF (direct or indirect) response is recorded. Pharmacologically induced changes in ABP, leg-cuff release, body tilt, hand-grip, lower-body negative pressure, squat–stand manoeuvres, slow breathing, transient compression of the carotid artery, etc., all can be classified as measurement methods. The accuracy of measurement methods is usually good because a known pattern of stimulus is helpful for detecting a synchronized response of CBF and thus assessing CA. However, the measurement methods can be performed in limited time and are usually not repeated more frequently than once a day.

In contrast, continuous monitoring methods are based on observing the CBF/FV response to continuous spontaneous fluctuations of CPP or ABP. The stimuli (ABP or CPP fluctuations) are usually weaker, not necessarily repetitive and, therefore the signal-to-noise ratio (SNR) remains more unfavourable. However, these methods have the advantage of assessing autoregulation continuously. Autoregulation is a quite fragile brain protective mechanism, it fluctuates in time as CPP may change, PaCO₂ concentration may change, body temperature, endothelial functions, level of anaesthesia, etc. may also fluctuate. Therefore, monitoring of CA continuously in time is desirable. Moreover, continuous monitoring allows for individual targeting of CPP or ABP levels to achieve optimal autoregulatory strength [38]. One important point to discuss is the differentiation between ‘static’ and ‘dynamic’ autoregulation assessment/monitoring methods. Static CA refers to steady-state autoregulation, measured with slow changes in CPP (or ABP), while dynamic CA characterize autoregulation through small changes or short-term oscillations in CPP (or ABP). These transients and oscillations cannot be too fast, as properly working autoregulation can be compared with a high-pass filter. In general, fluctuations of CPP/ABP faster than 0.05 Hz are believed to carry a diminished amount of information about CA in comparison to slower waves.

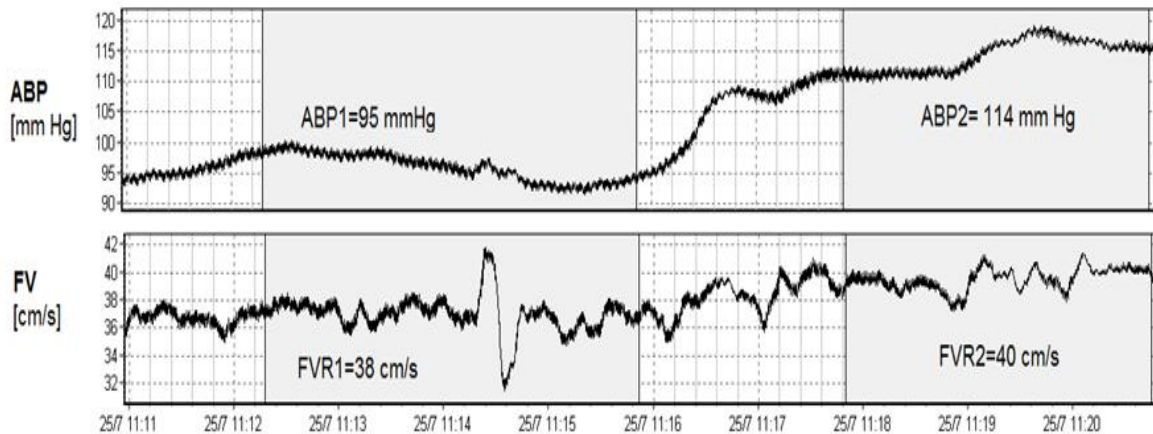


Figure 3.1 Example of evaluation of static rate of autoregulation. Arterial blood pressure has been increased from 95 mm Hg to 114 mm Hg with vasopressor. Changes in CBF were recorded using transcranial Doppler ultrasonography (FV). ABP: arterial blood pressure; FV: flow velocity.

In many studies, ‘static’ and ‘dynamic’ autoregulation have been compared and the correlation between the methods has always been far from perfect. However, comparisons between methods belonging to one family (static–static or dynamic–dynamic) are also not that exact. This is because each method has its own limited accuracy. It has not been definitively proven that ‘static’ and ‘dynamic’ components of autoregulation may be dissociated physiologically.

3.1 Current widely used methods for cerebral autoregulation assessment

Though it is clinically appealing to record spontaneous changes in ABP and CBF velocity, assessment of CA at rest may not reveal the full capacity of autoregulation because of the presence of intrinsic non-linearity. In addition to the TCD methods, other neuro-imaging techniques, such as magnetic resonance imaging (MRI), positron emission tomography (PET) or perfusion computed tomography (PCT), appear suitable because of their availability in acute care situations, high spatial resolution and excellent safety record. Through these techniques, the CBF, blood volume, oxygen extraction fraction (OEF) and oxygen consumption rate ($CMRO_2$) can be measured in multiple regions. The relationships between changes in blood volume and changes in CBF velocity or changes in $CMRO_2$ were analysed to assess CA [103], [115]. However, these methods, in general, are expensive and have a poor temporal resolution (\approx minutes) and can be challenging to use in bedside studies.

Most studies of CA relied on linear (cross-spectral or correlation-based) methods to assess the integrity of autoregulation. If the pressure–flow relation displays a low coherence (i.e. if it lacks linear dependence), often interpreted as the sign of intact CA [116], the relation between pressure and CBF cannot be quantified via linear

analyses. In other words, autoregulation itself creates uncertainty in its linear estimates. This is a problem of the analytical technique, not the input signal (spontaneous oscillations vs induced BP manipulation). The limitation can be overcome by using non-linear approaches.

Understanding the advantages as well as the limitations of these methods will be helpful for clinicians to choose appropriate methods for their studies of CA in clinical diagnosis or management.

3.1.1 Autoregulation index (ARI)

ARI is a gauging system to quantify the status of CA [12], [13]. The index is defined by introducing a sharp drop in ABP produced by a rapid deflation of thigh cuffs to grade the ensuing CBFV response with a parametric, second-order model [87]. It grades CA into 10 levels (from 0–9), where $ARI = 0$ shows that the changes in FV follow entirely the changes in ABP and thus reflects completely abolished autoregulation; $ARI = 9$, on the other hand, means that FV returns to the baseline value rapidly and therefore indicates highly effective autoregulation (Figure 3.2). At the heart of this method there is a second order differential equation that simulates 10 possible CBF velocity responses to an ideal step change of ABP by giving 10 sets of pre-defined parameters, including a damping factor, time constant and, gain parameter. By comparing the recorded CBF velocity with the 10 simulated CBF velocities, the index number is determined by finding the best match (Fig. 3.3).

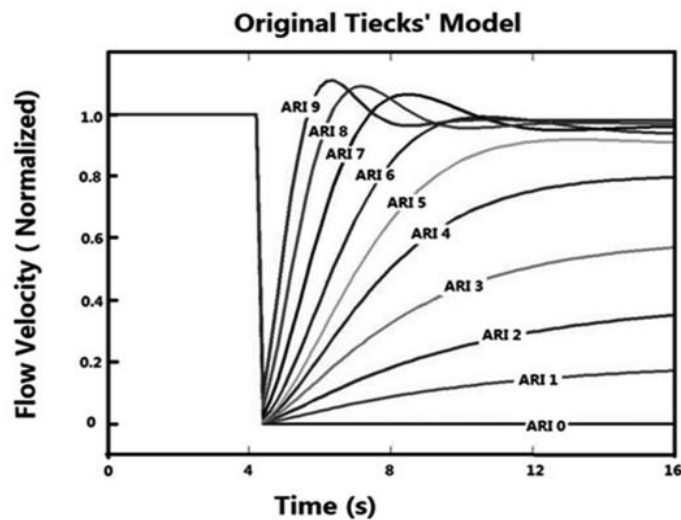


Figure 3.2 Response of cerebral autoregulation model to a step change in blood pressure.

Table 3.1 Parameters related to the autoregulation index[12]

| T,s | D | K | ARI | dROR,%/s |
|------|------|------|-----|------------------------------|
| ... | 0.00 | 0 | 0 | 0, No autoregulation |
| 2.00 | 1.60 | 0.20 | 1 | 2.5 |
| 2.00 | 1.50 | 0.40 | 2 | 5.0 |
| 2.00 | 1.15 | 0.60 | 3 | 10.0 |
| 2.00 | 0.90 | 0.80 | 4 | 15.0 |
| 1.90 | 0.75 | 0.90 | 5 | 20.0, Normal autoregulation |
| 1.60 | 0.65 | 0.94 | 6 | 30.0 |
| 1.20 | 0.55 | 0.96 | 7 | 40.0 |
| 0.87 | 0.52 | 0.97 | 8 | 60.0 |
| 0.65 | 0.50 | 0.98 | 9 | 80.0, Fastest autoregulation |

T is the time constant, D is a damping factor, K is the autoregulatory dynamic gain, ARI is the autoregulation index, and dROR is the dynamic rate of regulation.

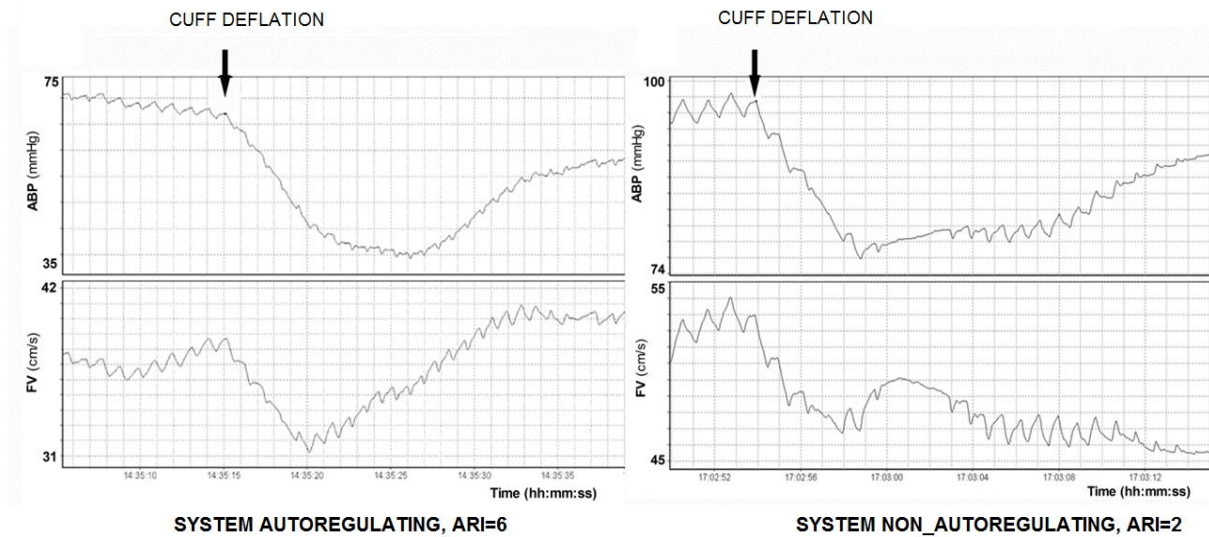


Figure 3.3 Example of deflation of leg cuffs to test cerebral autoregulation. On left: pattern specific for working autoregulation: In response to deflation, blood pressure (ABP) drops and so does blood flow velocity in MCA. With working autoregulation FV starts to recover before ABP increases back to baseline (left panel). With autoregulation disturbed, FV stays decreased, as long as ABP remains decreased[117].

ARI can also be derived from the analysis of spontaneous waves in ABP and FV, by means of impulse response (IR) estimation [31], [118]. In the original Tiecks model, $p(n)$ is the normalized change in ABP from its baseline value (the value before ABP drop). However, in IR based ARI, we use impulse signal as input and the baseline signal is assumed to be 0, so $p(n)$ equals the impulse ABP signal. $V(n)$ in Equation 3.4 presents the FV, and here, it means IR of Tiecks' model. f represents the sampling frequency. x_1 and x_2 are just intermediate variables, which were assumed to be equal to 0 initially [31].

$$p(n) = \begin{cases} 0, & n \neq 1; \\ 1, & n = 1; \end{cases} \quad (\text{Equation 3.1})$$

$$x_1(n) = x_1(n-1) + \frac{P(n) - x_2(n-1)}{f \cdot T} \quad (\text{Equation 3.2})$$

$$x_2(n) = x_2(n-1) + \frac{x_1(n) - 2D \cdot x_2(n-1)}{f \cdot T} \quad (\text{Equation 3.3})$$

$$V(n) = 1 + P(n) - K \cdot x_2(n) \quad (\text{Equation 3.4})$$

which can be written as a second-order equation:

$$f^2 T^2 x'' + 2 \cdot D \cdot f \cdot T x'(n-1) = P - x(n-1) \quad (\text{Equation 3.5})$$

$$V(n) = 1 + P(n) - K \cdot x(n) \quad (\text{Equation 3.6})$$

Or

$$f^2 T^2 V_n'' + 2DfTK \cdot V_{n-1}' + K \cdot V_{n-1} = f^2 T^2 P_n'' + 2DfTK \cdot P_{n-1}' + K \cdot P_{n-1} - K^2 P_n + K \quad (\text{Equation 3.7})$$

where V'' and V' refers to second derivative and first derivative of velocity, P'' and P' refers to second derivative and first derivative of pressure, T is the time constant, D is a damping factor, K is the autoregulatory dynamic gain, f is sampling frequency.

This grading method is simple and easy to implement and interpret. However, this method either requires manipulation of ABP or presumes a pre-defined linear and stationary relationship between ABP and CBF velocity, which is generally not true. The actual responses of CBF velocity are more diverse and dispersed. Therefore, the 10 pre-defined cases are not enough to explain all situations, resulting in inappropriate assignments of the index number in some cases and having large individual variability.

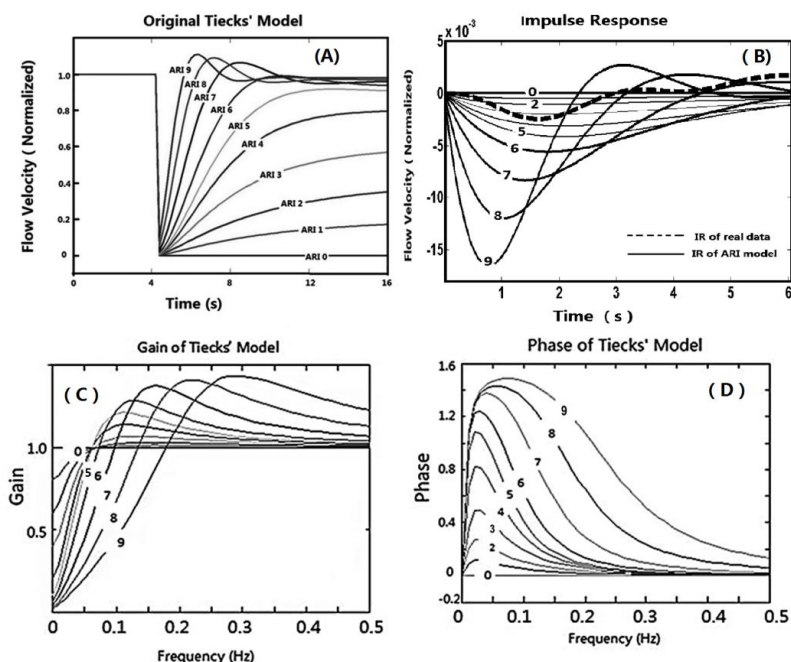


Figure 3.4 The upper panel shows the step response (A) and impulse response (B) of original Tiecks' model. The lower panel shows the transfer function (TF) characteristics of Tiecks' model (C and D). (A) From bottom to top, each line represents autoregulation index (ARI) value of 0 to 9, respectively. (B) From bottom to top, the solid lines stand for ARI 9 to ARI 0. The dashed line is a sample of the IR between real ABP and real FV of one patient. (C) The gain of Tiecks' model; (D) The phase of Tiecks' model[31].

3.1.2 Transfer function analysis (TFA)

Transfer function analysis has been used widely in renal autoregulation[119], [120], cardiovascular control[121] and respiratory sinus arrhythmia[122]. The basic idea of transfer function comes from looking at the frequency response of a linear system, describing the oscillatory components at individual frequencies of output signal through the input signal. Recently, the TFA method has been used to analyse the dynamic properties of CA, which is regarded as a high-pass filter [14]–[16]. The principle is that autoregulation is supposed to attenuate the influence of ABP on CBF velocity by preventing a direct transmission of pressure waves into blood flow waves at a low frequency range (normally <0.2 Hz) [17]. Three parameters, gain, phase shift and coherence, can be derived from the transfer function at each frequency[123], [124]. Gain quantifies the compression of the relative changes in the amplitude of CBF velocity to ABP, whereas phase shift indicates the time lag (given a specific frequency) between ABP and CBF velocity [99]. Gain is a continuous value. For example, a value of 0.5 suggests that 50% of the relative amplitude of CBF velocity is attenuated with respect to a unit of changes in ABP. Phase shift is denoted in degree or radians. The larger the phase of CBF velocity is shifted from ABP, the better the autoregulation is taking effect [126], [127]. Such a linear-response theory analysis does not consider the fact that slow fluctuations of CBFV may occur independently of changes in ABP, or may, in fact result from a non-linear relationship. Therefore, the criterion of coherence—the degree of linearity between input and output—is often used to test the validity of the model [120]. A

high coherence is thought to indicate a high reliability of the calculated phase and gain parameters because the assumption of linearity is clearly met, whereas a low coherence is thought to indicate a low reliability of phase and gain parameters, possibly caused by external noise or a non-linear relationship [17]. However, it can also be argued that coherence per se could be an indicator of CA, with high coherence indicating impaired CA (because in this situation slow variations in CBFV (output) are linearly and passively related to slow variations in ABP (input)), and low coherence indicating properly functioning CA (because in this situation the generally non-linear character of the physiological autoregulatory curve may reveal itself in a non-linear relationship between CBFV and ABP) [17], [128]. A series of studies of the performance and implementation of TFA by multi-centres were recently published by the society of Cerebral Autoregulation Research Network (CARNet) [126].

TF parameters can be obtained through the Fast Fourier Transform (FFT) algorithm below:

From the temporal sequences of ABP ($P(t)$) and FV ($V(t)$), the auto-spectrum and cross-spectrum of blood pressure ($P(f)$) and flow velocity ($V(f)$) can be obtained. They are calculated as the expected value of the complex product with themselves (Equation 3.8, Equation 3.9) by averaging four segments of data.

$$S_{pp}(f) = E[P(f) * P(f)] \quad (\text{Equation 3.8})$$

$$S_{vv}(f) = E[V(f) * V(f)] \quad (\text{Equation 3.9})$$

where $S_{pp}(f)$ and $S_{vv}(f)$ are the auto-spectra of ABP and FV, respectively. Similarly, the cross spectrum ($S_{pv}(f)$) is calculated through Equation 3.10. It provides a statement of how common activity between two signals is distributed across frequency. The cross-spectrum can also be calculated as the FFT of the crosscovariance function (ccvf). As the ccvf is not symmetric around $\tau = 0$, the cross-spectrum is a complex-valued function.

$$S_{pv}(f) = E[P(f) * V(f)] \quad (\text{Equation 3.10})$$

The coherence function is defined as a normalization of the cross spectrum by the product of the two auto-spectra, its value will be between 0 and 1 and can be calculated through Equation 3.11.

$$\gamma = \frac{\|S_{pv}(f)\|^2}{S_{pp}(f)S_{vv}(f)} \quad (\text{Equation 3.11})$$

Coherence reflects the linear relationship between input and output. For example, if input and output are identical processes, their power spectra are equal and to the cross-spectrum. In this case, the coherence will be 1 at all frequencies. However, if the input and output are completely independent, then the cross-spectrum will be 0, as is the coherence.

The TF is a complex-valued function, it can be obtained by Equation 3.12 and can be described as Equation 3.13, where H_r and H_i are the real part and imaginary parts of H_f .

$$H_f = \frac{Y_f}{X_f} \quad (\text{Equation 3.12})$$

$$H_f = H_R + H_I \cdot j \quad (\text{Equation 3.13})$$

The TF gain ($|H(f)|$) can tell us what magnitude of change in FV is caused by a change in MABP. The TF phase ($\varphi(f)$) describes the time shift from input to output at a specific frequency[129]. They can be obtained through Equation 3.14 and Equation 3.15.

$$|H(f)| = [H_I^2 + H_R^2]^{1/2} \quad (\text{Equation 3.14})$$

$$\varphi(f) = \tan^{-1} \left[\frac{H_I(f)}{H_R(f)} \right] \quad (\text{Equation 3.15})$$

Finally, the IR of the system can be obtained by the inverse FFT (IFFT) of the TF, as described in Equation 3.16. In this study, before doing ifft, the TF was filtered with a cut-off frequency of 0.5 Hz.

$$i_f(t) = \text{IFFT}[H(f)] \quad (\text{Equation 3.16})$$

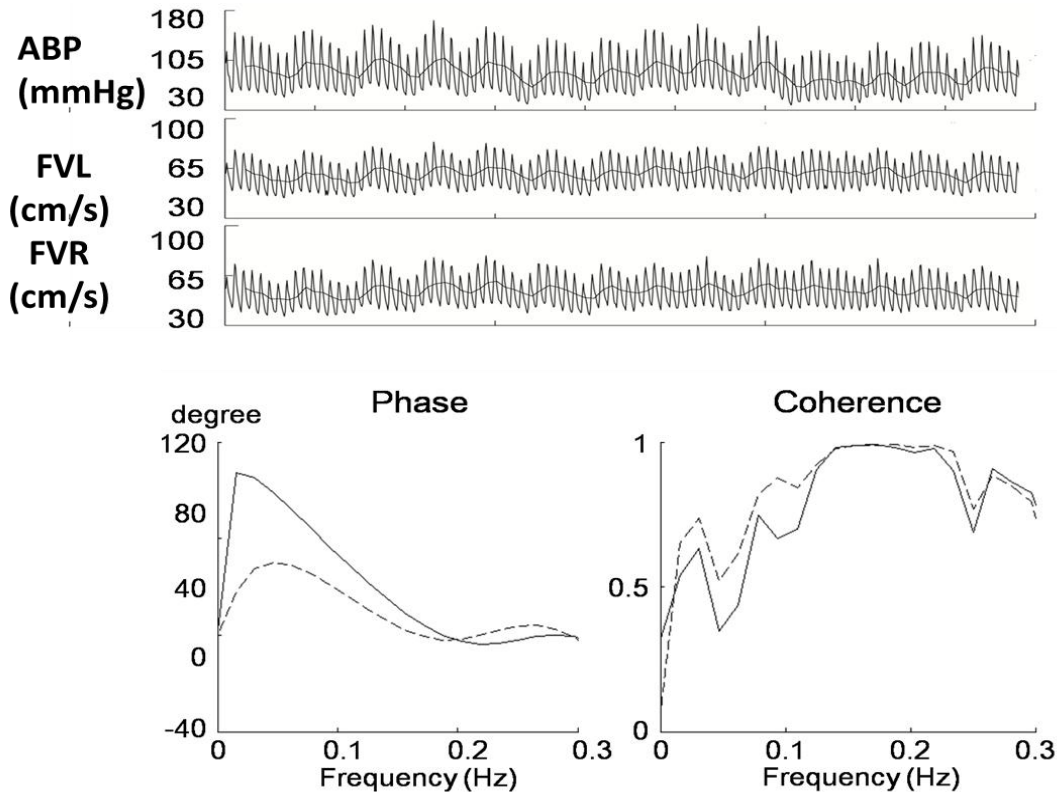


Figure 3.5 Analysis of the phase shift between slow fluctuation of mean ABP and blood flow velocity. High phase-shift at high coherence means good autoregulation. In this subject, compared with the right side (solid line), the

recovery of the blood flow of the left side (dashed line) was slower, the phase shift was lower, and the coherence was higher[130].

3.1.3 Time correlation

The time-correlation method allows continuous estimation of CA through a moving linear correlation between slow waves of ABP and ICP (pressure reactivity index, PRx), or CBF velocity and CPP (mean flow index, Mx), or ABP and PbtO₂ (TOx_a). These parameters can reflect the compliant ability of cerebral vessels in response to changes in ABP or CPP. They have been widely used for continuous monitoring of CA in patients requiring neuro intensive care predominantly. One of the limitations of this method is that calculation of the correlation coefficient may be influenced by the time scales used and signal preprocessing (e.g. degree of smoothing applied or detrending).

Mean Flow Index (Mx), Systolic Mx (Sx) and Diastolic Mx (Dx)

Mean flow index (Mx), estimates CA through the correlation coefficient between slow fluctuations (20 seconds to 3 minutes) of mean FV and CPP [23], [131]–[133]. It is a purely time-domain measurement, based on the concept that if CA is intact, there will be no correlation between changes in CPP and changes in FV ($Mx = \text{zero or negative}$), whereas when CA is exhausted changes in CPP will be directly correlated with changes in CBFV ($Mx \sim +1$). Importantly, Mx has been shown to be associated with outcome in different patient groups including carotid occlusive disease, stroke and subarachnoid haemorrhage [114], [134]–[140]. The maximal and minimal values of FV from every 1.5 s period were calculated and treated as the peak-systolic and end-diastolic components, respectively. Systolic Mx (Mxs) is the correlation coefficient between 10s mean of peak-systolic FV (FVs) and CPP; while diastolic Mx (Mxd) refers to the relationship between 10s mean value of end-diastolic FV (Fvd) [132]. The study showed that Sx had a better performance in distinguishing favourable and unfavourable outcomes than Mx.

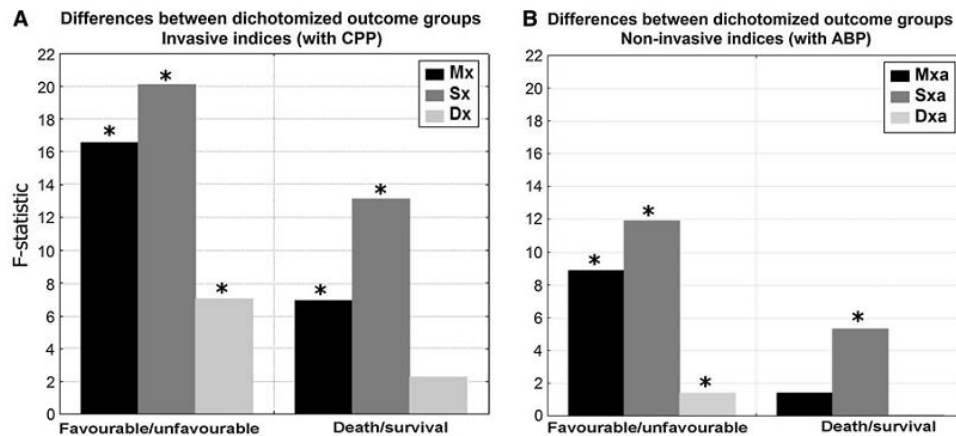


Figure 3.6 Graphs comparing the observed difference in analysed indices between favourable/unfavourable outcome and survival/death using invasive indices—with CPP (A) and non-invasive indices—with ABP(B) [132]. In all cases the biggest differences were observed for indices using systolic FV, regardless of the outcome measures and whether CPP or ABP was used for calculation, indices utilizing CPP for calculation demonstrate larger differences between

outcome groups than those using ABP. ABP arterial blood pressure, CPP cerebral perfusion pressure, Dx and Dxa diastolic flow velocity index using CPP and ABP, respectively, Mx and Mxa mean flow velocity index using CPP and ABP, respectively, Sx and Sxa systolic flow velocity index using CPP and ABP, respectively. *P < 0.05

Pressure reactivity index (PRx)

The pressure reactivity index (PRx) is a moving linear correlation between spontaneous slow waves of ABP and ICP, and can reflect the ability of cerebral vessels to change diameter in response to changes in blood pressure [21]. Studies also showed that PRx is a useful secondary index of vascular deterioration leading to a fatal outcome and a variable for setting the individual target for CPP management [141]–[143]. A significant increase in mortality after TBI has been demonstrated to occur with increasing PRx [144]. It is calculated as the moving linear correlation coefficient between 30 consecutive, 10-s averaged values of ABP and corresponding ICP signals [55], [145]. Averages over 10 secs were used to suppress the influence of the pulse and respiratory–frequency wave components. Under reduced intracranial compliance, a positive correlation between ABP and ICP at low frequency is indicative of passive cerebral vasculature and impaired autoregulation. Zero or negative correlation between ABP and ICP at the same frequency is indicative of reactive vasculature and intact autoregulation [57], [102], [146].

3.2 Wavelet analysis for CA autoregulation

However, the methods described above are either simple correlation indices (such as PRx), suitable for linear, stationary signal analyses, such as the TF approach [31], [32], or assume the system being analyzed are linear or the statistical parameters of the signals are constant over time (stationary signals) [31], [32]. With the clarification of the non-stationary nature and non-linearity of CA [28], [147], many attempts have been made to perform more sophisticated analyses to quantify the coupling mechanism of ABP and ICP, including high-order Volterra kernels, phase-synchronization methods, and WT signal-processing techniques [148]–[150]. The WT method, has been widely applied in geophysics and economics, and is particularly useful for analysing noisy, transient and non-stationary signals by enabling simultaneous optimal interpretation of spectral and temporal information using a data window of variable width [34], [151]. It is a method for decomposing a signal into a time-scale plane (the scale being roughly speaking an inverse of frequency) through the convolution of the signal with a scaled wavelet function [13], [14]. One advantage of wavelet analysis is the ability to reveal signal features with the right balance of the temporal and frequency resolution appropriate to the frequencies studied, higher temporal resolution for higher frequency and higher scale (inverse frequency) resolution for lower frequency [34], [35].

Two useful parameters that can be derived from WT include wavelet transform phase shift (WTP) and wavelet transform coherence (WTC); both can be calculated through the cross-wavelet transform (XWT). WTP characterizes the localised (in the time-frequency plane) phase difference between input (ABP) and output (ICP) in the time and frequency dimensions, while WTC, in very simplified terms, identifies local (again, in the time-frequency plane) correlations between two XWTs. In this way, locally phase-locked behaviour can be uncovered. A value of WTC = 1 indicates a high common power between two time series at a certain time and frequency. A value of WTC = 0, on

the other hand, is obtained for a vanishing correlation [152], [153], and is mathematically associated with high variance of the phase-shift estimator [154]. Therefore enforcing a certain minimal threshold for WTC is often used to guarantee a reliable phase and gain estimation [155].

There are also some other methods to study the non-linear relationship between ABP and FV or ICP, CA, such as multimodal pressure flow (MMPF) method, which is based on the Hilbert-Huang transform (HHT) [156]. The principle is to calculate the phase-shift between ABP and CBF velocity without assuming a linear relationship a priori. The ABP and CBF velocity are empirically decomposed into a series of modes from fast to slow waves, respectively. The mode that is considered the most relevant to autoregulation is then identified and the instantaneous phase of ABP and CBF velocity is computed by a Hilbert transform. The phase difference between the variables can then be calculated readily. Several studies have shown that it can deal with the non-linear relationship of ABP and CBF velocity. However, the validity and effectiveness of these methods need to be further tested or replicated in multi-centre studies. Table 3.2 contains a brief description of methods used in CA assessment.

3.3 Clinical application of CA assessment

Over the years, a dynamic patient-targeted CPP protocol, based on the CA ability of cerebral vasculature has been proposed. Since Czosnyka et al introduced PRx to assess CA, widely accepted as a marker for cerebral autoregulatory status in many neurocritical care settings [157], because it can be determined from periodic variations in ICP and MAP, two widely and commonly measured parameters in TBI patient modalities, without needing external stimuli. Moreover, taking the additional step of plotting PRx against CPP will often generate a ‘U’-shape curve, the base of which represents the CPP corresponding to the smallest value of PRx, where the CA response is most active [27]–[29], the point termed CPPopt. Steiner et al. introduced this concept in 2002 looking at CPPopt calculated from the whole monitoring period [36]. In 2012, Aries et al. proposed and tested an automated CPPopt algorithm based on a moving four-hour calculation window in a different (retrospective) cohort of TBI patients by showing improved outcome in patients with CPP close to the averaged automated CPPopt [38].

Over the years, other observational studies have confirmed that adult and paediatric patients whose median CPP is closer to their determined CPPopt seem to have better clinical outcomes [37], [159], [160]. A clinical trial of CPPopt-targeted therapy is now essential to determine whether CPPopt is purely prognostic, or if CPPopt represents a true physiologic target that, if achieved, will improve outcomes.

Problematic for the design of such a study is the fact that CPPopt can only be generated during approximately 44% of the monitoring time in these retrospective studies [161]. Weersink et al. identified six factors that were independently associated with the absence of the CPPopt curve [162]. Depreitere et al. introduced an innovative multi-window-based algorithm for CPPopt calculation using minute-by-minute monitoring data typically available from electronic medical records systems [161]. They used a low-resolution version of PRx, which they termed LAx, and calculated a moving weighted-average value of CPPopts based on seven windows of different length (1, 2, 4, 6,

8, 12, 24 hours), instead of a single four-hour-long moving window. The weighting system was based on two criteria: the better a 'U'-shape curve could be fitted and the lower the LAx value corresponding to the plot-specific CPPopt, the higher the weight of that window. Bases on their study, the mathematical approach needs to be improved further by increasing the window number and applying a weighting system that incorporates more characteristics of the PRx–CPP plot. Moreover, a validation study in a much larger population of TBI patients is necessary.

Table 3.2 Methods for cerebral autoregulation assessment and monitoring

| Method | Method | Monitors | Principle | Limitations |
|--------|--|---|---|---|
| Static | Pharmacological increase or decrease in ABP | TCD, PET, Perfusion Computed Tomography (CT) or Radionuclide CBF compared with CPP or ABP | <p>The test involves measurement of CBF at baseline and after a rise in ABP induced by a vasopressor. The static rate of autoregulation is calculated as the ratio of relative rise in cerebral vascular resistance (CVR) divided by relative rise in CPP or ABP[163].</p> $sRoR (\%) = 100 (\% \Delta CVR / \% \Delta CPP)$ <p>where $CVR = CPP / CBFV$</p> <p>an sRoR of 100% denotes ideal autoregulation, 0 indicates absolutely non-functioning autoregulation—see Fig. 3.1</p> <p>sROR: Static rate of autoregulation.</p> | If autoregulation is not working, pharmacological increases in ABP may cause a rise in ICP, leaving CPP unchanged. In such a situation, CBF remains unchanged, giving a false impression of autoregulation staying functional. Such a situation is named in the literature as ‘false autoregulation’. |
| | Brain imaging techniques: MRI, Perfusion CT | Arterio-jugular oxygen content difference (AJDO2) | When cerebral metabolic rate of oxygen is constant, changes in arterio-jugular differences of oxygen (AVDO2) reflect changes in CBF. In these situations relative changes in AVDO2 can be viewed as inverse changes in CBF and used as an evaluation method of CO2-reactivity and autoregulation. [164], [165]. | The method was not validated. Studies grading autoregulation on that basis of changes in AJDO2 need to be interpreted with caution. |
| | | MRI | MRI has high spatial resolution and the CA can be calculated by comparing the observed MRI signal intensity change ultrasound during a standardized thigh cuff maneuver[166]. | It is difficult to obtain beat-to-beat values of mean ABP inside the magnet. |

| | | | | |
|--------------------------------------|------------------------------------|--|--|--|
| | | Perfusion CT | Measurement of Xe-CBF using the CT method, before and after alteration of ABP (pharmacologically) or vasodilation by acetazolamide[167]. | If ICP is not measured, CPP may not follow changes in ABP or decrease in response to Xe or acetazolamide. This may disturb quantitative indices describing cerebrovascular reactivity. |
| Mixture of static and dynamic | Lower-body negative pressure | Radionuclide methods or TCD compared with ABP monitoring | Lower-body negative pressure produces arterial hypotension provoked by strong autonomic activation. Pulsatile lower-body negative pressure can also be used to induce slow changes in ABP and assess the phase shift between CBF and ABP slow rate waveforms. Zero phase shift indicates autoregulation is not working properly[168]. | It is very difficult to resolve information regarding pressure autoregulation and systemic responses (ABP, heart rate and PaCO ₂) observed during alteration of autonomic haemodynamic control. |
| Dynamic | Thigh-cuff test | TCD or near infrared spectroscopy (NIRS) compared with ABP | It involves inducing a temporary decrease in ABP after deflation of thigh cuffs, previously inflated above systolic ABP, and measuring the speed of response in CVR using a (parameter called RoR, rate of autoregulation)(Fig. 3.3). Alternatively, the response in CBF can be modelled as the step response of a high-pass filter. Autoregulation is described as the filter parameter, ARI[12]. | SNR may be low as response to thigh-cuff test may be weak. Therefore, it is advised to repeat the test three times. In conscious patients, inflating cuffs may be painful. In patients with depleted pressure–volume compensatory reserve, sudden decrease in ABP may lead to a rise in ICP–disturbing the assessment of autoregulation if ICP is not monitored. |
| | Transient hyperaemic response test | TCD | Doppler sonography FV recording of response to release of 6–9 seconds compression of the carotid artery. A positive hyperaemic response, indicated by CBFV during hyperaemia divided by baseline CBFV being greater than 1.1, denotes working autoregulation. Otherwise, autoregulation is judged as depleted[169]. | Carotid arteries need to be screened to eliminate cases with carotid plaque, in which carotid artery compression may pose a risk of embolization. Compressions producing baroreceptor activation of ABP regulation may produce false response; ABP monitoring is advised. |

| | | | |
|----------------------------|--|--|--|
| Time correlation | TCD compared with CPP or ABP | Mx, correlation between 30 consecutive 10-s averages of TCD mean CBF velocity and ABP. Alternative indices for systolic and diastolic FV (Sx and Dx) can be calculated[131]. | Long-term monitoring of the TCD signal is difficult, as the position of ultrasound probes cannot always be maintained. |
| | ABP and ICP | PRx, Correlation coefficient between 30 consecutive 10-s averages of mean ABP and ICP[21]. | Long term monitoring of TCD signal is difficult, as position of ultrasound probes cannot be always maintained. |
| | NIRS compared with CPP or ABP | COx or TOx, Pearson correlation between 30 consecutive 10-s means of ABP and tissue oxygenation index[108]. | Shows good affinity to gold standard assessment of LLA. NIRS signals, however, look like noise, and even if they are easier for long-term monitoring than TCD, one can never know when monitoring is valid or not. |
| | Diffuse correlation spectrometry (DCS) compared with ABP | It utilizes the intensity fluctuations of near-infrared light to noninvasively quantify CBF at the bedside[170][171]. | This is a new, emerging methodology, able to monitor instant CBF from near infrared spectroscopy changes. Clinical applications remain to be documented. The penetration depth of DCS, is limited compared to traditional clinical modalities, such as MRI and CT. |
| | PbtiO2 compared with CPP or ABP | ORx, Pearson correlation coefficient between intraparenchymal brain tissue oxygenation and CPP or ABP, calculated over longer (60 or 20 minutes) time window[111] | After years of reporting, still there is no convincing proof that ORx is an index of autoregulation. |
| Transfer-function analysis | TCD or NIRS, or DCS compared with ABP | If the cerebral circulation acts as a high-pass filter (high-frequency fluctuations in ABP pass through to FV unimpeded while lower frequencies are dampened), TF phase, gain and coherence can be studied[172]. | Phase shift is the most promising variable, but it can be evaluated only if the frequency of slow waves is stable—see Figure 3.5. Therefore, methods involving slow respirations or slow modulations of positive end-expiratory pressure (PEEP) are most promising in this area. |

| | | | | |
|--|--|-------------|---|---|
| | | | | |
| | Valsalva manoeuvre | TCD | The Valsalva manoeuvre produces phasic variations in ABP[173]. | During Valsalva, changes in ICP are possible. |
| | Multimodal pressure-flow (MMPF) analysis | ABP and TCD | Any 'complex' signal $S(t)$ can be represented as the superimposition of more basic (simpler) components: $S(t) = \sum S_k(t)$, where S_k are empirical modes(oscillators, in general non-sinusoidal). MMPF phase measure of autoregulation has much better repeatability/reproducibility than the traditional Fourier TFA[174]. | Computationally complex, mode selection subjective, use limited to the authors and direct collaborators |

CHAPTER 4 METHODOLOGICAL CONSIDERATIONS REGARDING PROJECTS INCLUDED IN THE THESIS

Despite advances in the application of CA assessment, there remain many uncertainties about the theoretical and pragmatic relationships between the indices. The gold standard reference for CA assessment in TBI is still to be determined. The methodology used in this thesis can be divided into three sections; first, the validation of relationships between current widely used CA parameters, including PRx, Mx, ARI and TF; second, introduction of a new method, a wavelet method for CA assessment; third, an improved method to calculate optimal CPP for clinical management of TBI patients.

4.1 General overview of the original projects included in this thesis

The protocol of this study is depicted in Figure 4.1. **The first step** was to validate the relationship between current CA parameters (PRx, Mx, CA, and TF parameters) through simulated data and real monitored data. Although a few comparisons have been published [23]–[29], they have been based on real measurements, which inevitably introduces confounding factors to the relationships such as poor fit of the assumed models or the presence of unknown extraneous ‘noise’ [30], i.e. components in ABP and CBFV that are not related to each other. The potential for differential sensitivity of the CA indices to these confounding factors makes meaningful comparisons between the different methods difficult.

Therefore, to cross-validate the relationships between the CA indices in a more controlled environment, and to try to find a reliable index to assess CA in TBI patients, this study used artificial or simulation data, with CBFV generated according to Tiecks’ ARI model [12] using real ABP signals as the input. Mx and TF parameters were calculated and compared with the ‘golden’ ARI values, which were used as a basic reference in this comparison. Through these artificial data, undisturbed by unknown confounding factors, the pure theoretical relationships between CA indices were studied. Afterwards, a retrospective study was conducted to analyse the relationship between these CA parameters via real data from a cohort of TBI patients admitted to Addenbrooke’s Hospital between 2003 and 2015.

The second step of this study was to introduce a new method, wavelet methodology, to assess CA. This method was implemented in our own software ICM+ (<http://www.neurosurg.cam.ac.uk/icmplus>). The mathematical principle of this method is described in the next chapter. To validate the wavelet calculation, a cohort of experimental data using piglets was first applied. After the validation, the wavelet method was applied into 515 TBI patients, and was compared with traditional CA parameters. The relationship between wavelet method and patients’ outcome was also studied.

The third step of this thesis was to find the best way to target optimal CPP for clinical management of TBI patients. The feasibility and impact on the outcome of strategies based on individualized CPP management following severe TBI were advocated by the Brain Trauma Foundation guidelines [175]. Attempts to identify an optimal cerebral perfusion pressure (CPPopt) individually based on CA has been approved through several studies. However, many

challenges still remain to improve the performance of CPPopt. The object of the present study was to investigate how the yield and the continuity of CPPopt can be enhanced, through a multi-window algorithm and a weighting system, which can maximally exploit and optimize the potential information about cerebral vascular pressure reactivity.

Figure 4.1 describes the framework of this thesis.

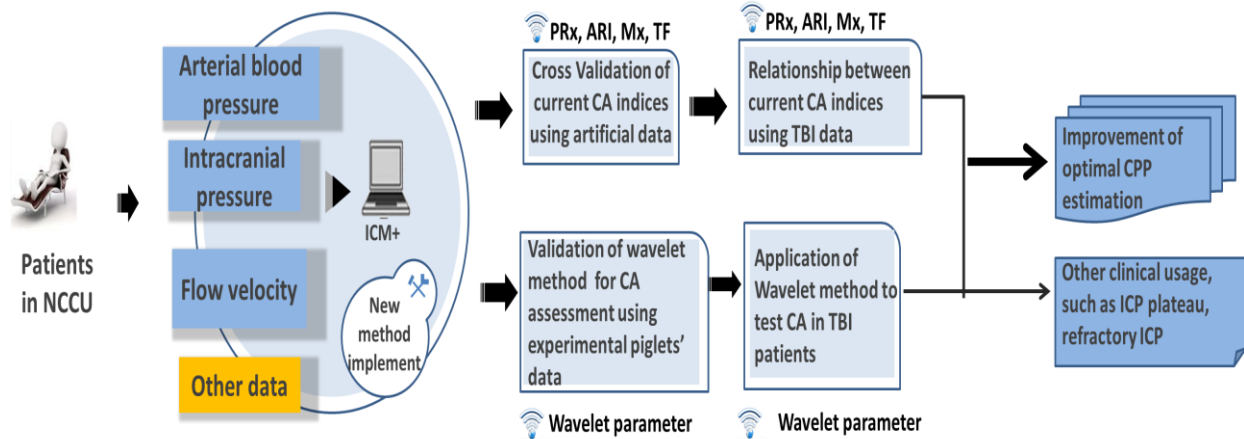


Figure 4.1 The framework of this research. First, is the validation of relationships between current widely used CA parameters, including pressure reactivity index (PRx), mean flow index (Mx), autoregulation index (ARI) and transfer-function (TF) parameters. Second, introduction of a new method, wavelet method for CA assessment. Third, optimal CPP estimation for clinical management of TBI patients.

4.2 Data collection

Monitoring in the intensive care unit is particularly vital, as patients deteriorate quickly and are at high risk of death or serious complications [176]. Health care monitoring requires the intensive use of information technologies to acquire and manage data, to transform the data into actionable information, and to disseminate this information so that it can be used effectively to improve patient care [177].

4.2.1 Intracranial pressure

In the NCCU, ICP can be extremely dynamic (Figure 4.2), with information included in the ICP waveform that may provide important information about intracranial pathology (Figure 4.3). Continuous ICP monitoring is applied for patients with severe TBI in some NCCUs and [178].

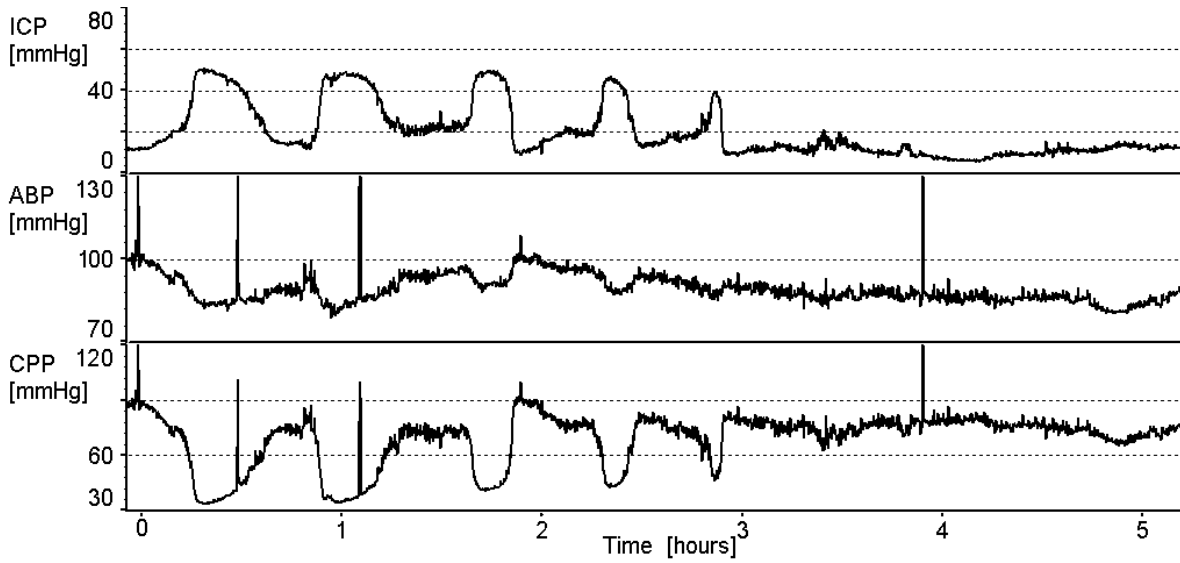


Figure 4.2 Intracranial pressure (ICP) can be highly dynamic in the neuro criticalcare unit [179].

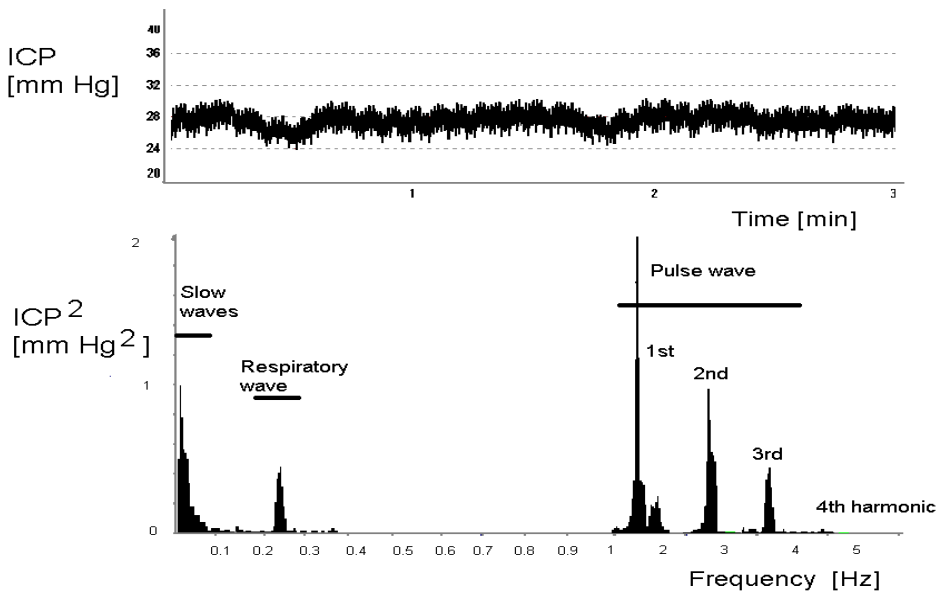


Figure 4.3 The waveforms of intracranial pressure (ICP) signal: pulse waves, respiratory waves and slow waves [179].

An intraventricular drain inserted into one of the lateral ventricles and connected to an external pressure transducer is still considered to be the ‘gold standard’ method [179], [180]. This method allows repetitive zeroing (at auditory meatus), ICP measurement and withdrawal of CSF (Figure 4.4). However, this method is most invasive, with a high

risk of infection at 6–11% [181], [182]. Several alternatives to the ventricular catheter include intraparenchymal probes, subarachnoid bolt or epidural pressure transducer (Figure 4.5) [50], [183]. The intraparenchymal probes most frequently used these days give higher precision than the other two [184]. It either uses a miniature strain gauge pressure sensor, which can transfer the changes in ICP into changes in resistance to measure, or the intraparenchymal probe uses a fiberoptic catheter, which tests the changes of ICP through changes in reflection of the light beam. The infection rate of the intraparenchymal probe is very low, but its main disadvantage is a small drift of the zero reference [185] that cannot be recalibrated once the sensor has been inserted.

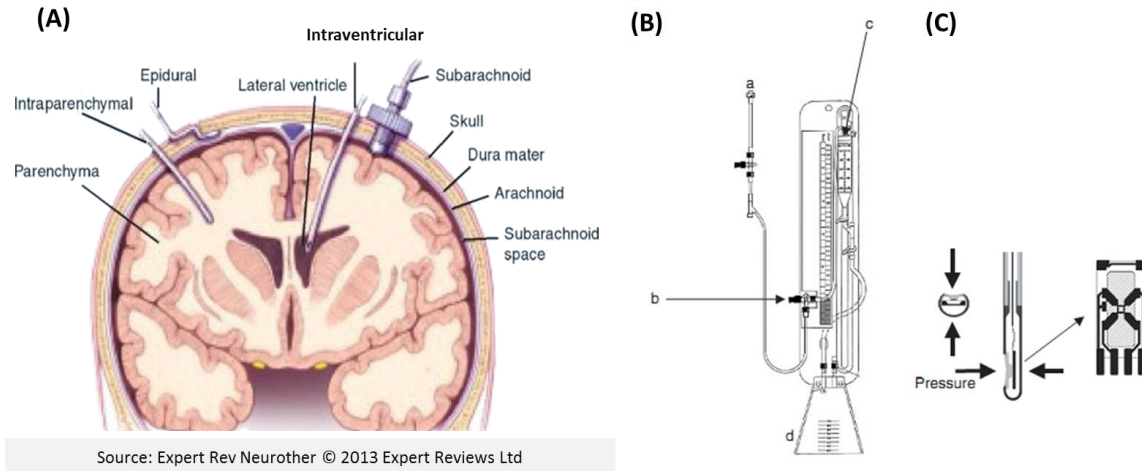


Figure 4.4 (A) ICP monitoring. Invasive probes are placed at specific neuroanatomic positions such as the lateral ventricle, parenchymal tissue, and the subarachnoid and epidural space [186]. (B) A typical system for ICP measurement via an intraventricular drain: a: connection with drain; b: zero (should be positioned at height of patient's ear) and three-way stopcock for connection with pressure transducer; c: drip chamber, adjustable in height over zero for CSF drainage. Depending on stopcock position (b) either pressure measurements or CSF drainage are possible; and d: CSF reservoir. (C) Possible configuration for the intraparenchymal probe. Pressure is sensed at the tip of the probe by a miniature sensor consisting of piezo-elements or other pressure sensitive elements arranged as a Wheatstone bridge.

4.2.2 Cerebral blood flow

Four major arteries supply blood to the brain: the left and right internal carotid arteries (ICA), and the left and right vertebral arteries (VA) (Figure 4.5). The carotid arteries contribute approximately 80% to the total CBF, the remaining 20% coming from the two VAs [187]. Within the cranium, the VAs join to form the basilar artery, which is in communication with the ICAs via the posterior communicating arteries at the so-called circle of Willis. Considerable anatomic variation exists in the circle of Willis. Based on a study of 1413 brains, the classic anatomy of the circle is only seen in 34.5% of cases [188]. At the circle of Willis each ICA splits into an anterior cerebral artery (ACA) and a middle cerebral artery (MCA), while the basilar artery divides into the left and right posterior arteries (PCA). These major arteries divide into smaller and smaller arteries before branching into the capillaries, from which exchange of metabolites between the blood and interstitial fluid of the brain occurs [189]. The

capillaries then unite into intracranial veins that employ the dural venous sinuses, which transport the venous blood from the brain.

As the largest branch of the internal carotid, the MCA supplies fresh blood to lateral side areas of the frontal, temporal and parietal lobes. It is the vessel most commonly affected by cerebrovascular accidents and is always used for diagnostic tests through neuroimaging tools, such as TCD.

CBF measurement was not possible until 1945, when Kety and Schmidt used a nitrous oxide method to determine the global CBF based on the Fick's principle [190]. However, this method was found to be cumbersome and required repeated blood sampling, other methods were introduced later, including Stochastic method, two compartmental models, hydrogen clearance method, microspheres technique, et al [191]. With the advent of computed tomography (CT) scans, methods have been developed for measurement of CBF using CT scans since CT scans are less time consuming, better availability, better delineation of morphology. Xenon enhanced CT and CT perfusion techniques have been used to test CBF[192], [193]. In recent years, methods based on other imaging techniques, such as single photon emission computed tomography (SPECT), magnetic resonance imaging (MRI), positron emission tomography (PET) have also been investigated . However, these methods only give snapshots of CBF and do not allow for continuous monitoring and are associated with a radiation dose. Optical approaches have gained increasing attention for detection of CBF as they are simple to use, bed side and reduced risk of radiation and shifting of patients to complex radiological suite[191]. Three methods are normally used based on optical techniques, i.e. laser Doppler flowmetry, optical micro-angiography, and optical imaging of indocyanine green molecular dynamics analysis.

Later, Transcranial Doppler (TCD) ultrasonography was introduced as an indirect assessment of blood flow [194] . It has several advantages in the NCCU, such as non-invasive detection, reproducible measurement and, safe procedure. However, it is movement sensitive and the result does depend on the operator's experience. It utilises the Doppler shift to assess the changes in flow velocity of the moving red blood cell. It should be remembered that TCD measures only the flow velocity and not the absolute CBF value, on assumption that the radius of arteries keep constant, then TCD can be used as a noninvasive estimate of CBF. TCD has been clinically used to monitor the CBF in cardiopulmonary bypass, carotid endarterectomy, head injury, vasospasm, brain death, etc. Its use also has been described to monitor the CBF in resuscitation during cardiac arrest[195], [196].

TCD ultrasonography is based on the principle of the Doppler effect [197]. According to this principle, ultrasound waves emitted from the Doppler probe are transmitted through the skull and reflected by moving red blood cells within the intracerebral vessels. The difference in the frequency between the emitted and reflected waves, is caused by the moving red blood cells (blood flow velocity). Because blood flow within the vessel is laminar, the Doppler signal obtained actually represents a mixture of different Doppler frequency shifts forming a spectral display of the distribution of the velocities of individual red blood cells on the TCD monitor (Figure 4.5) [194]. The relationship between flow velocity (reflector speed) and Doppler shift frequency is expressed below:

$$V_r (cm/s) = \frac{Doppler\ shift \times V_p (cm/s)}{2 \times F_i \times \cos(\theta)} \quad \text{Equation 4.1}$$

V_r refers to reflector speed, F_i refers to the incident frequency, θ is the angle of insonation, V_p refers to the propagation speed, which is a constant that can be obtained for various media.

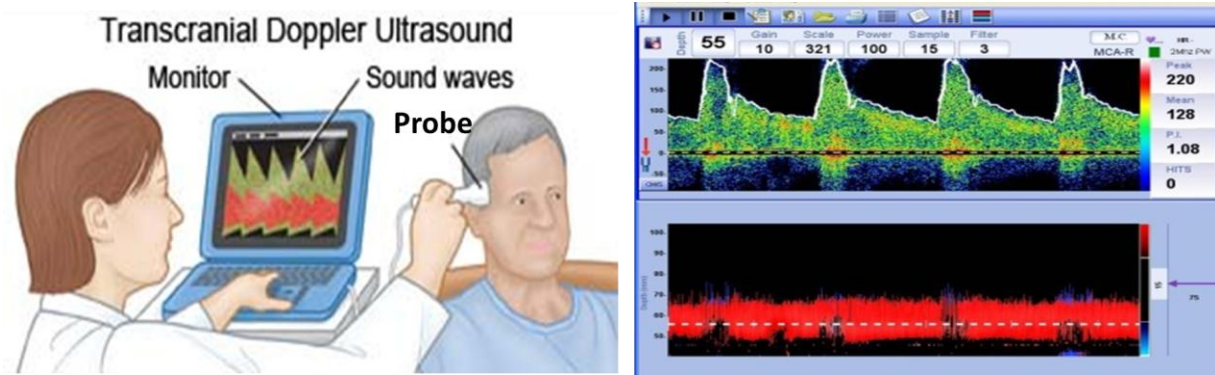


Figure 4.5 An example of spectral Doppler frequency display of the middle cerebral artery

Spectral analysis of the Doppler signal can then be used to obtain the envelope (the peak velocity in the middle of the artery), or the mean velocity. In general, four main acoustic windows have been used (Figure 4.6): (1) The transtemporal window; (2) the transorbital window; (3) the submandibular window and (4) the transforaminal window [194], [198]. In this study, we used TCD to monitor FV in MCA through the transtemporal window.

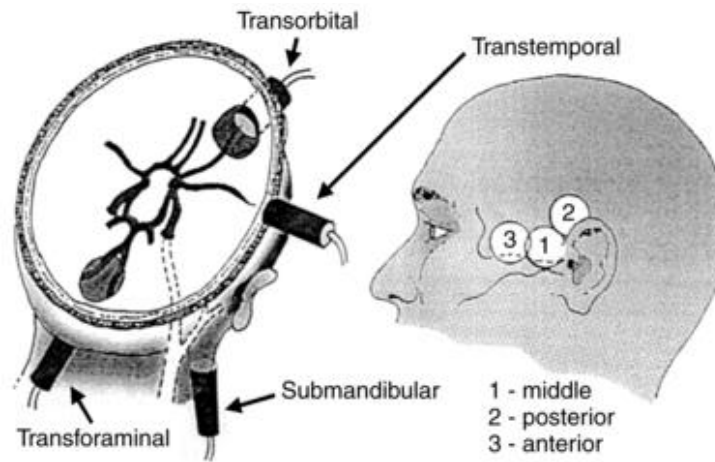


Figure 4.6 Four acoustic windows commonly used in transcranial Doppler examination: (1) transorbital window; (2) submandibular window; (3)transforaminal window; (4) transtemporal window.

4.2.3 Data monitoring

In this study, continuous monitoring of ABP, ICP and FV were obtained. ABP was monitored invasively through the radial or femoral artery using a standard pressure monitoring kit (Baxter Healthcare, CardioVascular Group, Irvine, CA). ICP was monitored using an intraparenchymal probe (Codman ICP MicroSensor, Codman & Shurtleff, Raynham, MA) inserted into the frontal cortex [38]. FV from MCA was monitored via the transtemporal windows bilaterally using Doppler Box (DWL Compumedics, Germany) or Neuroguard (Medasonic, CA) [132], [199], [200]. The intonation depth was from 4 to 6 cm and the examinations were performed during the first three days after head injury [201]. Each TCD recording lasted for 20 minutes to 2 hours.

All signals were sampled at 30–240 Hz (the sampling rates were increased over the years) and recorded using ICM+® software (University of Cambridge, Cambridge Enterprise, Cambridge, UK, <http://www.neurosurg.cam.ac.uk/icmplus>) through an A/D converter (DT9801, Data Translation, Marlboro, MA) or digitally directly from GE Solar monitors. Artefacts as sudden and short erratic peaks of the signal introduced by tracheal suctioning, arterial line flushing or transducer malfunction were removed manually. Data were recorded and analysed anonymously as part of a standard audit approved by the Neurocritical Care Users Group Committee (Figure 4.7).

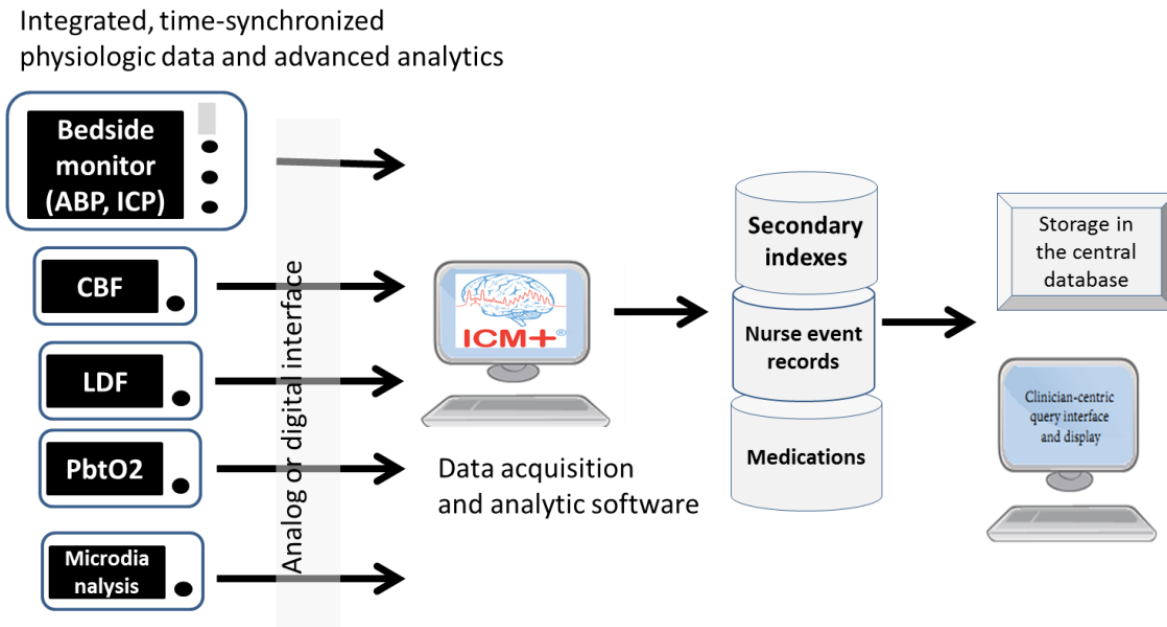


Figure 4.7 Data monitoring in neuro critical care unit in Addenbrooke's hospital, Cambridge

4.3 The database

Clinical data

Retrospective data from clinical patients and experimental piglets were employed in this study. For the analysis of the relationship between different methodologies of CA assessment, a database of patients with TBI admitted to the NCCU, Addenbrookes' Hospital, between 2003 and 2015, has been used. The data base comprises the largest population, with over 525 TBI patients archived.

Patients were managed according to current institutional TBI guidelines (adapted from Menon et al., 1999) [202]. In brief, patients were sedated, intubated, ventilated, and paralyzed with CPP managed according to ICP/ CPP management protocol for severe TBI. Interventions were aimed at keeping ICP < 20mmHg using positioning, sedation, muscle paralysis, moderate hyperventilation, ventriculostomy, osmotic agents and, induced hypothermia. CPP was maintained above 60 to 70 mmHg using vasopressors, inotropes, and intravenous fluids. Pressure reactivity parameters analysed in this study were not included in the protocol and therefore analysis of their association with the outcome was valid.

The relationship between the analysed CA parameters and patients' outcome at six months was evaluated. The Glasgow Outcome Scale (GOS) was used to assess patients' outcome at six months (obtained at rehabilitation clinic or by phone interview). For the purpose of the statistical analysis, the patients' outcomes were dichotomized in two ways: favourable outcome (good outcome and moderate disability) versus unfavourable outcome (severe disability, vegetative state and death); fatal outcome (death) versus non-fatal outcome (good outcome, moderate disability, severe disability and vegetative state). Although the dichotomisation might lose some group information and conceal any non-linearity in the relation between the variable and outcome, it greatly simplifies the statistical analysis and leads to easy interpretation and presentation of results. It separates patients' outcome into most obvious two groups[203].

Experimental piglets' data

In Chapter 5, a new method for CA assessment is introduced, which is the WT methodology. To validate the algorithm, two separate cohorts of subjects were analysed, one with induced, sinusoidal ABP waves at a frequency of 1/min and another with spontaneous ABP wave activity. All procedures were approved by the Johns Hopkins University Animal Care and Use Committee or the Baylor College of Medicine Animal Care and Use Committee and conformed to the standards of animal experimentation of the National Institutes of Health [204]. The piglets underwent induction of anaesthesia with inhaled isoflurane. Following tracheostomy and placement of central venous access subjects were maintained under anaesthesia with mechanical ventilation, narcotic infusion and isoflurane (0.5-0.8%) through the method previously described [205]. At the time of the experiments, the monitoring data were saved on hard disk digitally for further methodological studies .

The stability of the PRx in time series, and the SNR is improved by the use of controlled ABP wave activity [205]. This is mainly due to inadequate coherence between ABP and ICP. Low coherence between the ABP and ICP can result from physiologic events unrelated to autoregulation that can affect the ABP, ICP or, both. Periods without wave activity within the frequency range of the autoregulatory mechanism also have low coherence between ABP and ICP and result in random noise in the PRx. To examine the influence of those random effects on the relationship between the wPRx and PRx we performed analysis first on a dataset from experiments with induced high amplitude waveforms in ABP [205] and then repeated the analysis in a set of experiments with spontaneous ABP waves only [206].

In the first set the data were collected from 12 piglets, where regular, sinusoidal, ABP oscillations were induced using modulated positive end-expiratory pressure (PEEP) during volume-controlled ventilation [205]. A primary wave with a fixed tidal volume of 50 cc (cubic centimetres) at a rate between 15 and 25 min⁻¹ was applied to a customized ventilator (Impact Instrumentation, West Caldwell, NJ). A secondary wave component in a sine-wave pattern of one minute period was introduced into the PEEP control. Once a stable recording was obtained the piglets were haemorrhaged by syringe-pump withdrawal at a rate of 12% calculated blood volume/h, which allowed the procedure of gradual ABP reduction over 3-4 hours before demise.

In the second group, only spontaneous ABP and ICP signals from 16 piglets with naïve (n = 8) or elevated ICP (ICP = 20 mmHg, n = 8) were studied. For the elevated ICP group, artificial CSF (KCl 3.0 mmol/l, MgCl₂ 0.6 mmol/l, CaCl₂ 1.3 mmol/l, NaCl 131.8 mmol/l, NaHCO₃ 24.6 mmol/l, urea 6.7 mmol/l, and glucose 3.6 mmol/l) was infused in an external ventricular drain catheter at varying rates to achieve and maintain a steady-state ICP of ≈20 mmHg throughout the experiment [204], [206]. A 5F oesophageal balloon catheter (Cooper Surgical, Trundall, CT) was placed in the femoral veins and was gradually inflated by infusion of saline from a syringe pump slowly to lower CPP to 10 mmHg in both the naïve ICP group and elevated ICP group after achieving a steady state of mean ICP. The ABP was reduced continuously over the next three hours.

In both groups of experiments, ABP, ICP, and CBF were monitored continuously. ABP was transduced invasively with a clinical monitor (Marquette Solar 8000, GE Healthcare, Little Chalfont, UK). ICP was monitored through an external ventricular drain after craniotomy. Bilateral laser Doppler probes (Moor Instruments, Devon, UK) were placed to monitor CBF after additional craniotomies over each parietal cortex. The signals were all sampled at 200 Hz, digitized using an A/D converter (DT9801, Data Translation, Marlboro, MA), and were recorded using a laptop computer with ICM+® software (University of Cambridge, Cambridge Enterprise, Cambridge, UK, <http://www.neurosurg.cam.ac.uk/icmplus>). The data from both experiments were originally used in previous publications [204]–[206].

Data summary in different chapters

| Chapter | Data | M/F | Age | ABP |
|-------------|--|---------------------------|-------------------|---|
| Chapter 5.1 | 34 TBI patients data, 138 data recordings | 8 females and 26 males | 29 ± 16 years old | 82.0 ± 10.5 mmHg |
| Chapter 5.2 | 288 TBI patients | 66 females and 222 males | 33 ± 16 years old | 91.2 ± 11.9 mmHg |
| Chapter 6.1 | 12 piglets experimental data | / | / | Regular sinusoidal ABP oscillations were induced using modulated PEEP during ventilation. ABP was decreased through withdrawal. |
| Chapter 6.2 | 16 piglets experimental data | / | / | 8 piglets with naive ICP and 8 piglets with elevated ICP. |
| Chapter 6.3 | 515 TBI patients | 210 females and 305 males | 38 ± 16 years old | 94.8 ± 15.0 mmHg |
| Chapter 7.2 | 526 TBI patients | 219 females and 307 males | 38 ± 16 years old | 93.6 ± 8.3 mmHg |
| Chapter 7.3 | 427 TBI patients | 157 females and 270 males | 37 ± 16 years old | 93.3 ± 8.0 mmHg |
| Chapter 8.1 | 119 TBI patients, with 24 patients showed 30 plateau waves | 5 females and 19 males | 33 ± 13 years old | 94.2 ± 12.8 mmHg at baseline and 93.8 ± 11.5 mmHg at plateau |
| Chapter 8.2 | 12 patients | 3 females and 9 males | 27 ± 11 years old | 99.8 ± 17.0 mmHg at baseline and 96.7 ± 17.2 mmHg at plateau |

4.4 Statistical analysis

Statistical analyses were performed using the IBM SPSS Statistics (version 21 or version 19) software. The characters of relationships between various parameters were studied either using a linear regression method or non-

linear regression curve estimation method (polynomial regression and four-parameter logistic functions were employed). Pearson's correlation coefficient (r) was used to examine linearity of the relationships.

Independent-samples t-test was used to analyse the ability of different parameters in distinguishing patients' outcome groups (favourable versus unfavourable outcome, fatal versus non-fatal outcome). Results were considered as significant at $p < 0.05$.

When applicable, the receiver-operator characteristic curve (ROC) with calculation of the area under the curve (AUC) were used to compare the abilities of different parameters in distinguishing patients' outcome. Statistical differences between ROC curves were verified using DeLong's test for two correlated ROC curves (R package pROC) [207].

Bland-Altman plots were used to investigate the agreement between these parameters. In addition, R-software was used to test the statistical significance of the difference between the areas under the two ROC curves for different outcome groups. The specific statistical methods used in each project are described in detail in the respective chapters.

CHAPTER 5 RELATIONSHIP BETWEEN DIFFERENT CA PARAMETERS IN TBI

5.1 Cross-validation and cross-calibration of CA indices – a modelling study

5.1.1 Introduction

Accurate and quantitative assessment of CA is important, as transient episodes of cerebral ischaemia, or uncontrolled increases in CBF, are thought to be detrimental in a number of critical conditions, including stroke, subarachnoid haemorrhage and TBI [30], [113], [114]. As described in Chapter 3, many studies tried to assess CA using different methods. Initially, clinical studies mainly used ‘static’ methods to evaluate CA, which was assessed by analysing the CBF response to slow manipulations of ABP or CPP [5]–[8]. However, this process is not routinely applicable as it requires potentially harmful ABP manipulations [5]. Later on, TCD was introduced, which allowed dynamic CA assessment by analysing CBFV response to rapid changes in ABP, either externally induced or occurring spontaneously [9]–[11]. Most widely used methods for dynamic CA assessment includes ARI, Mx, transfer function analysis [19], [23], [132], [133]. As described in chapter 3, ARI grades FV response to changes in ABP into 10 levels. The Mx is a purely time-domain measurement, and has been shown to be associated with outcome in different patient groups [6], [114], [135], [136], [138], [140], [201]. In patients with no ICP monitoring, Mx is calculated using CBFV and ABP instead, and in the clinical literature this index is denoted as Mxa.

TFA assumes that functional CA can be described as a high-pass filter that readily transmits rapid (high-frequency) changes in ABP to CBFV, but attenuates the transmission of slower (LF) ABP perturbations to CBFV [159]. Parameters derived from TF include phase shift, gain and coherence [96], [160], [127], [129].

Although a few comparisons between these CA parameters have been published [22]–[29], they have been based on real measurements, which inevitably introduces confounding factors to the relationships, such as poor fit of the assumed models or the presence of unknown extraneous ‘noise’ [20], i.e. components in ABP and CBFV that are not related to each other. The potential for differential sensitivity of the CA indices to these confounding factors makes meaningful comparisons between the different methods difficult. To cross-validate the relationships between the CA indices in a more controlled environment, this study generated artificial CBFV according to Tiecks’ ARI model of CA [21] using real ABP signals from TBI patients as input. Using these signals, Mxa and TF parameters were calculated and compared with ARI values to elucidate the theoretical relationships between CA indices, undisturbed by unknown confounding factors. In addition, a varying degree of ‘exogenous’ noise was imposed on the simulated data to study its influence on these relationships.

5.1.2 Materials and methods

138 data recordings (lasting 30 minutes each) from 34 randomly selected patients suffering from TBI admitted in the NCCU, Addenbrooke’s Hospital, between 2003 and 2013 were retrospectively analysed. All recordings with available ABP were eligible for analysis. The inclusion criterion was invasive monitoring of ABP with at least half

an hour recording. All patients were sedated, ventilated and managed according to a CPP- and ICP-oriented protocols for management of head injury with CPP maintained at >60 mmHg and ICP < 20 – 25 mmHg [202].

Data monitoring

Data were collected as described in Chapter 4. Artefacts introduced by tracheal suctioning, arterial line flushing or transducer malfunction were removed. Data were recorded and analysed anonymously as part of a standard audit approved by the Neurocritical Care Users Group Committee.

Patients' demographics

The average age of this cohort was 28.8 years (standard deviation, SD, 15.9 years) with 8 females and 26 males. Mean ABP was 82.0 ± 10.5 mmHg (mean \pm SD) and average ICP was 19.9 ± 6.8 mmHg. The GOS scores at six months were distributed as follows: good outcome, $n = 10$ (29%); moderate disability, $n = 5$ (15%); severe disability, $n = 10$ (29%); persistent vegetative state, $n = 3$ (9%) and death, $n = 6$ (18%).

Data before 2000 were analysed under the approval of Addenbrooke's Hospital Neurocritical Care Unit Users Committee as part of an anonymised clinical audit. After 2000, informed consent was obtained from all patients (or their next of kin) for the use of collected data for research purposes. The study was approved by the relevant research ethics committee (29 REC 97/291).

5.1.3 Data analysis

Generation of artificial flow velocity waveforms

Artificial mean FV waveforms were generated according to the mathematical model proposed by Tiecks et al. [12] using real ABP recordings (Equations 3.1-3.4). The model provides a second-order high-pass filter representation of the relationship between ABP and CBFV that can be adjusted for different 'strengths' of autoregulation (graded by ARI). The strength of autoregulation is divided into 10 levels, according to a set of parameters: the time constant (τ), damping factor (D), and the autoregulatory dynamic gain (K) (Section 3.1.1).

Transfer-function phase, gain and coherence calculation

TF phase, gain and coherence between the real ABP and the generated flow velocities for the 138 recordings were calculated through the method described in chapter 3, Section 3.1.2. The analysis mainly focuses on two frequency ranges: very-low-frequency range (VLF, 0-0.05 Hz) and low frequency range (LF, 0.05-0.15Hz). We use gain_VLF as the abbreviation for gain in the VLF range, and gain_LF for the gain in the LF range. Similarly, phase_VLF and phase_LF refer to phase in the VLF and LF ranges, respectively, while coh_VLF and coh_LF stand for squared coherence in the VLF and LF ranges, respectively.

The generated FV and ABP were first normalized (mean subtracted, and divided by SD), and then divided into four data segments of 120-second duration (amounting to 50% segment overlap) and transformed with the FFT algorithm

(Welch method) [208], [210]–[213]. TF phase and gain between artificial CBFV and ABP were calculated in VLF and LF using the method described in Section 3.1.2. All the calculations were performed through a 300-second moving window and updated every 10 seconds.

Mxa calculation

The mean flow index (Mxa), time correlation coefficient between 10s averages of ABP and the artificial mean CBFV, was calculated using a 300s data window. All the parameters were averaged over each recording session for further analysis.

Adding noise to the artificial data and testing the robustness of CA parameters

To investigate the robustness of the examined parameters and their relationships in a more ‘real-life’ scenario, we simulated exogenous noise by adding coloured noise to the generated CBFV signals. We used a Gaussian white noise signal and filtered it using a low-pass filter (Butterworth) with the cut-off frequency at 0.2 Hz, and setting the signal-to-noise ratio (SNR) to 3 (the-low power noise), 0.9 (middle-power noise) and 0.3 (high-power noise).

Statistical analysis

SPSS software (version 19, IBM, Armonk, NY, USA) was used for statistical analysis. Curve fitting methods (polynomial regression and four-parameter logistic function) were used to describe cross-relationships between ARI, Mxa and TF parameters. Pearson’s correlation coefficient (r) was used to examine linearity of the relationship across certain value ranges. Results were considered significant at $p < 0.05$.

5.1.4 Results

Simulated cerebral blood flow velocity

Figure 5.1 shows one example of 10 normalized mean CBFVs (divided by the mean value of CBFV 9, upper panel) generated from a fragment of a real ABP signal recording (lower panel) using ARI ranging from 0 to 9. In the upper panel FV 0–9 correspond to ARI 0–9, respectively. Differences in amplitudes and phases of the waves are clearly visible.

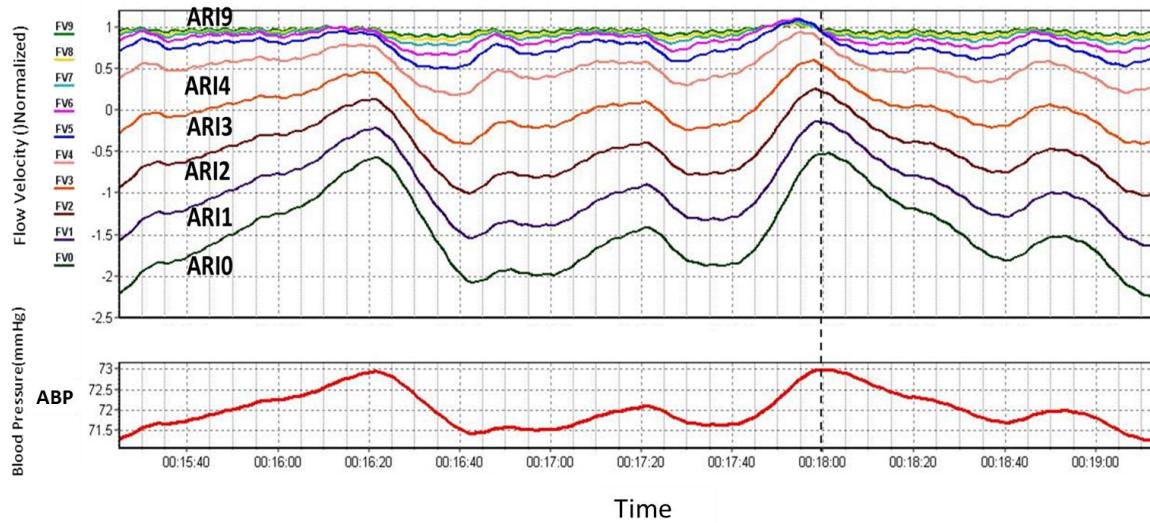


Figure 5.1 The real blood pressure (lower panel) and 10 artificial flow velocities (upper panel) generated for one patient. FV0 refers to the flow velocity generated according to the model with dysfunctional autoregulation (ARI 0). FV9 refers to the flow velocity generated in the model of ideal autoregulation (ARI 9). ARI: autoregulation index; FV: flow velocity.

Theory Relationship between ARI and Mxa

The relationship between ARI and Mxa through artificial data is shown in Figure 5.2. The non-linear character of the relationship can be captured using a 4-parameter logistic function: $Mxa = 1.02 - 0.69 / (1 + \exp(4.41 - ARI))$ ($r = 0.999$, Figure 5.2 A). From ARI 3 to ARI 6, the usual range of values seen in clinical practice, the relationship between these two indices is practically linear (Fig. 5.2 B, $Mxa = -0.151 \times ARI + 1.338$, $r = 0.885$).

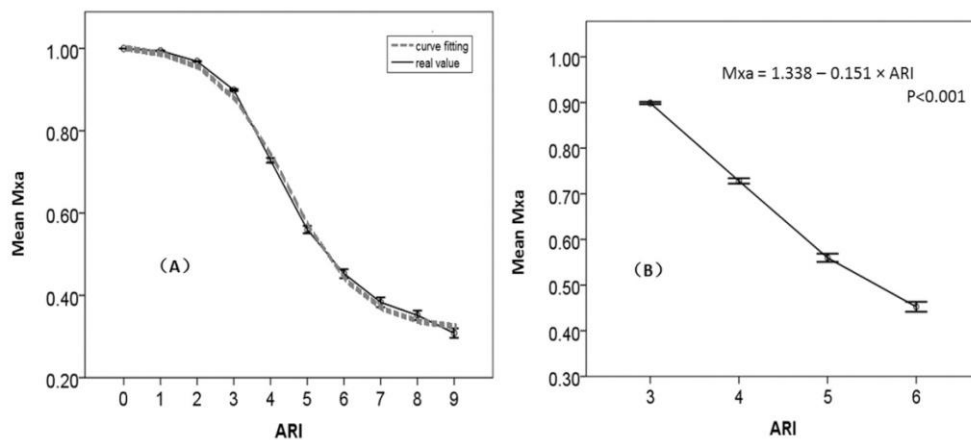


Figure 5.2 The relationship between mean Mxa and ARI. (A) The mean value of Mxa for different groups of artificial flow velocities generated from ARI0 to ARI9. (B) The mean value of Mxa from ARI3 to ARI6, and the

relationship is approximately linear between ARI 3 and 6. Mxa: mean flow index using arterial blood pressure as input; ARI: autoregulation index. Error bars: standard errors of the 138 simulated data.

Relationship between ARI and estimated TF parameters

Figure 5.3 describes the phase, gain and coherence relationships between ARI and TF in both VLF and LF ranges. There is a highly linear relationship between ARI and gain_VLF (Figure 5.3 A, $r = -0.995$, $p < 0.001$): $\text{gain_VLF} = 0.982 - 0.104 \times \text{ARI}$, and a non-linear, humped, relationship between ARI and gain_LF ($p < 0.001$).

Fig. 5.3 B depicts the relationship between phase and ARI. For both frequency ranges, this relationship is positive and highly monotonic. Furthermore, from ARI 3 to 6, it becomes almost purely linear ($\text{phase} = 13.82 \times \text{ARI} - 18.38$, $r = 0.986$ for the VLF range and $\text{phase} = 8.43 \times \text{ARI} - 13.89$, $r = 0.992$, for the LF range).

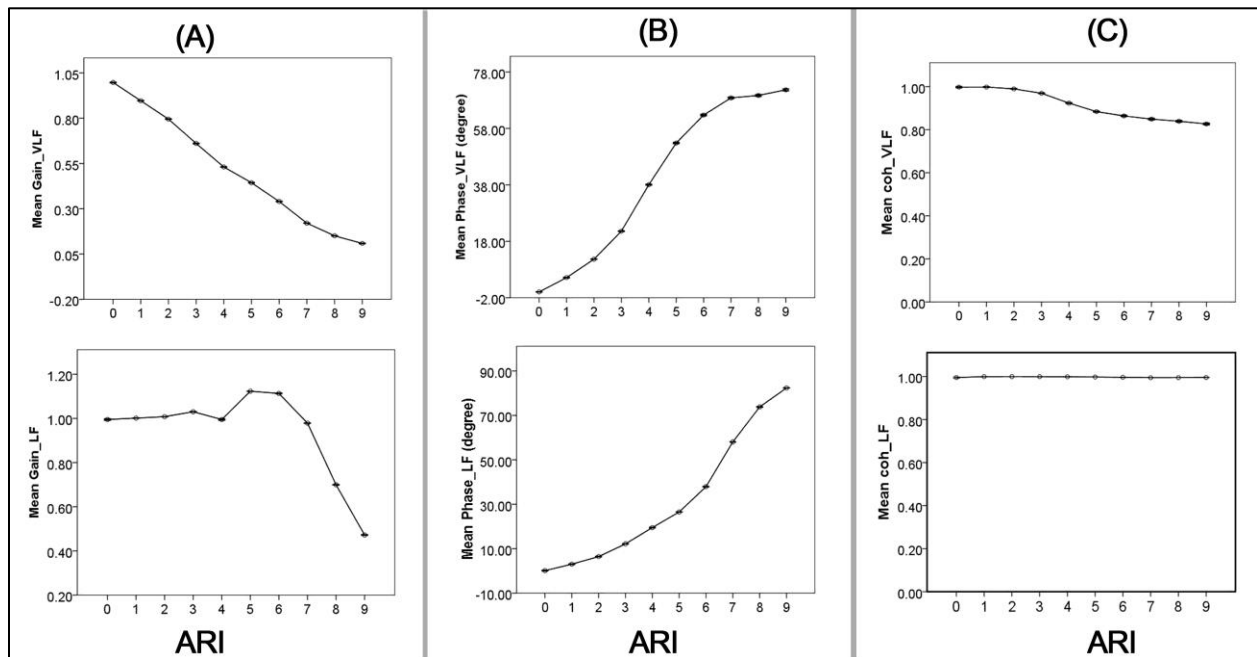


Figure 5.3 The relationship between ARI and the estimated transfer function parameters. ARI: autoregulation index; Gain_VLF: transfer function gain in very low frequency range; Gain_LF: gain in low frequency range; Phase_VLF: phase in very low frequency range; Phase_LF: phase in low frequency range; Coh_VLF: coherence in very low frequency range; Coh_LF: coherence at low frequency range. VLF: very low frequency range, 0-0.05 Hz; LF: low frequency range, 0.05-0.15 Hz. The points in the graphs are actually expressed as mean and error bar, however, as the data is simulated, the error is very tiny.

Relationship between Mxa and TF parameters

Figures 5.4 A to 5.4 C show the relationship between Mxa and estimated TF indices. A nearly linear, negative relationship exists between Mxa and Phase_VLF ($\text{Phase_VLF} = 106.13 - 99.24 \times \text{Mxa}$; $r = -0.941$), which is not quite the case for Mxa and phase_LF ($r = -0.894$). The gain in VLF was also monotonically, though not quite linearly, related to Mxa ($r = 0.928$), while the gain in LF did not show a consistent relationship with Mxa.

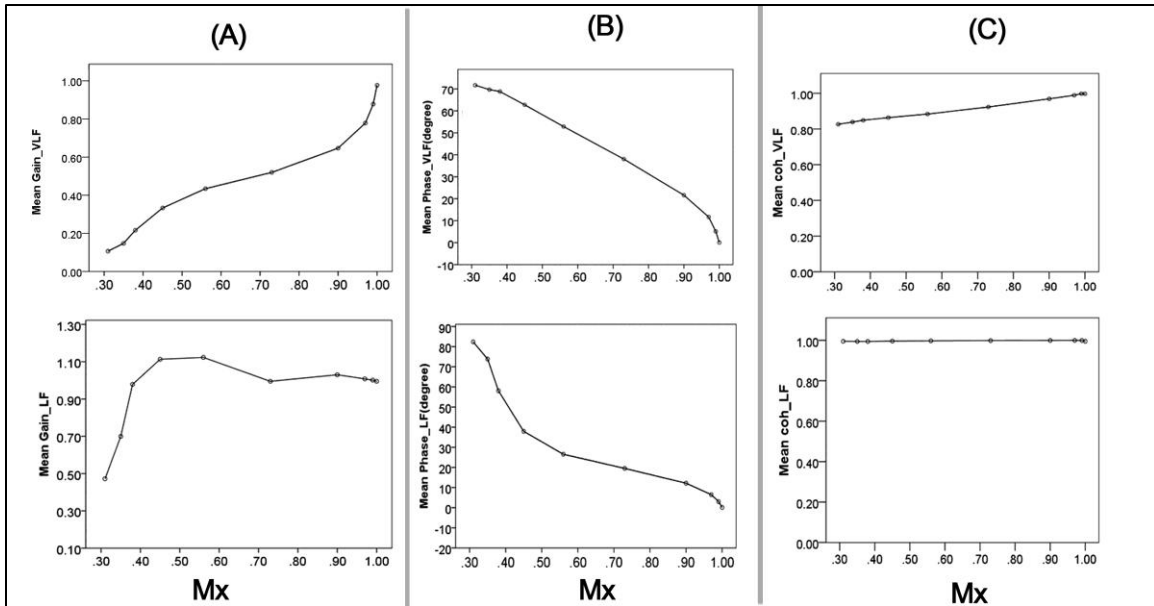


Figure 5.4 Relationship between Mxa with transfer function parameters. (A) The mean value of Mxa versus mean value of the gain in VLF and LF. (B) Mean Mxa versus the phase in VLF and LF. (C) Mean Mxa versus the coherence in VLF and LF. VLF: very low frequency (0-0.05 HZ), LF: low frequency (0.05-0.15 HZ). Mxa: mean flow index using ABP as input.

Analysis of the effects of exogenous noise

Figure 5.5 displays the relationship between Mxa and CBFV without noise as well as CBFV with three different levels of SNR corresponding to low-, middle- and high-noise power. Despite a general preservation of the overall character of the relationship between Mxa and ARI, the actual ‘steepness’ of this relationship, and its uncertainty, change with the different levels of noise.

Figure 5.5 D shows that, as expected, the coherence between ABP and CBFV decreased with noise added, furthermore, in the presence of noise, a clear monotonic relationship between the estimated coherence and ARI was revealed in the VLF range.

We also tested the relationship between estimated TF gain/phase and ARI under different levels of added noise (Figure 5.5, Table 5.1). With increased noise, more uncertainty was introduced into the CA parameter estimates, demonstrated by the increase in their standard errors. With the artificially calculated data, gain_VLF and gain_LF were increased while the noise was increased (Figure 5.5 B). The character of the relationship between TF phase and ARI remained almost the same, while the values were generally decreased in both the VLF and LF bands.

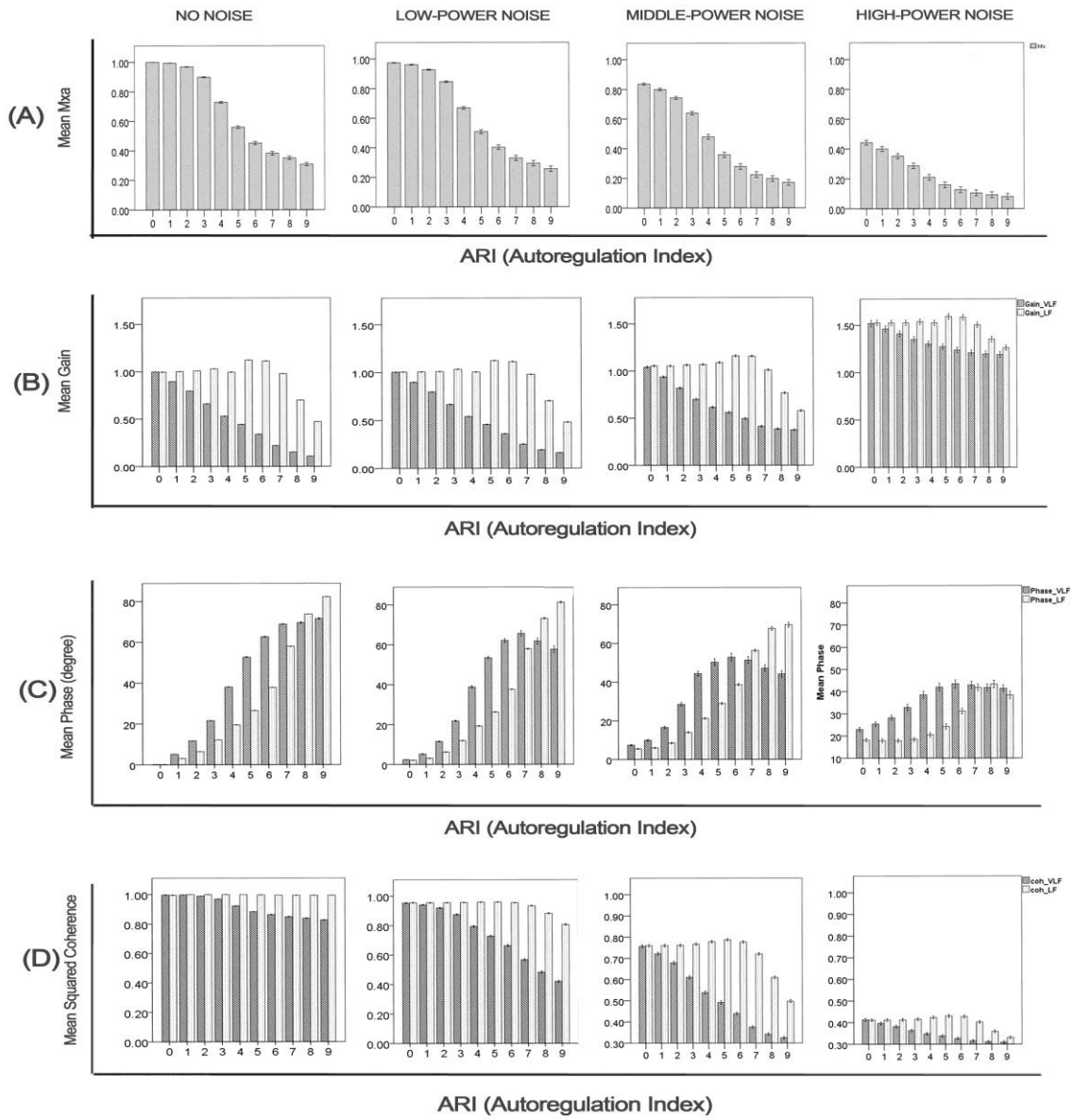


Figure 5.5 The relationships between Mxa, TF parameters and ARI with different intensities of added noise. In the panel grid, rows (from top to bottom) represent different indices: Mx, Gain, Phase and Coherence, and columns (from left to right) represent increasing intensity of noise. Black bar: VLF; Grey bar: LF. Mxa: mean flow index; ARI: autoregulation index; TF: transfer function. Error bars: standard error.

Table 5.1 The Pearson correlation coefficient (r) between ARI and other cerebral autoregulation parameters.

| | No Noise | Low Noise | Middle Noise | High Noise |
|-----------|----------|-----------|--------------|------------|
| Mxa | -0.926 | -0.88 | -0.802 | -0.519 |
| Gain_VLF | -0.995 | -0.983 | -0.889 | -0.298 |
| Gain_LF | -0.599 | -0.6 | -0.532 | -0.183 |
| Phase_VLF | 0.973 | 0.858 | 0.674 | 0.373 |
| Phase_LF | 0.966 | 0.95 | 0.917 | 0.547 |
| Coh_VLF | -0.934 | -0.924 | -0.87 | -0.425 |
| Coh_LF | -0.133 | -0.594 | -0.549 | -0.243 |

ARI: autoregulation index. TF: transfer function; Mxa: mean flow index using ABP as input; VLF: 0–0.05 Hz; LF: 0.05–0.15 Hz. Black: TF parameters in VLF; the p values for all the parameters in this form are below 0.01. Gain_VLF, Phase_VLF and Coh_VLF refer to gain, phase and squared coherence in the VLF range; Gain_LF, Phase_LF and Coh_LF refer to gain, phase and squared coherence in the LF range.

5.1.5 Discussion

This section used artificial data to explore rigorously the interrelationships between the commonly cited CA methodologies –TF analysis, non-parametric modelling and time-based correlation. Using this approach, the studied indices were cross-validated against each other to elucidate the true relationships between CA estimates; a relationship fully independent from the assumptions and uncertainties that plague experimental or clinical data. Finally, how these indices behave in response to sequential exogenous noise was investigated to explore the robustness of each CA index. Together, these analyses add insights to both the interpretation of previously published literature and the design of future cerebral haemodynamic investigations.

Mxa versus ARI

The character of the relationship between Mxa and ARI confirmed the general interchangeability of these two indices. However, because the actual shape of the relationship follows an inverted ‘S’-shape curve, Mxa may only be useful for grading CA in the middle range (ARI 2 to 7) because it saturates outside of this range (Figure 5.2). For noise-free simulation, the range that Mxa can be used as a scale is between 0.38 and 0.90, which equates to ARI 3 to 6. However, in practice, as shown by our noise simulations, one should expect this range to shorten and shift towards lower values of Mxa (Figure 5.6).

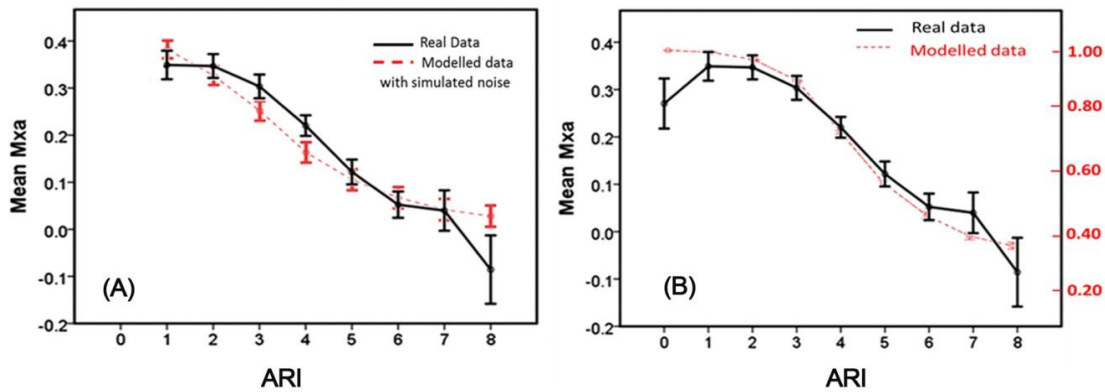


Figure 5.6 Comparison of Mxa-ARI relationship between real data and modelled data. The real curve measured in a cohort of TBI patients (solid black) is plotted against (A) curve obtained using modelled data under high-power noise conditions (red dashed line); and (B) against the pure, noise-free model generated curve, recalibrated using measured Mxa values for exhausted and intact autoregulation (red dashed line). ARI: autoregulation index; Mxa: Mean flow index using blood pressure as input.

Transfer function analysis versus ARI and Mxa

The phase showed a stable relationship with autoregulation indices in both frequency ranges. A negative, albeit non-linear, relationship between phase and ARI as well as phase and Mxa in both frequency ranges was demonstrated for ‘noise-free’ simulations. A roughly ‘S’-shape relationship exists between phase and ARI, with VLF showing a plateau for high ARI. The relationship between phase and Mxa was, as expected, inverse, and nearly linear for the LF range. This indicates that for a noise-free situation, a phase from 0 to 70 degrees in VLF and from 0 to 80 degrees in LF can be used to grade CA, with the former saturating at ARI of 7, while the latter spans the whole range of ARI. With ‘noise’ added, the relationship is flattened: the higher the noise power, the smaller the phase. This effect was particularly pronounced in the VLF range, while LF-derived phase kept its relationship to ARI relatively stable until high noise levels.

However, bearing in mind that values of ARI above 7 are unlikely to be observed in reality, and if they do occur their clinical significance is rather limited, the use of the LF or VLF range seems to provide equivalent information, as far as the relationship with ARI is concerned. Nevertheless, considering the highly non-linear relationship of the phase with Mxa in the LF region, our results seem to favour the use of the VLF range for the phase parameter.

The gain only showed a stable, non-linear relationship with ARI and Mxa in the VLF range. The higher gain was associated with lower ARI and higher Mxa. The gain in the LF band did not show a consistent relationship with either ARI or Mxa, and therefore its use in this range cannot be recommended. This relationship might be because the transfer function characteristics of Tiecks’ model shown in Figure 3.4, where the phase showed constant relationship with ARI, while gain demonstrated complex result with ARI in difference frequencies.

Simulated noise

By generating artificial CBFV data, the original analyses necessarily excluded all external noise from the CA estimates. To simulate a more realistic scenario and investigate the influences of the noise on CA assessment, we used three levels of intensity of added artificial noise (low-, middle- and high-power noise). How well such artificial noise approximates the real-world scenario of clinical CA assessment is not certain; however comparison with previously published data indicates that such artificial noise may be relevant [214]. In Figure 5.6 A, the relationship between ARI and Mxa using the noise-added artificial data of the current analysis is qualitatively similar to the relationship between ARI and Mxa derived from the real data of 288 TBI patients [214]. This reasonably good match between the noise-added simulated real data indicates that our rather simplistic approach provides a decent approximation to the exogenous noise seen in real data.

As expected, the intensity of noise has a big influence on all CA parameters, but particularly on the relationship between the coherence and ARI (Fig.5.5 D). On the one hand, in the presence of noise, notably at higher levels, there is a strong linear relationship between the VLF coherence and ARI seemingly providing justification for using coherence as a measure of CA (Table 5.2). However, the character of the coherence–ARI relationship changes dramatically at different noise intensities, and is almost completely flat in a noise-free model. This means using coherence to assess CA depends on having just the right amount of noise, which makes the applicability of coherence questionable.

The other TF parameters, Mxa and, their relationships to ARI were affected by the noise as well, to varying degrees. Interestingly, although the shape of the relationship curve between the parameters and ARI remained largely unchanged, the scaling was significantly affected. Therefore, in different ‘noise’ conditions (bearing in mind that by ‘noise’ we understand any exogenous process), the same TF parameter value or Mxa value will correspond to different ARI (i.e. strengths of autoregulation) levels. This can potentially explain the difficulties in comparing CA across different patient cohorts.

Recalibration of the various autoregulation indices according to the ‘background’ exogenous ‘noise’ for a particular patient population may therefore be necessary for consistent CA grading. This may not, of course, be a practical solution, as the level of ‘background noise’ will be unknown in reality, possibly varying and generally unmeasurable. However, if one, for example, compares the real Mxa–ARI characteristics measured in TBI patients with a curve obtained via simple recalibration of the pure model function using only two measured values of Mxa (for intact and exhausted autoregulation) in that cohort of patients (Fig. 5.6 B), it is easy to see the appeal of this sort of way of thinking.

5.1.6 Limitations

In this section, a particular model (Tiecks’ model) of CA was used to generate CBFV signals and whether it is the same as the noise-free physiological system still needs further investigation. Therefore, the relationships described will predominantly hold for that particular model and may not necessarily accurately reflect the actual relationships

in recorded datasets. However, the model has been shown to provide a good fit to the data recorded during leg-cuff tests, where a clearly defined stimulus (release of leg cuffs) was applied [215]. Furthermore, the observations in this section are rather generic for any type of high-pass-like relationship between ABP and FV and therefore the interpretations and recommendations are likely to hold in practice.

Finally, the representation of confounding exogenous processes and non-linear effects as an additive coloured Gaussian noise signal is a gross simplification. However, in the absence of a better model, this approach provides us with an adequate platform for investigating, at least qualitatively, the effects of these unknown factors on the performance and interrelationships of these CA indices.

5.1.7 Conclusions

This section explored theoretical relationships between the most commonly used indices of CA: ARI, Mxa and TF phase and gain. ARI, Mxa and TF phase (but not gain) were generally interchangeable while coherence should only be used with a full understanding of its interpretation and significance. The study also examined the influence of exogenous noise and highlighted the importance of considering the ‘recalibrating’ effects brought about by exogenous processes and model misfits.

5.2 Comparison of frequency- and time-domain methods of CA assessment in TBI

This study has been published as a full paper in the Journal of Cerebral Blood Flow & Metabolism [214].

The theoretical relationships and interchangeability of assessments of CA using ARI, Mx and TF parameters have been validated through the simulated data described above. However, how these commonly used parameters correlate with each other in real data analysis for TBI patients still needs further investigation. In this section, we analyse the relationship using real data. Moreover, the effects of different inputs (ABP or CPP) for CA assessment are also studied.

5.2.1 Materials and methods

A data base of 288 TBI patients admitted to the NCCU, Addenbrooke's Hospital in the United Kingdom between the years 2003 and 2013 (713 data recordings in total) was employed. The mean age of this population was 33 ± 16 years (mean \pm SD) and the mean Glasgow Coma Scale (GCS) at the scene was 6 ± 3 (mean \pm SD).

Daily TCD, used to monitor FV from the MCAs, was a part of the clinical assessment of the state of CA required by the clinical protocol. Data were recorded and analysed anonymously as part of a standard audit approved by the Neurocritical Care Users Group Committee. Patients were managed according to current institutional TBI guidelines [202], as described in Chapter 3. In brief, patients were sedated, intubated, ventilated and paralysed.

5.2.2 Monitoring and data analysis

ABP and CBFV were collected continuously as described in Chapter 4. ARI, PRx, TF phase, gain and coherence were calculated according to the method described in Sections 3.1.1-3.1.3. TF parameters mainly focused in two frequency ranges: 0–0.05 Hz (VLF) and 0.05–0.15 Hz (LF). Both ABP and CPP were used as input, and we use 'a' or 'c' for abbreviations (Table 5.2), for example, ARI_a refers to the ARI value between ABP and FV.

Table 5.2 Abbreviations used in this section

| Abbreviation | Full Name | Abbreviation | Full Name |
|--------------|--|--------------|---|
| Phase_a_VLF | Phase between ABP and FV at very low frequency | Phase_a_LF | Phase between ABP and FV at low frequency |
| Phase_c_VLF | Phase between CPP and FV at very low frequency | Phase_c_LF | Phase between CPP and FV at low frequency |
| Gain_a_VLF | Gain between ABP and FV at very low frequency | Gain_a_LF | Gain between ABP and FV at low frequency |
| Gain_c_VLF | Gain between CPP and FV at very low frequency | Gain_c_LF | Gain between CPP and FV at low frequency |
| Coh_a_VLF | Coherence between ABP and FV at very low frequency | Coh_a_LF | Coherence between ABP and FV at low frequency |
| Coh_c_VLF | Coherence between CPP and FV at very low frequency | Coh_c_LF | Coherence between CPP and FV at low frequency |
| ARic | Autoregulation index between CPP and FV | ARia | Autoregulation index between ABP and FV |
| Mxc | Mean flow index between CPP and FV | Mxa | Mean flow index between ABP and FV |

All autoregulatory indices were calculated from daily monitoring sessions and were then averaged for each patient, giving one value for each subject, which was compared with the patient's outcome later. The outcome was assessed with the GOS six months after injury via rehab clinic or phone interview, which we dichotomized into two groups: favourable group (good outcome, moderate disability) and unfavourable group (severe disability, vegetative state and death).

5.2.3 Statistical analysis

Statistical analysis was performed using the IBM SPSS Statistics (version 19) software. The cross-relationship between these autoregulation indices was studied using a non-linear regression curve-estimation method. The Pearson correlation coefficient r between these parameters was calculated. In addition, the independent-samples t -test was used to analyse differences in autoregulatory indices in the two outcome groups (favourable and unfavourable). Results were considered significant at $p < 0.05$.

5.2.5 Results

Patients' demography

Patients' demography were distributed as follows: good outcome, n = 75 (26%); moderate disability, n = 69 (24%); severe disability, n = 74 (26%); persistent vegetative state, n = 9 (3%) and death, n = 61 (21%). Fifty per cent of patients achieved a favourable outcome. An ARI value of 9 (both ARIa and ARIC) indicates hyperresponsive autoregulation, which is rarely seen in healthy subjects. In this study, fewer than eight ARI measurements of nine were observed. As this group was disproportionately smaller than other groups, it was excluded from further outcome analysis.

Table 5.3. Patients' Characteristics

| Index | Unit | Mean value | Standard Deviation |
|-------|------|------------|--------------------|
| ABP | mmHg | 91.24 | 11.93 |
| ICP | mmHg | 17.99 | 9.78 |
| FV | cm/s | 62.5 | 27.22 |
| CPP | mmHg | 73.2 | 12.8 |
| GOS | – | 2.69 | 1.44 |
| GCS | – | 6.6 | 3 |

ABP: arterial blood pressure; ICP: intracranial cerebral pressure; FV: flow velocity; CPP: cerebral perfusion pressure; GCS: Glasgow coma scale; GOS: Glasgow outcome scale.

Table 5.4 Mean Value of CA parameters

| | Mxa | Mxc | ARI a | ARI c | Phase_a (degree) | | Phase_c (degree) | | Gain_a | | Gain_c | | Coh_a (squared) | | Coh_c (squared) | |
|---------------|------|------|----------|----------|---------------------|------|---------------------|-------|--------|-----|--------|-----|--------------------|-----|--------------------|-----|
| | | | | | VL F | LF | VLF | LF | VLF | LF | VLF | LF | VLF | LF | VLF | LF |
| Mean value | 0.22 | 0.03 | 3.7 | 4.6 | 7.3 | 4.5 | -17.3 | -16.6 | 1.4 | 2.0 | 1.2 | 2.0 | 0.4 | 0.4 | 0.5 | 0.5 |
| S.D. | 0.23 | 0.29 | 1.7 | 2.1 | 24. 7 | 26.0 | 37.1 | 40.6 | 0.9 | 1.5 | 0.7 | 1.2 | 0.1 | 0.1 | 0.1 | 0.1 |

The relationship between parameters using CPP as input

The relationship between Mx and ARI using CPP as input is presented in Figure 5.7 A. ARI was significantly related to Mx, though non-linearly ($r = -0.404$, $p < 0.001$); from ARI = 0 to 2, Mx was constant, whereas from ARI 2–8 the relationship was strongly negative: $M_{xc} = 0.401 - 0.081 \times \text{ARIC}$ ($p < 0.001$, Figure 5.7 A).

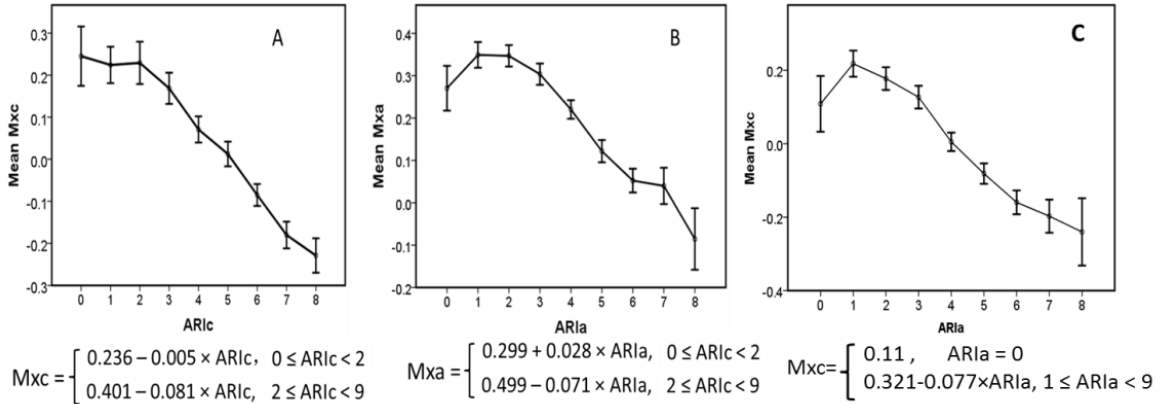


Figure 5.7 The relationship between ARI and Mx: (A) ARIC and Mxc (B) ARIa and Mxa (C) ARIa and Mxc. Error bars: standard deviation.

Of the TFs, only phase was correlated with ARI in the LF range ($p = 0.001$, $r = 0.126$, Figure 5.8 E), but not in the VLF range ($p = 0.235$, $r = -0.045$, Figure 5.8 B). The relationship between ARIC and phase_c_LF from ARIC = 1 to ARIC = 6, can be described by the linear model: $\text{Phase} = -28.68 + 4.22 \times \text{ARIC}$ ($p < 0.001$, Figure 5.8 E).

There was no significant relationship between ARIC and Gain_c in either of the frequency ranges ($p > 0.05$, Figure 5.8 A and Figure 5.8 D). No significant relationship was found between ARIC and squared coherence_c either ($p > 0.05$, Figure 5.8 C and Figure 5.8 F).

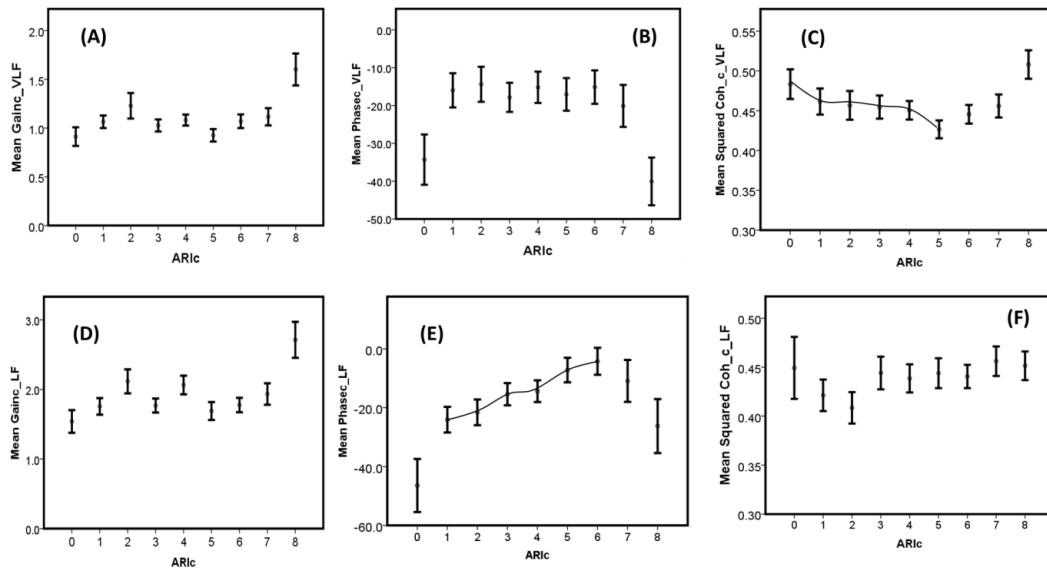


Figure 5.8 The relationship between ARic and Gain_c at VLF (A) and LF (B) as well as the relationship between ARic and Phase_c at VLF (C) and LF (D). Figures C and F show the relationship between ARic and squared coherence at VLF (E) and LF (F). VLF: very low frequency, 0-0.05 Hz; LF: low frequency, 0.05-0.15 Hz. The unit for phase is degree. Error bars: standard deviation.

The relationship between parameters using ABP as input

Using ABP as the input signal, the ARIa and Mxa were strongly correlated, presenting a significant negative, non-linear, relationship between them ($r = -0.38$, $p < 0.001$, Figure 5.9 B).

The relationship between ARIa and Mxc was also studied. A significant negative relationship between these two parameters is shown in Fig. 5.7 C ($r = -0.382$, $p < 0.001$). From ARIa = 1 to 9, the relationship can be described by a linear function: $Mxc = 0.401 - 0.081 \times ARIa$ ($p < 0.001$, Figure 5.9 C).

For TF parameters, ARI correlated significantly with phase_a in both VLF ($p < 0.001$, $r = 0.206$, Figure 5.9 B) and LF ranges ($p < 0.001$, $r = 0.291$, Figure 5.9 E). LF Phase_a and ARIa were linearly related: $Phase_a = -10.681 + 4.93 \times ARIa$ ($p < 0.05$, Figure 5.9 E). No obvious relationship between ARIa and Gain_a was found (Figure 5.9 A and Figure 5.9 D). The squared coherence_a was unrelated to ARIa at both frequency ranges (Figure 5.9 C and Figure 5.9 F).

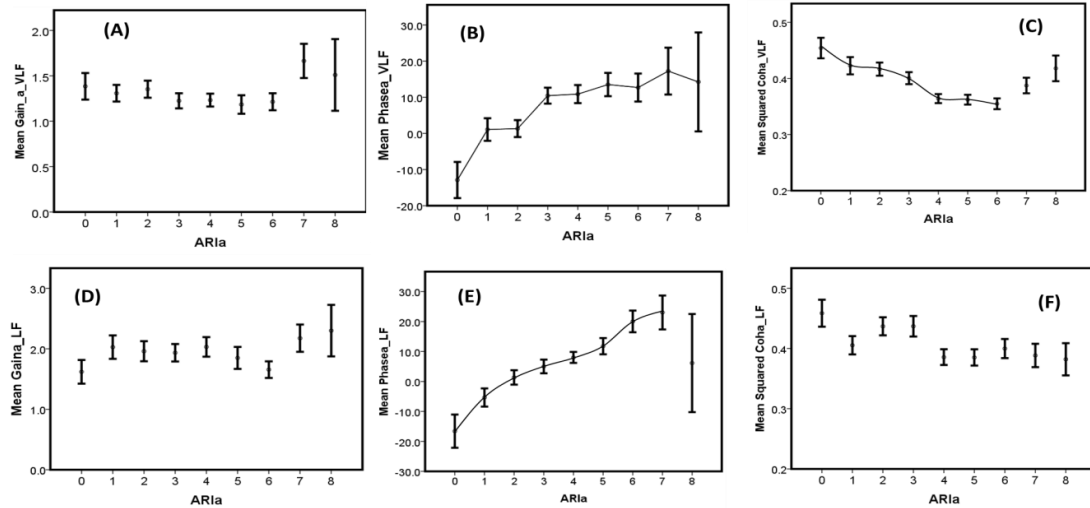


Figure 5.9 The relationship between ARIa and Gain_a at VLF (A) and LF (B) as well as the relationship between ARIa and Phase_a at VLF (C) and LF (D). E and F demonstrates the relationship between ARIa and squared coherence at VLF (E) and LF (F). VLF: very low frequency, 0-0.05 Hz; LF: low frequency, 0.05-0.15 Hz. Error bars: standard deviation.

Outcome analysis

Significant differences could be found in both ARI and Mx ($p < 0.05$, Figure 5.10) for the two groups of patients with dichotomized GOS scores (1–2: favourable or 3–5: unfavourable). Patients with favourable outcomes attained higher ARI values (ARIa: 4.09 ± 1.63 , ARIC: 4.89 ± 1.91) and lower Mx values (Mxa = 0.18 ± 0.24 and Mxc = -0.04 ± 0.29). For the unfavourable outcome group, mean ARI scores were lower (ARIa = 3.48 ± 1.64 , ARIC = 4.42 ± 1.97) and Mx scores were higher (Mxa = 0.26 ± 0.21 , Mxc = 0.09 ± 0.28). The differences between favourable and unfavourable outcome groups were greater for ARIa than for ARIC ($F = 9.56$; $p = 0.002$ and $F = 4.14$; $p = 0.043$, respectively). By contrast, Mxc showed much better performance in differentiating the two groups than Mxa ($F = 15.38$, $p < 0.0001$, $F = 10.08$, $p = 0.002$, respectively). Neither TF, gain, phase nor coherence showed any relationship with outcome in this cohort.

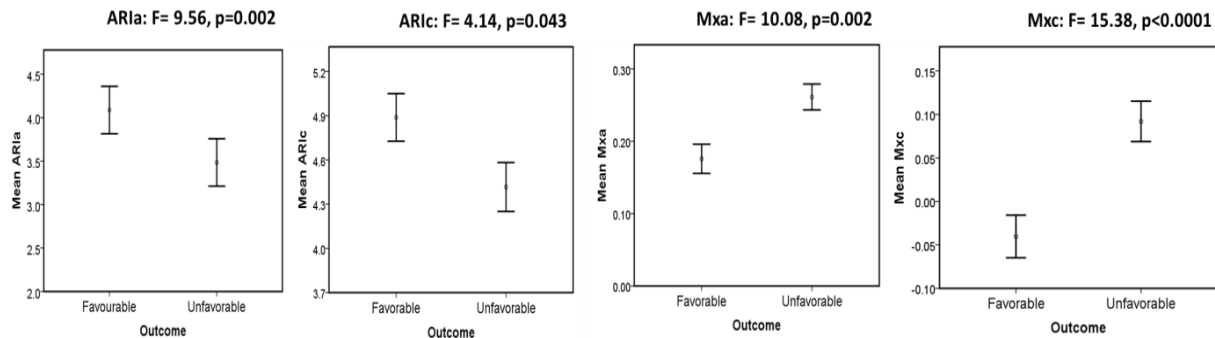


Figure 5.10 Mean values and SD in patients with favorable and unfavorable outcomes. (A) ARIa: ARI between ABP and FV; (B) ARIC: ARI between CPP and FV; (C) Mxa: Mx between ABP and FV; (D) Mxc: Mx between CPP and FV. Error bars: standard deviation.

5.2.6 Discussion

Mx and ARI as cerebral autoregulation indicators

Several methods for CA assessment using spontaneous fluctuations in ABP and FV (such as ARI, Mx, TF phase and gain) have been applied to patients with stroke, carotid stenosis and subarachnoid haemorrhage [139], [216], [217]. However, their application for TBI has not been fully validated. This paper compared the results of three important autoregulation monitoring methods in a cohort of TBI patients. The result showed a significant negative relationship between Mx and ARI. The linear relationship between ARI and Mx from ARI = 2 to ARI = 7 agreed with the findings in our previous study [201]. The finding that between ARI 0 to 2, Mx remained at ≈ 0.3 could indicate that 0.3 is the threshold for disturbed autoregulation and normal autoregulation, which was also found in a study by Sorrentino et al. [218].

Mx describes the stability of CBF in the face of CPP or ABP changes. It is a non-parametric, i.e. model-free, method and only assesses whether, and to what extent, variation in one parameter (pressure) is significantly associated with variations in the other (flow). It reflects the shape of Lassen's curve, with stable CBF within and pressure-passive CBF outside the limits of autoregulation. On the other hand, ARI explains how fast FV can recover from any changes in ABP or CPP and it is based on the mathematical model proposed by Tiecks. Therefore, as a parametric method, ARI depends on how accurately the model can reflect the physiology of the CBF autoregulation. Theoretically, if the assumptions are met, parametric methods will be more sensitive to changes in physiology than non-parametric methods. In this respect, if the Tiecks model describes the CA system accurately, ARI should perform with greater accuracy than Mx. On the other hand, if the model assumptions are not entirely met, a non-parametric method like Mx should give more reliable results. In the present study, the quality of fit of the estimated IR to the model, though satisfactory in most cases, was sometimes poor, suggesting assumption violation. Perhaps some sort of combination of these approaches might yield more satisfactory results.

Transfer function indices as cerebral autoregulation indicators

Many factors can cause rhythmic fluctuations in both ABP and ICP, such as pulse wave, respiratory wave and slow waves. However, the pulse wave and even the respiratory wave are too fast to engage CA effectively [129]. According to the 'high-pass filter' model, the variation in CBF due to changes in ABP would be effectively damped only in the LF range, and therefore LF waves are considered to be most relevant for testing/monitoring CA [210]. These slow waves can be generally classified further as A-waves, B-waves and C-waves [219]. A-waves, known also as 'plateau waves', are characterised by a steep increase in ICP reaching a plateau lasting for more than five minutes. B-waves, described originally by Lundberg, refer to the spontaneous fluctuations occurring in the frequency range of 0–0.05 Hz [219]–[221]. C-waves refer to oscillations with a frequency of 4–8 waves/min, often termed the Mayer (M) waves [219]. In this study, we chose two frequency ranges that include A-/B-waves (around 0–0.05 Hz) and M waves (0.05–0.15 Hz) to be our main targets for TFA.

TFA allows us to look at the character of transmission from input to output of a linear system at different frequencies. The TF characteristics are always described via two components: phase and gain. Theoretically, increases in steady-state cerebrovascular resistance or decreases in vascular compliance during cerebral vasoconstriction should be directly reflected in changes in gain and phase of the TF [222]. In this study, however, we found that only phase was consistently related to the strength of autoregulation as measured by ARI. A linear relationship existed between ARI (in the range of 1 to 6) and phase at LF range. This suggested that, at least in our cohort of patients, the model is best applicable to the frequency range of 0.05–0.15 Hz. The VLF cerebral FV may contain cerebral vasomotion itself rather than being a pure response. In contrast, as demonstrated in Figure 5.8 and Figure 5.9, there was no relationship between gain and ARI. This might potentially be explained by the nature of TF characteristics in Tiecks' model (Figure 3.2). In Tiecks' model, phase increases along with the increase of ARI across the frequencies of interest. In contrast, gain does not have a uniform relationship with ARI; at lower frequencies, lower gain corresponds with higher ARI, whereas at higher frequencies, higher gain corresponds with higher ARI.

Predictors of patients' outcome

Many investigations have indicated that the failure of CA after TBI is associated with a poor outcome [12], [131], [223], [224]. From this aspect, any reliable parameter that is claimed to assess CA should also have a significant relationship with patients' outcome. To test this notion on the studied parameters, autoregulation monitoring results were compared with GOS scores taken at six-month post injury. We demonstrated a significant reduction in ARI and an increase in Mx from favourable to unfavourable outcome. This was verified in a large sample, the previous findings that both ARI (AR_{Ia} and AR_{Ic}) and Mx (M_x_a and M_x_c) were significantly associated with outcome [201].

Mx, contrary to the other approaches studied here, is a non-parametric method, except for the fact that it requires prior removal (smoothing) of high-frequency variations (like pulse and respiratory component). In this study, M_x_c performed better than AR_{Ia}, indicating that its qualitative nature is on average more robust than linear modelling for CA assessment in TBI. Indeed, according to Lassen's curve, the relationship between CBF and CPP shows that CBF stays flat, constant, within the autoregulatory range. It is at the lower and upper limits of CA that the relationship becomes highly non-linear [225]. For TBI patients, the plateau length of Lassen's curve might be shortened to a great extent, thus making it more likely for CPP to be within the non-linear part. Therefore, linear modelling (Tiecks) may be less applicable for CA analysis in TBI. Mx, being more a qualitative than a quantitative method, is probably less sensitive to those effects.

Moreover, the actual 'driving force' of the CBF is CPP, not ABP alone. In patient populations where no pathology of increased ICP is expected, changes in CPP and ABP practically amount to the same thing. However, the same cannot be said for TBI, where intracranial-hypertension-induced high-amplitude ICP waves are common. In those patients, neglecting ICP effects will lead to increased estimation errors, illustrated by the fact that M_x_c showed a better correlation with the outcome than M_x_a. This is in agreement with a previous study of Lewis et al. [226].

Nevertheless, ARI showed better association with the outcome than using ABP alone. This effect is a little puzzling but is perhaps a consequence of a further violation of the linearity assumption of the underlying CA model introduced by the ICP-moderated feedback mechanism (explored by the popular PRx index [21], [37]). This, coupled with the lack of any association of phase and gain parameters to outcome may perhaps suggest that linear ‘high-pass filter’ model-based approaches to assessment of CA do not perform very well in severe TBI patients.

Limitations

In this study, the TCD technology was used to monitor FV for CA assessment. Because of issues with probe repositioning and fixation, it is currently only practical to make intermittent (e.g. daily) short recordings of FV and prolonged monitoring over hours and days is unfeasible. In TBI patients, with their highly dynamic course of pathology over the first few days post injury, such intermittent measurements are likely to miss the development of transient pathological processes, e.g. plateau waves, that are likely to affect the final outcome, thus weakening the associations to outcome measures. More frequent TCD examinations or development of self-focusing/adjusting ultrasound probes seem to be the only ways these problems can be overcome.

Finally, blood FV of MCA was used as a surrogate for CBF on the basis that the diameter of MCA remains constant during the monitoring period. However, there are still some ongoing discussions about the influences of diameter changes of MCA affecting the pressure–flow relationship. Many researchers have demonstrated that CBF velocity measurements correlated closely with changes in CBF in healthy volunteers and patients with extracranial or intracranial artery stenosis [13], [227]–[229], but whether this is also the case in severe TBI is not entirely certain.

Conclusion

This second study confirms that the IR-based ARI correlates significantly with the time correlation-based index Mx in TBI patients. Both parameters are significantly related to patients’ outcome, although Mx correlates more strongly than ARI. There is also a linear relationship between ARI and phase in the frequency range of 0.05–0.15 Hz. The TF parameters (phase and gain) have a poor relationship with the outcome; we cannot, therefore, recommend them for autoregulation measurements.

5.3 Conclusion

This chapter confirms the relationship between commonly used parameters for CA assessment through both simulated data and real TBI patients’ data. The results showed that the IR-based ARI correlates significantly with the time correlation-based index Mx. Both parameters are significantly related to patients’ outcome, although Mx correlates more strongly than ARI. There is also a linear relationship between ARI and phase in the frequency range of 0.05–0.15 Hz. The TF parameters (phase and gain) have a poor relationship with the outcome; we cannot, therefore, recommend them for autoregulation measurements.

CHAPTER 6 INTRODUCTION OF A NEW, TIME-FREQUENCY ANALYSIS METHOD FOR CA ASSESSMENT

6.1 Introduction

The interrelation between ABP, ICP and FV provides information about the functioning of CA[77], [128], [230]–[233]. However, the methods mentioned in the previous chapter, such as Mx, TF, ARI are either simple correlation indices or are assumed to be suitable for linear signal analysis. This chapter introduces a new time–frequency analysis method for CA assessment, the wavelet transform, which is suitable for non-stationary, noisy signal analysis. It is able to perform local analysis and reveal signal features with desired temporal–frequency resolution in different frequency ranges using a window of variable width [34], [151],[25], [26].

In this chapter, the WT algorithm is introduced as a fundamental method for CA assessment. WTP is calculated with WTC as a threshold, determined through a quantitative analysis using amplitude-adjusted ABP and ICP surrogate signals from more than 10000 computer simulations. A validation study was conducted on two cohorts of experimental piglet data. Then, the method was implemented into our own software ICM+® (University of Cambridge, Cambridge Enterprise, Cambridge, UK, <http://www.neurosurg.cam.ac.uk/icmplus>). Afterwards, the wavelet method was applied to 515 TBI patients and compared with traditional PRx. The relationship between the two parameters with patients’ outcome was also studied. Figure 6.1 describes the framework of this chapter.

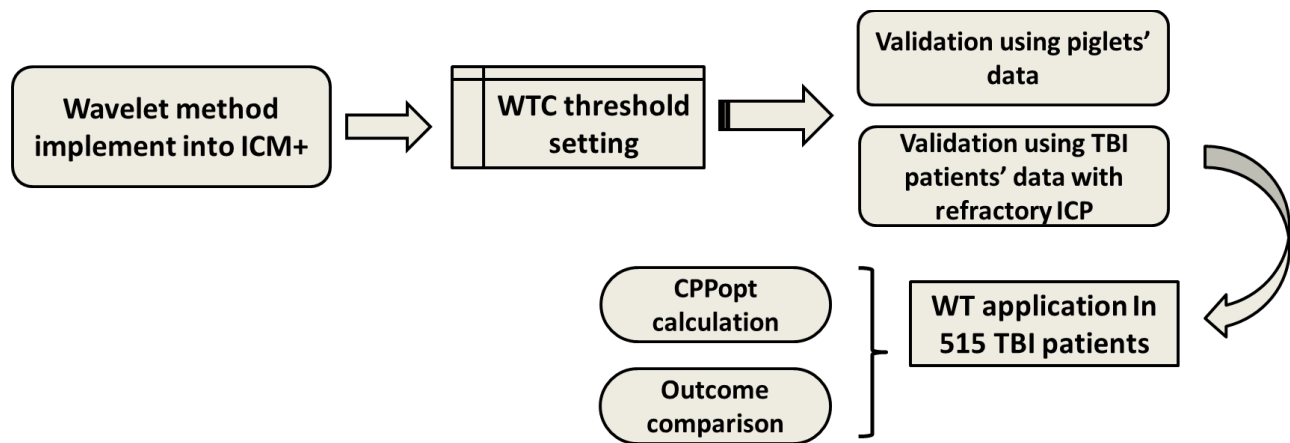


Figure 6.1 Flow Chart of chapter 6. WTC, wavelet transform coherence; TBI, traumatic brain injury; WT, wavelet transform; CPPopt, optimal CPP value.

6.2 Validation of Cerebral Autoregulation Assessment Using Wavelet Method

Paper submitted to JCBFM (December 2016)

6.2.1 Introduction

The aim of this study was to introduce wavelet-transform based method for CA assessment using continuous measurements of ABP and ICP and to validate the calculation of the wavelet method with PRx, a well-established CA index.

6.2.2 Materials and methods

Materials and Data recordings

Two separate cohorts of subjects were analysed for this study, one with induced, sinusoidal ABP waves at a frequency of 1/min and another with spontaneous ABP wave activity. The stability of the PRx in time series was tested, and the SNR is improved by the use of controlled ABP wave activity [205]. This is mainly due to inadequate coherence between ABP and ICP. Low coherence between the ABP and ICP can result from physiologic events unrelated to autoregulation that can affect the ABP, ICP or, both. Periods without wave activity within the frequency range of the autoregulatory mechanism also have low coherence between ABP and ICP and result in random noise in the PRx. To examine the influence of those random effects on the relationship between the wPRx and PRx, we performed analysis first on a dataset from experiments with induced high-amplitude waveforms in ABP [205] and then repeated the analysis in a set of experiments with spontaneous ABP waves only [206].

The hypotension experiment procedure was described in detail in Chapter 4. In the first set, the data were collected from 12 piglets, where regular, sinusoidal, ABP oscillations were induced using modulated PEEP during volume-controlled ventilation [205]. A primary wave with a fixed tidal volume of 50 cc at a rate between 15 and 25 min⁻¹ was applied to a customized ventilator (Impact Instrumentation, West Caldwell, NJ). A secondary wave component in a sine-wave pattern of one minute period was introduced into the PEEP control. Once stable recording was obtained, the piglets were haemorrhaged by syringe-pump withdrawal at a rate of 12% calculated blood volume/h, which allowed the procedure of gradual ABP reduction over 3–4 hours before demise. For later analysis, this group was labelled the PEEP Group.

In the second group, only spontaneous ABP and ICP signals from 16 piglets with naïve (n = 8) or elevated ICP (ICP = 20 mmHg, n = 8) were studied. A 5F oesophageal balloon catheter (Cooper Surgical, Trundall, CT) was placed in the femoral veins and was gradually inflated by infusion of saline from a syringe pump slowly to lower CPP to 10 mmHg in both the naïve ICP group and elevated ICP group after achieving a steady state of mean ICP. The ABP was reduced continuously over the next three hours. Later, this group was labelled as the non-PEEP Group.

All procedures were approved by the Johns Hopkins University Animal Care and Use Committee or the Baylor College of Medicine Animal Care and Use Committee and conformed to the standards of animal experimentation of the National Institutes of Health [154].

In both groups of experiments, ABP, ICP and CBF were monitored continuously through the method described in Section 4.3. ABP was transduced invasively with a clinical monitor (Marquette Solar 8000, GE Healthcare, Little Chalfont, UK). ICP was monitored through an external ventricular drain after craniotomy. Bilateral laser Doppler probes (Moor Instruments, Devon, UK) were placed to monitor CBF after additional craniotomies over each parietal cortex. The signals were all sampled at 200 Hz, digitized using an A/D converter (DT9801, Data Translation, Marlboro, MA), and recorded using a laptop computer with ICM+® software (University of Cambridge, Cambridge Enterprise, Cambridge, UK, <http://www.neurosurg.cam.ac.uk/icmplus>). The same software was later used for the retrospective analysis of all stored signals. The data from both experiments were originally used in previous publications [204]–[206].

Methodology

The continuous WT is defined as the convolution of a scaled mother wavelet function φ with the analysed signal $g(t)$,

$$W(s, \tau) = \int g(t) \varphi_s(t - \tau) dt \quad (\text{Equation 6.1})$$

In order to get the phase information, the most commonly used mother wave, the complex Morlet wave was applied, which is a Gaussian function modulated with a complex sinusoid, defined as

$$\varphi_0(t) = \pi^{-\frac{1}{4}} (e^{i2\pi f_0 t} - e^{-(2\pi f_0)^2/2}) e^{-t^2/2} \quad (\text{Equation 6.2})$$

where f_0 is the central frequency of the mother wavelet, t is time. The second term in the brackets is known as the correction term, as it corrects for the non-zero mean of the complex sinusoid of the first term [151]. In practice it becomes negligible and can be ignored when $f_0 \gg 0$, in which case, the Morlet wavelet can be written in a simpler form as [151]

$$\varphi_0(t) = \pi^{-\frac{1}{4}} e^{i2\pi f_0 t} e^{-t^2/2} \quad (\text{Equation 6.3})$$

We define the scale s as

$$f = f_0/s = w_0/2\pi s \quad (\text{Equation 6.4})$$

where w_0 is the reference coefficient, $w_0 = 2\pi f_0$, which shifts the balance between frequency resolution and time resolution.

Therefore, the wavelet function based on the Morlet wavelet function can be expressed as

$$\varphi(t/s) = \pi^{-\frac{1}{4}} e^{i\omega_0 t/s} e^{-(t/s)^2/2} \quad (\text{Equation 6.5})$$

The discrete form of the CWT of a sequence x_n is

$$W_n(s) = \sum_{n'=0}^{N-1} x_{n'} \varphi^* \left[\frac{(n'-n)\delta t}{s} \right] \quad (\text{Equation 6.6})$$

$$\varphi \left[\frac{(n'-n)\delta t}{s} \right] = \left(\frac{\delta t}{s} \right)^{\frac{1}{2}} \varphi_0 \left[\frac{(n'-n)\delta t}{s} \right] \quad (\text{Equation 6.7})$$

where φ^* is the complex conjugate of the normalized wavelet function; n is the time-series index, and δt is the sampling time.

The wavelet power density estimator of x_n is defined as $A = W_n(s)W_n(s)^*$, $W_n(s)^*$ is the complex conjugate of $W_n(s)$. The complex argument of the time series $W_n(s)$ gives a representation of the instantaneous phase of x_n .

The finite length of the analysed signal results in so called edge artefacts of WT. It is therefore, useful to introduce an index, the Cone of Influence (COI), in which the edge effect is significant and the power spectrum should be considered as dubious. For the Morlet wave, the COI is $s\sqrt{2}$, where the wavelet power for discontinuity at the edge drops by a factor of e^{-2} [205], [234]. The points within the edge effect area were removed prior to the phase/coherence point extraction. COI is larger for larger s .

The cross-wavelet transform

The cross-wavelet transform (XWT) of two time series x_n and y_n is defined as

$$W^{XY} = W^X W^{Y*} \quad (\text{Equation 6.8})$$

where $*$ denotes complex conjugation. The complex argument $\text{pha}(W^{xy})$ can be interpreted as the instantaneous phase difference between x_n and y_n in time-frequency space [155], [205], [210].

Wavelet transform coherence

WTC can be used to find correlated areas in time-frequency space of two signals. The squared WTC estimator is defined as the squared absolute value of the smoothed cross-wavelet spectrum, normalized by the smoothed wavelet power spectrum of the two signals,

$$C_n^2(s) = \frac{|\langle W_n^{xy}(s) \cdot s^{-1} \rangle|^2}{\langle W_n^{xx}(s) \cdot s^{-1} \rangle \langle W_n^{yy}(s) \cdot s^{-1} \rangle} \quad (\text{Equation 6.9})$$

where W_n^{xx} and W_n^{yy} are the wavelet spectral density functions, W_n^{xy} is the cross-wavelet spectrum and the angular brackets indicate the smoothing operator. This definition of the wavelet coherence corresponds to the Fourier-based coherence and maintains its value between 0 and 1.

The smoothing operator is achieved by a convolution in time and scale.

$$S(W) = S_{\text{scale}}(S_{\text{time}}(W_n(s))) \quad (\text{Equation 6.10})$$

where S_{scale} denotes smoothing along the wavelet scale axis and S_{time} means smoothing in time. The time convolution is performed with a Gaussian $e^{-n^2/2s^2}$, which is the absolute value of the wavelet function in each scale. The time convolution will double the edge artefact to $2s\sqrt{2}$. The scale convolution is performed by a rectangular window with a length of $\sigma_{j_0} \cdot s$, where $\sigma_{j_0} = 0.6$ is the empirical scale decorrelation length for the Morlet wavelet [235],

$$\langle W \rangle = [(c_1 w_n(s) * e^{-n^2/2s^2})_n * c_2 \Pi(\delta_{j_0} s)]_s \quad (\text{Equation 6.11})$$

c_1 and c_2 are normalization factors and Π is the rectangular function.

Wavelet coherence threshold evaluation

The Monte Carlo-simulations approach was used to evaluate the distribution of estimated wavelet coherence values corresponding to two uncorrelated signals. As described by Faes [236], coherence threshold levels depend on the choice of the surrogate signals used and their similarity to the analysed signals. To improve the accuracy of the analysis, we made the inputs of the simulation resemble the investigated signals of ABP and ICP as much as possible. This was done by randomly selecting a sample of 14 recordings from the experimental piglets' data, and generating amplitude-adjusted Fourier transform surrogates of real ABP and ICP, with amplitude kept but phase randomized through white noise generator [237]. By doing this, we could generate a test distribution of WTC values between ABP and ICP signals, in which the internal relationship has been destroyed [238].

Theoretically, the estimated WTC of such pairs of signals should be close to 0. The simulations were conducted 10000 times and WTC in the band of 0.0067–0.05 Hz was calculated. If the actual value of WTC was higher than the 95% of WTC values obtained in this artificial unrelated surrogate distribution, the WTC value was assumed to be high enough to indicate a significant relationship between input and output. We then estimated the significance level for each scale or central frequency, which equals angular frequency (w_0) divided by 2π . Four w_0 s were tried, namely, 2π , 10, 20 and 30 radians/second.

In the subsequent calculations, the estimated 95% confidence WTC threshold was used to reject corresponding phase values, which were deemed unreliable.

Wavelet transform pressure reactivity index (wPRx)

WTP between ABP and ICP in the frequency range 0.0067 Hz to 0.05 Hz was calculated through complex wavelet transform, described above. The Morlet mother wave was applied with the central frequency set at 1 Hz. A 500-second window was used to calculate WTP, and updated every 10 seconds. WTC was used to reject corresponding unreliable phase values, with the threshold calculated through the Monte Carlo-simulations approach (described above). Random noise is generated when the phase shift is calculated between two incoherent signals, thus coherence analysis acts as a filter to remove epochs with inadequate waveform activity for autoregulation analysis. Individual WTP values with WTC higher than the threshold were recorded, while the WTP values obtained with WTC lower than the threshold were deleted. The cosine of WTP was calculated afterwards, labelled as the wavelet-transform pressure reactivity index (wPRx), which limited the wPRx range between -1 (180 degrees phase shift) to $+1$ (0 degrees phase shift), and rendering a metric with direct correspondence to PRx. In addition, the cosine operation offers a practical solution to the problem of phase wrapping.

Determining the Lower Limit of Autoregulation for the piglet data

To compare the performance of PRx and wPRx, we measured the accuracy of wPRx and PRx to detect CPP below each subject's individual LLA derived from laser Doppler cortical blood flow monitoring. Delineation of the LLA with this experimental protocol using laser Doppler recordings has been described previously [204], [239]. Briefly, a scatter plot of one-minute average laser Doppler flow versus CPP was made for each piglet. The CPP at the left intersection of two lines defined by a piecewise linear regression model is defined as LLA (Fig. 6.2). When CPP is below LLA, the subject is asserted to have impaired CA and when CPP is above LLA the subject is asserted to have intact CA.

To delineate the accuracy of PRx and wPRx to detect CPP below LLA, both metrics were categorized and averaged in 5-mmHg bins of CPP for each piglet.

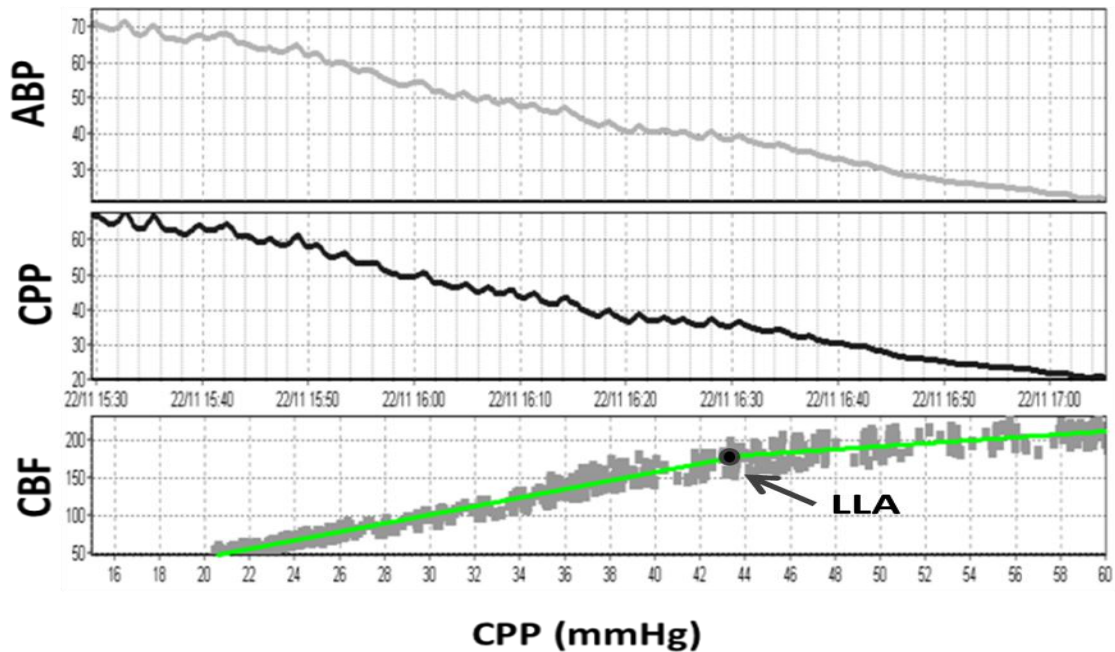


Figure 6.2 Demonstration of lower limit of autoregulation (LLA) using laser Doppler cerebral blood flow (CBF) and cerebral perfusion pressure (CPP) as a breakpoint between two linear sections estimated using the least mean square distance.

Pressure reactivity index (PRx)

The PRx was calculated according to previously published methods. First, ABP and ICP were filtered to remove pulse and respiratory frequency waveforms with 10 second averaging. A moving Pearson's correlation coefficient of 30 consecutive samples (300 seconds) renders the standard PRx [21]. In addition, we repeated the same calculation using a 500-second moving window (50 samples per PRx) for direct comparison to the wPRx which is done with a 500 second calculation period.

Statistical analysis

SPSS software (version 21, IBM, Armonk, NY, USA) was used for statistical analysis. Linear regression was used to describe relationships between PRx and wPRx. Pearson's correlation coefficient (r) was used to examine the linearity of the relationship. The independent-samples t-test was used to analyse the ability of PRx and wPRx in distinguishing intact CA (CPP above LLA) and impaired CA (CPP below LLA). A ROC test was also done, rendering an area under the ROC curve (AU-ROC) for each parameter. Statistical differences between AU-ROC were verified using DeLong's test for two correlated ROC curves (R package pROC) [157]. Bland-Altman plots

were used to investigate the agreement between the two variables. The Kruskal–Wallis test was used to compare the SDs of PRx and wPRx. The results were considered significant at $p < 0.05$.

6.2.3 Results

Wavelet transform calculation

A representative example of WTP and WTC between ABP and ICP from a single experimental dataset is shown in Fig. 6.2. With gradually decreased ABP (Fig. 6.3a), the phase shift between ABP and ICP showed a coupling decrease over time at the frequency of the input PEEP wave, demonstrated by the colour change from red to blue along the solid line in Fig. 6.3c. This change in phase shift from roughly three radians to less than one radian is interpreted as the transition from intact autoregulation to impaired autoregulation, induced by the overall lowering of the CPP. In the same protocol, the WTC at the same frequency remained stable and high across the whole period, shown by the red colour along the solid line in Fig. 6.3d. Fig. 6.3e shows the average value of WTC across the whole frequency range at each time point, and it was clear that for this sample, the frequency-averaged WTC was above the significance level in most time periods.

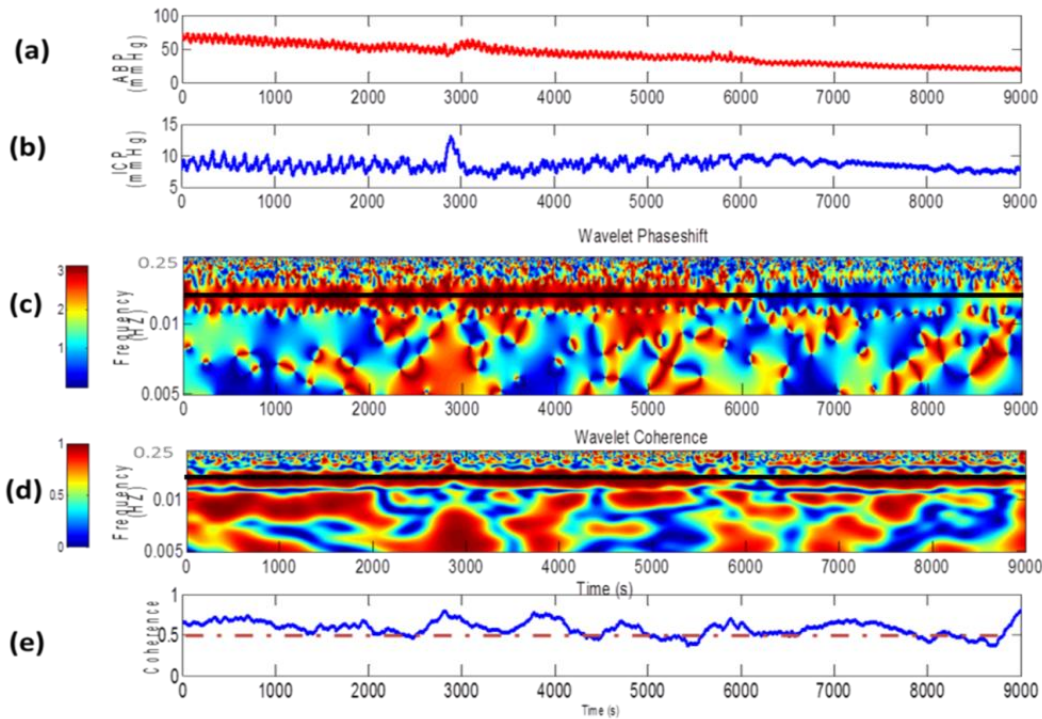


Figure 6.3 Demonstration of WTP and WTC between ABP and ICP of one piglet in the PEEP Group. (a) Arterial blood pressure, ABP. (b) Intracranial pressure, ICP. (c) The WTP map between ABP and ICP. Red color indicates higher value and blue color implies lower value. (d) The WTC map. (e) The average value of WTC across the whole frequency average at each time point. The dashed line is the significance level of WTC. The Morlet coefficient $w_0 = 2\pi$. WTP: wavelet-transform phase shift; WTC: wavelet-transform coherence.

Wavelet coherence threshold

The distribution of WTC using random, scrambled ICP and ABP is shown in Fig 6.4. The use of higher reference w_0 (higher central frequency) resulted in lower WTC thresholds. For w_0 of 2π , 10, 20, and 30 radians/second, the WTC threshold was 0.48, 0.46, 0.45 and 0.43 respectively. Although higher threshold will limit the dynamic range of the estimates, and lower values are preferred if possible, regarding to the bigger edge effect that higher w_0 will produce, the Morlet coefficient $w_0 = 2\pi$ (i.e. central frequency = 1 Hz) and WTC threshold of 0.48 were subsequently used for analysis.

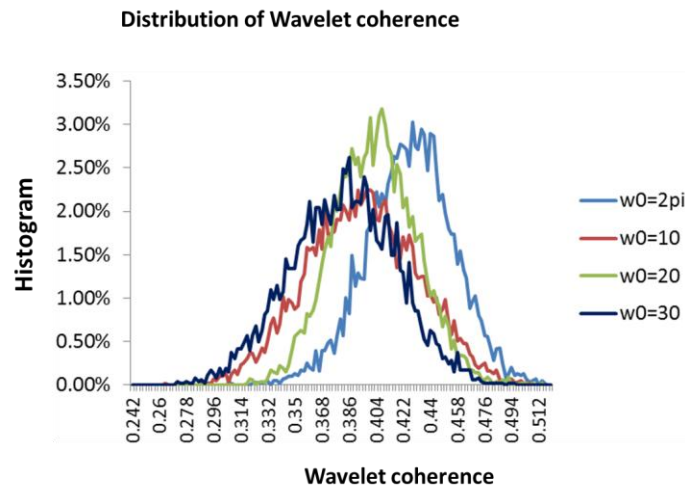


Fig.6.4 The distribution of wavelet transform coherence of 10000 simulations using Monte Carlo simulations based on surrogate signals of ICP and ABP, through different mother wave central frequencies, i.e. wavelet reference index w_0 . $w_0 = 2\pi, 10, 20, 30$.

The relationship between wPRx and PRx

Figure 6.5 shows the relationship between the 30-minute average values of wPRx and PRx. The strongest correlation between wPRx and PRx was observed when ABP oscillations were controlled with the PEEP modulation protocol ($r = 0.88$, Fig. 6.5A). In the non-PEEP Group, the correlation between wPRx and PRx was weaker ($r = 0.68$, Fig. 6.5B). The study showed no difference between PRx using a 500-second window and traditional PRx based on a 300-second window calculation ($p > 0.05$). Therefore, only the 300-window-based PRx was used for the subsequent analysis.

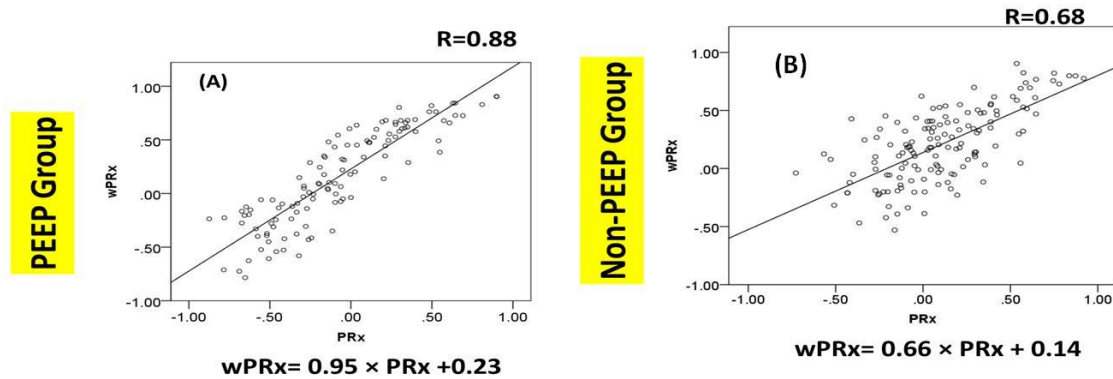


Figure 6.5 Relationships between PRx and wPRx in the PEEP wave-manipulated group (A) and in the spontaneous ABP waves (B). PRx: pressure reactivity index; wPRx: wavelet PRx; PEEP: positive end-expiratory pressure. Each dot represent 30-minutes average value of wPRx and PRx.

Stability of PRx and wPRx

For the first group, where the ABP was manipulated through regular sinusoid waves, there was no significant difference in standard deviation of PRx and wPRx (SD of PRx = 0.47 ± 0.06 , SD of wPRx = 0.48 ± 0.07 , $p > 0.05$). However, for the spontaneous group, wPRx showed a more stable result than PRx, demonstrated through lower SD (SD of PRx = 0.402 ± 0.19 , SD of wPRx = 0.34 ± 0.17 , $p < 0.001$).

Comparing wPRx and PRx against LLA in the PEEP Group

The purpose of determining LLA for each piglet was to have a standard against which to define good autoregulation (CPP above LLA) and bad autoregulation (CPP below LLA). The average LLA of the first group with ABP being manipulated through sinusoid waves was 33.75 mmHg (95% confidence interval (CI): 27.6–39.9 mmHg). Fig. 6.6 displays PRx and wPRx of a piglet in this group, normalized to LLA, taking the origin of the abscissa at the LLA. The mean PRx or wPRx value at each 5-mmHg bin was calculated and displayed. It is clearly seen that while CPP dropped below LLA, both PRx and wPRx were increased, demonstrating worse autoregulation with more positive values.

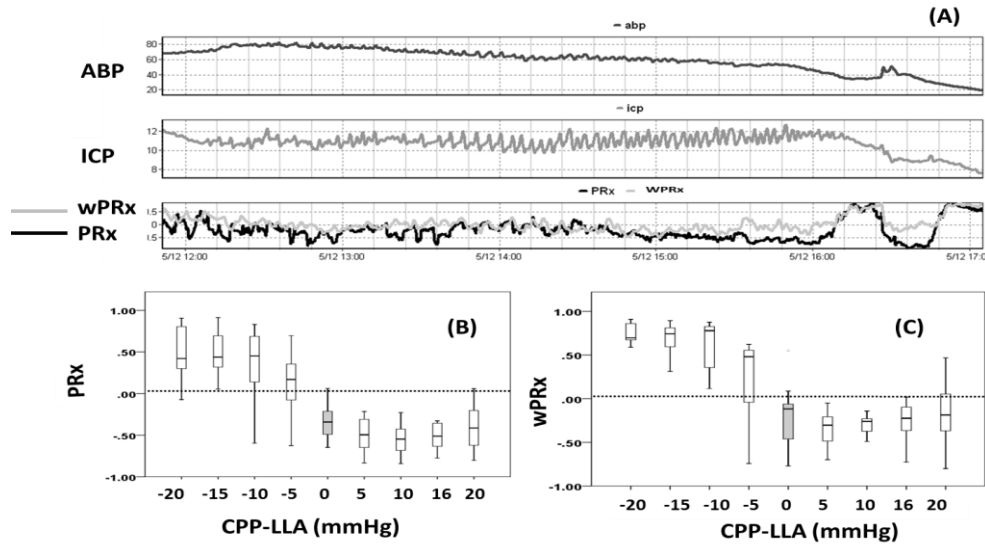


Figure 6.6 Comparison of PRx and wPRx against a standard LLA in PEEP group. (A) An example of ABP, ICP, PRx and wPRx along continuous ABP decrease. Cerebral autoregulation indices are binned in 5 mmHg increments of CPP for comparison against the LLA: (B) PRx, (C) wPRx. Positive CPP-LLA value is related with intact CA, and negative CPP-LLA implies impaired CA. PRx: pressure reactivity index; wPRx, wavelet pressure reactivity index, cosine of wavelet phase shift between arterial blood pressure and intracranial pressure, using wavelet coherence as threshold. Analysed frequency was 0.0067 – 0.05 Hz. LLA: lower limit autoregulation.

Previous studies have already compared PRx against LLA and demonstrated that higher PRx is linked to worse CA, represented by CPP below LLA[36], [204]. In this PEEP group, AUC-ROC curve validated that wPRx can differentiate normal and impaired CA as PRx ($p < 0.05$, Table 6.1). The DeLong’s test showed no significant difference between the two AUC-ROC curves of PRx and wPRx ($p = 0.78$, Table 1). In the non-PEEP Group, both wPRx and PRx can distinguish good and bad CA, no significant difference between the two AU-ROC values was found ($p > 0.05$).

Table 6.1 The ability of PRx and wPRx in distinguishing good CA (above LLA) and impaired CA (below LLA) for PEEP group and non-PEEP group (spontaneous ABP at naïve ICP and elevated ICP).

| | PEEP group | Non-PEEP group (Naïve ICP and elevated ICP together) |
|---|------------------|--|
| PRx | AUC-ROC=0.944 ** | AUC-ROC=0.85 ** |
| wPRx | AUC-ROC=0.931 ** | AUC-ROC=0.87 ** |
| P value between two AUC-ROC curves (PRx and wPRx) | $p = 0.781$ | $p = 0.779$ |

The area under the curve is where a value of 1 indicates maximum sensitivity and specificity. CA: cerebral autoregulation; ICP, intracranial pressure; LLA, lower limit of autoregation. PEEP: positive end-expiratory pressure. AUC-ROC: Area under a receiver-operator characteristic (ROC) test. ** means $p < 0.001$, demonstrating significant difference between good and bad CA.

Comparing wPRx and PRx against LLA in the non-PEEP Group

Fig. 6.7 shows an example of recordings of ABP and ICP in the non-PEEP Group at different brain compliance states (naïve ICP and elevated ICP = 20 mmHg).

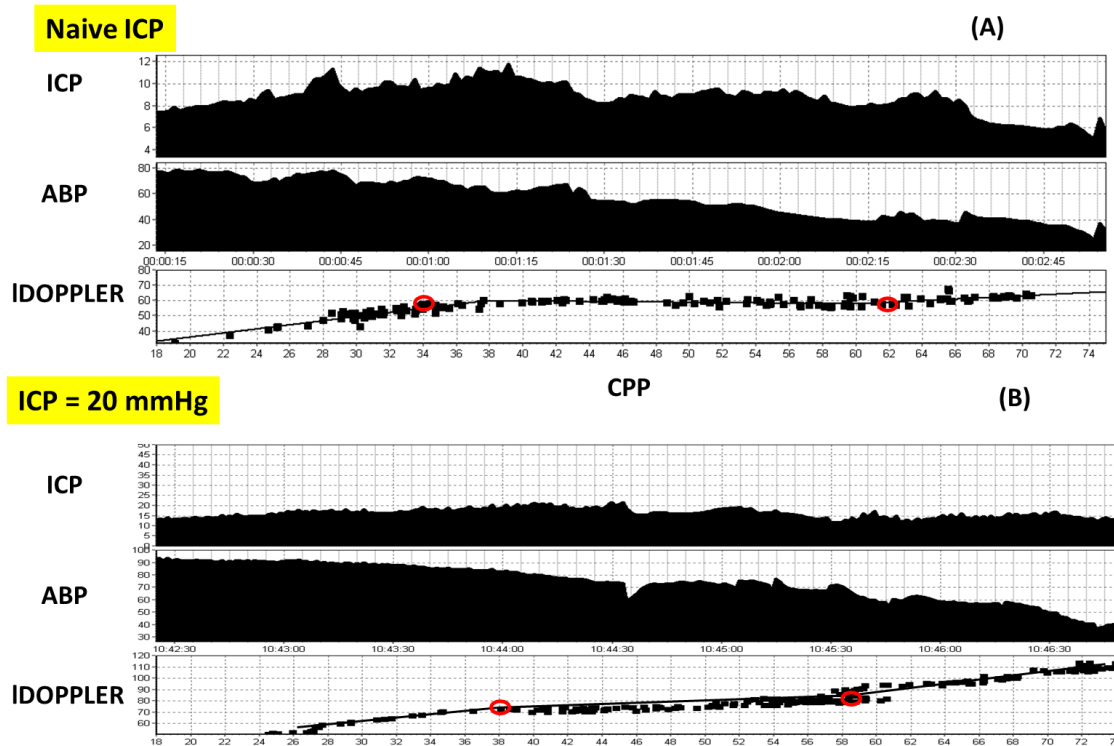


Figure 6.7 Influences of ICP on lower limit of autoregulation (LLA) . A, Determining LLA for one piglet with naive ICP. ABP (mmHg), ICP (mmHg), LD flux (LDOPPLER, AU), were recorded while a balloon catheter in the inferior vena cava was gradually inflated over two to four hours. B, example of a piglet with an ICP of 20 mmHg. Before a reduction in ABP, the ICP was increased to 20 mmHg by a steady-state infusion of artificial cerebrospinal fluid, which was maintained throughout the experiment.

The LLA was different among the two ICP levels, which matches the original, previously published analysis of this dataset [206]. The average LLA for the naïve and moderately elevated (ICP = 20 mmHg) was 31.1 mmHg (95% CI: 26.2–35.9 mmHg) and 37.8 mmHg (95% CI: 31.0–44.6 mmHg), respectively. Both PRx and wPRx showed a significant decrease from bad CA to intact CA at naïve ICP and elevated ICP ($p < 0.05$ Figure 6.8, Table 6.1).

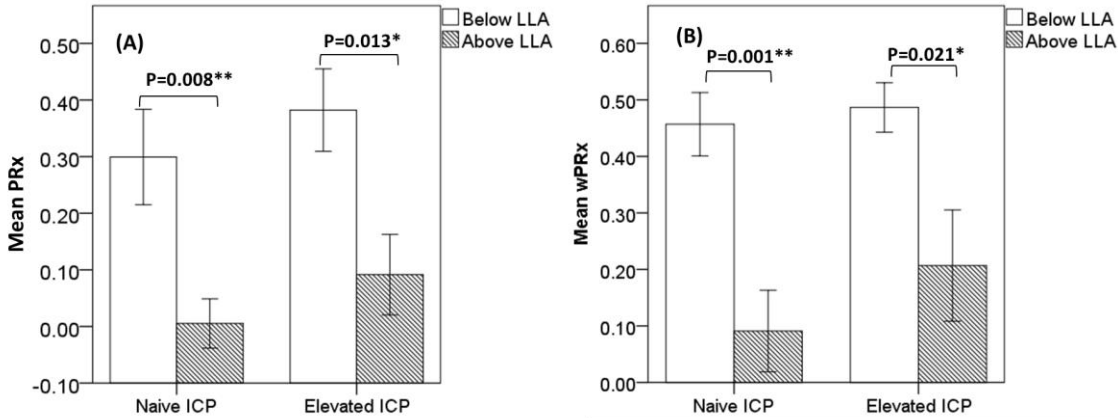


Figure 6.8 Performance of PRx and wPRx in distinguishing good cerebral autoregulation (CPP above LLA) and bad autoregulation (CPP below LLA) at two ICP levels. $p < 0.05$ implies significant difference. The white colour bar implies impaired CA with CPP below LLA; the striped bar refers to intact CA with CPP above LLA. Error bar: standard error. PRx: pressure index; wPRx: wavelet PRx; ICP, intracranial pressure; CPP, cerebral perfusion pressure; LLA, lower limit of autoregulation; CA: cerebral autoregulation.

6.2.4 Discussion

The main finding of this study was that wPRx and PRx have similar accuracy at delineation of the LLA, and wPRx demonstrates an improvement in precision over PRx by mitigating the noise introduced by the use of spontaneous ABP waves to monitor autoregulation. The PRx is mainly useful for delineation of the optimal CPP for patients with TBI. Deviation from optimal CPP defined by PRx monitoring is associated with death and permanent neurologic disability. Maintenance of CPP at the optimal range defined by PRx monitoring is associated with the highest rate of survival with intact neurologic function. Studies that have shown this are taken as evidence for the accuracy of PRx monitoring. However, it is known that the PRx is imprecise, due to transient fluctuations in the ABP and ICP signals unrelated to autoregulation. This imprecision necessitates prolonged time-averaging of the PRx reliably to delineate optimal CPP. Improvements in the precision of PRx monitoring have the potential to decrease this time requirement. The use of WT with coherence filtering, as demonstrated in this study, is a viable method to improve the SNR in the PRx and decrease the monitoring time required to find optimal CPP.

Wavelet analysis

The WT expands time series into a time–frequency space with desired temporal–frequency resolution, to fit various needs for non-stationary signal analysis [128]. In his review, Smith highlighted the use of wavelet-based techniques to aid the interpretation of complex time-variant signals by producing qualitative and quantitative evidence of cerebrovascular autoregulation that is ‘not possible using other methods’[33], [240]. To introduce the wavelet method to analyse CA through ABP and ICP is one of the main purposes of this study. The Morlet wavelet, a complex function, is a natural choice when phase feature extraction is needed. Coherence (in this case WTC)

threshold is often used to ensure a reliable estimate of the phase relationship between input and output. This combination of wavelet-derived instantaneous phase accompanied by coherence-derived quality control makes it a more robust method for non-stationary signal analysis.

However, defining an appropriate threshold for coherence is generally not trivial as it will vary depending on the values of various parameters of the estimation calculation process[236]. Therefore, we chose to establish that threshold using Monte Carlo simulations, in which surrogates of ABP and ICP with destroyed phase relationship were generated and analysed. This was also repeated for different Morlet mother wavelet central frequencies or angular frequencies (ω_0). The simulations showed that increasing ω_0 would shift the distribution of WTC towards lower values, thus decreasing the WTC threshold (effectively improving the statistical properties of the coherence estimation). However, high ω_0 results in a more pronounced edge effect (see Section 6.2.2), which reduces the effective data points for analysis, and that was ultimately considered to be of more importance to the current analysis than a small gain in the reliability of the coherence estimation.

Validation of wPRx

As the most frequently used parameter for CA assessment in TBI patients, PRx was applied as a ‘standard’ for comparison with wPRx. ICP and ABP are common modalities available in NCCUs, and PRx is perhaps the most extensively validated of all metrics of autoregulation. However, PRx is calculated as a simple moving linear correlation between mean ABP and ICP, and it has a low SNR due to extraneous effects influencing ICP or ABP. To remove the effects of noise from this source, and to examine the pure relationship between wPRx and PRx, we used recordings from experiments with a persistent, LF ABP wave introduced by adding a PEEP modulation to the ventilator [205], [206].

For this cohort of piglets’ data with regular fluctuations in ABP, wPRx is not expected to perform any better than PRx, as the strong, deterministic component of approximately fixed frequency and amplitude induced in ABP removes any advantages of a non-stationary approach. However, the good agreement of the two parameters validates that the wPRx principle works. The potential advantages of wPRx lie in dealing with the input signal (ABP) when it is composed of spontaneous slow waves of varying intensity and frequency. Transmission of these variable waves into the output signal (ICP) waveforms may be partially masked by other sources of fluctuations, thus causing the coherence to decrease. In this case, the phase relationship is unreliable, and thus an indiscriminate measure like PRx will return random noise. Using coherence as a filter to mitigate the noise caused by non-stationary signals can produce a more stable result, which is demonstrated in this study with increased stability of the wPRx when spontaneous ABP waveforms are used.

In both experiments, hypotension was induced by decreasing ABP manually until CPP was below the lower limit of CA, thus a clear CA state can be defined for impaired CA and intact CA [204], [206]. In both sets of experiments,

wPRx and PRx demonstrated similar results in distinguishing the two CA states. wPRx and PRx showed a significant increase from intact CA (above LLA) to impaired CA (below LLA).

Interpretation of PRx

Although a commonly used parameter for CA assessment in TBI, there are still some concerns about PRx with regard to its simplicity to assess the complex autoregulatory system. The high correlation between wPRx and PRx in this study provides further evidence that PRx is principally driven by the phase relationship between ABP and ICP [195].

6.2.5 Limitations

As is well known, ABP is not the only determinant of CBF. Other parameters, such as CO₂, have a vasodilatory effect on cerebral vessels[242]. If there are variations of CO₂ during the analysis period of wPRx, then ideally it should be considered, possibly via using multivariate wavelet analysis.

The dataset used in this study was from two groups of experimental piglets. The data of the PEEP Group validated wPRx for CA assessment, and the non-PEEP Group data showed wPRx with a more stable result. However, the analysis focused on the frequency range 0.0067 to 0.05 Hz, with Morlet wavelet with a central frequency of 1 Hz used as the mother wave. More frequency ranges and central frequencies can be tried in the future.

6.2.6 Conclusion

This section introduced the wavelet method to assess CA in two groups of hypotension experimental data from piglets [205], [206]. To exclude unclear noises that might be introduced into ABP or ICP, and examine the pure relationship between wPRx and PRx, the first experiment added a strong sinusoid wave to the ventilator to produce a persistent LF ABP. The result validated the wPRx principle through a significant linear relationship and high agreement between wPRx and PRx. Afterwards, spontaneous ABP waves and ICP waves of 20 piglets with hypotension experiments were applied, demonstrating the benefits of using wPRx to assess CA through lower SD. The result also showed that both PRx and wPRx can distinguish impaired CA and intact CA clearly.

6.3 Cerebovascular pressure reactivity using wavelet analysis in TBI

Paper submitted to PLOS Medicine (November 2016)

6.3.1 Introduction

Section 6.2 introduced a new, time–frequency-based method for CA assessment, and validated the algorithm through two cohorts of experimental piglets’ data. The third section of this chapter applies the WT approach to assess CA in 515 TBI patients. The method was compared with the well-known CA parameter, PRx. In addition, the clinical potential of PRx/wPRx is in examining it versus CPP, which allows indicating the range of CPP values where autoregulation is preserved, or most active, also offering an individualised target for CPP management, called CPPopt. In this section, we calculated the CPPopt according to both PRx and wPRx and then compared it with patients’ outcome after six-month admission.

6.3.2 Material and methods

A total of 515 TBI patients’ data were used, admitted to Addenbrooke’s Hospital between 2003 and 2015 with continuous monitoring of ABP and ICP. ABP and ICP were collected through the method described in Chapter 3. Artefacts introduced by tracheal suctioning, arterial line flushing or transducer malfunction were removed manually. The computerized data storage protocol was reviewed and approved by the local ethics committee of Addenbrooke’s Hospital, Cambridge University and the Neuro Critical Care Unit User’s Group. Patients were managed according to current institutional TBI guidelines (adapted from Menon et al., 1999) [202].

Data Analysis

CA parameters: Time-averaged values of ICP, ABP and CPP ($CPP = ABP - ICP$) were calculated using waveform time integration over 10-s intervals. PRx was calculated as a moving Pearson correlation coefficient between 10 s averages of ABP and mean ICP, using a 300 s data window [55].

Wavelet analysis. WTP between ABP and ICP in the frequency range 0.0067 Hz to 0.05 Hz was calculated through complex wavelet transform, described in Section 5.2 [155], [234]. The Morlet mother wave was applied with the central frequency set at 1 Hz. A 500-s window was used to calculate WTP, and updated every 10 s. The Monte Carlo simulation approach was applied to evaluate the distribution of estimated WTC values corresponding to two uncorrelated signals. 10000 simulations were conducted and the 95% confidence WTC threshold was used to reject corresponding phase values that were deemed unreliable. Individual WTP values with WTC higher than the threshold were kept, while the points with WTC lower than the threshold were ignored. The cosine of WTP was calculated afterwards, labelled wavelet (transform) pressure reactivity index (wPRx), which on one hand can limit the wPRx range from -1 to $+1$, making wPRx directly comparable with PRx; in addition, the result of this operation also help address the problem of phase wrapping.

Outcome analysis. To analyse the relationship between PRx/wPRx and outcome, the averaged values of each parameter were calculated across the whole monitoring period. The GOS was used to assess patients' outcome at six months (obtained at rehabilitation clinic or by phone interview). For the statistical analysis, the patients' outcomes were dichotomized in two ways: favourable outcome (good outcome and moderate disability) versus unfavourable outcome (severe disability, vegetative state and death); fatal outcome (death) versus non-fatal outcome (good outcome, moderate disability, severe disability and vegetative state).

Optimal cerebral perfusion pressure.

To test the ability of wPRx in the determination of the optimal cerebral perfusion pressure (CPPopt), the curve fitting methodology described by Aries et al. [38] was used to estimate CPPopt based on both wPRx (CPPopt_wPRx) and PRx (CPPopt_PRx) for this cohort of TBI patients. In summary, a 5-min median of CPP minute-by-minute time trend was calculated alongside PRx (or wPRx). These PRx (or wPRx) values were divided and averaged into CPP bins spanning 5 mmHg. An automatic curve fitting method was applied to the binned data to determine the CPP value with the lowest (w)PRx. CPPopt was calculated using a four-hour calculation window with an update every minute. The first CPPopt curve could be generated when at least 50% of the required data points of (w)PRx were available, i.e. after a minimum of two hours of monitoring. We calculated the average value of CPPopt across the whole monitoring period for each patient. In addition, the difference between median CPP and CPPopt was calculated continuously ($\Delta\text{CPP} = \text{median CPP} - \text{CPPopt}$) and averaged for the whole monitoring period.

6.3.3 Statistical analysis

Statistical analyses were performed using the IBM SPSS Statistics (version 21) software. The cross-relationship between PRx and wPRx was studied using a linear-regression method (one data per patient). Pearson's correlation coefficient (r) was used to examine the linearity of the relationship. The independent-samples t-test was used to analyse the ability of PRx and wPRx in distinguishing different outcome groups (favourable versus unfavourable outcome, fatal versus non-fatal outcome). Results were considered significant with $p < 0.05$. In addition, χ^2 tests were used to describe the 'degree of equivalence' of examined CA parameters with dichotomized patients' outcome groups by ROC curve analysis. R-software was used to test the statistical significance of the difference between the areas under two ROC curves for different outcome groups. The SDs of wPRx, PRx, CPPopt_PRx and CPPopt_wPRx were calculated to show the stability of these parameters.

6.3.4 Results

Patients' demographics

The group of patients included 210 females and 305 males. Their mean age was 38.4 ± 16 years (mean \pm SD), median GCS score was 7 (interquartile range, IQR: 3–9). The initial GCS and GOS scores were missing in 34 and 73 patients, respectively. The average ABP and ICP of this cohort were 94.8 ± 15 mmHg and 16.2 ± 12 mmHg,

respectively. Average CPP was 79.6 ± 15 mmHg. The outcome was distributed as follows: good recovery, $n = 75$ (17.0%); moderate disability, $n = 117$ (26.5%); severe disability, $n = 142$ (32.1%); persistent vegetative state, $n = 11$ (2.5%) and death, $n = 97$ (21.9%). The mean recording time per patient after artefact removal was 118.6 hours (range from 1 h to 536 h).

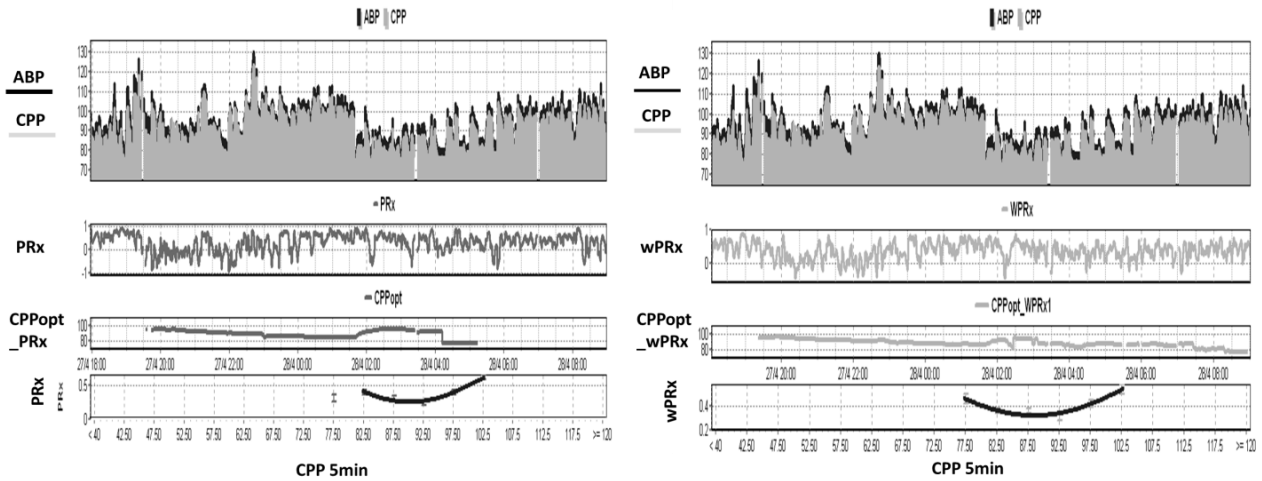


Figure 6.9 Example of data analysis using ICM+, showing time trends of arterial blood pressure (ABP), cerebral perfusion pressure (CPP), pressure reactivity index (PRx), wavelet pressure reactivity index (wPRx). The U-shape curves at the bottom panels were used to determine automated optimal CPP (CPPopt) with curve fitting software. The (w)PRx-CPP plot was created using CPP 5 minute mean value as x-axis, with averaged (w)PRx values in CPP bins spanning 5 mmHg as y-axis.

Relationship between PRx and wPRx

Figure 6.10 A shows the relationship between PRx and wPRx. There was a significant linear relationship between the two parameters, which can be described as: $wPRx = 0.81 \times PRx + 0.32$ ($p < 0.001$, $r = 0.79$). The SD of wPRx was significantly smaller than that of PRx ($wPRx 0.31 \pm 0.06$ vs $PRx 0.37 \pm 0.06$, $p < 0.001$).

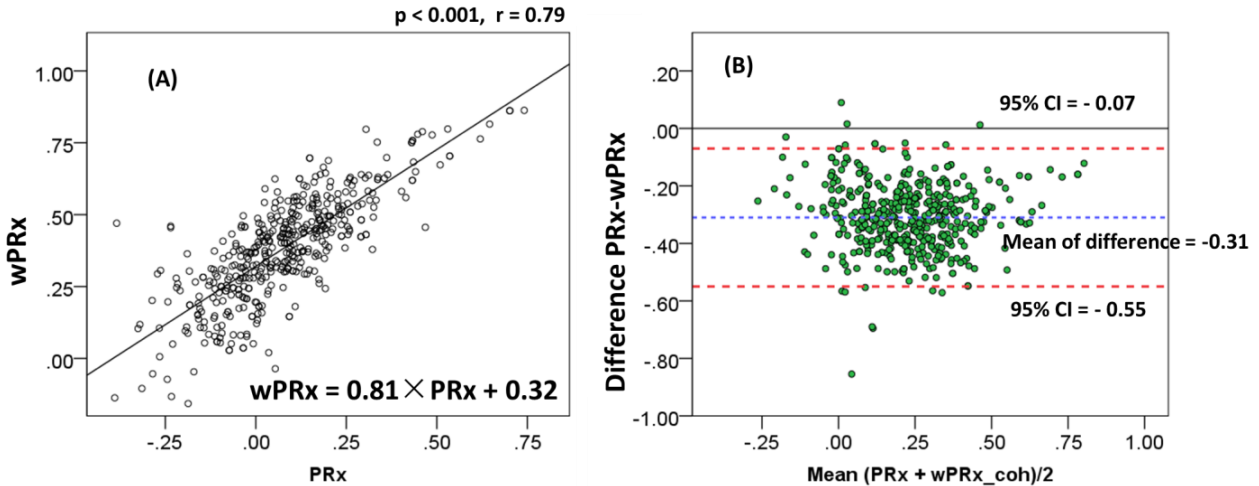


Figure 6.10 Relationship between PRx and wPRx (one dot per patient, $n=515$). A, there is a linear relationship between PRx and wPRx. B, Bland Altman plot of wPRx and PRx showing high agreement of the two parameters. PRx: pressure reactivity index; wPRx: wavelet PRx, the cosine of wavelet phase shift between arterial blood pressure and intracranial pressure (ICP).

Outcome analysis

A significant difference existed between favourable and unfavourable outcomes, demonstrated by both PRx and wPRx (Figure 5.11A–B). Mean (\pm SD) PRx was 0.03 ± 0.13 in the favourable outcome group and 0.10 ± 0.17 in the unfavourable group ($p < 0.001$, AUC = 0.613); wPRx was significantly different between patients with a favourable outcome compared with those with an unfavourable outcome (0.31 ± 0.17 vs 0.42 ± 0.18 , $p < 0.001$, AUC = 0.675). The R analysis showed a significant difference between the two ROC curves of PRx and wPRx ($z = 3.6$, $p = 0.0002$).

For the fatal and non-fatal groups, PRx and wPRx also showed significant differences between the two groups (Figure 5.11C–D). Mean (\pm SD) PRx was 0.05 ± 0.14 in the non-fatal outcome group and 0.15 ± 0.19 in the fatal group ($p < 0.001$, AUC = 0.66); wPRx was significantly different between patients with non-fatal outcome compared with those with fatal outcome (0.34 ± 0.17 vs 0.48 ± 0.19 , $p < 0.001$, AUC = 0.73). The R analysis of the two ROC curves showed better performance with wPRx than PRx in distinguishing the two groups ($z = 2.9941$, $p = 0.003$).

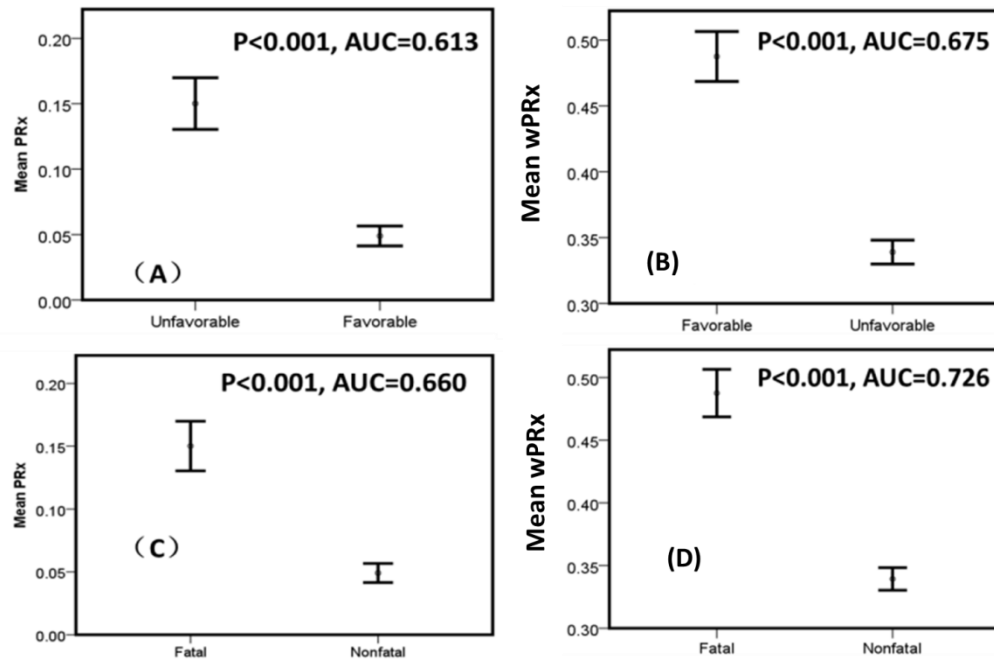


Figure 6.11 The mean values of PRx, and wPRx in different patients' outcome groups. Both parameters could distinguish between favourable and unfavourable outcomes, as well as between fatal and nonfatal outcomes. PRx: pressure reactivity index; wPRx: wavelet PRx, the cosine of wavelet phase shift between arterial blood pressure (ABP) and intracranial pressure (ICP). AUC: area under curve.

CPPopt analysis

Figure 6.12 shows the relationship between (w)PRx and binned CPP for 515 TBI patients using the data across the whole monitoring period. A linear relationship exists between average CPPopt_wPRx and CPPopt_PRx for the whole monitoring time, which can be described as $CPPopt_wPRx = 0.89 \times CPPopt_PRx + 10.42$ ($p < 0.001$, $r = 0.81$, Figure 6.12 C). Figure 6.12 A–B shows that for the total cohort of patients, the CPPopt would be 70 mmHg according to PRx methodology and 80 mmHg according to the wPRx methodology. A significant positive relationship exists between CPPopt_wPRx and mean CPP ($p < 0.001$, $r = 0.40$, Figure 6.12 D).

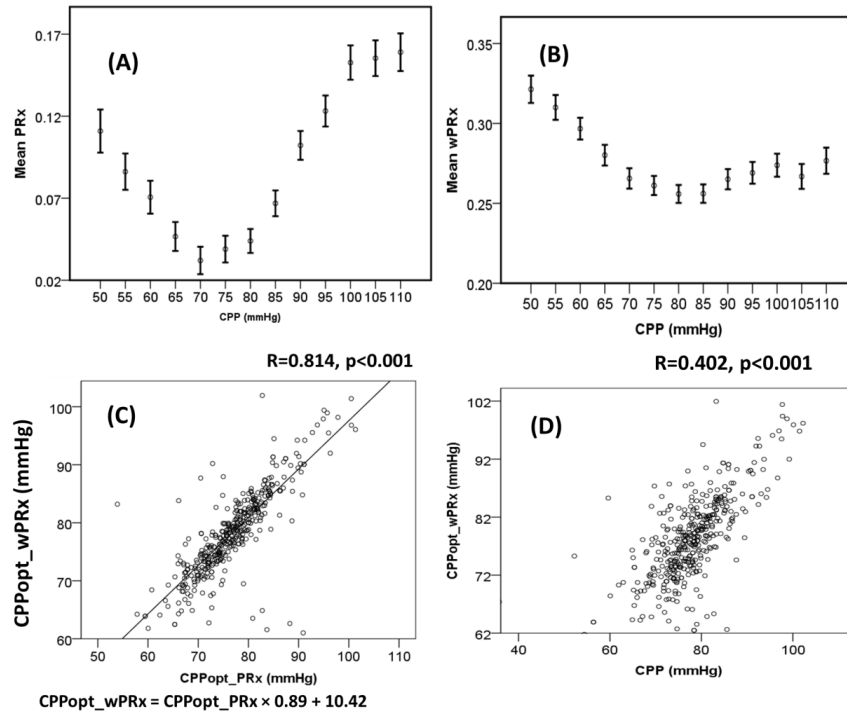


Figure 6.12 (A) PRx- vs CPP plot for the whole cohort. (B) wPRx-CPP plot for the whole cohort. (C) The relationship between CPPopt_wPRx and CPPopt_PRx (one dot per patient, n=515). (D) CPPopt_wPRx vs mean CPP (one value per patient). PRx: pressure reactivity index; wPRx: wavelet PRx, the cosine of wavelet phase shift between arterial blood pressure (ABP) and intracranial pressure (ICP).

An overall determination of an individual CPPopt across the whole time was possible in 502 patients according to wPRx or PRx. The CPPopt yield rate was significantly increased by using wPRx (CPPopt_PRx $53.2\% \pm 20$ vs CPPopt_wPRx $59.6\% \pm 27$, $p < 0.001$). SD of CPPopt_PRx and CPPopt_wPRx were 8.45 ± 2.90 and 7.05 ± 3.78 , respectively ($p < 0.001$).

Figure 6.13 demonstrates the relationship between favourable outcome, unfavourable outcome, mortality rate, severe disability rate and Δ CPP. The mortality increased steadily with the median CPP shifting below the threshold of CPPopt both according to both wPRx and PRx (Figure 6.13 C). An inverse 'U'-shape curve with the highest favourable outcome rate appeared at the smallest difference between CPP and CPPopt as seen in Fig.6.13 B. In contrast, the unfavourable outcome showed a rate increasing below or above CPPopt (Figure 6.13 A). The disability rate was increased while median CPP is above CPPopt (Figure 6.13 D).

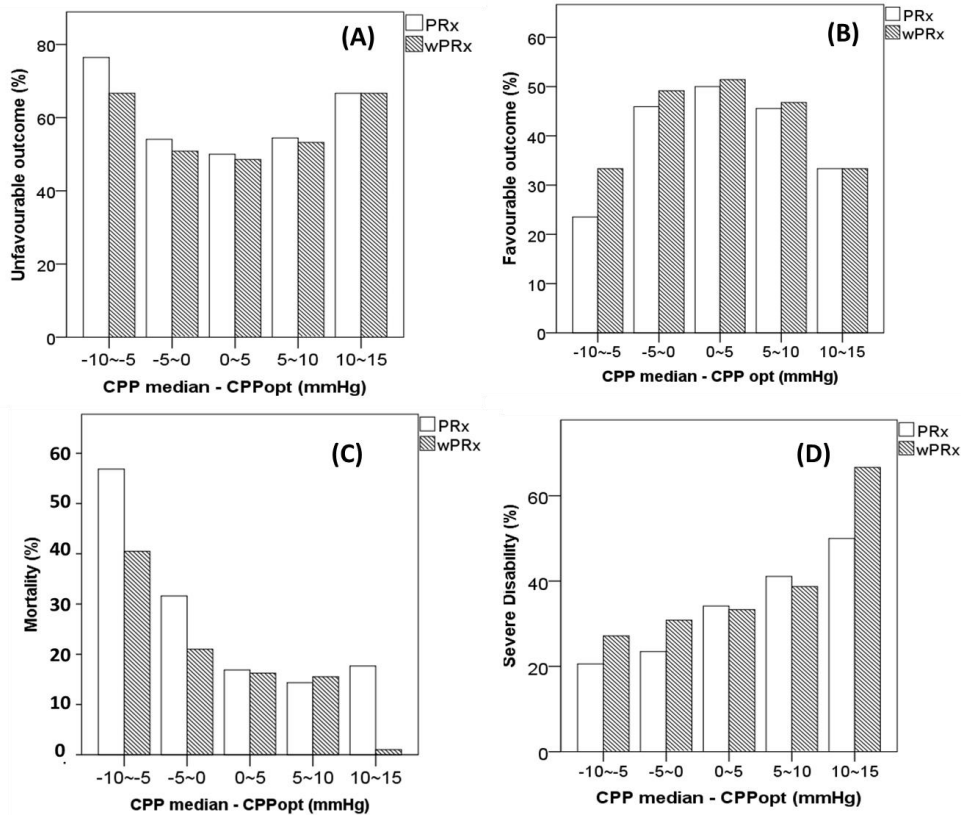


Figure 6.13 Graphs of the relationship between favourable outcome, unfavourable outcome, mortality rate, severe disability rate and the difference between median cerebral perfusion pressure (CPP) and optimal CPP according to PRx (CPPopt_PRx) and wPRx (CPPopt_wPRx). A, a ‘U’-shape curve demonstrating that the smallest incidence of unfavourable outcome was associated with median CPP around CPPopt. B, this graph shows the asymmetrical inverted ‘U’-shape curve between favourable outcome and the difference between the median CPP- CPPopt; C, the mortality increases steadily when median CPP is increasingly below CPPopt. D, severe disability increased while CPP median is above CPPopt.

Age and ICP

There was a significant relationship between PRx and age ($r = 0.24, p < 0.001$), also between wPRx and age ($r = 0.124, p = 0.01$) in this 515-cohort of TBI patients. CA seems to deteriorate with increase of age, shown by increased PRx and wPRx. wPRx showed a stronger relationship with ICP ($r = 0.32, p < 0.001$) than PRx did ($r = 0.11, p = 0.029$).

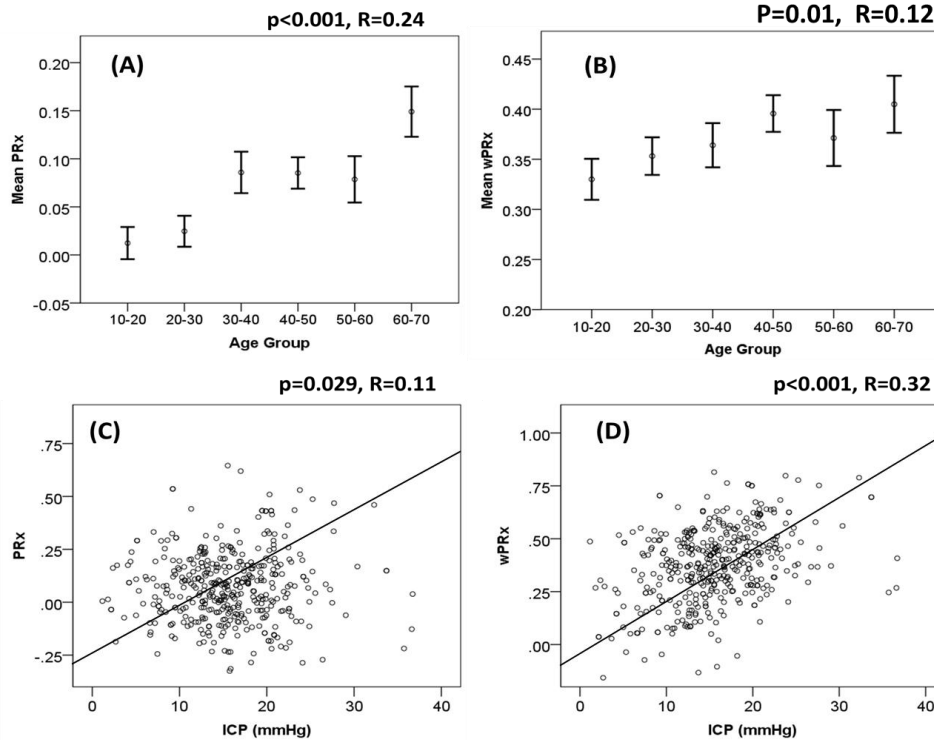


Figure 6.14 The relationship between cerebral autoregulation parameters and age. A, The mean PRx was increased with the age developing. B, wPRx also showed a slight increase while the age was increased. C, relationship between PRx and ICP (one dot per patient, n=515); D, relationship between wPRx and ICP (one dot per patient, n=515).

6.3.5 Discussion

The WT is a time–frequency method that facilitates more accurate analysis of biological signals containing components that are non-stationary[243]. We have developed and validated a wavelet-based methodology of continuous assessment of CA for 515 TBI patients. We have shown that there is a close relationship between wPRx and the established PRx index. For PRx, a negative correlation indicates a pressure-active vascular bed with preserved cerebrovascular reactivity, whereas a positive correlation indicates a pressure-passive vascular bed with impaired reactivity [243]. For wPRx, bigger wPRx values reflect smaller phase shifts between fluctuations in ABP and ICP. The fact that we have achieved such high correlation between the two indices strongly suggests that PRx actually represents a cosine of the phase shift between those two modalities.

Despite similar performance from both indices, the wPRx approach seemed to produce more stable time trends, as reflected by its smaller SD than PRx. The reason might be the robustness of the wavelet method; on the one hand, the application of WTC can guarantee the most associated values and remove unreliable points; on the other hand, the calculation of wPRx was focused on the specific frequency range of CA, while PRx covers the whole frequency band, which includes uncertain noises.

In this retrospective study, the wavelet method demonstrated better performances than PRx in distinguishing favourable and unfavourable outcomes, as well as fatal and non-fatal outcomes according to the GOS score. However, in the optimal CPP calculation, wPRx revealed an asymmetrical 'U'-shape curve, which might suggest that a CPP below the averaged optimal level can impair CA much more than a CPP above the averaged optimal level.

wPRx makes CPP_{opt} estimation more continuous and stable by showing higher yield rate and lower SD than PRx. Normal ageing is associated with many well-recognized changes in the cardiovascular system, such as increases in systolic blood pressure, decreases in systemic artery compliance, cardiac baroreceptor sensitivity and decrease of cortical CBF [244]–[248]. Several types of research have already studied the relationship between age and CA in healthy volunteers, and no relationship existed between CA and age using ABP and FV as input[249], [250]. However, in TBI patients, whether age influences CA is still not very clear. In this research, the analysis showed an age-related deterioration in CA, which means that dynamic CA in older TBI patients no longer performs as efficiently as in younger TBI patients. This relationship was captured by both PRx and wPRx.

6.3.6 Limitations

This retrospective analysis has been performed on a person for whom the outcome was known, more studies need to be done to analyse the ability of wPRx to predict patients' outcomes.

This research analysed the relationship between ABP and ICP in the frequency range 0.0067 Hz to 0.05 Hz. More signals and more frequency ranges can be tried.

6.3.7 Conclusion

This study validates a sophisticated, wavelet-based method for CA assessment in TBI patients. Based on our results, wPRx showed potential in distinguishing different patients' outcome groups and showed more stable behaviour, which can be used in optimal CPP determination.

6.4 Conclusion

This study introduced a new method for assessment of CA using wavelet-derived phase shift between ABP and ICP and validated it against PRx in two hypotensive experiments in piglets. To exclude other noise that PRx might contain and compare the new method with PRx purely, the study introduced sinusoid manipulated waves to ABP to induce persistent LF ABP waves. The result showed a significant linear relationship between wPRx and PRx. Moreover, this study employed spontaneous ABP and ICP from hypotensive piglets to show wPRx with a more stable result.

After being validated through the piglets' experimental data, the wPRx was applied to 515 TBI patients. wPRx was linearly related with PRx and showed a more stable result. It has also been demonstrated that wPRx can produce more continuous optimal CPP for this cohort of patients, showing a similar result with the outcome as PRx.

CHAPTER 7 AN INNOVATIVE METHOD TO MONITOR CPPopt IN TBI

7.1 Introduction

Survival after TBI depends on the control of intracranial hypertension and the provision of haemodynamic support to achieve an ‘adequate’ CBF, with CPP being one of the main driving forces. However, setting an adequate CPP target for the individual TBI patients at the bedside remains challenging. Maintaining a CPP above 70 mmHg was proposed as a method for preventing secondary injuries [1], [2]. However, a large randomized controlled trial could not demonstrate a benefit of a fixed CPP-targeted therapy [4]. The recent Brain Trauma Foundation guidelines advocated exploring the feasibility and the impact on the outcome of strategies based on individualized autoregulation-guided CPP management [2].

As described in Chapter 3, plotting PRx against CPP will often generate a ‘U’-shape curve, the minimum turning point of which represents the CPP corresponding to the smallest value of PRx, where the CA response is most active [27]–[29], and the point is termed CPPopt [38]. Observational studies have confirmed that adult and paediatric patients whose median CPP is closer to their determined CPPopt seem to have better clinical outcomes [37], [159], [160]. However, there are still some problems with traditional CPPopt, calculated through single 4-hour window such as low yield, high variability, which limit the clinical application of the method. Based on Depreitere’s method [161], which was introduced in 2014 using an innovative multi-window-based algorithm for CPPopt calculation, we extended this method to combine more windows and applied a weighting system that incorporates more characteristics of the PRx–CPP plot. Instead of using 7 windows of different length (1, 2, 4, 6, 8, 12, 24 hours), we use 36 windows from 2 hours to 8 hours, increased at 10-minute step. We also extended the weighting system criteria from 2 to 4. A validation study in a much larger population of TBI patients is conducted in this chapter.

7.2 Monitoring of CPPopt in TBI using a multi-window weighting algorithm based on PRx

Paper submitted to Critical Care Medicine (November 2016)

7.2.1 Materials and methods

Patients’ demographics

This section is a retrospective study on 526 severe TBI patients (391 males) admitted in the NCCU of Addenbrooke’s Hospital between 2003 and 2015. Mean age (SD) was 38.6 ± 16.5 years. Continuous recordings of ABP and ICP were part of the local monitoring protocol in severe TBI patients [251], recorded according to the method described in Chapter 3.

All patients were sedated, intubated and, mechanically ventilated during the recording period. A CPP/ICP-oriented protocol for TBI management was used with CPP maintained > 60 mmHg and ICP < 20 mmHg [251]. The baseline

neurological status of each patient was determined using the GCS. The post-resuscitation GCS was used in patients who had sedation discontinuation immediately following hospital admission. The clinical outcome was assessed at six months after hospital admission using the GOS [252]. Artefacts introduced by tracheal suctioning, arterial line flushing or transducer malfunction were removed manually. Data were recorded and analysed anonymously as part of a standard audit approved by Neurocritical Care Users Group Committee. The same software was later used for the retrospective analysis of all stored signals.

Preprocessing

Time averaged values of ICP, ABP, and CPP were calculated using waveform time integration over 60-sec intervals. Cerebrovascular PRx was calculated as a moving Pearson correlation coefficient between 30 consecutive, 10-s averaged values of ABP and corresponding ICP signals [21]. Averages over 10 s were used to suppress the influence of the pulse- and respiratory-frequency wave components. Artefacts were identified and excluded manually from analysis after the data collection.

Traditional CPPopt calculation

CPPopt was calculated according to a published curve-fitting algorithm using four hours of ABP and ICP recording (Aries et al. 2012) described in Chapter 5. In summary, a 5-min median CPP time trend was calculated alongside PRx. These PRx values were divided and averaged within CPP bins spanning 5 mmHg. The upper limit and lower limit of CPP for the CPPopt calculation were set at 40 and 120 mmHg, respectively. For each CPP bin, the corresponding values of PRx were assembled. The mean value and standard error (S.E.) of each bin were then plotted against the bin's mean CPP values to create the error bar chart representing the relationship between PRx and CPP. An automatic curve fitting method was applied to the error-bar plot to determine the CPPopt value automatically at the lowest associated PRx. The curve fitting error was calculated as the square root of SSE (average sum of the squared differences) between the 5 mmHg bin averaged PRx data and fitted values (Figure 6.1B, left panel).

Theoretically, this PRx-CPP relationship should form a smooth 'U'-shaped curve, i.e. with the best cerebrovascular pressure reactivity at the lowest point (vertex). Importantly, before the curve-fitting process, PRx data were first processed using a Fisher Transform, in order to achieve a normal distribution eliminating the ceiling effect of the maximum PRx value of 1.0[38].

Multi-window CPPopt calculation with weighting

In this study, we applied a multi-window approach for CPPopt, with the length of calculation window varying from two to eight hours, increased in 10-minute steps. Hence, for each time point, 36 PRx-CPP plots were generated after 8 hours of monitoring. These plots were given a combined weight factor based on three rules (see below), and the

final resulting CPPopt value was computed as the weighted average of the 36 available CPP values. The weighting rules were as follows:

1. The longer the window duration, the lower the weight factor (Figure 7.1A);
2. The smaller the curve ‘fit error’, the higher the weight factor (Figure 7.1B, the thick black line). Alternatively, the full ‘fit error’ was calculated as the error between the original PRx data points and the fitted curve, instead of the 5 mmHg bin average data and the fitted curve (Figure 7.1B);
3. Fitted curves that did not include the turning point with minimum value were also given lower weight (Figure 7.1C–D);

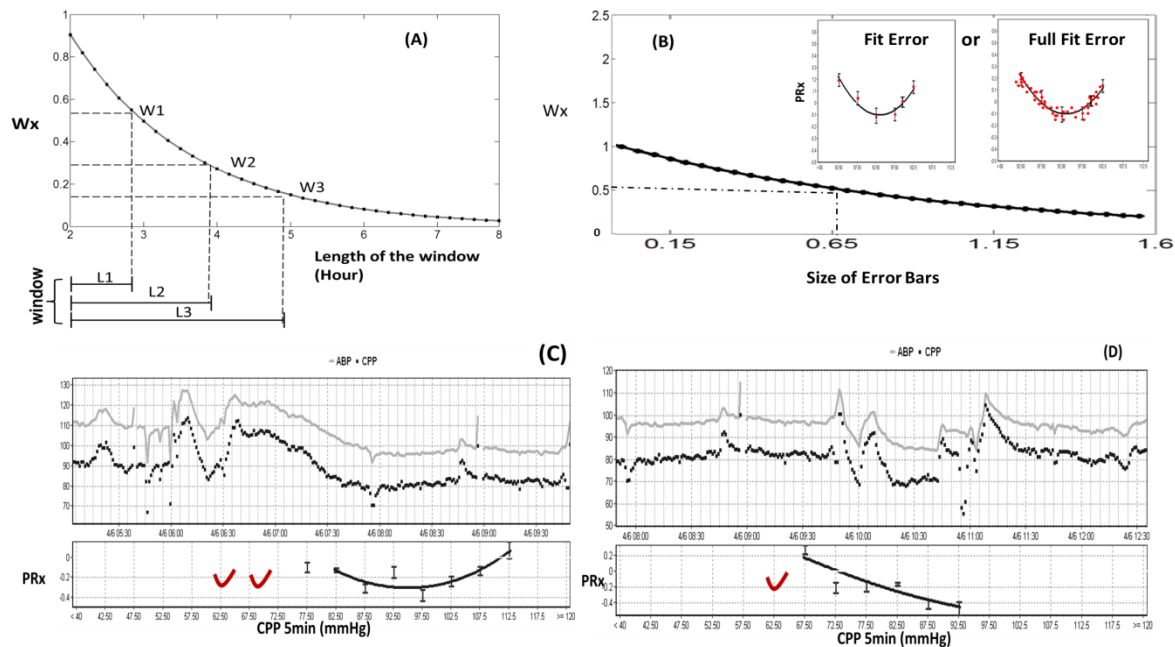


Figure 7.1 The three weighting rules for CPPopt calculation using multi-window approach. A, longer window duration lowers the weight factor; B, the smaller the curve ‘fit error’, the higher the weight factor; the fit error was calculated as the error between the original data points and the fitted curve (right panel), instead of between bin average data and the fitted curve (left panel) ; C-D: curve that includes the turning point of minimum value receives higher weight factor (C) then the one that does not (E). ABP: arterial blood pressure; CPP: cerebral perfusion pressure; PRx: pressure reactivity index; CPP 5min: 5-minute mean value of CPP.

The weighting process can be described mathematically as:

$$\text{Weight} = \frac{1}{e^{\text{window length}}} \times \frac{1}{e^{\text{full fit error}}} \times W_{\text{non-parabolic window}} \quad (\text{Equation 7.1})$$

Additional fit criteria

To try to improve the quality of individual curve fitting, the following two extra calculation options were investigated:

1. inclusion of error weighting (the S.E. of the error bars) in the process of curve fitting (Figure 7.2B) and
2. a criterion enforcing the curve to overlap (at least partially) the range of PRx values $<-0.3, 0.6>$ (Figure 7.2A), thus forcing the algorithm not to return any CPPopt value when PRx was always very high (complete loss of CA), or very low (entirely intact CA).

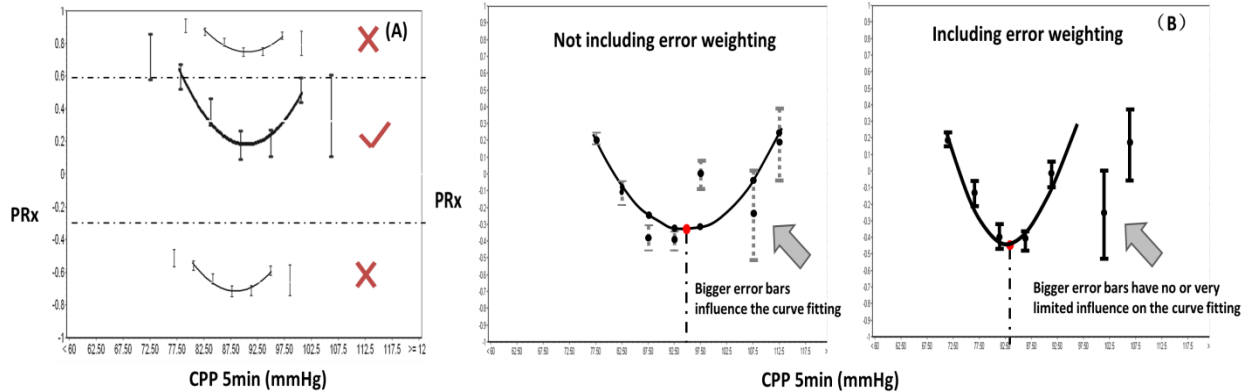


Figure 7.2 A, CPP bins were excluded for CPPopt calculation in the PRx regions of completely impaired (PRx > 0.6, upper panel) or completely working (PRx < -0.3, bottom panel) cerebral autoregulation. Figure 7.2B, inclusion of error weighting in the process of curve fitting (right panel) and exclusion of error weighting in the process of curve fitting (left panel). PRx represents pressure reactivity index.

CPPopt and outcome

Previously published papers from our group demonstrated that patients with averaged CPP close to CPPopt tended to have a more favourable outcome[38]. We repeated this same analysis on a larger number of patients using the new multi-window weighted CPPopt calculation method as well as the original single window (4 h) CPPopt calculation-approach. In order to investigate influence of the newly introduced parameters/options for the CPPopt calculation the analysis was repeated several times as detailed in Table 7.1. The following naming convention was adopted for the suffix of CPPopt parameters labels:

S–single-window calculation (a four-hour window);

M–multiple window calculation (36 windows);

Y–enforcing the curve to overlap a specific range of the y-axis (PRx values: -0.3 to 0.6);

E–error-bar weighting (the SE of the error bars);

W—using a weighting algorithm, each plot was given a combined weight factor based on the three rules (window length, full-fit error and vertex; Equation 7.1);

A – average.

Table 7.1 Abbreviations of labels for CPPopt calculation

| Label | Calculation window | Use error-bar weighting | Enforcing the curve to overlap a specific range of the y-axis | Use multi-window weighting system | Description |
|-------------|--------------------|-------------------------|---|-----------------------------------|--|
| CPPopt_S | Single | NA | NA | NA | Using four-hour window |
| CPPopt_SYE | Single | Y | Y | NA | Using four-hour window, with algorithm of error-bar weighting and forcing the curve to overlap the range of PRx values <-0.3, 0.6> |
| CPPopt_MA | Multiple | NA | NA | NA | Calculate the average value of CPPopts based on multi-window approach |
| CPPopt_MAYE | Multiple | Y | Y | NA | Calculate the average value of CPPopts based on multi-window approach, with algorithm of error-bar weighting and forcing the curve to overlap the range of PRx values <-0.3, 0.6> |
| CPPopt_MW | Multiple | NA | NA | Y | Calculate the weighted-average value of CPPopts based on multi-window approach; the weighting factors include window length, full-fit error and parabolic vertex |
| CPPopt_MWYE | Multiple | Y | Y | Y | Calculate the weighted-average value of CPPopts based on multi-window approach, with algorithm of error-bar weighting and forcing the curve to overlap the range of PRx values <-0.3, 0.6>; the weighting factors include window length, full-fit error and parabolic vertex |

Y: use this function, NA: not apply this function.

We calculated the difference between the median CPP (CPPmed) and each of the calculated CPPopt values every minute. Subsequently, for outcome analysis, these values were averaged over the whole monitoring period for each patient (Δ CPP). The outcome was dichotomized in two ways: favourable (good recovery, moderate and disability) vs unfavourable outcome (severe disability, persistent vegetative state and death) and mortality vs survival.

7.2.2 Statistical analysis

Statistical analysis was performed using the IBM SPSS Statistics (version 21) software. The yield was calculated as the ratio between the count of CPPopt and the count of CPP across the whole monitoring period in every patient. The stability of CPPopt was calculated as the SD of the differences between two consecutive values of CPPopt (CPPopt (t) – CPPopt (t – 1)) over the whole monitoring period. Fatal and non-fatal outcome groups were compared using the non-parametric Kruskal–Wallis test because the values in most groups were not normally distributed. ANOVA test was used to compare the yield of different CPPopt calculation methods (Table 7.3). We assumed $\alpha=0.05$. ROCs were used to compare the ability of different CPPopts to distinguish patients' outcomes, rendering an area under the ROC curve for each parameter [253]. Bland–Altman plots were used to investigate the agreement between CPPopt_S and CPPopt_MA for the pooled data of all TBI patients.

7.2.3 Results

Patient Demographics

The group of patients included 219 females and 307 males, with their characteristics described in Table 2. Their mean age was 38.6 ± 16.5 (mean \pm S.D.) years old, median GCS score was 7 (interquartile range [IQR]: 4-9). The GCS and GOS score were missing in 190 and 18 patients. The average ABP and ICP of this cohort was 93.6 ± 8.3 mmHg and 16.6 ± 9.9 mmHg, respectively. For the outcome analysis, patients with GOS score missing were excluded. The outcome was distributed as follows: good recovery, n= 84 (16.5%), moderate disability, n = 136 (26.8%), severe disability, n = 165 (32.5%); persistent vegetative state, n = 12 (2.3%); and death, n = 111 (21.9%). The mean recording time per patient after artefact removal was 142.0 hours (range from 1 hour to 697 hours).

Table 7.2 Patient demographics, clinical variables, and outcome

| | N | Age | GCS | ABP | ICP | CPP | PRx |
|----------------------------|----------------------------|---------------|--------------------|---------------|---------------|---------------|---------------|
| Death | 111 | 44.4 ±17.8 | 6.0 (IQR:3-8) | 94.2 ±14.0 | 20.4 ±12.3 | 75.0 ±13.6 | 0.16 ±0.20 |
| Vegetative state | 12 | 40.5 ±16.8 | 5.0 (IQR:3-9) | 90.3 ±11.6 | 16.1 ±8.3 | 72.9 ±9.5 | 0.06 ±0.20 |
| Severe disability | 165 | 39.0 ±15.4 | 6.0 (IQR:4-8) | 94.2 ±7.4 | 16.6 ±10.0 | 78.6 ±9.7 | 0.04 ±0.16 |
| Moderate disability | 136 | 35.7 ±15.4 | 7.0 (IQR: 4-10) | 92.8 ±8.3 | 15.3 ±8.8 | 77.8 ±8.2 | 0.04 ±0.16 |
| Good recovery | 84 | 34.9 ±16.6 | 8 (IQR:4-10.5) | 93.3 ±7.8 | 14.7 ±7.6 | 79.1 ±7.0 | 0.01 ±0.13 |
| Total | 526 (18 GOS missing) | 38.6 ±16.5 | 7 (IQR: 4-9) | 93.6 ±8.3 | 16.6 ±9.9 | 77.7 ±9.9 | 0.07 ±0.18 |

GOS, Glasgow Outcome Scale; M/F, males/females; GCS, Glasgow Coma Score; ABP, arterial blood pressure; ICP, intracranial pressure; CPP, cerebral perfusion pressure; PRx, pressure reactivity index. wPRx: wavelet pressure reactivity index; Values are shown as mean ± SD or median and interquartile region. SD: standard deviation; IQR: interquartile range. ABP, ICP, CPP, PRx and wPRx were averaged in each patient over the whole monitoring period.

CPPopt yield

Figure 7.3 shows two examples of CPPopt trends in TBI patients with long-term recordings. In both cases the single window CPPopt trend (CPPopt_S) contains many missing values (gaps) while the multi-window trend (CPPopt_MA) is entirely free of those gaps.

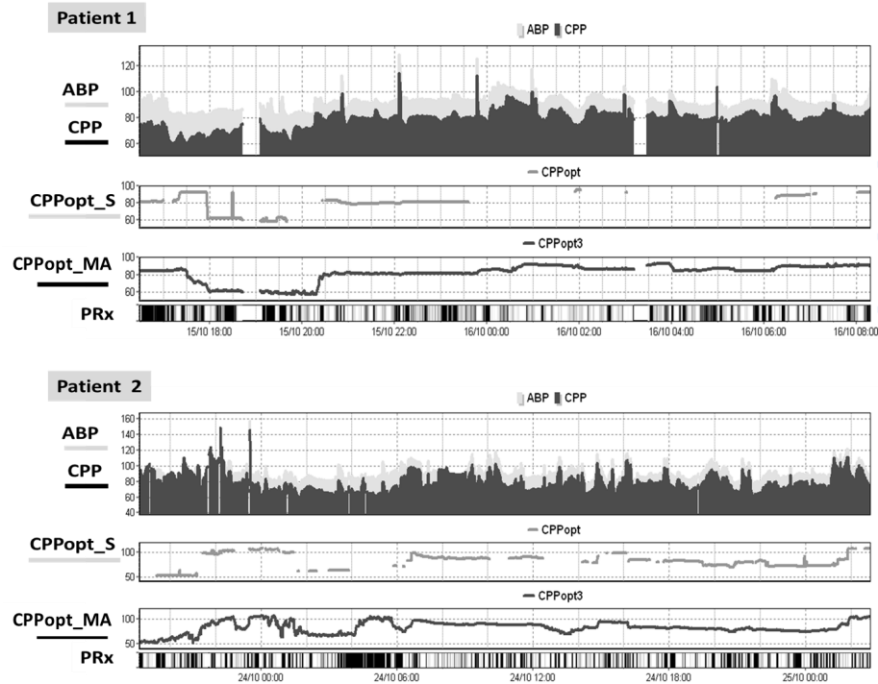


Figure 7.3 Examples of CPPopt trends. ABP: arterial blood pressure; CPP: cerebral perfusion pressure; CPPopt_S: CPPopt calculated according to PRx using a four-hour moving window; CPPopt_MA: a simple average value of CPPopt of window lengths varying from two hours to eight hours, with 10 minutes as the increasing step.

Table 7.3 shows the average (\pm SE) yield per patient result of CPPopt. The yield was significantly increased from 51% \pm 0.94% by using a single window to 94% \pm 2.1% ($p < 0.05$) while using the multi-window. There was no significant difference in CPPopt yield between different variants of the multi-window approach ($p > 0.05$).

Stability of CPPopt

The standard deviation of differences (SDD) between the sample-to-sample difference of CPPopt is shown in Table 7.3. The stability of CPPopt was improved significantly by using the multi-window algorithm; SDD of CPPopt_S was 0.83 \pm 0.015, while SDD of CPPopt_MA was 0.58 \pm 0.015 ($p < 0.05$).

Table 7.3 The yield result and standard deviation of differences (SDD) between two consecutive values of CPPopt across the whole recording duration of CPPopt using single-window calculation (CPPopt_S or CPPopt_SYE) and using the multi-window algorithm (CPPopt_M).

| | CPPopt_S | CPPopt_SYE | CPPopt_MA | CPPopt_MAYE | CPPopt_MW | CPPopt_MWYE |
|-----------------------|-------------------|-------------------|-------------------|-------------------|-------------------|-------------------|
| Yield (Mean \pm SE) | 50.5% \pm 0.94% | 46.1% \pm 0.95% | 94.2% \pm 2.11% | 92.3% \pm 2.09% | 94.2% \pm 2.13% | 92.3% \pm 2.08% |
| SDD (Mean \pm SE) | 0.83 \pm 0.015 | 0.74 \pm 0.014 | 0.58 \pm 0.015 | 0.61 \pm 0.016 | 0.69 \pm 0.016 | 0.72 \pm 0.019 |

PRx: pressure reactivity index. CPPopt_S: optimal CPP calculated using the single four-hour window; CPPopt_M: optimal CPP based on the multi-window algorithm.

Relationship between CPPopt_single window and CPPopt_multi-window

We use CPPopt_MA to represent the multi-window approach. There was a linear relationship between CPPopt_MA and CPPopt_S, shown in Figure 7.4A ($r = 0.89$). The Bland-Altman plot demonstrates high agreement between the two methods. For this cohort of patients, CPPopt varied from 60 mmHg to 110 mmHg. The faint, parallel lines in the charts are associated with CPPopt values obtained from ‘incomplete’ ‘U’- shape curves (i.e. only descending or ascending parts), and represent lowest/highest values of the CPP bins (central point) contained within the curve (thus explaining the granularity of 5mmHg).

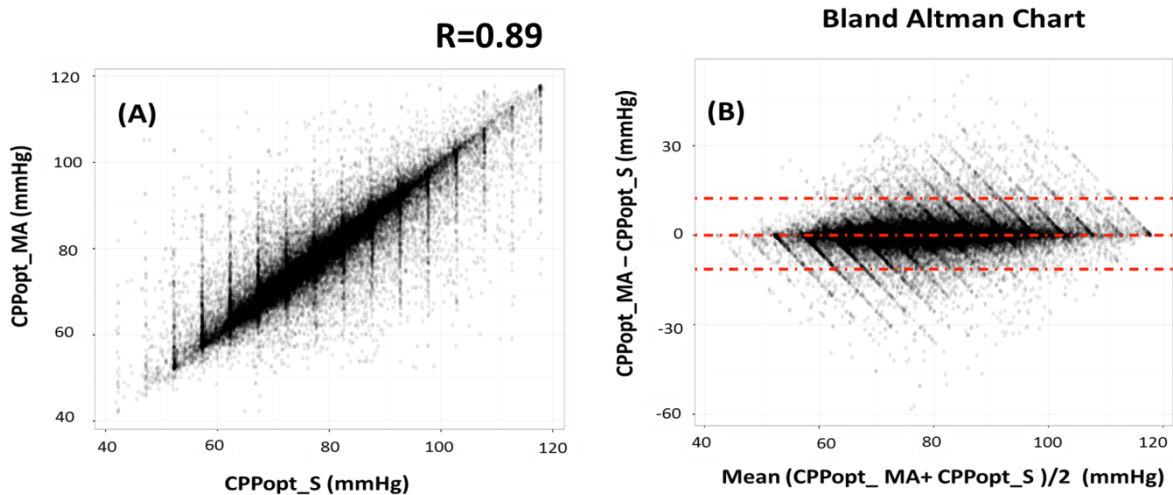


Figure 7.4 Relationship and Bland–Altman plot of CPPopt_S and CPPopt_MA. CPPopt_S refers to CPPopt calculated through a four-hour window and CPPopt_MA implies CPPopt calculated as the average value of multi-window CPPopts. Red lines: mean and 95% CI.

Outcome analysis

Figure 7.5 demonstrates the relationship between patients’ outcomes and Δ CPP (the difference between CPP and CPPopt). Both CPPopt_S and CPPopt_M variants showed similar performance in relation to patients’ outcome, with CPP values below CPPopt more likely to result in a fatal outcome.

For both approaches, the highest incidence of a favourable outcome was associated with averaged median CPP around CPPopt (Δ CPP = 0). A nearly linear relationship between median CPP values above the optimal CPP threshold (Δ CPP > 0) and severe disability rate can be seen.

A ROC test showed that Δ CPP based on a single window or multi-window can distinguish the fatal and non-fatal outcome group significantly ($p < 0.001$); AUC of Δ CPP based on CPPopt_S was 0.72 and AUC of Δ CPP based on CPPopt_MA was 0.69.

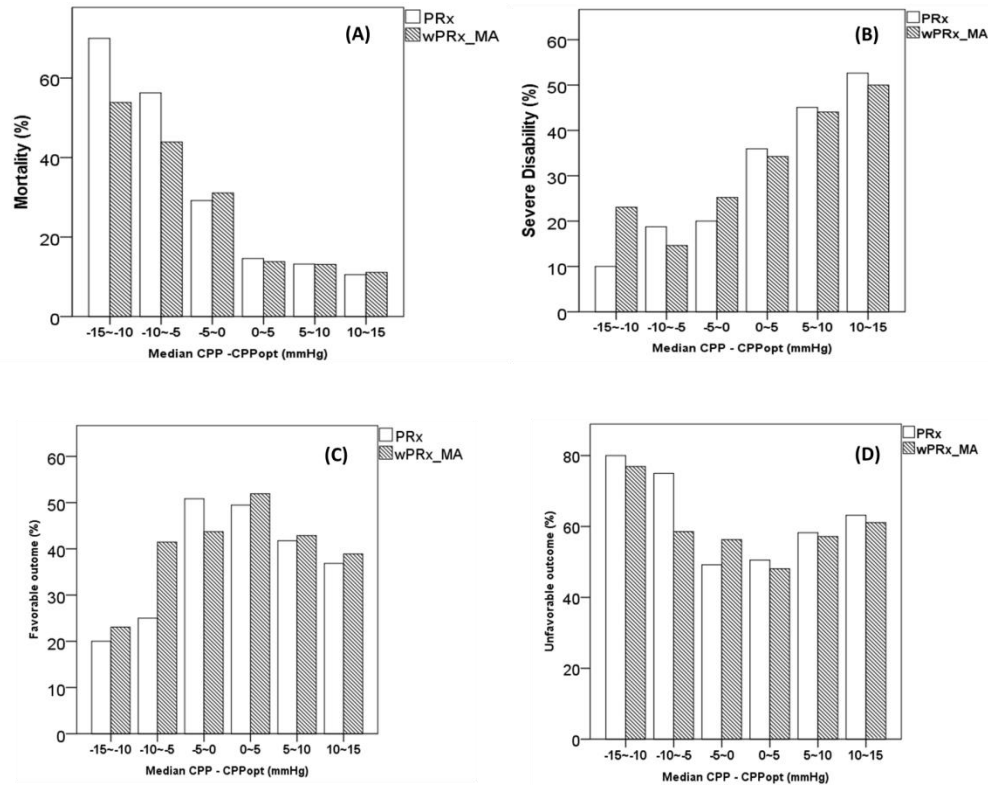


Figure 7.5 Graphs of the relationship between mortality, favourable outcome, severe disability, unfavourable outcome rate and the difference between averaged median cerebral perfusion pressure (CPP) and CPPopt using the moving window of four hours (A) and using weighted multi-window calculation (B).

7.3 Monitoring of CPPopt in TBI using a multi-window weighting algorithm based on wPRx

In Chapter 6, we introduced a new method for CA assessment, wavelet PRx (wPRx) and validated it versus PRx. The result showed that wPRx can reflect CA and distinguish good CA from impaired CA. In Section 7.3, we also applied the multi-window algorithm to wPRx, to see whether there is improvement against the traditional single-window method for CPPopt estimation.

7.3.1 Materials and data monitoring

Data of 427 TBI patients (70 females) admitted to the NCCU of Addenbrooke's Hospital between 2003 and 2015 were used. Continuous ABP and ICP were recorded through the method described in Chapter 3. The computerized data storage protocol was reviewed and approved by the local ethics committee of Addenbrooke's Hospital, Cambridge University and the Neurocritical Care Unit User's Group.

7.3.2 Methods

Time-averaged values of ICP, ABP and CPP were calculated using waveform time integration over 60-s intervals. Cerebrovascular PRx was calculated as a moving Pearson correlation coefficient between 30 consecutive, 10-s averaged values of ABP and corresponding ICP signals [21]. Averages over 10 s were used to suppress the influence of the pulse- and respiratory-frequency wave components. A positive correlation between ABP and ICP at low frequency is indicative of passive cerebral vasculature and impaired autoregulation. Zero or negative correlation between ABP and ICP at the same frequency is indicative of reactive vasculature and intact autoregulation [36].

The wavelet wPRx between ABP and ICP in the frequency range 0.0067 to 0.05 Hz was calculated. A Morlet wavelet was applied as the mother wavelet with the central frequency set at 1 Hz. wPRx was calculated as described in Section 6.1 using a 500-second window. Higher wPRx implies worse autoregulation; in contrast, lower wPRx demonstrates better autoregulation. Artefacts were identified and excluded manually from analysis after the data collection.

CPPopt_wPRx (CPPoptw) was calculated according to a curve-fitting algorithm described in the last section, with a 5-min median CPP time trend calculated alongside wPRx. These wPRx values were divided and averaged into CPP bins spanning 5 mmHg. An automatic curve-fitting method using a weighting system was applied to the binned data to determine the CPPopt value at the lowest associated wPRx. Before the curve fitting, wPRx data were first processed using a Fisher Transform to achieve a normal distribution, eliminating the ceiling effect of the maximum wPRx value of 1.0 [254]. The same strategy as Section 7.2 was applied to wPRx, with the calculation done through ICM+ software. The different simple codes in this section are described in Table 7.4.

Table 7.4 Abbreviations of codes using wPRx for CPPopt calculation through multi-window or single-window approach.

| Code | Window type | Use error weighting | Enforce y region (0–0.8) | Use weighting system (window length, fit error, non-parabolic and full-fit error) |
|--------------|------------------|---------------------|--------------------------|---|
| CPPoptw_S | Four hour window | NA | NA | NA |
| CPPoptw_SYE | Four hour window | Y | Y | NA |
| CPPoptw_MA | Multi-Window | NA | NA | NA |
| CPPoptw_MAYE | Multi-Window | Y | Y | NA |
| CPPoptw_MW | Multi-Window | NA | NA | Y |
| CPPopt_MWYE | Multi-Window | Y | Y | Y |

Y: use this criterion; NA: not applied in this calculation.

The difference between median CPP (CPPmed) and CPPoptw over the whole monitoring period was calculated, labelled as ΔCPPw . The outcome was dichotomized in two ways: favourable (good recovery, moderate and disability) vs unfavourable outcome (severe disability, persistent vegetative state and death) and fatal outcome (death) vs non-fatal outcome (persistent vegetative state, severe disability, moderate disability and good recovery). To test the extent of the erratic nature of CPPoptw, the SD of the difference between minute-to-minute CPPopt was calculated.

7.3.3 Statistical analysis

Statistical analysis was performed using the IBM SPSS Statistics (version 21) software. Groups were compared using the non-parametric Kruskal-Wallis test because the values in most groups were not normally distributed. ANOVA test was used to compare the yield of different CPPopt calculation methods (Table 7.5). We assumed $\alpha=0.05$. The ROC curve was used to compare the ability of different CPPopts to distinguish patients' outcomes. A ROC test was also done, rendering an area under the ROC curve for each parameter. Bland–Altman plots were used to investigate the agreement between CPPoptw_S and CPPoptw_MA.

7.3.4 Results

CPPopt_wPRx yield

Figure 7.6 shows CPPopt_wPRx using single window (CPPoptw_S) and multi-window weighted (CPPoptw_MWYE) approaches. The latter approach showed a more stable and continuous result.

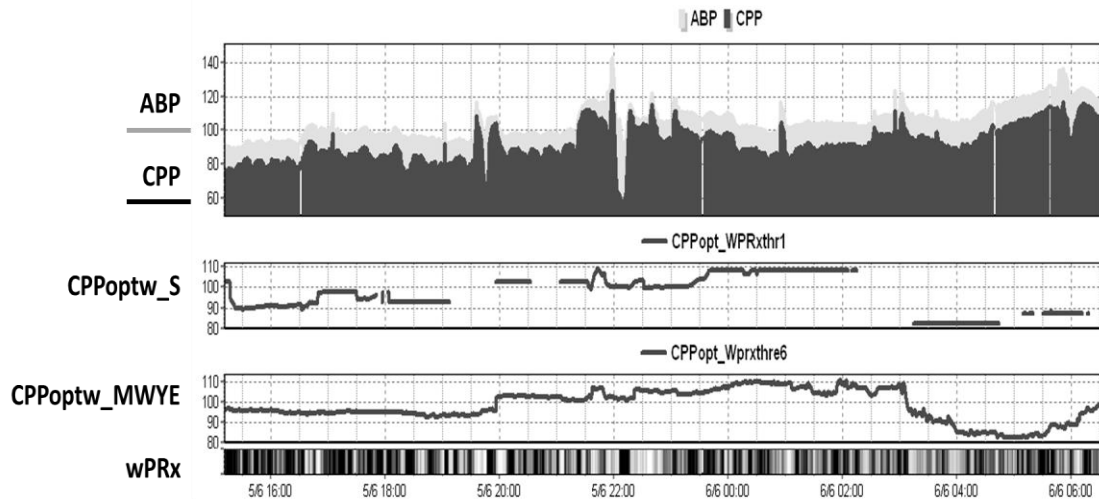


Figure 7.6 Demonstration of CPPopt calculation according to wPRx. ABP: arterial blood pressure; CPP: cerebral perfusion pressure; CPPoptw_S: CPPopt calculated according to wPRx through a 4-hour moving window; CPPoptw_MWYE: average value of CPPopts through various length moving windows, from two hours to eight hours, with 10 min as the increasing step.

Figure 7.7 shows that the average yield result of CPPopt_wPRx using 4 hour window was 52.5%, while the multi-window algorithm resulted in a significantly increased yield result of 94.5% ($p < 0.05$). The application of enforcing PRx region and using standard deviation in bins to weight the curving system, did not cause big difference.

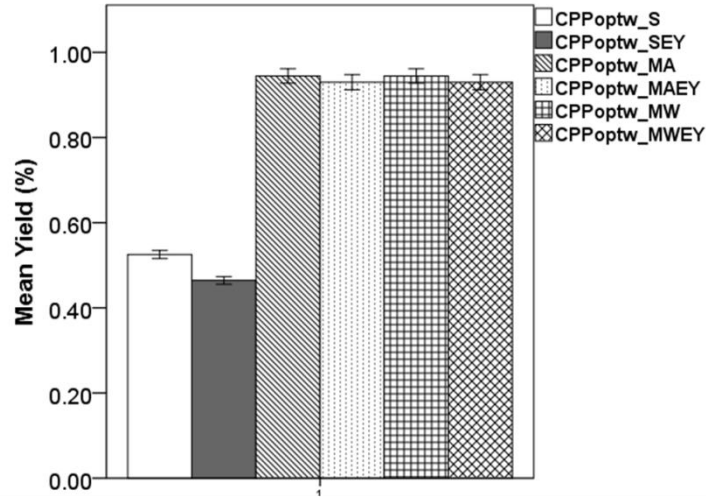


Figure 7.7 Yield result of CPPopt_wPRx using 4 hour window and multi-window. wPRx: cosine of wavelet phase shift between arterial blood pressure and intracranial pressure.

Variability of CPPopt_wPRx

The SDDs between the sample-to-sample differences of CPPopt_wPRx are shown in Table 7.5. No big differences between the stability of CPPopt_wPRx based on the single-window system and multi-window system were found ($p > 0.05$).

Table 7.5 The yield result and SDD between two consecutive values of CPPopt across the whole recording duration of CPPopt using the single-window calculation (CPPopt_S or CPPopt_SYE) and the multi-window algorithms (CPPopt_M).

| | CPPopt_S | CPPopt_SYE | CPPopt_MA | CPPopt_MAYE | CPPopt_MW | CPPopt_MWYE |
|-------------------|---------------|---------------|---------------|---------------|---------------|---------------|
| Yield (Mean ± SE) | 52.5% ± 0.94% | 46.5% ± 0.95% | 94.5% ± 2.11% | 93.0% ± 2.09% | 94.5% ± 2.13% | 93.0% ± 2.08% |
| SDD (Mean ± SE) | 0.49 ± 0.013 | 0.48 ± 0.013 | 0.36 ± 0.014 | 0.36 ± 0.015 | 0.41 ± 0.017 | 0.42 ± 0.018 |

Relationship between CPPopt_single window and CPPopt_multi-window

The CPPopt using a single window (four-hour window) is linearly related to CPPopt using the multi-window-average method (Figure 7.8, $p < 0.001$). The relationship can be expressed as: $\text{CPPoptw_MA} = 0.96 \times \text{CPPoptw_S} + 2.91$ ($r = 0.92$, $p < 0.001$). The result also showed that for this cohort of patients, CPPopt varied from 60 mmHg to 100 mmHg. The Bland–Altman analysis showed high agreement between the two CPPopts.

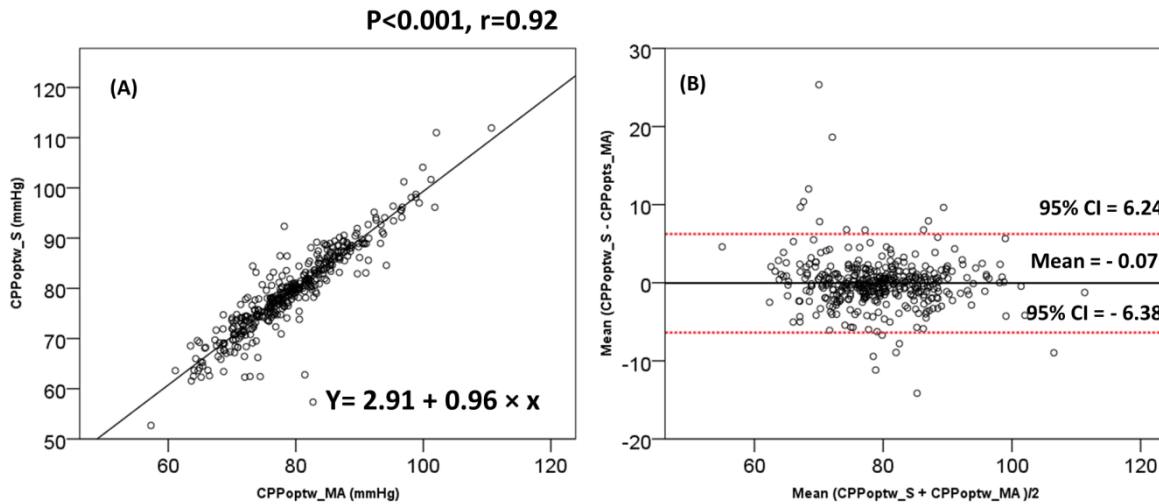


Figure 7.8 Relationship between CPPopt_wPRx using the four-hour window and using multi-window system. wPRx: cosine of wavelet phase shift between arterial blood pressure and intracranial pressure. Per point per patient (N=427).

Outcome analysis

Figure 7.9 demonstrates the relationship between patients' outcomes (the mortality rate, favourable outcome rate and severe disability rate) and the difference between CPP and CPPopt. The result shows that CPP close to CPPopt was related to a better outcome, either using a single window or multi-window (Figure 7.9A). The mortality increases steadily when median CPP is increasingly below the threshold of optimal CPP and decreases slightly with increasing values above optimal CPP (Figure 7.9C); a nearly linear relationship between median CPP values above the optimal CPP threshold and severe disability rate can be seen (Figure 7.9D). A 'U'-shape curve demonstrated that the smallest incidence of an unfavourable outcome was associated with median CPP around optimal CPP (Figure 7.9B).

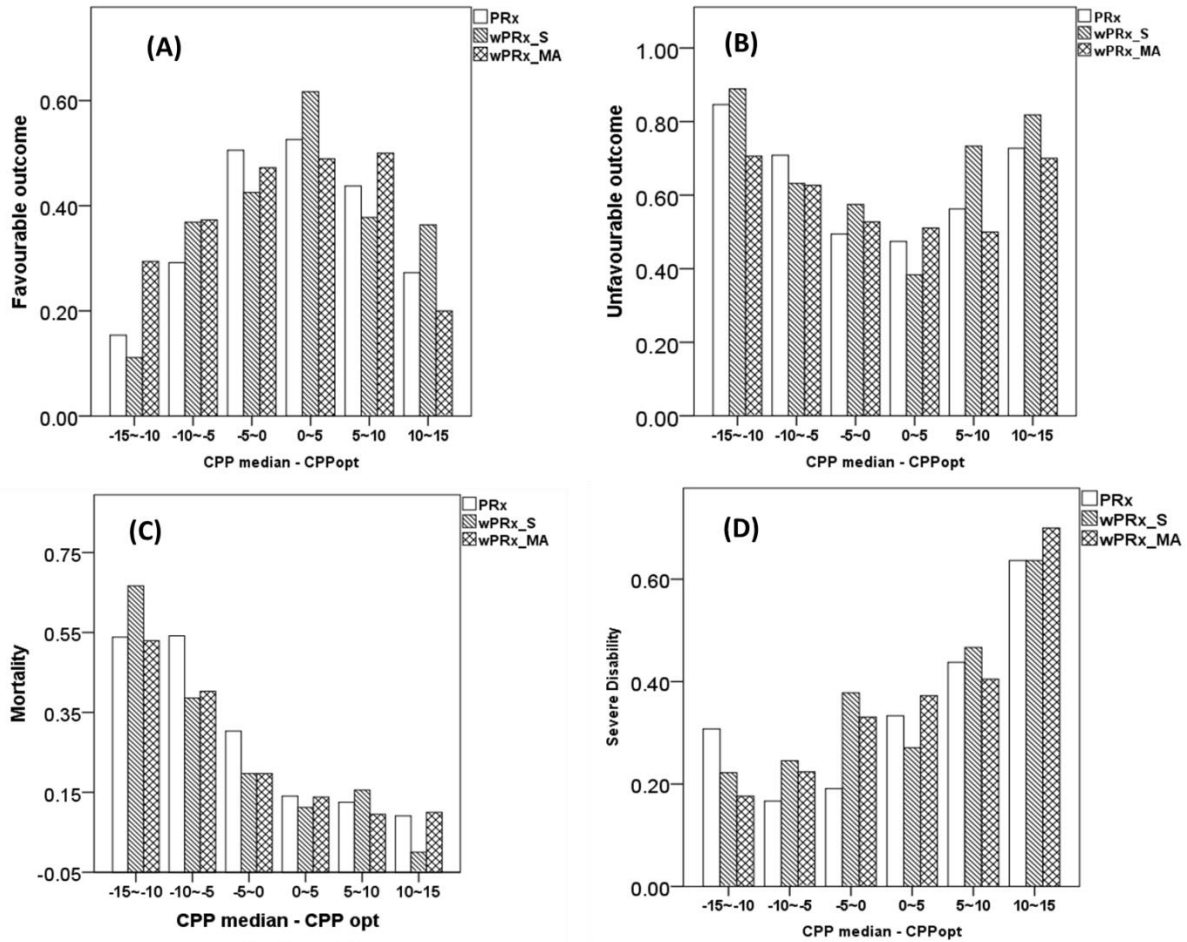


Figure 7.9 Graphs of the relationship between favourable outcome, unfavourable outcome, mortality and severe disability and the difference between cerebral perfusion pressure (CPP) and CPPopt_wPRx using the moving window of four hours and using a multi-window calculation.

7.4 Discussion

Although continuous assessment of CPPopt seems to have prognostic value, its potential for clinical use in an intervention study is limited in part because of its apparent instability and frequent discontinuities. We have built on concepts presented by Depreitere et al. and implemented a new method of CPPopt calculation that improves the quality of the curve fit and improves yield and stability by taking advantage of multiple calculations from incrementally extended data windows.

This method extended the number of windows that Depreitere et al. used from 7 to 36, varying from two hours to eight hours, and took more factors into account. The results showed a marked increase in CPPopt yield (>90%), and a significant improvement in the stability of CPPopt, compared with traditional single-window-based CPPopt. This was of course not unexpected, given the methodology involved. It is easy to see that the algorithm should be able to fit an acceptable curve from windows of increasing sizes, all the way up to eight hours. The averaging operation is also likely to have a stabilising effect on the CPPopt trend. The question is, however, if by increasing the window length as far back as eight hours, are we calculating values that may perhaps be less relevant to the current state? The first factor in our weighting system, the window length penalty, is such that a shorter window was given a higher weight to gauge the curve fitting, which should help to address this problem. The algorithm then favours the shorter windows, which are more related to the most recent changes in CA, thus leading to more local curve fits.

An ideal 'U'-shape curve with a clear minimum at the middle gives more confidence in identification of the best vasoreactivity (CPPopt), while only descending or ascending lines might introduce some underestimation or overestimation, although they also carry information about vasoreactivity[255]. In our weighting approach, higher weight was set to a perfect 'U'-shape curve and lower weight was assigned to only monotonic lines. Through this approach, we believe it can estimate the CPP point with the best autoregulation more reasonably.

Another criterion in the weighting approach was the fit error. To consider more data points, the full-fit error was calculated between the individual PRx data points and the fitted curve, with a higher weight assigned to the curve with a smaller fit error. Through this penalty, the curves that have better performances in curve fitting can have more influence in the final CPPopt calculation.

To make the CPPopt estimation more reasonable, we excluded the PRx/wPRx range of entirely intact CA ($PRx < -0.3$ or $wPRx < 0$, where no CPPopt is needed) and completely damaged CA ($PRx > 0.6$ or $wPRx > 0.8$, where CPPopt cannot be recommended even if there is a 'U'-shape curve). The current weighting parameters used in this study were decided roughly on a small sample study; further research needs to be done to find the best value of these different weighting factors. However, even with current settings, it already showed significant improvement in the estimation of CPPopt, which indicates future clinical use.

Both PRx and wPRx were used to estimate CPPopt. Previous studies have indicated a relationship between patients' outcome and deviation from CPPopt [204], [239], [256]. We did not expect the relationship with the outcome to change using the multi-window algorithm, as this is done on patient averaged values. What we did want to achieve is better stability and availability of the curve, without introducing errors that make the statistics with outcome worse. From this point, the fact that no significant difference was found between the recommended CPPopt using both multi-window or single-window approaches is actually reassuring.

Researchers have already confirmed that treating a patient with individualized optimal CPP has a better discrimination value than a fixed threshold of 60 or 70 mmHg[255]. This, larger, study of 515 TBI patients, showed CPPopt varying from 60 mmHg to 110 mmHg, sustaining the notion that one fixed CPP target for all patients may not be appropriate [2], [257], and that a dynamic CPP target based on pressure autoregulatory capacity is more likely to be recommended [216], [217]. With the presented multi-window methodology that ensures the CPPopt values available nearly 95% of the time, with markedly reduced short-term variability, the technique should be much more applicable to future clinical trials.

7.5 Conclusion

The new CPPopt methodology increased the availability of valid CPPopt values (according to PRx or wPRx) during most of the monitoring time. The method, which can easily be programmed in an automated tool at the bedside, has the potential to make the technique of 'optimal CPP' management widely applicable in most ICUs.

CHAPTER 8 CEREBRAL AUTOREGULATION DURING INTRACRANIAL HYPERTENSION

Raised ICP has been proved to be associated with a poorer outcome in the past [21], [260], [261]. A small study of severe TBI patients showed that some TBI patients whose initial CT scan was normal, with no mass lesion or midline shift, developed raised ICP greater than 20 mmHg that lasted more than five minutes [262], which can result in secondary injury. In adults, the normal ICP under resting conditions is 0–10 mmHg with 15 mmHg being the upper limit of normal. The main reasons for raised ICP include mass lesions, CSF accumulation, vascular congestion and cerebral oedema [263], [264]. Small increases in mass may be compensated for by a reduction in CSF volume and cerebral blood volume but, once such mechanisms are exhausted, ICP rises with increasing pulse pressure and the appearance of spontaneous waves (plateau and B-waves) [180]. Known as a Lundberg A-waves, an ICP plateau refers to sudden increases in ICP up to 50–80 mmHg lasting 5–20 min. It may be triggered by usual ICU procedures such as tracheal suctioning, lowering the head of the bed and routine hygiene [43].

A sudden transient decrease in ABP, with intact CA, will lead to a rapid compensatory dilation of cerebral blood vessels. Accordingly, the blood volume will be increased, which will in turn, under conditions of ‘tight’ brain, cause an increase in ICP. Based on the concept of CPP, the difference between ABP and ICP, this will bring further decrease in CPP and further vasodilation until maximum vasodilation is reached [180], [265]–[267]. This triggers a cycle that leads to ever reducing CPP vasodilatory cascade (Fig. 8.1).

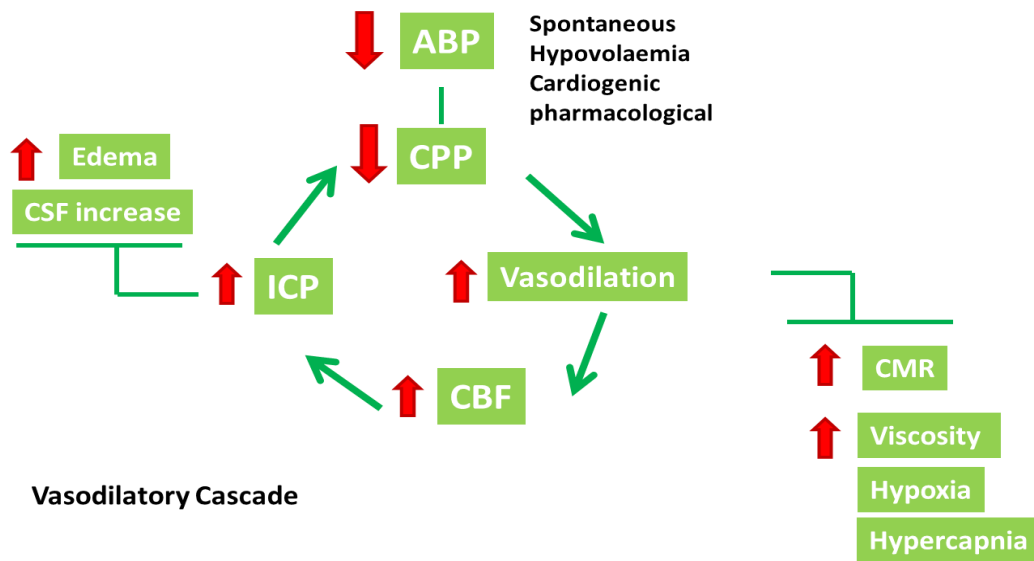


Figure 8.1 The complex vasodilatory cascade.

In the last three chapters, we have investigated the relationship between traditional CA assessment methods (e.g. PRx, TF phase and gain, ARI and Mx) in TBI patients, we also introduced a sophisticated new method for CA

assessment in TBI, the WT method (wPRx). The multi-window approach improved targeted optimal CPP significantly in clinical practice, with a more stable result than with the single-window algorithm.

In this chapter, we tried these different methodologies for CA assessment in some special clinical cases, they are ICP plateau waves and patients with refractory ICP to see the performance of these parameters.

8.1 Cerebral autoregulation assessment in plateau waves

The result presented in this section have been published in *Acta Neurochir Suppl.* 2016 [268].

8.1.1 Introduction

ICP plateau waves refer to ICP rising up to 50–100 mmHg for 5 to 20 min, returning to normal values either spontaneously or in response to treatment [109], [180], [269]. The rapid termination of the wave has been described by a vasoconstriction cascade model in which active vasoconstrictive events lead to decreases in CBV and ICP and an increase in CPP [216], [223]. Theoretically, plateau waves are always associated with degradation of the CBF autoregulation ability as the vessels reach the state of maximum dilation [270].

Many methodologies have been introduced to assess CA, both in the frequency domain and the time domain. In this section, we used plateau wave recordings from TBI patients as a ‘test bench’ to compare the performance of those parameters in their ability to distinguish between the ICP baseline and plateau phases. Furthermore, we calculated ARI, Mx and TF parameters using either ABP or CPP as inputs and FV as output.

8.1.2 Materials and methods

119 TBI patients admitted to Cambridge University Hospital (Addenbrooke’s) between 2003 and 2013 were studied retrospectively (total number of 495 daily recordings). Daily TCD recording to assess CA may be considered in standard management in our NCCU. Data were recorded and analysed anonymously as part of a standard clinical audit approved by the Neurocritical Care Users Group Committee. Continuous ICP signals and FV of MCA were monitored in the way described in Chapter 3. The complete dataset has been screened for plateau waves and this resulted in a reduced dataset of 30 plateau waves recordings, in 24 patients.

The ARI value was calculated by comparing IRs estimated from real data with IRs derived from Tiecks’ model (described in Section 3.1). TF gain, phase as well as coherence in the frequency range of 0.01–0.05 Hz (VLF) and 0.05–0.15 Hz (LF) were calculated through the FFT algorithm, as described in Section 3.2. Both ABP and CPP were used as input and here we use ‘a’ or ‘c’ for abbreviation, for example, gain_a_VLF refers to the gain between ABP and FV at the VLF range (Table 8.1). All the calculations were updated every 10 s.

Table 8.1 Abbreviations used in this section

| Abbreviation | Full Name | Abbreviation | Full Name |
|--------------|-------------------------------------|--------------|-------------------------------------|
| Phase_a_VLF | Phase between ABP and FV at VLF | Phase_a_LF | Phase between ABP and FV at LF |
| Phase_c_VLF | Phase between CPP and FV at VLF | Phase_c_LF | Phase between CPP and FV at LF |
| Gain_a_VLF | Gain between ABP and FV at VLF | Gain_a_LF | Gain between ABP and FV at LF |
| Gain_c_VLF | Gain between CPP and FV at VLF | Gain_c_LF | Gain between CPP and FV at LF |
| Coh_a_VLF | Coherence between ABP and FV at VLF | Coh_a_LF | Coherence between ABP and FV at LF |
| Coh_c_LF | Coherence between CPP and FV at LF | Coh_c_VLF | Coherence between CPP and FV at VLF |

Mean flow index (Mx) was calculated as a moving Pearson’s correlation coefficient using 5 min long windows of 10 s averages of CPP and FV. The results were averaged for each recording, labelled here as Mxc. In addition, the calculations were repeated using ABP as input, instead of CPP, labelled here as Mxa.

Statistical analysis

Statistical analysis of variables was performed using the IBM SPSS Statistics (version 19) software. Results are presented as a mean value \pm SD. t-tests were used to analyse differences in autoregulatory indices between baseline and plateau. The Pearson correlation coefficient between these parameters was calculated, recorded as r. Results were considered significant at $p < 0.05$.

8.1.3 Results

The average values of ABP, ICP and FV for all 24 patients can be found in Table 8.2. During the plateau, mean ICP increased from 21.7 ± 8.3 mmHg to 43.8 ± 12.7 (mean \pm SD, $p < 0.05$) accompanied by a decrease in FV ($p < 0.05$) and CPP ($p < 0.05$). However, mean ABP did not show a very significant difference between baseline and plateau.

An example of the behaviour of ABP, ICP, CPP and FV is presented in Figure 8.2.

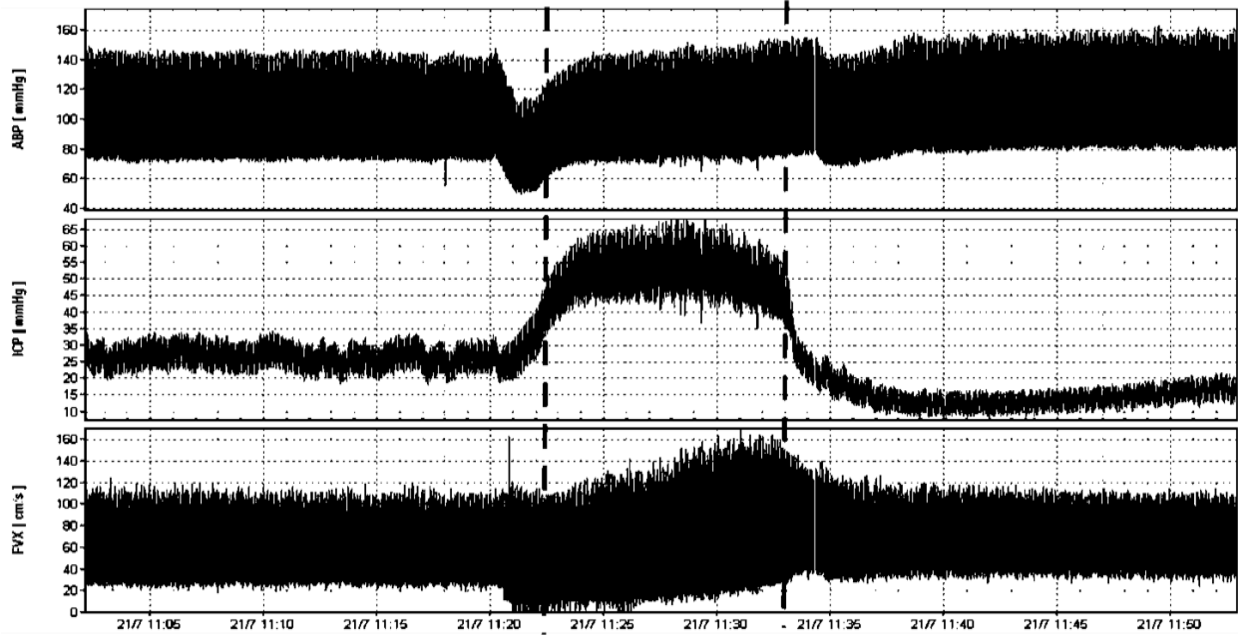


Figure 8.2 An example of a plateau wave, ABP: arterial blood pressure; ICP: intracranial blood pressure; FVX: flow velocity .

Table 8.2 Mean values of ABP, ICP, CPP and FV at baseline and plateau

| | ABP (mmHg) | ICP (mmHg) | CPP (mmHg) | FV (cm/s) | Mxa | Mxc | ARIa | ARIc |
|----------|-------------|-------------|-------------|-------------|-------------|-------------|-------------|-------------|
| Baseline | 94.2 ± 12.8 | 21.7 ± 8.3 | 72.5 ± 4.5 | 56.5 ± 31.4 | 0.21 ± 0.34 | 0.12 ± 0.40 | 3.39 ± 1.58 | 4.02 ± 2.46 |
| Plateau | 93.8 ± 11.5 | 49.9 ± 15.3 | 43.8 ± 12.7 | 48.6 ± 27.7 | 0.28 ± 0.42 | 0.47 ± 0.47 | 2.18 ± 1.99 | 2.45 ± 2.21 |

Mxa: mean flow index (Mx) between ABP and FV; Mxc: Mx between CPP and FV; ARIa: ARI between ABP and FV; ARIc: ARI between CPP and FV. Format: mean value ± SD.

Following the rise in ICP, the ARI decreased significantly in both ARIa ($p = 0.013$) and ARIc ($p = 0.014$) indicating deterioration of CA during the plateau phase (Figure 8.3A and Figure 8.3B, Table 8.3). The index Mxc increased significantly from 0.12 ± 0.40 at the baseline to 0.47 ± 0.47 at the plateau ($p = 0.004$), again showing deterioration of autoregulation. However, we could not find a significant difference between baseline and plateau when using Mxa (Figure 8.3C, $p = 0.472$).

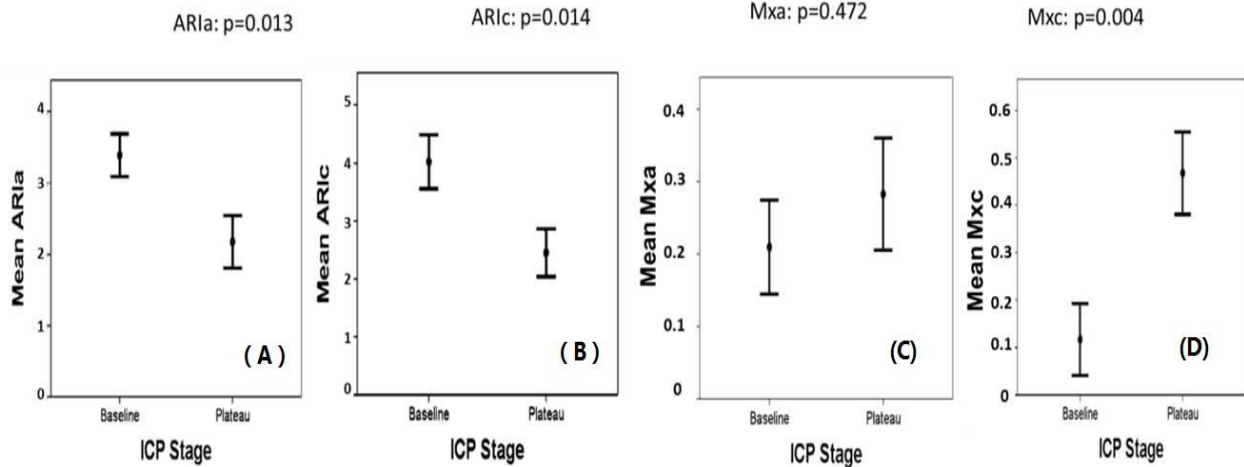


Figure 8.3 Autoregulation indices (ARIa and ARIc) and mean flow indices (Mxa and Mxc) during baseline and plateau. Error bars: SE.

Table 8.3 Mean values of CA parameters during baseline

| ICP Stage | | Phase_a (degree) | | Phase_c (degree) | | Gain_a | | Gain_c | | Coh_a | | Coh_c | |
|-----------|------------|------------------|-------|------------------|-------|--------|------|--------|------|-------|------|-------|------|
| | | VLF | LF | VLF | LF | VLF | LF | VLF | LF | VLF | LF | VLF | LF |
| Baseline | Mean value | -3.64 | 3.38 | -46.6 | -31.4 | 0.95 | 2.10 | 0.79 | 1.81 | 0.35 | 0.35 | 0.46 | 0.41 |
| | SD | 44.7 | 27.2 | 57.2 | 48.2 | 0.60 | 2.17 | 0.47 | 1.17 | 0.11 | 0.11 | 0.13 | 0.12 |
| Plateau | Mean value | -1.12 | 11.33 | -15.3 | -15.1 | 0.69 | 1.20 | 1.30 | 2.27 | 0.44 | 0.39 | 0.50 | 0.43 |
| | SD | 26.76 | 15.35 | 37.85 | 34.25 | 0.54 | 0.87 | 1.42 | 2.22 | 0.12 | 0.14 | 0.16 | 0.12 |

Phase_a: phase between ABP and FV; Phase_c: phase between CPP and FV ; Gain_a: gain between ABP and FV; Gain_c: gain between CPP and FV; VLF: 0–0.05 Hz; LF: 0.05–0.15 Hz.

Only Phase_c in the VLF range (0–0.05 Hz) showed a significant difference between baseline and plateau ($p = 0.02$). Neither Phase_a nor Gain_a was associated with an increased ICP at the plateau (Figure 8.4, $p > 0.05$). For Coh_a and Coh_c, there was a significant increase in Coh_a_VLF from 0.35 ± 0.11 at the baseline to 0.44 ± 0.12 at the plateau ($p = 0.004$). No significant differences were found in other coherence values ($p > 0.05$).

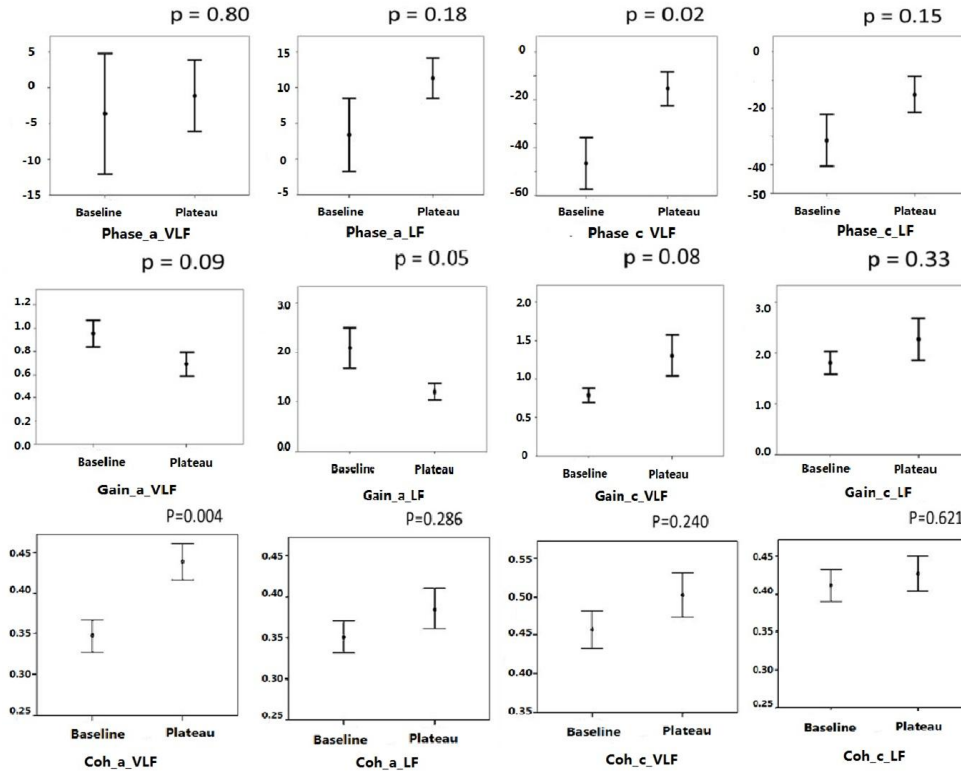


Figure 8.4 Mean value of phase and gain and coherence of transfer function at baseline and plateau. Gain_a_VLF: TF gain between ABP and FV at 0~0.05 HZ; Gain_a_LF: TF gain between ABP and FV at 0.05~0.15 HZ; Gain_c_VLF: TF gain between CPP and FV at 0~0.05 HZ; Gain_c_LF: TF gain between CPP and FV at 0.05~0.15 HZ.

8.1.4 Discussion

During plateau waves, ICP increases due to vasodilation followed by an increase in blood volume. After the vessel dilates to its maximum size, the vascular resistance and the compliance of large cerebral arteries reach their extreme levels [266], [271]–[273]. The CBF autoregulation ability will be weakened accordingly because the vessels lose their pressure reactivity. This degradation in CA was depicted in the ARI being significantly decreased at the top of the ICP plateau and in the Mx being significantly increased. This finding suggests a possible negative relationship between Mx and ARI. Changes in Mxc are more pronounced from baseline to plateau than changes in Mxa. This finding has also been observed in previous studies [21], [120], [266]. On the other hand, ARI proved to be sensitive to changes in autoregulation induced by the plateau waves, although less significantly than Mxc in our material, irrespective of whether ABP or CPP was used as input. This is perhaps because the model that ARI is based on explicitly uses ABP as input. If CPP is used as input instead, this is likely to introduce errors in the estimation of ARI. On the other hand, neglecting ICP waves by using ABP as the input, is likely to introduce errors in assessment

of autoregulation, particularly when a high amplitude of ICP slow waves is expected, as seen during plateau waves. This might explain why both ARIa and ARIC demonstrated similar sensitivity to changes in autoregulation induced by plateau waves, which was lower than Mx.

The increase of coherence between ABP and FV at the ICP plateau implies a more direct transmission from input to output, suggesting a loss of autoregulation. However, the TF did not behave consistently. Theoretically, if we consider CA as a high-pass filter, the better autoregulation is, the bigger time delay from input to output is and the smaller the gain is. In this study, neither phase nor gain demonstrated a significant difference between baseline and plateau. In some cases, the TF phase even increased during the plateau. This finding may reflect the non-linear effects of the CA system.

8.1.5 Conclusion

This study confirms that both ARI (ABP- or CPP-based) and mean FV index Mx (CPP-based) could be used reliably as indicators of deteriorating CA. On the other hand, the TF-derived parameters, phase, gain and coherence, showed rather inconsistent behaviour in our group of patients and thus their use in TBI patients with plateau waves is perhaps not advisable.

8.2 Wavelet method for CA assessment in TBI patients with refractory ICP

8.2.1 Introduction

Intracranial hypertension is commonly encountered in TBI patients, intracranial haemorrhage and ischaemia. Refractory-raised ICP, which leads to a reduction of cerebral perfusion, is associated with poor prognosis, and is potentially life threatening if not immediately corrected [274]. Few specific treatment options for intracranial hypertension have been subjected to randomized trials and it challenges the critical care team [234]. Defined as the difference between mean ABP and ICP, CPP can be reduced by an increase in ICP, a decrease in blood pressure or a combination of both factors. Through the normal CA, the brain is able to maintain a constant CBF within a normal autoregulatory range of CPP via vasodilation or vasoconstriction. However, after brain injury, the ability of the brain to autoregulate may be absent or impaired, thus resulting in similar responses of CBF following changes in CPP [276]. Therefore, it is important to find a good way to assess the interrelation and influence between ABP, ICP and FV, which provides information about the functionality of CA.

A major limitation of the classical spectral analysis is the steady-state assumption. It requires, at some level, disregarding the dynamic, complex and noisy characteristics of the continuous physiological adjustments required to maintain stable cerebral perfusion [188]. Thus, time–frequency methods have been introduced to detect the dynamic behaviour of ABP and ICP [277], [278]. The WT method, which has been widely applied in geophysical and economic fields, is found to be particularly useful for analysing noisy, intermittent and non-stationary signals [151]. It is a method of decomposing a signal into a time–scale plane through the convolution of the signal with a wavelet function [175]. One advantage of wavelet analysis is the ability to perform local analysis and reveal signal features with desired temporal–frequency resolution in different frequencies, higher temporal resolution for higher frequency and higher scale (inverse frequency) resolution for lower frequency [175], [176].

The aim of this study is to apply the wavelet method to TBI patients with refractory ICP and compare it with pressure reactivity index (PRx) and the TFA method.

8.2.2 Materials and methods

Recordings of 12 patients (3 females) aged between 16 and 43 years with refractory high ICP admitted to Addenbrooke's Hospital between the years of 2003 and 2012 were studied. Patients were selected from a larger database of previously presented cases [238] containing both baseline and high ICP (higher than 45 mmHg). The study had local research ethics approval and all subjects gave informed consent.

Continuous ABP was measured with an arterial line zero calibrated at the level of the right atrium (Baxter Healthcare Corp, USA). Continuous ICP was monitored in the frontal lobe with a strain gauge transducer (Codman, Codman and Shurtleff Inc., Raynham, MA, USA) implanted intraparenchymally. Signals from the bedside monitors, including ABP and ICP were sampled at 30–200 Hz and recorded by software ICM+® (Cambridge Enterprise Ltd,

Cambridge, UK, <http://www.neurosurg.cam.ac.uk/icmplus>) or, before 2001, using waveform recorder WREC for DOS (W. Zabolotny, Warsaw University of Technology). Artefacts introduced by tracheal suctioning, arterial line flushing or transducer malfunction were removed. Data were recorded and analysed anonymously as part of a standard audit approved by the Neurocritical Care Users Group Committee.

Methodologies

Wavelet analysis. WTP between ABP and ICP in the frequency range 0.0067 Hz to 0.05 Hz was calculated through complex wavelet transform, as described in the Appendix. A Morlet mother wave was applied with the central frequency set at 1 Hz. A 500-second window was used to calculate WTP, and updated every 10 seconds. Monte Carlo simulations approach was applied to evaluate the distribution of estimated WTC values corresponding to two uncorrelated signals. 10000 simulations were conducted and the 95% confidence WTC threshold was used to reject corresponding phase values that were deemed unreliable. Individual WTP values with WTC higher than the threshold were kept, while the points with WTC lower than the threshold were ignored. The cosine of WTP was calculated afterwards, labelled the wavelet (transform) pressure reactivity index (wPRx), which on the one hand can limit the wPRx range between -1 and $+1$, making wPRx directly comparable with PRx; in addition, the result of this operation also helps address the problem of phase wrapping.

Pressure Reactivity Index: The mean pressure reactivity index (PRx) was calculated as the time correlation coefficient between 10 s averages of ABP and mean ICP, using a 300 s data window. Positive PRx indicates a passive relationship between ABP and ICP, while PRx close to 0 or negative implies good autoregulation.

TF transform: TF phase and gain between the real ABP and ICP were calculated through the method described in Section 3.1.2. The analysis was focused on the frequency range 0.0067 to 0.05 Hz. Generated FV and ABP were first normalized (mean subtracted and divided by the SD), and then divided into four data segments of 120-second duration (amounting to 50% segment overlap) and transformed with the FFT algorithm (Welch method) [141], [144]–[147]. TF phase and gain between artificial CBFV and ABP were calculated using the method described in Section 3.1.2. All the calculations were performed through a 300-second moving window and updated every 10 seconds.

The average values of these CA parameters were calculated for two ICP states: ICP baseline (ICP < 25 mmHg) and ICP plateau (with high ICP > 45 mmHg).

Precision analysis

A comparison between the precision of the PRx, wPRx and TF was conducted using the method described in Brady's research [205]. The precision was calculated as the median absolute deviation divided by the range of possible values (RPV). For PRx and wPRx, the RPV is -1 to $+1$; and for TFP, the RPV is $0-180^\circ$ due to the absolute function applied to the phase calculation; for TF gain, in this analysis, the RPV is 4.

Statistical analysis

SPSS software (version 21, IBM, Armonk, NY, USA) was used for statistical analysis. A curve-fitting method (linear regression) was used to describe cross-relationships between PRx and WTP. Pearson's correlation coefficient (r) was used to examine the linearity of the relationship. Results were considered significant at $p < 0.05$. An independent-samples t-test was used to analyse differences in autoregulatory indices in different CA groups according to LLA or ICP state.

A ROC test was also done for CA groups, rendering an area under the ROC curve for each metric.

8.2.3 Results

Impaired CA during refractory ICP

Figure 8.5 demonstrates an example of signals and CA parameters for a TBI patient with refractory ICP. From baseline to high ICP, the CA deteriorated, as shown by increased wPRx and PRx.

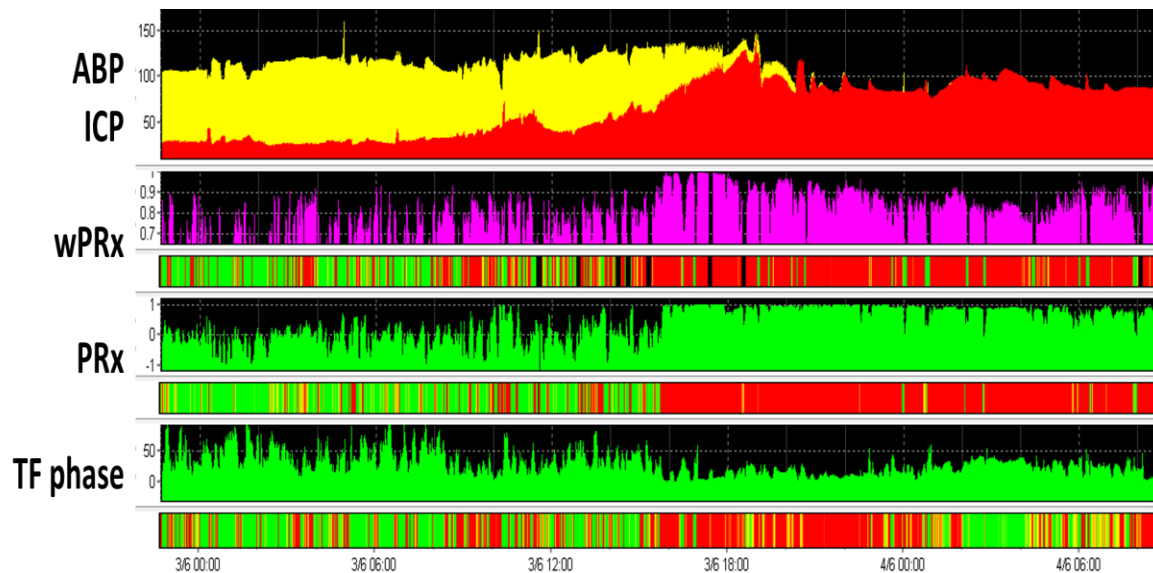


Figure 8.5 An example of a traumatic brain injury patient with refractory intracranial pressure.

Relationship between CA parameters and their precision

The relationship between one hour average of wPRx and PRx is shown in Figure 8.6. There is a significant positive relationship between wPRx and PRx ($r = 0.848$, $p < 0.001$, Figure 8.6A). The average precision for PRx, wPRx, TF phase and TF gain was 0.13 ± 0.07 (Mean \pm SD), 0.08 ± 0.05 , 0.11 ± 0.04 and 0.08 ± 0.05 . The difference between wPRx and PRx was significant ($p = 0.038$, Figure 8.6B).

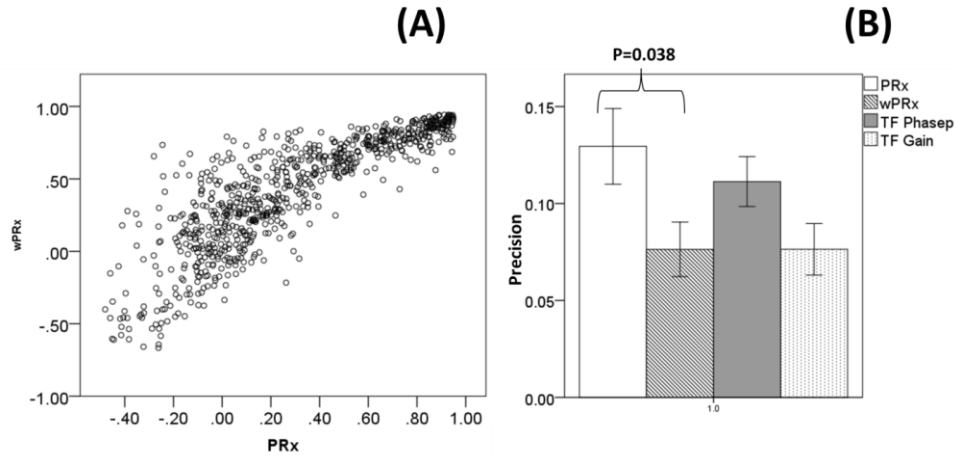


Figure 8.6 (A) Relationship between wPRx and PRx. (B) The precision of the four CA parameters: PRx, wPRx, TF phase and TF gain. Each dot represents one hour average of wPRx and PRx.

The ability of CA parameters in distinguishing refractory ICP

Figure 8.7 demonstrates that both PRx and wPRx can distinguish baseline and plateau ICP, while AUC of PRx equalled 0.882 and AUC of wPRx was 0.843. Either TF phase or TF gain can distinguish different ICP states ($p > 0.05$).

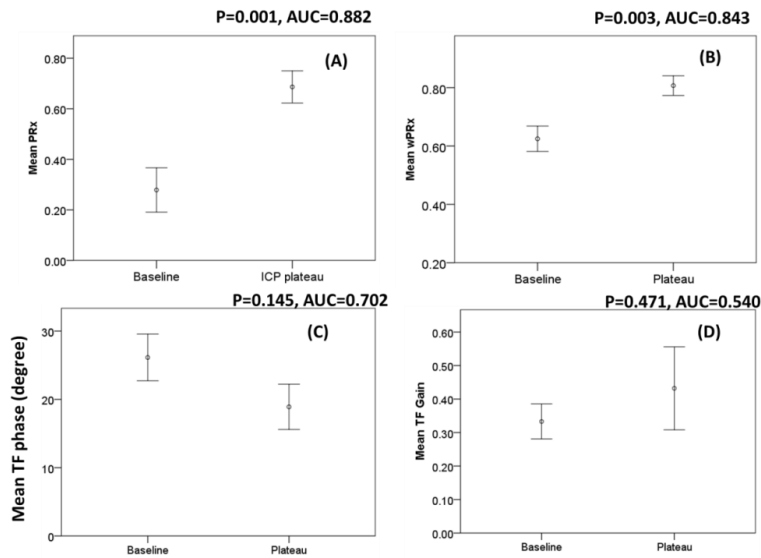


Figure 8.7 Average value of different CA parameters in two ICP states: baseline and plateau. ICP: intracranial pressure; CA: cerebral autoregulation; TF: transfer function; PRx: pressure reactivity index; wPRx: wavelet pressure reactivity index. Average value of all patients during baseline and plateau.

8.2.4 Discussion

Refractory ICP can always happen after brain trauma, which is very dangerous and needs immediate clinical action. CA is a potentially important parameter to use to monitor the brain state of the patients. In this study, the average ICP was increased from 24 ± 8 mmHg to 64 ± 22 mmHg, and the CA significantly deteriorated; this also matched the result from a previous study on the ICP plateau [279].

In this study, there is a significant linear relationship between wPRx and PRx, which again validates the calculation of CA through the wavelet method. Although both wPRx and PRx can distinguish different ICP states, wPRx showed a more stable result than PRx. This might be for two reasons: 1. The wavelet mainly focused on a specific frequency range, and is able to eliminate noises in unrelated bands, while PRx analysed the data across the whole frequency range. 2. The application of WTC can exclude the data points with an unreliable relationship between ABP and ICP, making the assessment more robust. TF behaved poorly in distinguishing different ICP states.

8.2.5 Conclusion

This section proved that even in sudden emergent cases of TBI, such as refractory ICP, both wPRx and PRx can be used to assess CA as a reliable tool, and both parameters can distinguish refractory ICP, with wPRx performing more stably. The TF did poorly in this situation.

8.3 Conclusion

This chapter applied different CA assessment methods to other clinical cases, ICP plateau and refractory ICP. The result showed that CA deteriorated during high ICP, and PRx, wPRx can distinguish ICP baseline and high ICP significantly.

CHAPTER 9 CONCLUSIONS AND FUTURE DIRECTIONS

In conclusion, it can be stated that all hypotheses listed in Chapter 1 were positively verified.

In detail:

1. This study examined the relationship between different commonly used methods for CA assessment, such as Mx, TF, ARI through a group of simulated data based on Tiecks' model and a cohort of TBI patients. The result showed strong relationship between ARI and Mx, as well as ARI and TF phase. It proved the interchangeability of these indices from theoretical and practical point of view. It also demonstrated that Mx and ARI were generally related with patients' outcome. Different input (ABP or CPP) will have influences on the CA indices.

2. A new autoregulation index (wPRx) based on time-frequency analysis, wavelet transform, was introduced and validated in two groups of experimental hypotension piglets' data. The wPRx was compared with a well-established parameter, PRx, and the result showed a strongly positive, approximately linear, relationship between wPRx and PRx. Afterwards, the wPRx was applied in 515 TBI patients, where similar strong relationship between wPRx and PRx was demonstrated, with wPRx showing more stable result.

3. The final aim of this project was to improve the estimation of CPPopt using the CA parameters for clinical guidance. A multi-window and weighting approach to estimate CPPopt for TBI patients was introduced and its performance scrutinised in a cohort of TBI patients. The results showed that the new proposed approach hugely improved the yield rate, from 55% to higher than 90% of the whole monitoring period offering significantly more stable behaviour, and all of that without worsening the relationship with outcome. The method, which can easily be programmed in an automated tool at the bedside, has the potential to make the technique of pressure autoregulation-steered management widely applicable in most ICUs.

4. In addition, this study also tested the performances of CA parameters in cerebral autoregulation during intracranial hypertension. The result showed deteriorated CA at high ICP, such as ICP plateau and refractory ICP.

Future continuation of the work presented here should include further investigation of the wavelet PRx index in order to unleash the full potential of the time-frequency localised 'PRx'. And without a doubt more work should be put into fine-tuning the algorithm of optimal CPP calculation. In particular the future work, could be broadly divided into several aspects:

1. The wavelet method in different clinical scenarios

An understanding of the physiology, pathophysiology, monitoring, and treatment of cerebral autoregulation is key in the evolution of clinical management of brain injury patients. This study validated a new time-frequency method, wavelet method (wPRx) for CA assessment, in traumatic brain injury. The result showed a great potential for its

application at bedside. However, more validations need to be done to extend this methodology into different modalities and different brain pathologies, such as tumour, stroke, brain haemorrhage and encephalitis. At the same time, various inputshave to be tried, because ICP is not a routine monitoring procedure for some of these brain injuries.

2. The time trends of dynamic cerebral autoregulation

Dynamic cerebral autoregulation is probably altered in acute brain injury, however, the temporal course of dynamic cerebral autoregulation and its correlation with clinical factors and outcomes are poorly understood [253]. In this study, the CA parameters were averaged across the whole monitoring time. For the future study, more efforts should focus on the time change (e.g. day-to-day change) and investigate how the trend will influence patient outcome.

3. Further exploration of the multi-window system

Based on Depreitere's method, the new multi-window algorithm for CPPopt calculation used in this study has already increased yield significantly, but there is still room for improvement. The comparison between different weighting strategies did not show big differences suggests that more investigations about weighting parameters need to be done. The weight factors of window length, 'fit error' and curves shape were fixed values in this study (0.5, 1, 0.1 respectively), that could be optimised to strike a balance between yield, reliability and variability of the measure in the future. Moreover, whether a combination of 36 windows is necessary, and the influence of the criterion of enforcing y axis needs to be studied. For CPPopt calculation using PRx or wPRx, we applied the same set of weighting factors which could be optimized. Investigations can be conducted with one parameter being changed and keeping others fixed, to find the most important factor.

4. A randomized clinical trial

The current retrospective studies already showed good patient outcome is related with small difference between CPP and CPPopt, which makes a randomized clinical trial assessing the effect of CPPopt in the management of TBI patient necessary. The multi-window algorithm introduced in Chapter 7 made CPPopt available during almost the whole monitoring period which makes the clinical application of CPPopt possible. The next step could be gently apply the CA parameters into clinical management. The patients can be divided into two groups as suggested in CONGITATE project, one was controlled group with CPP managed according to Brain Trauma Foundation guideline, between 60 and 70 mmHg (CPPopt information is recorded but hidden for the treating clinicians.); the other was experimental group, with CPP is targeted at CPPopt, and while no CPPopt is demonstrated, then CPP is managed according to Brain Trauma Foundation guidelines. The trial might contribute to the future individualize optimal CPP management guidelines for TBI and potentially improve patient outcome.

5. wPRx threshold for bad cerebral autoregulation

This study already showed advantage of wPRx as a more stable parameter to assess CA. There is a strong relationship between wPRx and PRx, and previous studies proved that PRx of 0.3 as a threshold of patients' bad or impaired CA, and PRx below 0 indicating good CA. In this study, we found wPRx can distinguish patient outcome more obviously, however, a certain threshold has not been spotted yet. Future study should try to find the threshold to make the method more practical and clinically useful.

6. Multi-window method applied to other patients

Besides CPPopt assessment inTBI, researchers also applied similar algorithm to different patients, such as infants. In a population of preterm infants, Costa et al used tissue oxygenation heart rate reactivity index (TOHRx), which is the correlation coefficient between slow waves of heart rate (HR) and tissue oxygenation index (TOI) measured with NIRS, to calculate optimal ABP value (ABPopt) [280]. The result showed infants who had an ABP lower than optimal ABP by at least 4 mm Hg had greater mortality rate. In their study, the determination of individual ABPopt was possible in 81.5% infants. The multi-window algorithm, introduced in this study could be a potential tool to improve the yield of ABPopt.

REFERENCES

- [1] M. J. Rosner and S. Daughton, "Cerebral perfusion pressure management in head injury.," *The Journal of trauma*, vol. 30, no. 8, pp. 933-940-941, 1990.
- [2] G. J. Carney N, Totten AM, O'Reilly C, Ullman JS, Hawryluk GW, Bell MJ, Bratton SL, Chesnut R, Harris OA, Kisson N, Rubiano AM, Shutter L, Tasker RC, Vavilala MS, Wilberger J, Wright DW, "Guidelines for the Management of Severe Traumatic Brain Injury, Fourth Edition," *Neurosurgery*, 2016.
- [3] R. M. Chesnut, N. Temkin, N. Carney, S. Dikmen, C. Rondina, W. Videtta, G. Petroni, S. Lujan, J. Pridgeon, J. Barber, J. Machamer, K. Chaddock, J. M. Celix, M. Cherner, and T. Hendrix, "A trial of intracranial-pressure monitoring in traumatic brain injury.," *N. Engl. J. Med.*, vol. 367, no. 26, pp. 2471–81, 2012.
- [4] C. S. Robertson, A. B. Valadka, H. J. Hannay, C. F. Contant, S. P. Gopinath, M. Cormio, M. Uzura, and R. G. Grossman, "Prevention of secondary ischemic insults after severe head injury.," *Crit. Care Med.*, vol. 27, no. 10, pp. 2086–2095, 1999.
- [5] R. B. Panerai, "Assessment of cerebral pressure autoregulation in humans--a review of measurement methods.," *Physiol. Meas.*, vol. 19, no. 3, pp. 305–38, Aug. 1998.
- [6] M. Reinhard, M. Roth, B. Guschlbauer, a Harloff, J. Timmer, M. Czosnyka, and a Hetzel, "Dynamic cerebral autoregulation in acute ischemic stroke assessed from spontaneous blood pressure fluctuations.," *Stroke.*, vol. 36, no. 8, pp. 1684–9, Aug. 2005.
- [7] W. Rudziński, M. Swiat, M. Tomaszewski, and J. Krejza, "Cerebral hemodynamics and investigations of cerebral blood flow regulation.," *Nucl. Med. Rev. Cent. East. Eur.*, vol. 10, no. 1, pp. 29–42, 2007.
- [8] W. D. Obrist, H. K. Thompson, H. S. Wang, and W. E. Wilkinson, "Regional cerebral blood flow estimated by 133-xenon inhalation.," *Stroke*, vol. 6, no. 3, pp. 245–56, 2011.
- [9] M. Chacón, J. L. Jara, and R. B. Panerai, "A new model-free index of dynamic cerebral blood flow autoregulation.," *PLoS One*, vol. 9, no. 10, p. e108281, 2014.
- [10] R. Aaslid, K. F. Lindegaard, W. Sorteberg, and H. Nornes, "Cerebral autoregulation dynamics in humans.," *Stroke*, vol. 20, no. 1, pp. 45–52, 1989.
- [11] A. Kalanuria, P. a. Nyquist, R. a. Armonda, and A. Razumovsky, "Use of Transcranial Doppler (TCD) Ultrasound in the Neurocritical Care Unit," *Neurosurg. Clin. N. Am.*, vol. 24, no. 3, pp. 441–456, 2013.
- [12] F. P. Tiecks, A. M. Lam, R. Aaslid, and D. W. Newell, "Comparison of Static and Dynamic Cerebral Autoregulation Measurements," *Stroke*, vol. 26, no. 6, pp. 1014–1019, 1995.
- [13] R. Aaslid, D. W. Newell, R. Stooss, W. Sorteberg, and K. F. Lindegaard, "Assessment of cerebral autoregulation dynamics from simultaneous arterial and venous transcranial Doppler recordings in humans.," *Stroke.*, vol. 22, no. 9, pp. 1148–1154, 1991.
- [14] L. A. Lipsitz, S. Mukai, J. Hamner, M. Gagnon, and V. Babikian, "Dynamic regulation of middle cerebral artery blood flow velocity in aging and hypertension.," *Stroke.*, vol. 31, no. 8, pp. 1897–903, 2000.
- [15] R. Zhang, J. H. Zuckerman, K. Iwasaki, T. E. Wilson, C. G. Crandall, and B. D. Levine, "Autonomic neural control of dynamic cerebral autoregulation in humans.," *Circulation*, vol. 106, no. 14, pp. 1814–20, 2002.

- [16] A. S. S. Meel-van den Abeelen, D. M. Simpson, L. J. Y. Wang, C. H. Slump, R. Zhang, T. Tarumi, C. A. Rickards, S. Payne, G. D. Mitsis, K. Kostoglou, V. Marmarelis, D. Shin, Y. C. Tzeng, P. N. Ainslie, E. Gommer, M. Müller, A. C. Dorado, P. Smielewski, B. Yelicich, C. Puppo, X. Liu, M. Czosnyka, C. Y. Wang, V. Novak, R. B. Panerai, and J. A. H. R. Claassen, “Between-centre variability in transfer function analysis, a widely used method for linear quantification of the dynamic pressure-flow relation: The CARNet study,” *Med. Eng. Phys.*, vol. 36, no. 5, pp. 620–627, 2014.
- [17] R. Zhang, J. H. Zuckerman, C. A. Giller, and B. D. Levine, “Transfer function analysis of dynamic cerebral autoregulation in humans,” *Am. J. Physiol.*, vol. 274, no. 1 Pt 2, pp. H233-41, 1998.
- [18] R. B. Panerai, R. P. White, H. S. Markus, and D. H. Evans, “Grading of cerebral dynamic autoregulation from spontaneous fluctuations in arterial blood pressure.,” *Stroke.*, vol. 29, no. 11, pp. 2341–2346, 1998.
- [19] M. Czosnyka, P. Smielewski, P. Kirkpatrick, D. K. Menon, and J. D. Pickard, “Monitoring of cerebral autoregulation in head-injured patients.,” *Stroke.*, vol. 27, no. 10, pp. 1829–1834, 1996.
- [20] M. Czosnyka, P. Smielewski, S. Piechnik, L. a Steiner, and J. D. Pickard, “Cerebral autoregulation following head injury.,” *J. Neurosurg.*, vol. 95, no. 5, pp. 756–763, 2001.
- [21] M. Czosnyka, P. Smielewski, P. Kirkpatrick, R. J. Laing, D. Menon, and J. D. Pickard, “Continuous assessment of the cerebral vasomotor reactivity in head injury,” *Neurosurgery*, vol. 41, no. 1, pp. 11–19, 1997.
- [22] K. M. Brady, J. O. Mytar, J. K. Lee, D. E. Cameron, L. a. Vricella, W. R. Thompson, C. W. Hogue, and R. B. Easley, “Monitoring cerebral blood flow pressure autoregulation in pediatric patients during cardiac surgery,” *Stroke*, vol. 41, no. 9, pp. 1957–1962, 2010.
- [23] M. J. Lang EW, Mudaliar Y, Lagopoulos J, Dorsch N, Yan A, Griffith J, “Review of Cerebral Autoregulation: Assessment and Measurements,” *Australas. Anaesth.*, pp. 161–172, 2005.
- [24] G. G. Eriksen VR, Hahn GH, “Cerebral autoregulation in the preterm newborn using near-infrared spectroscopy: a comparison of time-domain and frequency-domain analyses,” *J Biomed Opt*, vol. 20, p. 37009, 2015.
- [25] M. Balestreri, M. Czosnyka, L. a. Steiner, M. Hiler, E. a. Schmidt, B. Matta, D. Menon, P. Hutchinson, and J. D. Pickard, “Association between outcome, cerebral pressure reactivity and slow ICP waves following head injury,” *Acta Neurochir. Suppl.*, no. 95, pp. 25–28, 2005.
- [26] D. K. Radolovich, M. J. H. Aries, G. Castellani, a. Corona, a. Lavinio, P. Smielewski, J. D. Pickard, and M. Czosnyka, “Pulsatile intracranial pressure and cerebral autoregulation after traumatic brain injury,” *Neurocrit. Care*, vol. 15, no. 3, pp. 379–386, 2011.
- [27] R. B. Panerai, N. P. Saeed, and T. G. Robinson, “Cerebrovascular effects of the thigh cuff maneuver.,” *Am. J. Physiol. Heart Circ. Physiol.*, vol. 308, no. 7, pp. H688-96, 2015.
- [28] R. B. Panerai, “Nonstationarity of dynamic cerebral autoregulation.,” *Med. Eng. Phys.*, Oct. 2013.
- [29] F. P. Tiecks, A. M. Lam, B. F. Matta, S. Strebel, C. Douville, and D. W. Newell, “Effects of the valsalva maneuver on cerebral circulation in healthy adults. A transcranial Doppler Study.,” *Stroke*, vol. 26, no. 8, pp.

- 1386–1392, 1995.
- [30] R. B. Panerai, “Cerebral autoregulation: from models to clinical applications,” *Cardiovasc.Eng.*, vol. 8, no. 1, pp. 42–59, 2008.
- [31] X. Liu, M. Czosnyka, J. Donnelly, K. P. Budohoski, G. V Varsos, N. Nasr, K. M. Brady, M. Reinhard, P. J. Hutchinson, and P. Smielewski, “Comparison of frequency and time domain methods of assessment of cerebral autoregulation in traumatic brain injury,” *J. Cereb. Blood Flow Metab.*, vol. 11, no. October, pp. 1–9, 2014.
- [32] R. Zhang, J. H. Zuckerman, C. A. Giller, and B. D. Levine, “Transfer function analysis of dynamic cerebral autoregulation in humans,” *Am. J. Physiol.*, vol. 274, pp. 233–241, 1998.
- [33] P. S. Addison, “A Review of Wavelet Transform Time-Frequency Methods for NIRS-based Analysis of Cerebral Autoregulation,” *IEEE Rev. Biomed. Eng.*, vol. PP, no. 99, p. 1, 2015.
- [34] K. Keissar, L. R. Davrath, and S. Akselrod, “Coherence analysis between respiration and heart rate variability using continuous wavelet transform,” *Philos. Trans. A. Math. Phys. Eng. Sci.*, vol. 367, no. 1892, pp. 1393–1406, 2009.
- [35] D. Maraun and J. Kurths, “Cross wavelet analysis: significance testing and pitfalls,” *Nonlinear Process. Geophys.*, vol. 11, no. 4, pp. 505–514, 2004.
- [36] L. Steiner, M. Czosnyka, and S. Piechnik, “Continuous monitoring of cerebrovascular pressure reactivity allows determination of optimal cerebral perfusion pressure in patients with traumatic brain injury,” *Crit. Care*, 2002.
- [37] C. Zweifel, A. Lavinio, L. A. Steiner, D. Radolovich, P. Smielewski, I. Timofeev, M. Hiler, M. Balestreri, P. J. Kirkpatrick, J. D. Pickard, P. Hutchinson, and M. Czosnyka, “Continuous monitoring of cerebrovascular pressure reactivity in patients with head injury,” *Neurosurg. Focus*, vol. 25, no. 4, p. E2, 2008.
- [38] M. J. H. Aries, M. Czosnyka, K. P. Budohoski, L. a. Steiner, A. Lavinio, A. G. Koliass, P. J. Hutchinson, K. M. Brady, D. K. Menon, J. D. Pickard, and P. Smielewski, “Continuous determination of optimal cerebral perfusion pressure in traumatic brain injury,” *Crit. Care Med.*, vol. 40, no. 8, pp. 2456–2463, 2012.
- [39] N. a Lassen, “Cerebral blood flow and oxygen consumption in man,” *Physiol. Rev.*, vol. 39, no. 2, pp. 183–238, 1959.
- [40] H. Johnston and J. O. Rowan, “Raised intracranial pressure and cerebral blood flow,” *J. Neurol. Neurosurg. Psychiatry*, vol. 37, pp. 392–402, 1974.
- [41] A. A. Lassen NA, “The upper limit of autoregulation of cerebral blood flow—on the pathogenesis of hypertensive encephalopathy,” *Scand J Clin Lab Invest.*, vol. 30, no. 2, pp. 113–116, 1972.
- [42] N. a Lassen, “Cerebral blood flow and oxygen consumption in man,” *Physiological reviews*, vol. 39, no. 2, pp. 183–238, 1959.
- [43] A. Monro, *Observations on the Structure and Function of the Nervous System*. Edinburgh: Creech & Johnston, 1783.
- [44] G. Kellie, “Appearances observed in the dissection of two of three individuals; death from cold and

- congestion of the brain,” *Trans. Medico-Chirurgical Soc. Edinburgh*, vol. 1, pp. 84–169, 1824.
- [45] R. B. P Reilly, *Head Injury 2Ed: Pathophysiology & Management*. CRC Press, 2005.
- [46] B. Mokri, “The Monro-Kellie hypothesis: applications in CSF volume depletion.,” *Neurology*, vol. 56, no. 12, pp. 1746–1748, 2001.
- [47] D. Greitz, R. Wirestam, A. Franck, B. Nordell, C. Thomsen, and F. Ståhlberg, “Pulsatile brain movement and associated hydrodynamics studied by magnetic resonance phase imaging. The Monoro-Kellie doctrine revisited,” *Neuroradiology*, vol. 34, no. 5, pp. 370–380, 1992.
- [48] D. Greitz, “Radiological assessment of hydrocephalus: new theories and implications for therapy.,” *Neurosurg. Rev.*, vol. 27, no. 3, pp. 145-165-167, 2004.
- [49] S. Qvarlander, B. Lundkvist, L.-O. D. Koskinen, J. Malm, and A. Eklund, “Pulsatility in CSF dynamics: pathophysiology of idiopathic normal pressure hydrocephalus.,” *J. Neurol. Neurosurg. Psychiatry*, vol. 84, no. 7, pp. 735–41, 2013.
- [50] L. A. Steiner and P. J. D. Andrews, “Monitoring the injured brain: ICP and CBF,” *British Journal of Anaesthesia*, vol. 97, no. 1. pp. 26–38, 2006.
- [51] T. Kocher, *Hirnerschütterung, Hirndruck und chirurgische Eingriffe beim Hirnerkrankungen, in Nothnagel: Spezielle Pathologie und Therapie*. Vienna, 1901.
- [52] P. P. Ryder, H. W., Espey, F. F., Kristoff, F. V. and Evans, “Observations on the interrelationships of intracranial pressure and cerebral blood flow.,” *J. Neurosurg.*, vol. 8, pp. 46–58, 1951.
- [53] M. W. Eng H.Lo, Josephine Lok, Mingming Ning, *Vascular Mechanisms in CNS Trauma*. New York: Springer science + business media, 2014.
- [54] C. G. Lisa Hill, “cerebral blood flow and intracranial pressure,” *Anaesth. Tutor. week*, 2007.
- [55] M. Czosnyka, S. Piechnik, H. K. Richards, P. Kirkpatrick, P. Smielewski, and J. D. Pickard, “Contribution of mathematical modelling to the interpretation of bedside tests of cerebrovascular autoregulation.,” *J. Neurol. Neurosurg. Psychiatry*, vol. 63, no. 6, pp. 721–31, 1997.
- [56] D. Clarke and L. Sokoloff, *Circulation and Energy Metabolism of the Brain*. 1999.
- [57] Paulson OB, Strandgaard S, and Edvinsson L, “Cerebral autoregulation.,” *Cerebrovasc. brain Metab. Rev.*, vol. 2, no. 2, pp. 161–192, 1990.
- [58] N. Lassen, “Cerebral blood flow and oxygen consumption in man.,” *Physiol. Rev.*, vol. 39, no. 2, pp. 183–238, 1959.
- [59] M. J. Cipolla, “The Cerebral Circulation,” in *Colloquium Series on Integrated Systems Physiology: From Molecule to Function to Disease*, 2009, pp. 1–59.
- [60] A. M. H. S. Strandgaard, D. Sengupta, E. T. Mackenzie, J. O. Rowan, J. Olesen, E. Skinhøj, N. A. Lassen, “The Lower and Upper Limits for Autoregulation of Cerebral Blood Flow,” in *Cerebral Circulation and Metabolism*, New York: Springer Berlin Heidelberg, 1975, pp. 3–5.
- [61] S. J. Phillips and J. P. Whisnant, “Hypertension and the brain. The National High Blood Pressure Education Program.,” *Arch. Intern. Med.*, vol. 152, no. 5, pp. 938–945, 1992.

- [62] S. Schwab, R. Kollmar, D. F. Hanley, and W. Hacke, "Critical Care Neurology," in *Neurological Disorders: Course and Treatment: Second Edition*, 2003, pp. 721–747.
- [63] G. Osol, J. F. Brekke, K. McElroy-Yaggy, and N. I. Gokina, "Myogenic tone, reactivity, and forced dilatation: a three-phase model of in vitro arterial myogenic behavior.," *Am. J. Physiol. Heart Circ. Physiol.*, vol. 283, no. 6, pp. H2260-7, 2002.
- [64] D. Heistad and H. Kontos, "Cerebral circulation," in *Handbook of Physiology, Section 2: The Cardiovascular System Volume III, Peripheral Circulation and Organ Blood Flow, Part 1*, 1983, pp. 137–82.
- [65] H. a Kontos, E. P. Wei, R. M. Navari, J. E. Levasseur, W. I. Rosenblum, and J. L. Patterson, "Responses of cerebral arteries and arterioles to acute hypotension and hypertension.," *Am. J. Physiol.*, vol. 234, pp. H371–H383, 1978.
- [66] N. N. Ekström-Jodal B, Häggendal E, Linder LE, "Cerebral blood flow autoregulation at high arterial pressures and different levels of carbon dioxide tension in dogs.," *Eur Neurol.*, vol. 6, no. 1, pp. 6–10.
- [67] S. Strandgaard, J. V Jones, E. T. MacKenzie, and A. M. Harper, "Upper limit of cerebral blood flow autoregulation in experimental renovascular hypertension in the baboon," *Circ. Res.*, vol. 37, no. 2, pp. 164–167, 1975.
- [68] E. Teasdale, E. Cardoso, S. Galbraith, and G. Teasdale, "CT scan in severe diffuse head injury: physiological and clinical correlations," *J. Neurol. Neurosurg. Psychiatry*, vol. 47, no. January, pp. 600–603, 1984.
- [69] S. E. and J. A., "Cerebral blood flow and intracranial pressure," *Anaesth. Intensive Care Med.*, vol. 9, no. 5, pp. 222–225, 2008.
- [70] C. S. Roy and C. S. Sherrington, "On the Regulation of the Blood-supply of the Brain.," *J. Physiol.*, vol. 11, no. 1–2, p. 85–158.17, 1890.
- [71] A. Norup Nielsen and M. Lauritzen, "Coupling and uncoupling of activity-dependent increases of neuronal activity and blood flow in rat somatosensory cortex.," *J. Physiol.*, vol. 533, no. Pt 3, pp. 773–785, 2001.
- [72] O. B. Paulson and E. A. Newman, "Does the release of potassium from astrocyte endfeet regulate cerebral blood flow?," *Science*, vol. 237, no. 4817, pp. 896–8, 1987.
- [73] C. Iadecola, "Does nitric oxide mediate the increases in cerebral blood flow elicited by hypercapnia?," *Proc. Natl. Acad. Sci. U. S. A.*, vol. 89, no. 9, pp. 3913–3916, 1992.
- [74] E. C. Peterson, Z. Wang, and G. Britz, "Regulation of cerebral blood flow," *International Journal of Vascular Medicine*, vol. 2011. 2011.
- [75] D. A. Pelligrino, R. L. Gay 3rd, V. L. Baughman, and Q. Wang, "NO synthase inhibition modulates NMDA-induced changes in cerebral blood flow and EEG activity," *Am J Physiol*, vol. 271, no. 3 Pt 2, pp. H990-5, 1996.
- [76] J. H. Lee, D. F. Kelly, M. Oertel, D. L. McArthur, T. C. Glenn, P. Vespa, W. J. Boscardin, and N. a Martin, "Carbon dioxide reactivity, pressure autoregulation, and metabolic suppression reactivity after head injury: a

- transcranial Doppler study.," *J. Neurosurg.*, vol. 95, no. 2, pp. 222–232, 2001.
- [77] K. H. Chan, J. D. Miller, N. M. Dearden, P. J. Andrews, and S. Midgley, "The effect of changes in cerebral perfusion pressure upon middle cerebral artery blood flow velocity and jugular bulb venous oxygen saturation after severe brain injury," *J Neurosurg*, vol. 77, no. 1, pp. 55–61, 1992.
- [78] E. Bor-Seng-Shu, W. S. Kita, E. G. Figueiredo, W. S. Paiva, E. T. Fonoff, M. J. Teixeira, and R. B. Panerai, "Cerebral hemodynamics: concepts of clinical importance.," *Arquivos de neuro-psiquiatria*, vol. 70, no. 5, pp. 352–356, 2012.
- [79] H. D. Busija DW, "Factors involved in the physiological regulation of the cerebral circulation," *Rev Physiol Biochem Pharamacol*, vol. 101, pp. 161–211, 1984.
- [80] N. Charkoudian and J. a Rabbitts, "Sympathetic neural mechanisms in human cardiovascular health and disease.," *Mayo Clin. Proc.*, vol. 84, no. 9, pp. 822–30, 2009.
- [81] W. T. Talman and D. Nitschke Dragon, "Neuronal nitric oxide mediates cerebral vasodilatation during acute hypertension," *Brain Res.*, vol. 1139, no. 1, pp. 126–132, 2007.
- [82] T. W. McAllister, "Neurobiological consequences of traumatic brain injury," *Dialogues Clin. Neurosci.*, vol. 13, no. 3, pp. 287–300, 2011.
- [83] J. L. Miller, J. D. Jones, P. A., Dearden, N. M. and Tocher, "Progress in the management of head injury.," *Br. J. Surg.*, vol. 79, pp. 60–64, 1992.
- [84] M. Faul, L. Xu, M. M. Wald, and V. G. Coronado, "Traumatic brain injury in the United States: emergency department visits, hospitalizations and deaths 2002–2006," ... , 2010.
- [85] A. M. Marek Majdan, Dominika Plancikova, Alexandra Brazinova, Martin Rusnak, Daan Nieboer, Valery Feigin, "Epidemiology of traumatic brain injuries in Europe: a cross-sectional analysis," *Lancet Public Heal.*, vol. 1, pp. e76–83, 2016.
- [86] and A. I. R. M. Wouter Peeters, Ruben van den Brande, Suzanne Polinder, Alexandra Brazinova, Ewout W. Steyerberg, Hester F. Lingsma, "Epidemiology of traumatic brain injury in Europe," *Acta Neurochir*, vol. 157, no. 10, pp. 1683–1696, 2015.
- [87] "Centers for Disease Control and Prevention. Nonfatal Traumatic Brain Injuries Related to Sports and Recreation Activities Among Persons Aged ≤ 19 Years — United States, 2001–2009.," *MMWR*, vol. 60, no. 39, pp. 1337–1342, 2011.
- [88] D. J. Thurman, C. M. Branche, and J. E. Snizek, "The epidemiology of sports-related traumatic brain injuries in the United States: recent developments.," *J. Head Trauma Rehabil.*, vol. 13, no. 2, pp. 1–8, 1998.
- [89] A. Brazinova, V. Rehorcikova, M. S. Taylor, V. Buckova, M. Majdan, M. Psota, W. Peeters, V. Feigin, A. Theadom, L. Holkovic, and A. Synnot, "Epidemiology of traumatic brain injury in Europe: a living systematic review," *J. Neurotrauma*, p. neu.2015.4126, 2015.
- [90] J. Ghajar, "Traumatic brain injury," *Lancet*, vol. 356, no. 9233, pp. 923–929, 2000.
- [91] S. T. Dawodu, "Traumatic Brain Injury (TBI) - Definition, Epidemiology, Pathophysiology," *Sports Medicine*, 2011. [Online]. Available: <http://emedicine.medscape.com/article/326510-overview>.

- [92] J. D. Corrigan, K. Smith-Knapp, and C. V Granger, "Outcomes in the first 5 years after traumatic brain injury.," *Arch. Phys. Med. Rehabil.*, vol. 79, no. 3, pp. 298–305, 1998.
- [93] H. E. Jacobs, "The Los Angeles Head Injury Survey: procedures and initial findings.," *Arch. Phys. Med. Rehabil.*, vol. 69, no. 6, pp. 425–431, 1988.
- [94] H. E. Jacobs, "The Los Angeles Head Injury Survey: Project rationale and design implications," *J. Head Trauma Rehabil.*, vol. 2, no. 3, pp. 37–50, 1987.
- [95] E. C. Jünger, D. W. Newell, G. a Grant, a M. Avellino, S. Ghatan, C. M. Douville, a M. Lam, R. Aaslid, and H. R. Winn, "Cerebral autoregulation following minor head injury.," *J. Neurosurg.*, vol. 86, pp. 425–432, 1997.
- [96] G. J. Bouma, J. P. Muizelaar, K. Bando, and A. Marmarou, "Blood pressure and intracranial pressure-volume dynamics in severe head injury: relationship with cerebral blood flow.," *J. Neurosurg.*, vol. 77, no. 1, pp. 15–19, 1992.
- [97] R. Ishii, "Regional cerebral blood flow in patients with ruptured intracranial aneurysms.," *J. Neurosurg.*, vol. 50, no. 5, pp. 587–94, 1979.
- [98] O. J. Heilbrun MP, "Regional cerebral blood flow studies in subarachnoid hemorrhage," *Eur Neurol*, vol. 8, no. 1, pp. 1–7, 1972.
- [99] G. J. Bouma and J. P. Muizelaar, "Cerebral blood flow, cerebral blood volume, and cerebrovascular reactivity after severe head injury.," *J. Neurotrauma*, vol. 9 Suppl 1, no. March, pp. S333–48, 1992.
- [100] T. W. Overgaard J, "Cerebral circulation after head injury. 1. Cerebral blood flow and its regulation after closed head injury with emphasis on clinical correlations.," *J Neurosurg*, vol. 41, no. 5, pp. 531–41, 1974.
- [101] J. M. Simard and M. Bellefleur, "Systemic arterial hypertension in head trauma," *Am. J. Cardiol.*, vol. 63, no. 6, pp. C32–C35, 1989.
- [102] E. W. Lang and R. M. Chesnut, "Intracranial pressure and cerebral perfusion pressure in severe head injury.," *New Horiz.*, vol. 3, no. 3, pp. 400–409, 1995.
- [103] C. S. Robertson, R. K. Narayan, Z. L. Gokaslan, R. Pahwa, R. G. Grossman, P. Caram, and E. Allen, "Cerebral arteriovenous oxygen difference as an estimate of cerebral blood flow in comatose patients.," *J. Neurosurg.*, vol. 70, no. 2, pp. 222–230, 1989.
- [104] C. Hawthorne and I. Piper, "Monitoring of intracranial pressure in patients with traumatic brain injury," *Frontiers in Neurology*, vol. 5 JUN. 2014.
- [105] L. Dunn, "Raised intracranial pressure.," *J. Neurol. Neurosurg. Psychiatry*, vol. 2, no. 3, pp. i23–i27, 2002.
- [106] et al. Bratton SL, Chestnut RM, Ghajar J, McConnell Hammond FF, Harris OA, Hartl R, "Guidelines for the management of severe traumatic brain injury. VIII. Intracranial pressure thresholds.," *J Neurotrauma*, vol. 24, no. Suppl 1, pp. S55–810, 2007.
- [107] J. Dinsmore, "Traumatic brain injury: an evidence-based review of management," *Contin. Educ. Anaesthesia, Crit. Care Pain*, vol. 13, no. 6, pp. 189–195, 2013.
- [108] J. Donnelly, K. P. Budohoski, P. Smielewski, and M. Czosnyka, "Regulation of the cerebral circulation:

- bedside assessment and clinical implications.,” *Crit. Care*, vol. 20, no. 1, p. 129, 2016.
- [109] P. J. Czosnyka M, Smielewski P, Piechnik S, Schmidt EA, Al-Rawi PG, Kirkpatrick PJ, “Hemodynamic characterization of intracranial pressure plateau waves in head-injured patients,” *J. Neurosurg.*, vol. 91, no. 1, pp. 11–9, 1999.
- [110] M. Czosnyka, P. Smielewski, P. Kirkpatrick, R. J. Laing, D. Menon, and J. D. Pickard, “Continuous assessment of the cerebral vasomotor reactivity in head injury.,” *Neurosurgery*, vol. 41, pp. 11-17-19, 1997.
- [111] M. Jaeger, M. U. Schuhmann, M. Soehle, C. Nagel, and J. Meixensberger, “Continuous monitoring of cerebrovascular autoregulation after subarachnoid hemorrhage by brain tissue oxygen pressure reactivity and its relation to delayed cerebral infarction,” *Stroke*, vol. 38, no. 3, pp. 981–986, 2007.
- [112] K. P. Budohoski, M. Czosnyka, P. Smielewski, M. Kasproicz, A. Helmy, D. Bulters, J. D. Pickard, and P. J. Kirkpatrick, “Impairment of cerebral autoregulation predicts delayed cerebral ischemia after subarachnoid hemorrhage: a prospective observational study.,” *Stroke.*, vol. 43, no. 12, pp. 3230–7, 2012.
- [113] J. Liu, Y. Wang, Y. Akamatsu, C. C. Lee, R. A. Stetler, M. T. Lawton, and G. Y. Yang, “Vascular remodeling after ischemic stroke: Mechanisms and therapeutic potentials,” *Prog. Neurobiol.*, vol. 115, pp. 138–156, 2013.
- [114] M. J. H. Aries, J. W. Elting, J. De Keyser, B. P. H. Kremer, and P. C. a J. Vroomen, “Cerebral autoregulation in stroke: A review of transcranial doppler studies,” *Stroke*, vol. 41, no. 11. pp. 2697–2704, 2010.
- [115] A. L. Lin, P. T. Fox, Y. Yang, H. Lu, L. H. Tan, and J. H. Gao, “Evaluation of MRI models in the measurement of CMRO₂ and its relationship with CBF,” *Magn. Reson. Med.*, vol. 60, no. 2, pp. 380–389, 2008.
- [116] G. H. Hahn, K. B. Christensen, T. S. Leung, and G. Greisen, “Precision of coherence analysis to detect cerebral autoregulation by near-infrared spectroscopy in preterm infants.,” *J. Biomed. Opt.*, vol. 15, no. 3, pp. 37002-1-37002–10, 2010.
- [117] K. P. Budohoski, M. Czosnyka, P. J. Kirkpatrick, P. Smielewski, L. a Steiner, and J. D. Pickard, “Clinical relevance of cerebral autoregulation following subarachnoid haemorrhage.,” *Nat. Rev. Neurol.*, vol. 9, no. 3, pp. 152–63, 2013.
- [118] R. B. Panerai, R. P. White, H. S. Markus, and D. H. Evans, “Grading of cerebral dynamic autoregulation from spontaneous fluctuations in arterial blood pressure.,” *Stroke.*, vol. 29, no. 11, pp. 2341–6, Dec. 1998.
- [119] N. Holstein-Rathlou, A. Wagner, and D. Marsh, “Tubuloglomerular feedback dynamics and renal blood flow autoregulation in rats.,” *Am. J. Physiol.*, vol. 260, no. 1 Pt 2, pp. F53-68, 1991.
- [120] A. P. Blaber, R. L. Bondar, F. Stein, P. T. Dunphy, P. Moradshahi, M. S. Kassam, and R. Freeman, “Transfer function analysis of cerebral autoregulation dynamics in autonomic failure patients,” *Stroke*, vol. 28, no. 9, pp. 1686–1692, 1997.
- [121] M. Pagani, V. Somers, R. Furlan, S. Dell’Orto, J. Conway, G. Baselli, S. Cerutti, P. Sleight, and a Malliani, “Changes in autonomic regulation induced by physical training in mild hypertension.,” *Hypertension*, vol.

- 12, no. 6, pp. 600–610, 1988.
- [122] J. P. Saul, R. D. Berger, M. H. Chen, and R. J. Cohen, “Transfer function analysis of autonomic regulation. II. Respiratory sinus arrhythmia,” *Am. J. Physiol.*, vol. 256, no. 1 Pt 2, pp. H153–61, 1989.
- [123] P. A. Bendat JS, *Random Data: Analysis and Measurement Procedures*. New York: John Wiley & Sons, 1986.
- [124] P. R.B., “System identification of human cerebral blood flow regulatory mechanisms,” *Cardiovasc. Eng.*, vol. 4, no. 1, pp. 59–71, 2004.
- [125] M. Reinhard, T. Müller, B. Guschlbauer, J. Timmer, and a Hetzel, “Transfer function analysis for clinical evaluation of dynamic cerebral autoregulation--a comparison between spontaneous and respiratory-induced oscillations.,” *Physiol. Meas.*, vol. 24, no. 1, pp. 27–43, Mar. 2003.
- [126] J. A. Claassen, A. S. Meel-van den Abeelen, D. M. Simpson, R. B. Panerai, and international Cerebral Autoregulation Research Network (CARNet), “Transfer function analysis of dynamic cerebral autoregulation: A white paper from the International Cerebral Autoregulation Research Network.,” *J. Cereb. Blood Flow Metab.*, vol. 36, no. 4, pp. 665–80, 2016.
- [127] H. H. Hu, T. B. Kuo, W. J. Wong, Y. O. Luk, C. M. Chern, L. C. Hsu, and W. Y. Sheng, “Transfer function analysis of cerebral hemodynamics in patients with carotid stenosis,” *J. Cereb. Blood Flow Metab*, vol. 19, no. 4, pp. 460–465, 1999.
- [128] C. a Giller, “The frequency-dependent behavior of cerebral autoregulation.,” *Neurosurgery*, vol. 27, no. 3. pp. 362–8, 1990.
- [129] R. R. Diehl, D. Linden, D. Lücke, and P. Berlit, “Spontaneous blood pressure oscillations and cerebral autoregulation.,” *Clin. Auton. Res.*, vol. 8, pp. 7–12, 1998.
- [130] J. Chen, J. Liu, W.-H. Xu, R. Xu, B. Hou, L.-Y. Cui, and S. Gao, “Impaired dynamic cerebral autoregulation and cerebrovascular reactivity in middle cerebral artery stenosis.,” *PLoS One*, vol. 9, no. 2, p. e88232, 2014.
- [131] M. Czosnyka, P. Smielewski, P. Kirkpatrick, D. K. Menon, and J. D. Pickard, “Monitoring of cerebral autoregulation in head-injured patients,” *Stroke*, vol. 27, no. 10, pp. 1829–1834, 1996.
- [132] K. P. Budohoski, M. Reinhard, M. J. H. Aries, Z. Czosnyka, P. Smielewski, J. D. Pickard, P. J. Kirkpatrick, and M. Czosnyka, “Monitoring cerebral autoregulation after head injury. Which component of transcranial Doppler flow velocity is optimal?,” *Neurocrit. Care*, vol. 17, no. 2, pp. 211–218, 2012.
- [133] M. Reinhard, S. Rutsch, and A. Hetzel, “Cerebral autoregulation in acute ischemic stroke,” *Perspect. Med.*, vol. 1, no. 1–12, pp. 194–197, 2012.
- [134] M. Reinhard, M. Roth, B. Guschlbauer, A. Harloff, J. Timmer, M. Czosnyka, and A. Hetzel, “Dynamic cerebral autoregulation in acute ischemic stroke assessed from spontaneous blood pressure fluctuations,” *Stroke*, vol. 36, no. 8, pp. 1684–1689, 2005.
- [135] M. Reinhard, T. a. Gerds, D. Grabiak, P. R. Zimmermann, M. Roth, B. Guschlbauer, J. Timmer, M. Czosnyka, C. Weiller, and a. Hetzel, “Cerebral dysautoregulation and the risk of ischemic events in occlusive carotid artery disease,” *J. Neurol.*, vol. 255, no. 8, pp. 1182–1189, 2008.

- [136] S. K. Piechnik, X. Yang, M. Czosnyka, P. Smielewski, S. H. Fletcher, A. L. Jones, and J. D. Pickard, "The continuous assessment of cerebrovascular reactivity: a validation of the method in healthy volunteers.," *Anesth. Analg.*, vol. 89, no. 4, pp. 944–9, 1999.
- [137] M. Czosnyka, P. Smielewski, A. Lavinio, J. D. Pickard, and R. Panerai, "An assessment of dynamic autoregulation from spontaneous fluctuations of cerebral blood flow velocity: a comparison of two models, index of autoregulation and mean flow index.," *Anesth. Analg.*, vol. 106, no. 1, p. 234–9, table of contents, Jan. 2008.
- [138] P. Smielewski, M. Czosnyka, P. Kirkpatrick, and J. D. Pickard, "Evaluation of the transient hyperemic response test in head-injured patients.," *J. Neurosurg.*, vol. 86, no. 5, pp. 773–8, 1997.
- [139] M. Reinhard, M. Roth, T. Müller, M. Czosnyka, J. Timmer, and a. Hetzel, "Cerebral autoregulation in carotid artery occlusive disease assessed from spontaneous blood pressure fluctuations by the correlation coefficient index," *Stroke*, vol. 34, no. 9, pp. 2138–2144, 2003.
- [140] M. Czosnyka, P. Smielewski, Z. Czosnyka, S. Piechnik, L. a Steiner, E. Schmidt, I. Gooskens, M. Soehle, E. W. Lang, B. F. Matta, and J. D. Pickard, "Continuous assessment of cerebral autoregulation: clinical and laboratory experience.," *Acta Neurochir. Suppl.*, vol. 86, pp. 581–5, 2003.
- [141] C. F. Contant, a B. Valadka, S. P. Gopinath, H. J. Hannay, and C. S. Robertson, "Adult respiratory distress syndrome: a complication of induced hypertension after severe head injury.," *J. Neurosurg.*, vol. 95, no. 4, pp. 560–568, 2001.
- [142] M. DK, "Procrustes, the traumatic penumbra, and perfusion pressure targets in closed head injury," *Anesthesiology*, vol. 98, no. 4, p. 805–7., 2003.
- [143] E. Sorrentino, J. Diedler, M. Kasprovicz, K. P. Budohoski, C. Haubrich, P. Smielewski, J. G. Outtrim, A. Manktelow, P. J. Hutchinson, J. D. Pickard, D. K. Menon, and M. Czosnyka, "Critical thresholds for cerebrovascular reactivity after traumatic brain injury," *Neurocrit. Care*, vol. 16, no. 2, pp. 258–266, 2012.
- [144] M. Czosnyka, D. Radolovich, M. Balestreri, A. Lavinio, P. Hutchinson, I. Timofeev, P. Smielewski, and J. D. Pickard, "Gender-related differences in intracranial hypertension and outcome after traumatic brain injury," *Acta Neurochir Suppl*, vol. 102, pp. 25–28, 2008.
- [145] L. a. Lipsitz, S. Mukai, J. Hamner, M. Gagnon, and V. Babikian, "Dynamic Regulation of Middle Cerebral Artery Blood Flow Velocity in Aging and Hypertension," *Stroke*, vol. 31, no. 8, pp. 1897–1903, 2000.
- [146] J. P. Muizelaar, J. D. Ward, A. Marmarou, P. G. Newlon, and A. Wachi, "Cerebral blood flow and metabolism in severely head-injured children Part 2: Autoregulation," *J Neurosurg*, vol. 71, pp. 72–76, 1989.
- [147] R. B. Panerai, S. L. Dawson, and J. F. Potter, "Linear and nonlinear analysis of human dynamic cerebral autoregulation.," *Am. J. Physiol.*, vol. 277, no. 3 Pt 2, pp. H1089-99, 1999.
- [148] G. D. Mitsis, M. J. Poulin, P. A. Robbins, and V. Z. Marmarelis, "Nonlinear modeling of the dynamic effects of arterial pressure and CO₂ variations on cerebral blood flow in healthy humans," *IEEE Trans. Biomed. Eng.*, vol. 51, no. 11, pp. 1932–1943, 2004.
- [149] G. D. Mitsis, R. Zhang, B. D. Levine, and V. Z. Marmarelis, "Modeling of nonlinear physiological systems

- with fast and slow dynamics. II. Application to cerebral autoregulation,” *Ann. Biomed. Eng.*, vol. 30, no. 4, pp. 555–565, 2002.
- [150] M. Latka, M. Turalska, M. Glaubic-Latka, W. Kolodziej, D. Latka, and B. J. West, “Phase dynamics in cerebral autoregulation,” *Am. J. Physiol. Heart Circ. Physiol.*, vol. 289, no. 5, pp. H2272–H2279, 2005.
- [151] P. Addison, *The Illustrated Wavelet Transform Handbook*. 2002.
- [152] a B. Rowley, S. J. Payne, I. Tachtsidis, M. J. Ebden, J. P. Whiteley, D. J. Gavaghan, L. Tarassenko, M. Smith, C. E. Elwell, and D. T. Delpy, “Synchronization between arterial blood pressure and cerebral oxyhaemoglobin concentration investigated by wavelet cross-correlation,” *Physiol. Meas.*, vol. 28, no. 2, pp. 161–73, Feb. 2007.
- [153] P. Kvandal, L. Sheppard, S. A. Landsverk, A. Stefanovska, and K. A. Kirkeboen, “Impaired cerebrovascular reactivity after acute traumatic brain injury can be detected by wavelet phase coherence analysis of the intracranial and arterial blood pressure signals,” *J. Clin. Monit. Comput.*, vol. 27, no. 4, pp. 375–383, 2013.
- [154] R. A. D. Peter J. Brockwell, *Time series: theory and methods*. New York, NY: Springer Series in Statistics, 1991.
- [155] a. Grinsted, J. C. Moore, and S. Jevrejeva, “Application of the cross wavelet transform and wavelet coherence to geophysical time series,” *Nonlinear Process. Geophys.*, vol. 11, no. 5/6, pp. 561–566, 2004.
- [156] V. Novak, A. C. C. Yang, L. Lepicovsky, A. L. Goldberger, L. a Lipsitz, and C.-K. Peng, “Multimodal pressure-flow method to assess dynamics of cerebral autoregulation in stroke and hypertension,” *Biomed. Eng. Online*, vol. 3, no. 1, p. 39, 2004.
- [157] E. W. Lang, M. Kasprowicz, P. Smielewski, E. Santos, J. Pickard, and M. Czosnyka, “Short pressure reactivity index versus long pressure reactivity index in the management of traumatic brain injury,” *J. Neurosurg.*, vol. 122, no. 3, pp. 588–94, 2015.
- [158] R. Sánchez-Porras, E. Santos, M. Czosnyka, Z. Zheng, A. W. Unterberg, and O. W. Sakowitz, “‘Long’ pressure reactivity index (L-PRx) as a measure of autoregulation correlates with outcome in traumatic brain injury patients,” *Acta Neurochir. (Wien)*, vol. 154, no. 9, pp. 1575–1581, 2012.
- [159] C. Dias, M. J. Silva, E. Pereira, E. Monteiro, I. Maia, S. Barbosa, S. Silva, T. Honrado, A. Cerejo, M. J. H. Aries, P. Smielewski, J. A. Paiva, and M. Czosnyka, “Optimal Cerebral Perfusion Pressure Management at Bedside: A Single-Center Pilot Study,” *Neurocrit. Care*, vol. 23, no. 1, pp. 92–102, 2015.
- [160] P. M. Lewis, M. Czosnyka, B. G. Carter, J. V. Rosenfeld, E. Paul, N. Singhal, and W. Butt, “Cerebrovascular Pressure Reactivity in Children With Traumatic Brain Injury*,” *Pediatr. Crit. Care Med.*, vol. 16, no. 8, pp. 739–749, 2015.
- [161] B. Depreitere, F. Güiza, G. Van den Berghe, M. U. Schuhmann, G. Maier, I. Piper, and G. Meyfroidt, “Pressure autoregulation monitoring and cerebral perfusion pressure target recommendation in patients with severe traumatic brain injury based on minute-by-minute monitoring data,” *J. Neurosurg.*, vol. 120, no. 6, pp. 1451–7, 2014.
- [162] C. S. A. Weersink, M. J. H. Aries, C. Dias, M. X. Liu, A. G. Koliass, J. Donnelly, M. Czosnyka, M. M. C.

- van Dijk, J. Regtien, D. K. Menon, P. J. Hutchinson, and P. Smielewski, "Clinical and Physiological Events That Contribute to the Success Rate of Finding "Optimal" Cerebral Perfusion Pressure in Severe Brain Trauma Patients.," *Crit. Care Med.*, 2015.
- [163] E. W. Lang, H. M. Mehdorn, N. W. C. Dorsch, and M. Czosnyka, "Continuous monitoring of cerebrovascular autoregulation: a validation study," *J. Neurol. Neurosurg. Psychiatry*, vol. 72, no. 5, pp. 583–586, 2002.
- [164] L. A. Steiner, J. P. Coles, A. J. Johnston, D. A. Chatfield, P. Smielewski, T. D. Fryer, F. I. Aigbirhio, J. C. Clark, J. D. Pickard, D. K. Menon, and M. Czosnyka, "Assessment of cerebrovascular autoregulation in head-injured patients: A validation study," *Stroke*, vol. 34, no. 10, pp. 2404–2409, 2003.
- [165] J. Sahuquillo, M. A. Poca, A. Ausina, M. Báguena, R. M. Gracia, and E. Rubio, "Arterio-jugular differences of oxygen (AVDO₂) for bedside assessment of CO₂-reactivity and autoregulation in the acute phase of severe head injury," *Acta Neurochir. (Wien)*, vol. 138, no. 4, pp. 435–444, 1996.
- [166] N. P. Saeed, M. A. Horsfield, R. B. Panerai, A. K. Mistri, and T. G. Robinson, "Measurement of cerebral blood flow responses to the thigh cuff maneuver: a comparison of TCD with a novel MRI method," *J. Cereb. Blood Flow Metab.*, vol. 31, no. 5, pp. 1302–1310, 2011.
- [167] M. Wintermark, J.-P. Thiran, P. Maeder, P. Schnyder, and R. Meuli, "Simultaneous Measurement of Regional Cerebral Blood Flow by Perfusion CT and Stable Xenon CT: A Validation Study," *AJNR Am. J. Neuroradiol.*, vol. 22, no. 5, pp. 905–914, 2001.
- [168] J. W. Taylor, J. A., Tan, C. O., Hamner, "Assessing Cerebral Autoregulation via Oscillatory Lower Body Negative Pressure and Projection Pursuit Regression.," *J. Vis. Exp.*, vol. 94.
- [169] P. Smielewski, M. Czosnyka, P. Kirkpatrick, H. McEroy, H. Rutkowska, and J. D. Pickard, "Assessment of cerebral autoregulation using carotid artery compression.," *Stroke.*, vol. 27, no. 12, pp. 2197–203, 1996.
- [170] E. M. Buckley, A. B. Parthasarathy, P. E. Grant, A. G. Yodh, and M. A. Franceschini, "Diffuse correlation spectroscopy for measurement of cerebral blood flow: future prospects.," *Neurophotonics*, vol. 1, no. 1, p. 11009, 2014.
- [171] T. Durduran, C. Zhou, E. M. Buckley, M. N. Kim, G. Yu, R. Choe, J. W. Gaynor, T. L. Spray, S. M. Durning, S. E. Mason, L. M. Montenegro, S. C. Nicolson, R. A. Zimmerman, M. E. Putt, J. Wang, J. H. Greenberg, J. A. Detre, A. G. Yodh, and D. J. Licht, "Optical measurement of cerebral hemodynamics and oxygen metabolism in neonates with congenital heart defects," *J Biomed Opt.*, vol. 15, no. 3, p. 37004, 2010.
- [172] R. Zhang, J. H. Zuckerman, C. A. Giller, and B. D. Levine, "Transfer function analysis of dynamic cerebral autoregulation in humans.," *Am. J. Physiol.*, vol. 274, pp. 233–241, 1998.
- [173] F. P. Tiecks, C. Douville, S. Byrd, A. M. Lam, and D. W. Newell, "Evaluation of impaired cerebral autoregulation by the Valsalva maneuver," *Stroke*, vol. 27, no. 7, pp. 1177–1182, 1996.
- [174] M.-T. Lo, K. Hu, Y. Liu, C.-K. C.-K. Peng, and V. Novak, "Multimodal Pressure Flow Analysis: Application of Hilbert Huang Transform in Cerebral Blood Flow Regulation.," *EURASIP J. Adv. Signal Process.*, vol. 2008, no. 617, pp. 1–15, 2008.

- [175] B. T. F. A. A. of N. S. C. of N. Surgeons., "Guidelines for the Management of Severe Traumatic Brain Injury 3rd Edition," *J. Neurosurg.*, vol. 24, Suppl, no. 212, pp. S1-106, 2007.
- [176] G. Robertson, "Time Series Understanding in the Intensive Care Unit," University of Edinburgh, 2015.
- [177] M. A. De Georgia, F. Kaffashi, F. J. Jacono, K. A. Loparo, M. A. De Georgia, F. Kaffashi, F. J. Jacono, and K. A. Loparo, "Information Technology in Critical Care: Review of Monitoring and Data Acquisition Systems for Patient Care and Research," *Sci. World J.*, vol. 2015, pp. 1–9, 2015.
- [178] S. L. Bratton, R. M. Chestnut, J. Ghajar, F. F. McConnell Hammond, O. a Harris, R. Hartl, G. T. Manley, A. Nemecek, D. W. Newell, G. Rosenthal, J. Schouten, L. Shutter, S. D. Timmons, J. S. Ullman, W. Videtta, J. E. Wilberger, and D. W. Wright, "Guidelines for the management of severe traumatic brain injury. VI. Indications for intracranial pressure monitoring.," *J. Neurotrauma*, vol. 24 Suppl 1, no. 212, pp. S37–S44, 2007.
- [179] J. D. P. M Czosnyka, "Monitoring and interpretation of intracranial pressure," *J Neurol Neurosurg Psychiatry*, vol. 75:813-821, 2004.
- [180] N. Lundberg, "Continuous recording and control of ventricular fluid pressure in neurosurgical practice.," *Acta Psychiatr. Scand. Suppl.*, vol. 36, no. 149, pp. 1–193, 1960.
- [181] P. J. Aucoin, H. R. Kotilainen, N. M. Gantz, R. Davidson, P. Kellogg, and B. Stone, "Intracranial pressure monitors. Epidemiologic study of risk factors and infections.," *Am. J. Med.*, vol. 80, no. 3, pp. 369–376, 1986.
- [182] C. G. Mayhall, N. H. Archer, V. A. Lamb, A. C. Spadora, J. W. Baggett, J. D. Ward, and R. K. Narayan, "Ventriculostomy-related infections. A prospective epidemiologic study.," *N. Engl. J. Med.*, vol. 310, no. 9, pp. 553–9, 1984.
- [183] G. Citerio and P. J. D. Andrews, "Intracranial pressure Part two: Clinical applications and technology," in *Applied Physiology in intensive care medicine*, 2009, pp. 109–112.
- [184] M. D. Bullock RM, Chesnut RM, Clifton GL, Ghajar J, "Guidelines for the management of severe traumatic brain injury.," *J Neurotrauma*, vol. 17, pp. 451–554, 2000.
- [185] G. Citerio, I. Piper, M. Cormio, D. Galli, S. Cazzaniga, P. Enblad, P. Nilsson, C. Contant, and I. Chambers, "Bench test assessment of the new Raumedic Neurovent-P ICP sensor: A technical report by the BrainIT group," *Acta Neurochir. (Wien).*, vol. 146, no. 11, pp. 1221–1226, 2004.
- [186] A. Cyrous, B. O'Neal, and W. D. Freeman, "New approaches to bedside monitoring in stroke.," *Expert Rev. Neurother.*, vol. 12, no. 8, pp. 915–28, 2012.
- [187] K. Devault, P. Gremaud, V. Novak, M. S. Olufsen, G. Vernières, and P. Zhao, "Blood Flow in the Circle of Willis: Modeling and Calibration.," *Multiscale Model. Simul.*, vol. 7, no. 2, pp. 888–909, 2008.
- [188] M. R. Bergman RA, Afifi AK, "Circle of Willis," *Illus. Encycl. Hum. Anat. Var.*, vol. 11, 2005.
- [189] K. N. Kayembe, M. Sasahara, and F. Hazama, "Cerebral aneurysms and variations in the circle of Willis.," *Stroke*, vol. 15, no. 5, pp. 846–850, 1984.
- [190] S. C. Kety SS, "Determination of cerebral blood flow in man by the use of nitrous oxide in low

- concentrations,” *Am J Physiol*, vol. 143, pp. 53–66, 1945.
- [191] M. Sethuraman, “Cerebral blood flow monitoring,” *J. Neuroanaesth. Crit. care*, vol. 2, no. 3, pp. 204–214, 2015.
- [192] H. Yonas, D. Johnson, and R. Pindzola, “Xenon-enhanced CT of cerebral blood flow,” *Sci Am Sci Med*, 1995.
- [193] M. N. Kim, T. Durduran, S. Frangos, B. L. Edlow, E. M. Buckley, H. E. Moss, C. Zhou, G. Yu, R. Choe, E. Maloney-Wilensky, R. L. Wolf, M. S. Grady, J. H. Greenberg, J. M. Levine, A. G. Yodh, J. A. Detre, and W. A. Kofke, “Noninvasive measurement of cerebral blood flow and blood oxygenation using near-infrared and diffuse correlation spectroscopies in critically brain-injured adults,” *Neurocrit. Care*, vol. 12, no. 2, pp. 173–180, 2010.
- [194] R. Aaslid, *Transcranial Doppler Sonography*. Springer-Verlag Wien, 1986.
- [195] M. S. Salvadori A, Pasquier P, Jarrassier A, Schaal JV, “Transcranial Doppler to measure cerebral blood flow in management of traumatic brain injury.,” *Injury*, vol. 45, pp. 1801–1802, 2014.
- [196] V. J. Jimenez CF, Padro PP, Garcia AS, “Cerebral blood flow measured by transcranial doppler ultrasound during manual chest wall or automated LUCAS-2 compressions during cardiopulmonary resuscitations.,” *Emergencias*, vol. 24, pp. 47–49, 2012.
- [197] S. Purkayastha and F. Sorond, “Transcranial doppler ultrasound: Technique and application,” *Semin. Neurol.*, vol. 32, no. 4, pp. 411–420, 2012.
- [198] M. P. Spencer and D. Whisler, “Transorbital Doppler diagnosis of intracranial arterial stenosis.,” *Stroke.*, vol. 17, no. 5, pp. 916–21, 2010.
- [199] R. Aaslid, T. M. Markwalder, and H. Nornes, “Noninvasive transcranial Doppler ultrasound recording of flow velocity in basal cerebral arteries.,” *J. Neurosurg.*, vol. 57, no. 6, pp. 769–774, 1982.
- [200] S. Sarkar, S. Ghosh, S. K. Ghosh, and a. Collier, “Role of transcranial Doppler ultrasonography in stroke,” *Postgrad. Med. J.*, vol. 83, no. 985, pp. 683–689, 2007.
- [201] M. Czosnyka, P. Smielewski, A. Lavinio, J. D. Pickard, and R. Panerai, “An assessment of dynamic autoregulation from spontaneous fluctuations of cerebral blood flow velocity: a comparison of two models, index of autoregulation and mean flow index.,” *Anesth. Analg.*, vol. 106, no. 1, p. 234–9, table of contents, Jan. 2008.
- [202] D. K. Menon, “Cerebral protection in severe brain injury: physiological determinants of outcome and their optimisation.,” *Br. Med. Bull.*, vol. 55, no. 1, pp. 226–258, 1999.
- [203] P. R. Douglas G Altman, “The cost of dichotomising continuous variables,” *BMJ*, vol. 332, no. 7549, p. 1080, 2006.
- [204] K. M. Brady, J. K. Lee, K. K. Kibler, R. B. Easley, R. C. Koehler, and D. H. Shaffner, “Continuous measurement of autoregulation by spontaneous fluctuations in cerebral perfusion pressure: comparison of 3 methods.,” *Stroke.*, vol. 39, no. 9, pp. 2531–2537, 2008.
- [205] K. M. Brady, R. B. Easley, K. Kibler, D. W. Kaczka, D. Andropoulos, C. D. Fraser, P. Smielewski, M.

- Czosnyka, G. J. Adams, C. J. Rhee, and C. G. Rusin, "Positive end-expiratory pressure oscillation facilitates brain vascular reactivity monitoring," *J. Appl. Physiol.*, vol. 113, pp. 1362–1368, 2012.
- [206] K. M. Brady, J. K. Lee, K. K. Kibler, R. B. Easley, R. C. Koehler, M. Czosnyka, P. Smielewski, and D. H. Shaffner, "The lower limit of cerebral blood flow autoregulation is increased with elevated intracranial pressure," *Anesth. Analg.*, vol. 108, no. 4, pp. 1278–1283, 2009.
- [207] A. X. Robin, N. Turck, A. Hainard, F. Lisacek, J. Sanchez, M. Müller, and M. X. R. Xavierrobinunigech, "Package ' pROC ,' " *2012-09-10 09:34:56*, no. 1, pp. 1–71, 2013.
- [208] J. a H. R. Claassen, B. D. Levine, and R. Zhang, "Dynamic cerebral autoregulation during repeated squat-stand maneuvers.," *J. Appl. Physiol.*, vol. 106, no. 1, pp. 153–160, Jan. 2009.
- [209] R. B. Panerai, "System Identification of Human Cerebral Blood," vol. 4, no. 1, pp. 59–71, 2004.
- [210] R. Zhang, J. H. Zuckerman, C. a Giller, and B. D. Levine, "Transfer function analysis of dynamic cerebral autoregulation in humans.," *Am. J. Physiol.*, vol. 274, no. 1 Pt 2, pp. H233-41, Jan. 1998.
- [211] D. K. Radolovich, M. J. H. Aries, G. Castellani, A. Corona, A. Lavinio, P. Smielewski, J. D. Pickard, and M. Czosnyka, "Pulsatile intracranial pressure and cerebral autoregulation after traumatic brain injury," *Neurocrit. Care*, vol. 15, no. 3, pp. 379–386, 2011.
- [212] R. B. Panerai, J. M. Rennie, A. W. R. Kelsall, and D. H. Evans, "Frequency-domain analysis of cerebral autoregulation from spontaneous fluctuations in arterial blood pressure," *Med. Biol. Eng. Comput.*, vol. 36, no. 3, pp. 315–322, 1998.
- [213] R. R. Diehl, D. Linden, D. Lücke, and P. Berlit, "Phase relationship between cerebral blood flow velocity and blood pressure. A clinical test of autoregulation.," *Stroke.*, vol. 26, no. 10, pp. 1801–1804, 1995.
- [214] X. Liu, M. Czosnyka, J. Donnelly, K. P. Budohoski, G. V Varsos, N. Nasr, K. M. Brady, M. Reinhard, P. J. Hutchinson, and P. Smielewski, "Comparison of frequency and time domain methods of assessment of cerebral autoregulation in traumatic brain injury," *J. Cereb. Blood Flow Metab.*, vol. 11, no. October, pp. 1–9, 2014.
- [215] A. H. van Beek, J. A. Claassen, M. G. O. Rikkert, and R. W. Jansen, "Cerebral autoregulation: an overview of current concepts and methodology with special focus on the elderly," *J. Cereb. Blood Flow & Metab.*, vol. 28, no. 6, pp. 1071–1085, 2008.
- [216] K. P. Budohoski, M. Czosnyka, P. Smielewski, G. V Varsos, M. Kasprovicz, K. M. Brady, J. D. Pickard, and P. J. Kirkpatrick, "Cerebral autoregulation after subarachnoid hemorrhage: comparison of three methods.," *J. Cereb. Blood Flow Metab.*, vol. 33, no. 3, pp. 449–56, Mar. 2013.
- [217] M. Oeinc, F. Neunhoeffler, K.-J. Buttler, S. Meckel, B. Schmidt, M. Czosnyka, C. Weiller, and M. Reinhard, "Dynamic cerebral autoregulation in acute intracerebral hemorrhage.," *Stroke.*, vol. 44, no. 10, pp. 2722–8, 2013.
- [218] E. Sorrentino, K. P. Budohoski, M. Kasprovicz, P. Smielewski, B. Matta, J. D. Pickard, and M. Czosnyka, "Critical thresholds for transcranial doppler indices of cerebral autoregulation in traumatic brain injury," *Neurocrit. Care*, vol. 14, no. 2, pp. 188–193, 2011.

- [219] J. J. Lemaire, T. Khalil, F. Cervenansky, G. Gindre, J. Y. Boire, J. E. Bazin, B. Irthum, and J. Chazal, "Slow pressure waves in the cranial enclosure," *Acta Neurochir. (Wien)*, vol. 144, no. 3, pp. 243–254, 2002.
- [220] J. K. Krauss, D. W. Droste, M. Bohus, J. P. Regel, R. Scheremet, D. Riemann, and W. Seeger, "The relation of intracranial pressure B-waves to different sleep stages in patients with suspected normal pressure hydrocephalus," *Acta Neurochir. (Wien)*, vol. 136, no. 3–4, pp. 195–203, 1995.
- [221] L. M. Auer and I. Sayama, "Intracranial pressure oscillations (B-waves) caused by oscillations in cerebrovascular volume," *Acta Neurochir. (Wien)*, vol. 68, no. 1–2, pp. 93–100, 1983.
- [222] U. Johnson, P. Nilsson, E. Ronne-Engström, T. Howells, and P. Enblad, "Favorable outcome in traumatic brain injury patients with impaired cerebral pressure autoregulation when treated at low cerebral perfusion pressure levels," *Neurosurgery*, vol. 68, no. 3, pp. 714–721, 2011.
- [223] M. Barth, B. Moratin, M. Dostal, A. Kalenka, J. Scharf, and K. Schmieder, "Correlation of clinical outcome and angiographic vasospasm with the dynamic autoregulatory response after aneurysmal subarachnoid hemorrhage.," *Acta Neurochir. Suppl.*, vol. 114, pp. 157–160, 2012.
- [224] M. Czosnyka, M. Balestreri, L. Steiner, P. Smielewski, P. J. Hutchinson, B. Matta, and J. D. Pickard, "Age, intracranial pressure, autoregulation, and outcome after brain trauma.," *J. Neurosurg.*, vol. 102, pp. 450–454, 2005.
- [225] a M. Harper and H. I. Glass, "Effect of alterations in the arterial carbon dioxide tension on the blood flow through the cerebral cortex at normal and low arterial blood pressures.," *J. Neurol. Neurosurg. Psychiatry*, vol. 28, no. 5, pp. 449–452, 1965.
- [226] P. M. Lewis, P. Smielewski, J. D. Pickard, and M. Czosnyka, "Dynamic cerebral autoregulation: should intracranial pressure be taken into account?," *Acta Neurochir. (Wien)*, vol. 149, no. 6, p. 549–55; discussion 555, Jul. 2007.
- [227] F. S. Larsen, K. S. Olsen, B. a Hansen, O. B. Paulson, and G. M. Knudsen, "Transcranial Doppler is valid for determination of the lower limit of cerebral blood flow autoregulation.," *Stroke*, vol. 25, no. 10, pp. 1985–8, 1994.
- [228] K. F. Lindegaard, T. Lundar, J. Wiberg, D. Sjoberg, R. Aaslid, and H. Nornes, "Variations in middle cerebral artery blood flow investigated with noninvasive transcranial blood velocity measurements," *Stroke*, vol. 18, no. 6, pp. 1025–1030, 1987.
- [229] R. Zhang, K. Behbehani, and B. D. Levine, "Dynamic pressure-flow relationship of the cerebral circulation during acute increase in arterial pressure," *J Physiol*, vol. 587, no. Pt 11, pp. 2567–2577, 2009.
- [230] H. N. R. Aaslid, T. Lundar, K. F. Lindegaard, "Estimation of Cerebral Perfusion Pressure from Arterial Blood Pressure and Transcranial Doppler Recordings," *Intracranial Press. VI*, pp. 226–229, 1986.
- [231] K. S. Shigemori M, Nakashima H, Moriyama T, Tokutomi T, Nishio N, Harada K, "Noninvasive study of critical thresholds of intracranial pressure and cerebral perfusion pressure for cerebral circulation and brain function," *Neurol Res*, vol. 11, no. 3, pp. 165–8, 1989.
- [232] M. Czosnyka, B. F. Matta, P. Smielewski, P. J. Kirkpatrick, and J. D. Pickard, "Cerebral perfusion pressure

- in head-injured patients: a noninvasive assessment using transcranial Doppler ultrasonography.," *J. Neurosurg.*, vol. 88, no. 5, pp. 802–808, 1998.
- [233] B. Schmidt, M. Czosnyka, J. J. Schwarze, D. Sander, W. Gerstner, C. B. Lumenta, J. D. Pickard, and J. Klingelhöfer, "Cerebral vasodilatation causing acute intracranial hypertension: a method for noninvasive assessment.," *J. Cereb. Blood Flow Metab.*, vol. 19, no. 9, pp. 990–996, 1999.
- [234] K. Keissar, L. R. Davrath, and S. Akselrod, "Coherence analysis between respiration and heart rate variability using continuous wavelet transform.," *Philos. Trans. A. Math. Phys. Eng. Sci.*, vol. 367, no. 1892, pp. 1393–1406, 2009.
- [235] C. Torrence and G. P. Compo, "A Practical Guide to Wavelet Analysis," *Bull. Am. Meteorol. Soc.*, vol. 79, no. 1, pp. 61–78, 1998.
- [236] L. Faes, G. D. Pinna, A. Porta, R. Maestri, and G. Nollo, "Surrogate data analysis for assessing the significance of the coherence function," *IEEE Trans. Biomed. Eng.*, vol. 51, no. 7, pp. 1156–1166, 2004.
- [237] T. Schreiber and A. Schmitz, "Surrogate time series," *Phys. D Nonlinear Phenom.*, vol. 142, no. 3–4, pp. 346–382, 2000.
- [238] J. Theiler, S. Eubank, A. Longtin, B. Galdrikian, and J. Doyné Farmer, "Testing for nonlinearity in time series: the method of surrogate data," *Phys. D Nonlinear Phenom.*, vol. 58, no. 1–4, pp. 77–94, 1992.
- [239] J. Lee, K. Kibler, P. Benni, and R. Easley, "Cerebrovascular reactivity measured by near-infrared spectroscopy," *Stroke*, 2009.
- [240] M. Smith, "Shedding light on the adult brain: a review of the clinical applications of near-infrared spectroscopy.," *Philos. Trans. A. Math. Phys. Eng. Sci.*, vol. 369, no. 1955, pp. 4452–69, 2011.
- [241] P. M. Lewis, J. V. Rosenfeld, R. R. Diehl, H. M. Mehdorn, and E. W. Lang, "Phase shift and correlation coefficient measurement of cerebral autoregulation during deep breathing in traumatic brain injury (TBI)," *Acta Neurochir. (Wien)*, vol. 150, pp. 139–146, 2008.
- [242] T. Peng, A. B. Rowley, P. N. Ainslie, M. J. Poulin, and S. J. Payne, "Wavelet phase synchronization analysis of cerebral blood flow autoregulation.," *IEEE transactions on bio-medical engineering*, vol. 57, no. 4, pp. 960–8, Apr-2010.
- [243] P. Kvandal, L. Sheppard, S. a Landsverk, A. Stefanovska, and K. a Kirkeboen, "Impaired cerebrovascular reactivity after acute traumatic brain injury can be detected by wavelet phase coherence analysis of the intracranial and arterial blood pressure signals.," *J. Clin. Monit. Comput.*, vol. 27, no. 4, pp. 375–83, Aug. 2013.
- [244] B. J. Carey, R. B. Panerai, and J. F. Potter, "Effect of aging on dynamic cerebral autoregulation during head-up tilt.," *Stroke*, vol. 34, no. 8, pp. 1871–1875, 2003.
- [245] K. W., "Evaluation of cardiovascular risk in the elderly: the Framingham Study," *Bull N Y Acad Med*, vol. 54, pp. 573–591, 1978.
- [246] J. L. Fleg, "Alterations in cardiovascular structure and function with advancing age," *Am. J. Cardiol.*, vol. 57, no. 5, 1986.

- [247] B. Gribbin, T. G. Pickering, P. Sleight, and R. Peto, "Effect of Age and High Blood Pressure on Baroreflex Sensitivity in Man," *Circ. Res.*, vol. 29, no. 4, pp. 424–431, 1971.
- [248] M. Wagner, A. Jurcoane, S. Volz, J. Magerkurth, F. E. Zanella, T. Neumann-Haefelin, R. Deichmann, O. C. Singer, and E. Hattingen, "Age-related changes of cerebral autoregulation: New insights with quantitative T2*-mapping and pulsed arterial spin-labeling MR imaging," *Am. J. Neuroradiol.*, vol. 33, no. 11, pp. 2081–2087, 2012.
- [249] B. J. Carey, P. J. Eames, M. J. Blake, R. B. Panerai, and J. F. Potter, "Dynamic cerebral autoregulation is unaffected by aging.," *Stroke.*, vol. 31, no. 12, pp. 2895–2900, 2000.
- [250] A. T. Yam, E. W. Lang, J. Lagopoulos, K. Yip, J. Griffith, Y. Mudaliar, and N. W. C. Dorsch, "Cerebral autoregulation and ageing," *J. Clin. Neurosci.*, vol. 12, no. 6, pp. 643–646, 2005.
- [251] H. C. Patel, D. K. Menon, S. Tebbs, R. Hawker, P. J. Hutchinson, and P. J. Kirkpatrick, "Specialist neurocritical care and outcome from head injury," *Intensive Care Med.*, vol. 28, no. 0342–4642 (Print), pp. 547–553, 2002.
- [252] B. Jennett and M. Bond, "Assessment of outcome after severe brain damage.," *Lancet*, vol. 1, no. 7905, pp. 480–484, 1975.
- [253] N. a Obuchowski, "Receiver operating characteristic curves and their use in radiology.," *Radiology*, vol. 229, no. 1, pp. 3–8, 2003.
- [254] C.-W. Lu, M. Czosnyka, J.-S. Shieh, A. Smielewska, J. D. Pickard, and P. Smielewski, "Complexity of intracranial pressure correlates with outcome after traumatic brain injury.," *Brain*, vol. 135, pp. 2399–408, 2012.
- [255] M. J. H. Aries, M. Czosnyka, K. P. Budohoski, A. G. Koliass, D. K. Radolovich, A. Lavinio, J. D. Pickard, and P. Smielewski, "Continuous monitoring of cerebrovascular reactivity using pulse waveform of intracranial pressure," *Neurocrit. Care*, vol. 17, no. 1, pp. 67–76, 2012.
- [256] L. A. Steiner, M. Czosnyka, and S. K. Piechnik, "Continuous monitoring of cerebrovascular pressure reactivity allows determination of optimal cerebral perfusion pressure in patients with traumatic brain injury," *Crit. Care*, vol. 30, no. 4, pp. 733–738, 2002.
- [257] C. Eker, B. Asgeirsson, P. Grände, W. Schalén, and C. Nordström, "Improved outcome after severe head injury with a new therapy based on principles for brain volume regulation and preserved microcirculation.," *Crit. Care Med.*, vol. 26, no. 11, pp. 1881–1886, 1998.
- [258] M. J. Aries, M. Czosnyka, K. P. Budohoski, L. A. Steiner, A. Lavinio, A. G. Koliass, P. J. Hutchinson, K. M. Brady, D. K. Menon, J. D. Pickard, and P. Smielewski, "Continuous determination of optimal cerebral perfusion pressure in traumatic brain injury," *Crit Care Med*, vol. 40, no. 8, pp. 2456–2463, 2012.
- [259] T. Howells, K. Elf, P. a Jones, E. Ronne-Engström, I. Piper, P. Nilsson, P. Andrews, and P. Enblad, "Pressure reactivity as a guide in the treatment of cerebral perfusion pressure in patients with brain trauma," *J. Neurosurg.*, vol. 102, no. 2, pp. 311–317, 2005.
- [260] J. D. Miller, D. P. Becker, J. D. Ward, H. G. Sullivan, W. E. Adams, and M. J. Rosner, "Significance of

- intracranial hypertension in severe head injury.,” *Journal of neurosurgery*, vol. 47, no. 4. pp. 503–16, 1977.
- [261] D. Pitts, L. H., Kaktis, J. V., Juster, R. and Heilbrun, *ICP and outcome in patients with severe head injury, in Intracranial Pressure IV*. Berlin: Springer-Verlag, 1980.
- [262] M. G. O’Sullivan, P. F. Statham, P. A. Jones, J. D. Miller, N. M. Dearden, I. R. Piper, S. I. Anderson, A. Housley, P. J. Andrews, S. Midgley, and et al., “Role of intracranial pressure monitoring in severely head-injured patients without signs of intracranial hypertension on initial computerized tomography,” *J Neurosurg*, vol. 80, no. 1. pp. 46–50, 1994.
- [263] L. TW., “Increased intracranial pressure,” *Clin. Neurosurg.*, vol. 16, pp. 436–71, 1969.
- [264] M. JD, “Normal and increased intracranial pressure.,” in *Northfield’s surgery of the central nervous system 2nd ed*, London: Blackwell, 1987, pp. 7–57.
- [265] R. M. J, *The vasodilatory cascade and intracranial pressure*. Springer Berlin Heidelberg, 1986.
- [266] M. Hayashi, H. Kobayashi, H. Kawano, S. Yamamoto~, and T. Maeda, “Cerebral blood flow and ICP patterns in patients with communicating hydrocephalus after aneurysm rupture,” *J Neurosurg*, vol. 61, pp. 30–36, 1984.
- [267] I. D. Risberg J, Lundberg N, “Regional cerebral blood volume during acute transient rises of the intracranial pressure (plateau waves),” *J Neurosurg*, vol. 31, no. 3, pp. 303–10, 1969.
- [268] S. P. Liu 1, Czosnyka M, Pickard JD, Varsos GV, Nasr N, “Derangement of cerebral blood flow autoregulation during intracranial pressure plateau waves as detected by time and frequency-based methods,” *Acta Neurochir Suppl.*, vol. 122, pp. 233–8, 2016.
- [269] M. J. Rosner and D. P. Becker, “Origin and evolution of plateau waves. Experimental observations and a theoretical model.,” *J. Neurosurg.*, vol. 60, no. 2, pp. 312–324, 1984.
- [270] M. L. Daley, C. W. Leffler, M. Czosnyka, and J. D. Pickard, “Plateau waves: Changes of cerebrovascular pressure transmission,” in *Acta Neurochirurgica, Supplementum*, 2005, no. 95, pp. 327–332.
- [271] C. J. Avezaat and J. H. van Eijndhoven, “Clinical observations on the relationship between cerebrospinal fluid pulse pressure and intracranial pressure.,” *Acta Neurochir. (Wien).*, vol. 79, no. 1, pp. 13–29, 1986.
- [272] R. Johnston, “Cerebrospinal Fluid Pulse Pressure and Craniospinal Dynamics. A Theoretical, Clinical and Experimental Study,” *J Neurol Neurosurg Psychiatry*, vol. 47, no. 11, p. 1265, 1984.
- [273] M. Czosnyka, H. K. Richards, H. E. Whitehouse, and J. D. Pickard, “Relationship between transcranial Doppler-determined pulsatility index and cerebrovascular resistance: an experimental study,” *J Neurosurg.*, vol. 84, no. 1, pp. 79–84, 1996.
- [274] J. D. Robinson, “Management of Refractory Intracranial Pressure,” *Crit. Care Nurs. Clin. North Am.*, vol. 28, no. 1, pp. 67–75, 2016.
- [275] M. K. Bader, R. Arbour, and S. Palmer, “Refractory increased intracranial pressure in severe traumatic brain injury: barbiturate coma and bispectral index monitoring.,” *AACN Clin. Issues*, vol. 16, no. 4, pp. 526–41, 2005.
- [276] L. Rangel-Castillo and C. S. Robertson, “Management of Intracranial Hypertension,” *Critical Care Clinics*,

- vol. 22, no. 4. pp. 713–732, 2006.
- [277] S. Cerutti, a M. Bianchi, and L. T. Mainardi, “Advanced spectral methods for detecting dynamic behaviour.,” *Auton. Neurosci.*, vol. 90, no. 1–2, pp. 3–12, 2001.
- [278] L. Keselbrener and S. Akselrod, “Selective discrete Fourier transform algorithm for time-frequency analysis: method and application on simulated and cardiovascular signals.,” *IEEE Trans. Biomed. Eng.*, vol. 43, no. 8, pp. 789–802, 1996.
- [279] C. M. Lang EW, Kasproicz M, Smielewski P, Pickard J, “Changes in Cerebral Partial Oxygen Pressure and Cerebrovascular Reactivity During Intracranial Pressure Plateau Waves,” *Neurocrit Care*, vol. 23, no. 1, pp. 85–91, 2015.
- [280] C. S. Da Costa, M. Czosnyka, P. Smielewski, S. Mitra, G. N. Stevenson, and T. Austin, “Monitoring of cerebrovascular reactivity for determination of optimal blood pressure in preterm infants,” *J. Pediatr.*, vol. 167, no. 1, pp. 86–91, 2015.